VOLUME 14 NUMBER 2 2021 ISSN 2218-7979
eISSN 2409-370X

International Journal of Biology and Chemistry

Al-Farabi Kazakh National University

International Journal of Biology and Chemistry is published twice a year by
al-Farabi Kazakh National University, al-Farabi ave., 71, 050040, Almaty, Republic of Kazakhstan
website: http://ijbch.kaznu.kz/

Any inquiry for subscriptions should be sent to:
Prof. Mukhambetkali Burkitbayev, al-Farabi Kazakh National University
al-Farabi ave., 71, 050040, Almaty, Republic of Kazakhstan
e-mail: Mukhambetkali Burkitbayev@kaznu.kz

EDITORIAL

The most significant achievements in the field of natural sciences are reached in joint collaboration, where important roles are taken by biology and chemistry. Therefore publication of a Journal, displaying results of current studies in the field of biology and chemistry, facilitates highlighting theoretical and practical issues and distribution of scientific discoveries.

One of the basic goals of the Journal is to promote the extensive exchange of information between the scientists from all over the world. We welcome publishing original papers and materials of biological and chemical conferences, held in different countries (by prior agreement, after the process of their subsequent selection).

Creation of International Journal of Biology and Chemistry is of great importance, since scientists worldwide, including other continents, might publish their articles, which will help to widen the geography of future collaboration.

The Journal aims to publish the results of the experimental and theoretical studies in the field of biology, biotechnology, chemistry and chemical technology. Among the emphasized subjects are: modern issues of technologies for organic synthesis; scientific basis of the production of physiologically active preparations; modern issues of technologies for processing of raw materials; production of new materials and technologies; study on chemical and physical properties and structure of oil and coal; theoretical and practical issues in processing of hydrocarbons; modern achievements in the field of nanotechnology; results of studies in various branches of biology, chemistry and related technologies.

We hope to receive papers from the leading scientific centers, which are involved in the application of the scientific principles of biological and chemical sciences on practice and fundamental research, related to production of new materials, technologies and ecological issues.

IRSTI 28.23.23 https://doi.org/10.26577/ijbch.2021.v14.i2.01

A.S. Makhmet[1], M.G. Sharaev[2], A.E. Dyusembaev[1], A.M. Kustubayeva[1]*

[1]Al-Farabi Kazakh National University, Almaty, Kazakhstan
[2]Skolkovo Institute of Science and Technology, Moscow, Russia
*e-mail: almkusto@kaznu.kz

Machine learning for brain signal analysis

Abstract. Machine learning (ML) is an effective tool for analysing signals from the human brain. Machine Learning techniques provide new insight into the understanding of brain function in healthy subjects and patients with neurological and mental disorders. Here we introduce the application of machine learning to brain signal analysis, specifically using two widely used brain signal collection methods: functional magnetic resonance imaging (fMRI) and Electroencephalography (EEG). The article provides a brief overview of the theoretical concept of machine learning and its types: supervised, unsupervised and reinforcement learning. The potential of machine learning applications in pathology is discussed. Differences between EEG and fMRI methods regarding machine learning application and an overview of the techniques employed in different research studies are reviewed. The new machine learning methods invented for analysis of brain signals in the resting state and during the performance of the different cognitive tasks would be useful and worth considering in other domains, not limited to medicine.

Key words: EEG, fMRI, machine learning, MVPA, brain signal analysis.

Introduction

Machine learning applications are effective in solving many modern problems. Its widespread use has induced the emergence of a large amount of literature. The present article aims to provide a brief introduction to machine learning techniques and its application in brain signals analysis, specifically to fMRI and EEG signals.

First, we provide a brief overview of the theoretical concept of machine learning. Machine learning is a scientific discipline in which techniques are designed so that machines can computationally efficiently extract patterns, structures or relationships from data. It is a relatively new discipline, which lies at the intersection of two fields: mathematics and computer science. The majority of machine learning techniques are based on the following mathematical realms: linear algebra, analytic geometry, matrix decomposition, probability theory, vector calculus and optimization [1].

A learning process outcome would be called a model. Machine learning models describe relationships within observed data. A typical dataset that is considered in ML problems consists of dependent and independent variables. Independent variables can also be referred to as features, while a dependent variable, which depends on independent variables, is referred to as a target.

Machine learning techniques are based on regression, dimensionality reduction, density estimation and classification [1]. The key objective in regression and classification problems is to build a model that would map inputs x to corresponding values y, where x represents feature matrix and y represents a target vector [1]. The difference is that in regression the outputs are continuous values, whereas in classification the outputs are discrete (or categorical) values. The key objective in dimensionality reduction problems is to reduce the number of features in the feature matrix, with minimum loss of potentially valuable information [1]. The key objective in density estimation problems is to describe a dataset from the perspective of a probability distribution [1].

Nowadays there are many different types of learning that exist in Machine learning. Traditionally, machine learning approaches are divided into three broad categories: supervised, unsupervised, and reinforcement learning. Reinforcement learning is a type of learning, in which an 'agent' learns how to act in an environment by continuously getting 'feedback' from that environment. In supervised learning, a model is trained on labeled data to learn a relationship between features and a target variable. Next, to

evaluate the performance of the model, the model is tested on previously 'unseen' data. Model training is the process during which a machine learns patterns and structure from available data. In contrast to the supervised learning approach, the unsupervised approach works with unlabeled data, and a model is built to discover patterns and structures within the data. Supervised learning is used in regression and classification algorithms, whereas unsupervised learning is used in dimensionality reduction, density estimation, anomaly detection, autoencoding and clustering techniques. In supervised learning, we are able to evaluate our model by comparing predicted and actual labels of test data. In contrast, in unsupervised learning there are no labels to predict, and, therefore, there is no direct evaluation for unsupervised learning. However, an output of an unsupervised learning task is often used to construct an input (informative features) to the subsequent supervised learning task, and it can be evaluated via results of the subsequent supervised learning task and answer the question, "Was the pattern discovered in unsupervised learning useful?" [2].

Machine learning application in clinics

Medicine and pathology in particular are arguably the most promising domains to apply machine learning: what could be more inspiring than contributing to saving millions of lives from complex diseases or improving the quality of life of those who are paralyzed? With each year there is an increased number of publications presenting applications of machine learning algorithms to medical data, yet this has not resulted in many meaningful contributions to clinical care [2]. The main reason is possibly low AI/ML algorithms trustworthiness, which comprises several parts: is the algorithm accurate and robust, how fair and transparent are its decisions, and finally, how interpretable are these decisions to the medical community [3]. While high accuracy and robustness (for example to low quality data) are well-known desired properties of AI/ML systems in all applied fields, model interpretability becomes crucial, especially in a clinical setting. Another factor that makes it difficult to apply machine learning to medical data is that acquisition of data is a costly and lengthy process. For example, for brain signal analysis to acquire data using fMRI, one must have an fMRI scanner, which is considered to be expensive, and not many research groups can afford it. Comparatively, getting other types of data is much easier. For example, Netflix possesses all the data that is needed in order to build its own recommendation system, because it analyses traffic that a user generates when interacting with a Netflix website or application.

Both supervised and unsupervised learning are used in pathology and human functions. One example is analysis of data obtained from patients with Heart Failure with preserved Ejection Fraction (HFpEF) [2]. HFpEF is a complex condition and reflects multiple dominant pathophysiologic processes. The idea of the analysis was to group patients on the basis of qualitative echocardiographic and clinical variables. Initially, there were 67 different features; after removing highly correlated features, there were 46 predictors (features). Next, a regularized form of a clustering algorithm was applied: clusters were determined by using multivariate Gaussian distributions and using means and standard deviation assigned to each feature [2]. The clusters were formed by calculating a joint probability of membership for each patient. Results of the comparison of the calculated clusters have demonstrated the differences across many phenotypic variables. These phenotypic clusters resulted in becoming features in the supervised learning model that predicted survival of HFpEF patients.

Study of signals of the brain, the most complex structure in the body, may help understand brain functioning in normal versus neurological or mental disorder brain conditions. Many studies use supervised learning approaches to diagnose a brain function pathology or classify symptom severity from concurrent neuroimaging data. Among brain function disorders are attention-deficit/hyperactivity disorder, autism, depression, and schizophrenia [4]. Moreover, machine learning technology is able to detect deviations from normative development trajectories as risk factors for psychopathology. Defining an age of an individual based on brain activity network patterns can be used to elucidate atypical development in children and adults with Tourette syndrome [4]. There is a growing number of studies using brain connectivity approaches [5]. This method is based on graph theory and determines functional, structural, and causal dynamical networks. Therefore, brain connectivity measurements appear to serve as variables to determine whether it is possible to predict subsequent diagnosis or treatment outcomes.

Apart from supervised learning in brain signal analysis, an unsupervised learning approach can be used to cluster patients into subgroups with categorically different patterns of neuroimaging features. The application of reinforcement learning is also considered in the field of neuroscience [6-7]. It is worth mentioning that the Reinforcement learning

approach itself gets its aspiration from the cognitive neuroscience field, as it tries to mimic brain function.

There are different techniques for measuring and mapping brain activity. These include Electroencephalography (EEG), functional magnetic resonance imaging (fMRI), Positron emission tomography (PET) and Magnetoencephalography (MEG). Our focus in this article is on the two most popular noninvasive and safe methods to obtain brain signals during the cognitive task or resting states: fMRI and EEG.

Machine learning in functional MRI signal analysis

FMRI measures brain neural activity via magnetic properties of blood, namely, the blood-oxygen level dependent (BOLD) signal. The method is based on the fact that with an increase in the activity of a particular area of the brain, blood flow to this area also increases, which means that the parameters of blood movement and level of oxygen in the vascular bed change. A typical neuroimaging experiment holds for several sessions (runs) per subject. In fMRI, the whole brain is scanned for the duration of a session, resulting in many brain images per time unit, called volumes. The scanning rate affects the spatial and temporal resolutions of images. FMRI has good spatial resolution and a satisfactory level of temporal resolution, even though these spatial and temporal resolutions are attained at the expense of each other.

For one to perform an effective fMRI analysis, the data collected should first undergo the preprocessing stage. Preprocessing typically includes Realigning and Unwarping the Data, Slice-time correction, Co-registration, Segmentation, Normalization, and Smoothing steps. The last Smoothing step is in many cases omitted to avoid distortion of neural activity intensity per voxel.

The first types of analyses that prevailed in the analysis of fMRI data were univariate and mass-univariate. In univariate analysis, an amplitude of a signal elicited from a voxel, which is a 3-dimensional pixel of a brain (usually 3mm*3mm*3mm), is analyzed in the context of each voxel separately. In mass-univariate analysis, a statistical inference about brain region responses to particular stimuli is made on the basis of the average activation value of a region calculated using univariate analysis conducted for each voxel in that region of a brain. Nowadays univariate and mass-univariate analysis is enhanced by Multivoxel pattern analysis (MVPA), the first concept of which appeared in the early 2000s. It also operates at a level of a voxel, however, the MVPA approach considers the fMRI analysis problem as a classification problem. Multivoxel pattern analysis has become a new paradigm for fMRI analysis in the world of neuroimaging.

The MVPA approach allows to ‘decode’ fMRI signals and maps them to sensory and motor events or participant’s mental state [8]. A brain activity that was triggered by a certain experimental condition is recorded and represented as a pattern of voxels for that condition. In MVPA, each voxel constitutes a dimension in space, correspondingly, every pattern of voxels i.e., brain activity can be represented as a dot in that voxel space. Thus, many points (voxel patterns) form clouds in the voxel space. Figure 1 shows a simple voxel space structure: the number of dimensions was simplified to 3 voxels, red dots represent condition A and blue dots represent condition B. The plane separates two clouds. Such representation of fMRI data makes it possible to apply different supervised methods, such as support-vector machine (SVM) and linear discriminant analysis (LDA).

Functional MRI analysis is complicated by the vast number of voxels that are treated as features in classification methods. This creates a problem of “Curse of dimensionality”: a number of available voxels reaches more than 30,000, whereas the number of trials (samples) are at the highest 100 [9]. Different approaches are employed to reduce data dimensionality and thus select only ‘useful’ voxels. Two of the main standard approaches are region of interest (ROI) and Searchlight. Regions in ROI can be selected on the basis of anatomical structure, or on the results of application of the ANOVA method. In the latter, voxels are selected on the ANOVA test of response of each voxel to the experimental conditions [10]. After ROI selection, a functional connectivity matrix can be calculated and vectorized in different ways. Obtained low-dimensional feature vectors are then used in ML models as predictors of various diseases, see for example [11].

In the Searchlight method, a classifier is consequently trained on a small spherical cluster of voxels, centered at each voxel of the indicated areas (usually the whole brain is selected). Classification accuracies for each spherical cluster are calculated and are assigned respectively to the central voxels of the clusters. The subsets of clusters with good classification accuracy are identified, then either all voxels of these subsets are selected or the central voxels of the clusters of these subsets are selected [12].

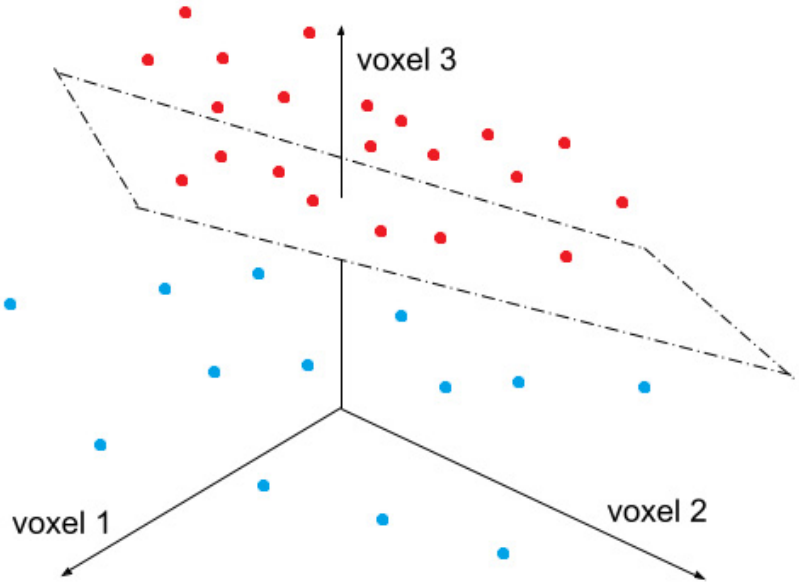

Figure 1 – Representation of brain activities of different conditions in voxel space

Common statistical approaches to dimensionality reduction, like ICA and PCA can also be successfully applied to select features. An example of ICA application is Hunyadi's [12] study of localization of epileptogenic zones, where ICA was applied to select epileptic components that later have been fed to classification algorithms [12]. Graph-theoretical approaches could be applied to fMRI-based connectivity matrices resulting in informative features for depression diagnostics [13].

Bleigh-Cohen [14] has proposed a new classification method called SBFE: patients with complex psychopathology were classified using data driven ROI search coupled with whole-brain machine-learning. SBFE showed 91% accuracy in classifying schizophrenia patients with and without OCD [14]. They state that in contrast to standard ROI driven analyses, SBFE was able to classify schizophrenia patients with and without OCD with 91% accuracy. Thus, the application of this approach can have promising results when needed to delineate patients of one complex psychiatric morbidity with the presence of different symptoms.

De Martino [15] in his work has introduced recursive feature elimination (RFE) strategy. It uses SVM reclusively to remove irrelevant voxels and assess informative spatial patterns. The method has increased sensitivity for discriminative patterns.

According to Duff [16], the number of pre-processing and feature generation methods impacts prediction accuracy more consistently than the choice of a classifier.

In many projects, the most popular choice of learning algorithms in fMRI analysis is SVM [17]. Among other different machine learning approaches in MVPA are Clustering algorithms [18], deep neural networks [19], and Representational Similarity Analysis [20]. In some recent work, there are first attempts to make deep neural networks models on fMRI data interpretable for particular clinical diagnostics tasks, see [21-22] for details. An advantage of using deep learning over non-deep learning approaches is that features can be automatically learned by neural networks, thus eliminating the need to conduct manual feature extraction and selection steps. Feature selection and extraction steps are performed by special structures of deep learning architecture, called convolutional and pooling layers.

In fMRI, due to the scarcity of samples compared to the number of features, the cross-validation technique is often used. Cross-validation is one of the ML techniques to improve the efficiency of the algorithm by iteratively splitting data into different training/testing sets, and thus artificially increasing the overall training sample of the model. There are different strategies for selecting the validation fold. One of the popular strategies in MVPA is leave-subject-out or also known as leave-one-out (LOO-CV), where records of one subject are assigned to be a test dataset [23].

Usually, experiments in neuroscience are constructed in such a way that there is a balanced number of records with different labels in a dataset. Nevertheless, studies with unbalanced datasets can also take place: an example is the study of intrusive memory formation, in which Clark [24] attempted to predict mental health symptoms by reconstructing idiosyncratic cognitive events. The labels of the conditions were not known at the time of the experiment. Therefore, balancing techniques were needed to be employed prior to classifying the records.

As in any medical problem, sensitivity and specificity are highly important metrics for evaluating model testing results in fMRI. Accuracy itself will not be enough to provide a full picture of the effective metric. In many studies, the ROC and Precision-Recall (PR) curve is employed as an evaluation metric.

Machine learning in EEG analysis

In contrast to fMRI, EEG is an economical and easy-to-operate tool for recording brain activity [25]. It records the brain's electrical activity over a period of time. Electrochemical processes occurring in the neuronal activity of the brain resulted in electrical oscillations on the brain surface with different amplitude and frequency – alpha, beta, gamma, theta, and delta rhythms. The relationship between these rhythms depends on external stimuli and the state of the human brain. These rhythms may differ in different brain conditions. For example, Gollan's study of Frontal alpha EEG asymmetry confirms that depressed patients have a significantly higher difference in alpha rhythms between the left and right frontal part of the hemisphere than healthy participants [26].

Analysis of EEG has made it possible to develop brain-computer-interface systems. Brain-computer interface (BCI) system is an application that reads EEG signals in real-time and sends the decoded signals to an external device.

The list of the neurological disorders that can be studied using EEG signals includes but is not limited to epilepsy, seizure prediction, Alzheimer's disease, Mild Cognitive Impairment (MCI), Parkinson's disease, Creutzfeldt-Jakob Disease, sleep studies, schizophrenia, analysis of emotional states [21]. Using machine learning classification methods, it is possible to predict and prevent the development of depression [27].

EEG signals have better temporal resolution than fMRI signals, but the spatial resolution is low [28]. EEG signals are collected by electrodes placed on the participant's head. Each electrode represents an EEG channel and records a brain signal from a part of the brain that is closer to the electrode. Nevertheless, the location of an electrode may not correspond to the exact location of the brain source [29]. This constitutes an inverse problem that exists in EEG concerning localizing a brain source that elicited a particular EEG signal [30].

Although both EEG and fMRI methods employ signal processing techniques for feature extraction, it should be noted that EEG mostly employs time series processing techniques, whereas fMRI combines image processing and time-series processing techniques. In contrast to fMRI, where features are the signal intensity value at each voxel, EEG features can be EEG bands spectral powers, coherence and interhemispheric asymmetry and other possible measured parameters from time-series.

EEG analysis is conducted in either time domain or frequency domain. Time-domain techniques encompass wavelet transform and connectivity metrics, whereas frequency domain encompasses Fourier transform and further work with signal spectrum. Physical stimuli induce changes in EEG signals called Event-related potentials. These potentials can be associated with mental activity and occur during stimulus perception or preparation and execution of actions. All types of EEG parameters may serve as features for machine learning to predict the brain activity in specific conditions. For example, the authors used coherence parameters of resting state to classify depressed patients and healthy participants [31]. Machine learning is currently being applied to EEG data collected from healthy and depressed patients to predict performance differences between these two groups during a decision task [32], during an emotional regulation task [33] and vigilance objectives [34].

Deep learning approaches are becoming more popular in EEG analysis. Thus, Acharya [21] uses Convolutional Neural Network as a classifier to predict depressed or healthy people. The proposed solution by Achraya [21] used a Backpropagation algorithm to train the network, adaptive moment estimation to optimize the parameters of the network structure and dropout technique to avoid overfitting. A cross-validation strategy with 10 folds was used to test the dataset. Classification with Convolutional Neural Network has helped to achieve accuracy, sensitivity, and specificity over 90% for each left and right hemisphere.

Conclusion

The studies reviewed in the present article demonstrate the progress that has been made due to the use of machine learning techniques in fMRI analysis, EEG analysis and in the brain signal processing field overall. With technological advances and increasing computational efficiency (Moore's law), the accuracy of the classification models in fMRI and EEG analysis may increase, even without changing the methodology of the machine learning application.

Machine learning has made enormous progress in the last two decades largely due to the growth of computing power and the emergence of deep learning; and its techniques have proved to be a valuable tool in gaining more insights from data in any domain that can possess a vast amount of data. Therefore, researchers in any field that deals with big data should be aware of the applicability and capability of machine learning techniques to be able to leverage them to their benefits. The new ML methods discovered or invented while solving cognitive science-related problems may be useful and worth considering in solving problems in other domains beyond medicine.

Funding

Research was supported by research grant from Ministry of Education and Science of Kazakhstan to A.M. Kustubayeva (AP08856595 "EEG/MRI study of brain development, emotional-cognitive functions, and genetic markers in different age groups").

M.G. Sharaev was supported by RFBR, research project 18-29-01032.

References

1. Deisenroth M.P., Faisal A.A., Ong C.S. (2021) Mathematics for Machine Learning. Cambridge University Press, 14-16 p.

2. Deo R.C. (2015) Machine Learning in Medicine. *Circulation*., vol. 132, no. 20, pp. 1920–1930. http://dx.doi.org/10.1161/CIRCULATIONAHA.115.001593.

3. Qayyum A., Qadir J., Bilal M., Al Fuqaha A. (2020) Secure and Robust Machine Learning for Healthcare: A Survey. *IEEE Reviews in Biomedical Engineering.,* vol. 14, pp. 156-180. https://doi.org/10.1109/rbme.2020.3013489.

4. Nielsen A.N., Gratton C., Church J.A., Dosenbach N.U.F., Black K.J., Petersen S.E., et al.. (2019) Atypical Functional Connectivity In Tourette Syndrome differs between Children and Adults. *Biological Psychiatry*., vol. 87, no. 2, pp. 164-173. http://dx.doi.org/10.1016/j.biopsych.2019.06.021

5. Rubinov M., Sporns O. (2010). Complex network measures of brain connectivity: Uses and interpretations. *NeuroImage, vol. 52, no. 3, p. 1059–1069.* doi:10.1016/j.neuroimage.2009.10.003. https://doi.org/10.1016/j.neuroimage.2009.10.003.

6. Botvinick M., Wang J.X., Dabney W., Miller K.J., Kurth-Nelson Z. (2020) Deep Reinforcement Learning and Its Neuroscientific Implications. *Neuron*,. vol. 107, no. 4, pp. 603-616. https://doi.org/10.1016/j.neuron.2020.06.014.

7. Niv Y. (2009). Reinforcement learning in the brain. *Journal of Mathematical Psychology*., vol. 53, no. 3, pp. 139–154.https://doi.org/10.1016/j.jmp.2008.12.005.

8. Haynes J-D, Rees G. (2006) Decoding mental states from brain activity in humans. *Nature Reviews Neuroscience*., vol. 7, no. 7, pp. 523–534. http://dx.doi.org/10.1038/nrn1931.

9. Hirose S, Nambu I, Naito E. (2015) An empirical solution for over-pruning with a novel ensemble-learning method for fMRI decoding. *Journal of Neuroscience Methods*., vol. 239, pp. 238–245. http://dx.doi.org/10.1016/j.jneumeth.2014.10.023.

10. Jamshy S., Perez O., Yeshurun Y., Hendler T., Intrator N. (2012) Searchlight Based Feature Extraction. In: Langs G., Rish I., Grosse-Wentrup M., Murphy B. (eds) Machine Learning and Interpretation in Neuroimaging. *Lecture Notes in Computer Science*, vol. 7263. Springer, Berlin, Heidelberg. https://doi.org/10.1007/978-3-642-34713-9_3.

11. Sharaev M., Artemov A., Kondrateva E., Sushchinskaya S., Burnaev E., Bernstein A., et al. (2018) MRI-Based Diagnostics of Depression Concomitant with Epilepsy: In Search of the Potential Biomarkers. Proceedings of IEEE international conference on data science and advanced analytics. Turin, Italy, P. 555. https://www.doi.org/10.1109/DSAA.2018.00071.

12. Hunyadi B, Tousseyn S, Dupont P, Van Huffel S, De Vos M, Van Paesschen W. (2015) A prospective fMRI-based technique for localising the epileptogenic zone in presurgical evaluation of epilepsy. *NeuroImage*., vol. 113, pp. 329–339. http://dx.doi.org/10.1016/j.neuroimage.2015.03.011.

13. Sharaev M., Artemov A., Kondrateva E., Ivanov S., et al. (2018) Learning Connectivity Patterns via Graph Kernels for fMRI-Based Depression Diagnostics. Proceedings of IEEE international conference on data mining workshops. Singapore, Sin-

gapore, P. 308. https://www.doi.org/10.1109/ICDMW.2018.00051.

14. Bleich-Cohen M., Jamshy S., Sharon H., Weizman R., Intrator N., Poyurovsky, M., et al. (2014) Machine learning fMRI classifier delineates subgroups of schizophrenia patients. *Schizophrenia Research*., vol. 160 no. 1-3, pp. 196–200. http://dx.doi.org/10.1016/j.schres.2014.10.033.

15. De Martino F, Valente G, Staeren N, Ashburner J, Goebel R, Formisano E. (2008) Combining multivariate voxel selection and support vector machines for mapping and classification of fMRI spatial patterns. *NeuroImage*., vol. 43, no. 1, pp. 44–58. http://dx.doi.org/10.1016/j.neuroimage.2008.06.037.

16. Duff K. (2012) Evidence-Based Indicators of Neuropsychological Change in the Individual Patient: Relevant Concepts and Methods. *Archives of Clinical Neuropsychology*., vol. 27, no. 3, pp. 248–261. http://dx.doi.org/10.1093/arclin/acr120.

17. Yamamoto M, Bagarinao E, Kushima I, Takahashi T, Sasabayashi D, Inada T, Suzuki M, Iidaka T, Ozaki N. (2020) Support vector machine-based classification of schizophrenia patients and healthy controls using structural magnetic resonance imaging from two independent sites. *PLoS One*., vol.15, no. 11. https://doi.org/10.1371/journal.pone.0239615.

18. Aljobouri H.K., Jaber H.A., Koçak O.M., Algin O, Çankaya I. (2018) Clustering fMRI data with a robust unsupervised learning algorithm for neuroscience data mining. *Journal of Neuroscience Methods*., vol. 299, pp. 45–54. http://dx.doi.org/10.1016/j.jneumeth.2018.02.007.

19. Svanera M, Savardi M, Benini S, Signoroni A, Raz G, Hendler T, et al. (2019) Transfer learning of deep neural network representations for fMRI decoding. *Journal of Neuroscience Methods*., vol. 328, 108319. https://doi.org/10.1016/j.jneumeth.2019.108319.

20. Kriegeskorte N. (2008) Representational similarity analysis – connecting the branches of systems neuroscience. *Frontiers in Systems Neuroscience*., vol. 2, no 4., http://dx.doi.org/10.3389/neuro.06.004.2008.

21. Li X., Dvornek N.C., Zhou Y., Zhuang J., Ventola P., Duncan J.S. (2019) Graph Neural Network for Interpreting Task-fMRI Biomarkers. Proceedings of international conference on medical image computing and computer assisted intervention. Shenzhen, China, P. 485.

22. Yan W., Calhoun V., Song M., Cui Y., et al. (2019) Discriminating schizophrenia using recurrent neural network applied on time courses of multi-site FMRI data. *EBioMedicine*. https://doi.org/10.1016/j.ebiom.2019.08.023.

23. Lueken U, Straube B, Yang Y, Hahn T, Beesdo-Baum K, Wittchen H-U, et al. (2015) Separating depressive comorbidity from panic disorder: A combined functional magnetic resonance imaging and machine learning approach. *Journal of Affective Disorders*., vol. 184, pp. 182–192. http://dx.doi.org/10.1016/j.jad.2015.05.052.

24. Clark I.A., Niehaus K.E., Duff E.P., Di Simplicio M.C., Clifford G.D., Smith S.M., et al. (2014) First steps in using machine learning on fMRI data to predict intrusive memories of traumatic film footage. *Behaviour Research and Therapy*., vol. 62, pp. 37–46. http://dx.doi.org/10.1016/j.brat.2014.07.010.

25. Acharya U.R., Oh S.L., Hagiwara Y., Tan J.H., Adeli H., Subha D.P. (2018) Automated EEG-based screening of depression using deep convolutional neural network. *Computer Methods and Programs in Biomedicine.,* vol. 161, pp. 103–113. http://dx.doi.org/10.1016/j.cmpb.2018.04.012.

26. Gollan J.K., Hoxha D., Chihade D., Pflieger M.E., Rosebrock, L., Cacioppo, J. (2014). Frontal alpha EEG asymmetry before and after behavioral activation treatment for depression. *Biological Psychology*., vol. 99, pp. 198–208. https://doi.org/10.1016/j.chiabu.2020.104358.

27. Bachmann M, Päeske L, Kalev K, Aarma K, Lehtmets A, Ööpik P, et al. (2018) Methods for classifying depression in single channel EEG using linear and nonlinear signal analysis. *Computer Methods and Programs in Biomedicine*., vol. 155, pp. 11–17. http://dx.doi.org/10.1016/j.cmpb.2017.11.023.

28. Liley D.T.J., Frascoli F. (2010) Approaches to Modelling the Dynamical Activity of Brain Function Based on the Electroencephalogram. In: Dewar R.L., Detering F. (eds) *Complex Physical, Biophysical and Econophysical Systems*. World Scientific Lecture Notes in Complex Systems, vol. 9. World Scientific Publishing Co., Singapore, Singapore. https://doi.org/10.1142/9789814277327_000.

29. Teplan M. (2002) Fundamentals of EEG measurement. *Measurement Science Review*., vol. 2, no. 2, pp. 1-11

30. Michel C.M., Brunet D. (2019) EEG Source Imaging: A Practical Review of the Analysis Steps. *Frontiers in Neurology*., vol 10. https://doi.org/10.3389/fneur.2019.00325

31. Ledovsky A., Mnatsakanian E., Sharaev M., Burnaev E. (2019) O-21 Separation of major depression patients from healthy controls using machine learning approach to resting-state EEG. *Clinical*

Neurophysiology., vol. 130, no. 7, p. e28. https://doi.org/10.1016/j.clinph.2019.04.337.

30. Kustubayeva A., Kamzanova A., Kudaibergenova S., Pivkina V., Matthews G. (2020) Major depression and brain asymmetry in a decision-making task with negative and positive feedback. *Symmetry*., vol. 12, no. 12, pp. 1–25. https://doi.org/10.3390/sym12122118.

33. Kustubayeva A., Tolegenova A., Matthews G. (2013) EEG-brain activity in different strategies of emotions' self-regulation: Suppression and reappraisal. *Psikhologicheskii Zhurnal.,*, 34(4), pp. 58–68. https://doi.org/10.3390/brainsci9090225.

34. Kamzanova A., Kustubayeva A., Matthews G. (2012) Diagnostic monitoring of vigilance decrement using EEG workload indices. Proceedings of the Human Factors and Ergonomics Society Annual Meeting. Boston, Massachusetts, USA. P. 203. https://doi.org/10.1177/1071181312561019.

IRSTI 34.31.17 https://doi.org/10.26577/ijbch.2021.v14.i2.02

M. Mutalkhanov, K. Sissemali*, A. Alnurova, A. Akilbekova,
M. Tauasarova, Z. Bassygarayev, K. Boguspaev
Al-Farabi Kazakh National University, Almaty, Kazakhstan
*e-mail: kuanishsissemali@gmail.com

Determination of the correlation between the accumulation of pigments and natural rubber in Tau-saghyz

Abstract. Natural rubber is a valuable polymer used in a wide variety of industries, from tire manufacturing to medical products and applications in the food industry. The tau-sagyz rubber plant (*Scozonera tau-saghyz* Lipcsh et Bosse) is one of the few plants in the world that can be used in the production of natural rubber when cultivated in culture. To increase the productivity of plants, it is necessary to establish factors affecting the biosynthesis of natural rubber. In our studies, the level of pigments (chlorophyll–a, b, carotenoids) was chosen as a factor that may have a positive effect on the accumulation of rubber in the roots of *S. tau-saghyz*. For this purpose, samples (leaves, roots) were taken from 3 groups of plants (north, south, east) in the Karatau mountains of the Kurman-Tas range. The extraction of pigments from leaf samples was carried out with acetone, and the extraction of rubber from the roots was carried out with hexane. The obtained data on the content of pigments and rubber in the samples were statistically processed using the t-test and Pearson correlation analysis. As a result, a statistical difference in the values of pigment accumulation in leaves and rubber in roots between the 3 studied groups of plants is shown. On the other hand, a very low level of correlation was found between the accumulation of pigments in the leaves and rubber in the roots in all three groups. The obtained results reliably showed that the level of pigment accumulation in the leaves does not affect the accumulation of rubber in the roots of Tau-sagyz.
Key words: Tau-saghyz, pigment accumulation, natural rubber, correlation.

Introduction

The importance of development of alternative crops for the natural rubber production. Natural rubber (NR) is a high molecular weight polymer found in more than 2,500 plant species [1;2]. Unfortunately, only few of these species can produce NR with desirable characteristics. NR is used as the raw material for the multiple types of products, such as medical devices, surgical gloves, aircraft, car tires, engineering components, pacifiers, clothes, toys and other [3]. NR possesses several properties that makes it so attractive for industrial use, including high tensile, tear, fatigue strength, ability to stick to itself and to other materials, moderate resistance to environmental damage by heat, light and ozone water, bacterial and viral barrier properties [4].

Currently the majority of NR is collected from tropical tree, member of family Euphorbiaceae *Hevea brasiliensis* (Muell Arg). The tree is native to rainforests of Amazon region in South America. This includes forests of Brazil, Venezuela, Ecuador, Colombia, Peru, and Bolivia [5]. However, due to the increase of demand for NR, *Hevea* were introduced to other countries. Currently the main producers of NR are Asian countries, in particular: Thailand with 35 % of worldwide NR supply and Indonesia with 30 % of worldwide NR supply [6]. However, the fact that NR is extracted exclusively from *Hevea* is a big disadvantage and possesses a big threat for entire rubber industry. An example of such threats is pathogens that can either significantly decrease quantity and quality of extracted rubber, as well as wipe an entire plantation of *Hevea* [7]. This became possible because of lack of genetic variability that could slow the infection's progression. Strategic pathogens include *Microcyclus ulei* (South American leaf blight (SALB), *Phytopthora* spp. (abnormal leaf fall), *Oidium Heveae* (powdery mildew), *Cornyespora cassiicola* (Corneyspora leaf fall), *Corticium salmonicolor* (pink disease), *Rigidoporus* spp. (white root disease) [8]. Another disadvantage of *Hevea* exclusive rubber production is its cultivation restrictions. *Hevea* has very strict environmental growing requirements. This prevents its cultivation on landscapes located outside of certain tropical region, while simultane-

ously makes it extremely susceptible to climate changes [1]. This characteristic also makes its cultivation a significant part of deforestation problem, since to establish the plantation a corporation or individual farmer must clear the land from forest to plant rubber trees [9]. The cost of *Hevea* originated NR is another disadvantage. Since latex harvesting is done manually by tapping the bark of rubber tree it is very labour-intensive process [10]. Combine it with fast increase of tapper's age due to unwillingness of younger generation to become tappers since it considered a low-class traditional job and not classified as a profession [11]. Combined with annually increasing demand for NR, increasing shortage of skilled tappers it leads to an increase of *Hevea* harvested rubber cost [1]. However, *Hevea* alone cannot satisfy the demand for NR. According to "Statista" website the worldwide demand for NR keeps growing annually as industries keep growing and developing. For example, in 2010 in the world has consumed around 10.7 million tons of NR (cis-1,4-polyisoprene), while in 2019 this number reached up to 13.7 million tons of NR [12]. This means that the shortage of rubber in 2019 were equal to around 100 thousand tones. This situation has sparked an interest of in alternative rubber producing crops. Currently guayule (*Parthenium argentatum*) and Russian dandelion (*Taraxacum kok-saghyz*) are the most well-known and promising ones [13].

Scorzonera tau-saghyz a potential rubber crop. Tau-saghyz inhabits stony-rubble slopes of Karatau mountain plateaus at 500-2000 meters above sea level [14;15]. Tau-saghyz is a member of Asteraceae family, perennial, dicotyledon plant with diploid set of chromosomes (n=14) [16]. Tau-saghyz was initially discovered during Soviet Union times during exploration of mountains of South Kazakhstan. This discovery pushed the All-Union Research Institute of Rubber and Gutta-Percha to establish research centers in villages Burnyi and Atabayevo as well as a research station in the central part of the Karatau ridge [14]. Tau-saghyz could become a strategic crop for Kazakhstan because its ability to synthesize and store NR. *Scorzonera tau-saghyz* is one of the plant species capable of synthesizing NR in quantities sufficient to be considered a rubber crop. In *Scorzonera tau-saghyz* NR is synthesized and stored mainly inside the underground stem (caudex) and root. Previously obtained data on rubber content of tau-saghyz showed that it could accumulate up to 40 % of dry mass of the roots consists of rubber. Plant stores rubber in its roots and underground stem. If the root is damaged latex appears on the surface of the wood in form of milky-white or yellowish-green coloured substance which quickly coagulates on air (Figure 1).

Figure 1 – Latex appearing on the surface of cut root. Photo by Mutalkhanov M., 2019

Unfortunately, the population of tau-saghyz has been reduced drastically during the years of World War II (1941-1945). During this period for the needs of military industry, more than 12 million roots were harvested, dry weight of which were equal to approximately 908 metric tons is to [17]. These events had significant impact on population of tau-saghyz, which was significantly damaged by the end of these years. As result in 1978 *Scorzonera tau-saghyz* was included into The Red Book of the USSR and further into the Red Book of the KazSSR and Red Book of the Republic of Kazakhstan [14]. There are several variations of tau-saghyz. The most notable ones were identified at following locations: Kaynar-Bastau (eastern part of Karatau mountain), Jelagan-Ata (central part Karatau mountain) and Leontyevka (eastern part of Karatau mountain) [18].

Currently the population of *Scorzonera tau-saghyz* has started to recover. However, there are number of factors limiting its recovery in natural conditions. These factors include its weak competitiveness, low seed germination rate and intensive conversion of the territory into pastures and plantations. Combination of these factors significantly slows down recovery of population both inside and outside of natural reserve [14]. One of the ways to solve this problem is application of microclonal propagation from apical meristem. As well as cultivation at controlled conditions within a laboratory and on a field. As result of such projects population of *Scorzonera tau-saghyz* started to recover. Currently tau-saghyz is included into the decree of the Government of the Republic of Kazakhstan of October 31, 2006 "On approval of the Lists of rare and endangered species of animals and plants" and is protected by law [19]. The

plant can be found on the territory of Karatau state natural reserve.

Morphology of Tau-saghyz. Scorzonera tau-saghyz is a woody semi shrub plant. The height of its aerial part could reach up to 25-40 cm. The aerial part of the plant takes form of a rosette, shaped as squat hemispherical cushions. Compactization of these cushions could either be sparse or mildly dense. On Figure 2 a typical look of *S. tau-saghyz* cushion is presented.

Figure 2 – Aerial part of *Scorzonera tau*-saghyz. Photo by Mutalkhanov M., 2019

These cushions are made of multiple short, densely branched, thick, woody, perennial branches. These branches typically grow from area close to the root collar. In general, these rosettes reach up to 30 cm. in diameter. However, the environmental conditions in which plant was growing could significantly alter the diameter, sometimes it could reach up to 100 cm [20].

The stem is covered by multiple dry leaves. The colour of these leaves varies from gray-brown to dark green with weak gloss, the texture of covering leaves is rough. Almost all of the leaves are sedated into deltoid base. Typically, the rosette contains between 6 and 24 leaves. Typically, the colour of leaves is greyish green, ends of the leaves have sharp edge of reddish-brown colour. The surface of the leaf may be either smooth or mildly pubescent. The lower part of the leaf has a distinct furrow on it. The central bigger one forms a distinct keel; the lateral ones are smaller and located along the central. The furrows are white coloured with distinct gloss. Leaves are expanded into an axil shaped like a delta. On the exterior the axil is smooth, cream coloured and glossy. An interior of the axil is densely covered by silky, slightly curly, light-brown, shiny hairs, up to 3-4 mm long [20]. The rosette's base is approximately 1 cm wide. There are several rows of scales covering this base. The external scales are 9 mm long and wide, round shaped but with distinct point at the top, internal ones are up to 3 cm long, lanceolate and elongated. The scales are semi-transparent, with dark brown coloration. The central vein of these leaves is more prominent, and the multiple (up to 10) lateral veins are less noticeable. They're bare outside, and slightly pubescent inside at the foundation, with a tiny amount of hair [20]. The underground part of the plant (caudex) compared to the short but highly branched aerial part is significantly longer, with scree habitats resulting in highest length of underground stem. The bark of the underground part is bare, with rough texture, and has a dark brown colour. Each branch of caudex ends with a rosette of leaves or sometimes it can end with a flowering shoot [14; 20]. Caudex has several purposes, for example: nutrients and water storage, nutrients transmission, as well as participation in vegetative reproduction of the plant, which remains the main mean of reproduction. Inside the caudex *S. tau-saghyz* have a multinucleated tube-like cell called laticifers. In these laticifers occurs the reaction of polymerization, which leads to the synthesis of cis-1,4-polyisoprene or NR.

Rubber biosynthesis. NR is a cis-1,4-polyisoprene polymer that consists of Isopentenyl pyrophosphate (IPP) monomers. IPP is an isoprenoid precursor which acts as an intermediate in the mevalonate (MVA) and in the non-mevalonate (MEP) pathway of isoprenoid precursor biosynthesis. IPP for rubber biosynthesis could either be derived through the MVA pathway occurring in cytosol or through MEP pathway occurring in plastids [8]. Studies performed on *Hevea* revealed that latex carbon used during rubber biosynthesis does not come directly from photosynthetic apparatus, but from stored carbohydrates like starch [21].

Indication of phonotypical traits could be associated (directly or indirectly) with increased accumulation of rubber is the main goal during the development of commercially viable rubber crop. It's suggested that increased quantities of pigments could have a beneficial effect, due to the increased supply of carbon which further will be used during rubber biosynthesis.

Materials and methods

Plant materials. Samples of the leaves, caudices and roots of *Scorzonera tau-saghyz* were collected by digging from wild fields at Karatau mountains in the Turkestan district. In particular, on the Kurmantas ridge (Figure 3-a) and Kanyon-Teris Akkan (Figure 3-b) in the national park. Samples were collected from May to June 2019.

The samples were collected from the plants growing on two ridges of mountains: south, north and west. The number of samples taken constituted 34 from south and west ridges and 32 from north ridge. Obtained samples were transported to Laboratory of ecological biotechnology at Al-Farabi Kazakh National University (KazNU). To preserve harvested samples during the transportation collected leaves, caudices and roots were stored in liquid nitrogen. After the samples got delivered, they were stored at -80□ until use.

*Pigment extraction and quantification***.** Determination of pigment quantity were performed using Arnon (1945) method [22]. 1 g of defrosted leaves were taken and grounded in 5 ml of 90 % acetone using pestle and mortar. Obtained extract were transferred to centrifuged at 5000 rpm for 5 min. After centrifugation complete the supernatant were transferred into clean tubes, while avoiding disrupting the pellet. The examination of the supernatant was performed on spectrophotometer. Light absorption read at wavelength of 663, 645, and 441 nm. Quantity of pigment was calculated using Holm-Wettstein formulas (1.1-1.4):

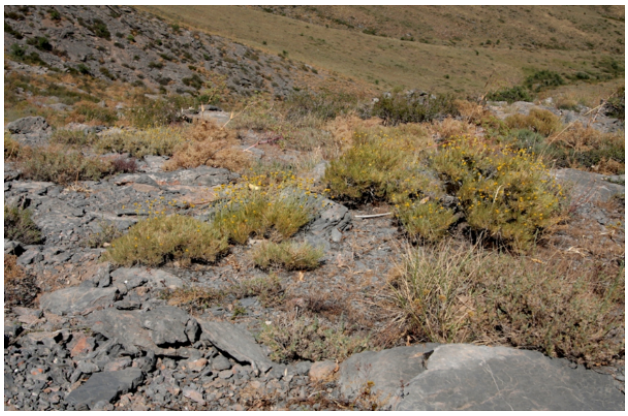

a

b

Figure 3 – Karatau mountains area where samples taken. Photo by Mutalkhanov M., 2019.
Note: a – Kurmantas ridge; b – Caniyon-Teris Akkan

$$C_{Ch_A}\ (\mu g/ml) = 9.784\ (A_{662}) - 0.990\ (A_{644}) \quad (1.1)$$

$$C_{Ch_b}\ (\mu g/ml) = 21.426\ (A_{662}) - 4.650\ (A_{644}) \quad (1.2)$$

$$C_{Ch_{a+b}}\ (\mu g/ml) = 5.134\ (A_{662}) - 20.436\ (A_{644}) \quad (1.3)$$

$$C_{Carotenoid} = 4{,}695\ (A_{441}) - 0.268\ (C_{Ch_{a+b}}) \quad (1.4)$$

where:

A662- light absorption at wavelength of 662nm

A644-light absorption at wavelength of 644nm

A441 – light absorption at wavelength of 441nm

Rubber extraction and purification. Root samples washed with running water to clean them of the soil. After washing, the roots were air dried in the shade. These roots transferred to KazNU where they have been stored at -80□ for 3 months. The root samples were grinded into powder by mill. Approximately 4g of powder is then transferred to Erlenmeyer flask with 50ml hexane. The remaining hexane were removed by

IKA RV05 basic rotary evaporator (IKAWerkeGmbH & Co. KG, Germany) with IKA HP4 basic water bath (IKAWerkeGmbH & Co. KG, Germany) have been used. After that the remainings were dried in a VD115 vacuum dryer (BINDERGmbH, Germany) at 24 °C for 22–24 h. All procedures performed at 23-25 °C.

Statistical analysis. The difference in pigment and rubber content between the groups examined using two-tailed t-test. Correlation analysis between pigment and rubber content performed using Pearson correlation. The calculations were performed using Microsoft Excel Add-on XLStat (ver. 2020.4) by Addinsoft.

Results and discussion

Differences in pigments and rubber content. Determination of pigment content in leaves of Tau-saghyz revealed that the content of pigments in leaves strongly depends on location of slope. So, the mean pigment content in leaves from East samples were highest, followed by South and North samples respectively (Table 1). The same pattern observed during determination of carotenoid content. T-test have shown that groups from different slopes .

Table 1 – The results of the t-test analysis of pigments and rubber content between groups

Substance	Groups	$t_{Observed}$	$t_{Critical}$	DF	alpha
Chlorophyll-A	East-North	3.809	1.998	65	0.05
	South-North	2.420	1.998	65	0.05
	South-East	1.376	1.998	66	0.05
Chlorophyll-B	East-North	3.902	1.998	65	0.05
	South-North	1.431	1.998	65	0.05
	South-East	1.696	1.997	66	0.05
Chlorophyll total	East-North	3.951	1.998	65	0.05
	South-North	2.200	1.998	65	0.05
	South-East	1.412	1.997	66	0.05
Carotenoid	East-North	3.755	1.998	65	0.05
	South-North	2.296	1.999	65	0.05
	South-East	1.260	1.997	66	0.05
Rubber	East-North	0.280	1.998	65	0.05
	South-North	0.125	1.998	65	0.05
	South-East	0.195	1.997	66	0.05

The t-test showed that $t_{Observed} > t_{Critical}$ (3.809>1.998 with DF = 65, alpha = 0.05), which shows a statistically significant difference between East and North with 95 % probability. A similar analysis of the following groups established a significant difference between South and North (2.420>1.998; DF = 65, alpha = 0.05). At the same time, South and East (1.376<1.998; DF = 66, alpha = 0.05) showed no difference between each other. Content of chlorophyll-B differed between East and North (3.902>1.998; DF = 65, alpha = 0.05). However, no difference indicated between South-North (1.431<1.998; DF = 65, alpha = 0.05) and South-East (1.696<1.998; DF = 66, alpha = 0.05). Total chlorophyll content differed between the East-North (3.951>1.998; DF = 65, alpha = 0.05) and South-North (2.200>1.998; DF = 65, alpha = 0.05) slopes. At the same time, South-East (1.412<1.998; DF = 66, alpha = 0.05) showed no difference between each other. Carotenoid content were different between the East-North (3.755>1.998; DF = 65, alpha = 0.05) and South-North (2.296>1.998; DF = 65, alpha = 0.05) slopes. At the same time, South-East (1.260<1.998; DF = 66, alpha = 0.05) showed no difference between each other. Rubber accumulation shown no statistically difference between the groups East-North (0.280>1.998; DF = 65, alpha = 0.05), South-North (0.125>1.998; DF = 65, alpha = 0.05) and South-East (0.195<1.998; DF = 66, alpha = 0.05). Results show that plants from South and East have significantly higher quantities of pigments compared to North. On the other hand content of rubber showed no difference between the groups.

Correlation analysis of the rubber content and the pigments content. To determine the degree of association between the accumulation of photosynthetic pigments in the leaves and the accumulation of rubber in the roots, the linear correlation coefficient r-Pearson used (Table 2).

Table 2 – The results of the correlation analysis between the pigments content in leaves and the content of rubber in roots in samples from Karatau mountains slopes

	Rubber		
Slopes	North	East	South
Ch-a	0.169	-0.090	-0.263
Ch-b	0.094	-0.088	-0.286
Ch-a+b	0.150	-0.088	-0.293
Car	0.225	-0.098	-0.099

Data from the correlation analysis between the rubber content in roots and the pigment content in leaves of *Scorzonera tau-saghyz* shows that rubber content in roots has very weak correlation with all four pigment variants. Among the groups only north, which showed lowest mean quantity of pigments, displayed positive correlation. On the other hand south and east, which showed the higher mean quantity of pigments, displayed negative correlations. However, due to the weak association between pigments and rubber quantities, it is suggested that pigment quantity not associated with rubber accumulation in roots.

Obtained data aligns with data obtained by Thaler P. et al. (2016) [23], who tracked the movement of carbon isotope ^{13}C throughout the body of *Hevea*, which allowed them to track the distribution of carbon in organism of plant. According to their findings carbon for rubber biosynthesis do not come directly from photosynthetic apparatus. Instead it "accumulated in mixed pool of carbohydrates within the plant". Possible reason for the lack of correlation may be the fact that there is a direct competition for organic compounds between the processes of biomass accumulation and rubber accumulation. Taking into account the fact that rubber is a secondary metabolite, its possible that the accumulation of biomass will be of paramount importance for the organism. Moreover, since the samples of leaves and roots collected during the flowering phase of tau-saghyz, the costly process of rubber formation were suppressed.

Conclusion

NR is biopolymer used in wide variety of industries. *S. tau-saghyz* is a plant that can be used as an alternative rubber crop, which in term could have a beneficial effect on economy and industry of the country. During experiment samples of leaves and roots collected from 3 groups of wild plants(South, East, North) undergo the pigment and rubber extraction processes. Results of t-test indicated clear difference in pigment content between North and South, East, while non have been indicated between South and East. In case of rubber accumulation. t-test showed lack of statistically significant difference between all three groups.

Pearson correlation analysis showed that all of the pigment variants have very weak correlation with rubber accumulation. Because of that it were considered negligible. Possible reason for it being direct competition for organic compounds between the processes of biomass accumulation and rubber accumulation. Its possible that collection of rubber while plant is in dormant state could increase rubber yield due to the absence of the competition.

Acquired data shows that pigment content cannot be used as a mean to identify plants with high rubber productivity. Researches on other mechanisms are required in order to identify phenotypical traits associated with increased rubber content.

Funding

The work was financially supported by MES RK within the Project No. AP08053131 Efficient editing of the *Scorzonera Tau-Saghyz* genome using CRISPR/Cas9 technology to obtain genetically improved plants with an increased content of natural rubber (for 2020-2022 yy).

References

1 van Beilen J., Poirier Y. (2007) Establishment of new crops for the production of natural rubber. Trends Biotechnol., vol. 25, no. 11, pp. 522-529. https://doi: 10.1016/j.tibtech.2007.08.009.

2 Rasutis D, Soratana K, McMahan C.M., Landis A.E. (2015) A sustainability review of domestic rubber from the guayule plant. Ind Crops Prod., vol. 70. pp. 383–394. doi:10.1016/j.indcrop.2015.03.042

3 Beliczky L. S., Fajen J. (2012) Encyclopaedia of Occupational Health and Safety 4th Edition. Chapter 80 – Rubber Industry. https://www.iloen-

cyclopaedia.org/contents/part-xii-57503/rubber-industry.

4 Industrial Rubber Goods: The Buyer's Guide. (from July 1, 2020, corrected at July 3, 2019, accessed at July 6, 2021). http://www.industrialrubbergoods.com/natural-rubber.html.

5 Rainforest-Alliance. (from June 24, 2021, corrected at June 29, 2021, accessed at July 3, 2021). https://www.rainforest-alliance.org.

6 Bottier C. (2020) Biochemical composition of *Hevea* brasiliensis latex: A focus on the protein, lipid, carbohydrate and mineral contents. ADV BOT RES., vol. 93, pp. 201–237. https://doi.org/10.1016/bs.abr.2019.11.003.

7 Buranov A. U., Elmuradov B. J. (2010) Extraction and Characterization of Latex and Natural Rubber from Rubber-Bearing Plants. J. Agric. Food Chem., vol. 58, no. 2, pp. 734–743

8 Cao X., Yan J., Lei, J., Li, J., Zhu, J., Zhang, H. (2017) De novo Transcriptome Sequencing of Me-JA-Induced *Taraxacum kok-saghyz* Rodin to Identify Genes Related to Rubber Formation. Sci. Rep., vol. 7. https://doi.org/10.1038/s41598-017-14890-z.

9 Warren-Thomas E.M., Edwards D.P., Bebber D.P. et al. (2018) Protecting tropical forests from the rapid expansion of rubber using carbon payments. Nat. Commun., vol.9, pp. 911. https://doi.org/10.1038/s41467-018-03287-9.

10 Mooibroek H., Cornish K. (2000) Alternative sources of Natural Rubber. Appl. Microbiol. Biotechnol., vol. 53, pp. 355-365. https://doi.org/10.1007/s002530051627.

11 Hazir M., Kadir R., Gloor E., Galbraith D. (2017) Effect of agroclimatic variability on land suitability for cultivating rubber (*Hevea brasiliensis*) and growth performance assessment in the tropical rainforest climate of Peninsular Malaysia. Clim. Risk Manag., vol. 27, pp. 100-203. https://doi.org/10.1016/j.crm.2019.100203.

12 Statista. (from June 29, 2021, corrected at July 2, 2021, accessed at July 4, 2021). https://www.statista.com/topics/3268/rubber/#dossierKeyfigures.

13 Cornish K. (2011) Similarities and differences in rubber biochemistry among plant species. Phytochemistry., vol. 57. – pp. 1123-1134. https://doi.org/10.1016/s0031-9422(01)00097-8.

14 Boguspaev K.K., Adil'baev Zh.A., Faleev D.G., Zhanataev Sh.A., Turasheva S.K., Sambetov K.K. (2013) Perspektivy razrabotki tehnologij vosstanovlenija populjacii rastenij tau-sagyza (*Scorzonera tau-saghyz* (Lipsch. et Bosse) v Karatauskom gosudarstvennom prirodnom zapovednike [Prospects for the development of technologies for restoring the plant population of tau-sagyz (*Scorzonera tau-saghyz* (Lipsch. et Bosse) in the Karatau State Nature Reserve]. Vestnik KazNU. Serija jekologicheskaja. vol. 2, pp. 38. https://pandia.ru/text/80/317/71142.php.

15 Plants For A Future Database (from June 16, 2021, with corrections at June 20, 2021, accessed at June 26, 2021). https://pfaf.org

16 Bordbar F., Makki P., Alifarsangi F. (2019) Karyotype Investigations in Iranian *Scorzonera tortuosissima* and *S. intricata*, Asteraceae. Cytologia, vol. 84, no. 1, pp. 69–72. https://doi.org/10.1508/cytologia.84.69.

17 Arias M., Hernandez M., Remondegui N., Huvenaars K., van Dijk P., Ritter E. (2016) First genetic linkage map of *Taraxacum koksaghyz* Rodin based on AFLP, SSR, COS and EST-SSR markers. Sci. Rep. vol.6. https://doi.org/10.1038/srep31031.

18 Bondarenko P. V., Tarakanov S.G. (1941) Tau-sagyz. Priemy vyrashhivanija v Srednej Azii [Tau-sagyz. Cultivation techniques in Central Asia]. Tashkent: AN SSSR, Uzbekskij filial. Izdatel'stvo UzFAN.

19 Collection of acts of the President of the Republic of Kazakhstan and the Government of Republic of Kazakhstan. (2006) "On approval of the list of environmental protection objects of special ecological, scientific and cultural significance" . vol. 40, pp.444.

20 Kul'tijasov M.V. (1938) Tau-Sagyz i vvedenie ego v kul'turu [Tau-Sagyz and its introduction into culture]. Moskva: Izdatel'stvo Akademii nauk SSSR. pp. 45-51

21 Men, X., Wang, F., Chen, G. Q., Zhang, H. B., & Xian, M. (2018). Biosynthesis of Natural Rubber: Current State and Perspectives. Int. J. Mol. Sci., vol. 20, no. 1, pp. 50. https://doi.org/10.3390/ijms20010050.

22 Yavorska N., Vorobets N. (2019) Photosynthetic Pigments in Shoots of *Vaccinium corymbosum* L. (Cv. Elliott). Agrobiodivers. improv. nutr., health life qual., vol. 3. pp. 93-100. https://doi.org/10.15414/agrobiodiversity.2019.2585-8246.093-100.

23 Thaler P., Duangngam O., Kasemsap P., Sathornkich J., Chayawat C., Satakhum D., Priault P., Desalme D., Chantuma P.,Ghashghaie J., Epron D. (2016) The source of latex. Tracing carbon from leaf photosynthesis to latex metabolism in rubber trees using carbon sTable isotopes. CRRI and IRRDB International Rubber Conference. Cambodia, P. 260-268.

IRSTI 34.29.01 https://doi.org/10.26577/ijbch.2021.v14.i2.03

A.S. Abdygalieva* , Zh.O. Ospanbaev

Kazakh research Institute of agriculture and crop production, Almaty region, Kazakhstan
*e-mail: abdygalieva.03@gmail.com

Assessment of the current state of populations and study of phytochemical features of *Conium maculatum* L. in the Ili-Alatau mountains

Abstract. A comprehensive study of the anatomical structure of the plant *Conuim maculatum* L. from the genus Ariaceae Lindl., which has valuable medicinal properties is presented. Currently, the medicinal plant *Conuim maculatum* L. is widely used in folk medicine. This plant is used by specialists for the prevention of various diseases, especially for the treatment of various types of cancer, as well as for the preparation of active painkillers and anti-inflammatory drugs. The article analyzes the current state of the plant *Conuim maculatum* L. in the Ili-Alatau, diagnostic signs were identified and the main features of its anatomical structure were analyzed. The article analyzes in detail the biological features of the medicinal plant *Conuim maculatum* L., the main promising distribution zones of the plant in the country, and also describes the systematic classification, phytochemical features and chemical structure of this species. Eco-phytocenotic features of *Conuim maculatum* L. are shown on a population growing at the foothills of the Ili-Alatau. The work on determining the chemical composition of the species *Conuim maculatum* L. was carried out at the research center of medicinal plants of the al-Farabi Kazakh National University.

Key words: *Conuim maculatum* L., botany, population, phytochemistry, anatomy, morphology.

Introduction

Currently, one of the pressing problems facing domestic scientists is the production of medicinal preparations necessary for medicine from plants with medicinal properties, increasing their effectiveness. Undoubtedly, the medicine made at the expense of medicinal plants has a number of advantages over synthetic ones [1,2]. This is due to the fact that phytopreparations obtained on the basis of medicinal plants are highly effective in the treatment of neglected diseases in the human body and cause minimal damage to the environment. Therefore, it is necessary to turn plants with medicinal properties into the main source of raw materials for the pharmaceutical industry, by integrating scientific work with practical work aimed at the systematic study of medicinal plants and the use of medicinal plants as raw materials for the production of medicines [3]. Inflammation as a pathological process is the most common form of the disease among people, the exacerbation of such diseases, the long-term persistence of symptoms of this disease in the human body leads to a decrease in the ability to work of a person, so the development of drugs to stabilize this problem is one of the most pressing issues today [4-6]. The flora of modern Kazakhstan includes about 6,000 plant species. Among them, more than 1,500 species of plants with healing properties have been registered. However, only more than 60 medicinal plants are officially included in the State Pharmacopoeia of the Republic of Kazakhstan, but despite this, such medicinal plants as *Conuim (C.) maculatum* L. require a full-scale systematic study [7]. This plant, which has a small source base, is used only in folk medicine for the treatment of inflammatory diseases, asthma, seizures and other diseases [8].

C. maculatum L. contains biologically active constituents of various chemical structures. Therapeutic effect of this plant on the human body is very large, as it is a part of the phenolic combined type, and a valuable medicinal plant in the fight against diseases and bacteria.

Recently, the range of application of *C. maculatum* L. significantly expanded, and now they are used not only in the treatment of rheumatological diseases, but also for the prevention of thrombosis in immunocompetent diseases and the prevention of the initial stage of atherosclerosis. They can be used in small operations, in the treatment of cardiovascular diseases, in oligomenorrhea, in Alzheimer's disease, in dementia and oncology. In particular, it is widely used for the prevention of colon cancer [9-11]. For

the localization of various malignant neoplasms, anti-inflammatory drugs act individually, the number of phytopreparations that act simultaneously in several aspects is limited in traditional and official medicine. Numerous data shows that it has a pronounced effect on many models of the disease, more effectively than other synthetic drugs. For example, with the help of histamine, serotonin, dextran, formalin, egg white, acetylsalicylic acid or phenylbutazone, you can quickly, but not for long, relieve edema, and in the fight against slow-developing and prolonged inflammation (kaolin, carrageenin) [11,12].

The plant itself contains up to 1-2% of the alkaloid, the alkaloid content in the leaves – 0.1 %, in the flower – 0.24 %, a large amount of the alkaloid is contained in the seeds – 1.6% and essential oil and caffeic acid – 0.08% [13-15].

The purpose of the current research is a systematic study of the biological, anatomical features of this rich in alkaloids medicinal plant and the study of the areas of its distribution.

Materials and methods

Object of research. Four species of the hemlock family Conium L. (Apiaceae Lindl.) are widely distributed in Europe, Siberia and Asia Minor, including Kazakhstan [16-18]. *Conium Maculatum* L. a two-year-old plant, reaching 2 m in height, blooms in May-June and bears fruit in June-July. Such a plant grows like a weed and they can often be found at the foot of roads, in the garden, on the slopes of mountains, in meadows in all regions of the republic, except for the desert [19,20].

All parts of the plant are poisonous and have an unpleasant smell due to the presence of an alkaloid in them. The fruits of the plant contain up to 2% alkaloid, coniin, coumarin, flavonoids, monoterpenoid and hydrocarbons, etc. [21,22]. The population materials were collected in the Almaty region, Karasai district, the foothills of the Zailiysky Alatau, and Raiymbek rural district. Coordinates above sea level: H = 860 m, N = 4311’201”, E=07642’202”.

Methods of research. The objects of the study were the vegetative organs (root, stem, leaf) *C. maculatum* L. (Apiaceae Lindl.). Samples of plant raw materials-spotted hemlock were collected in August 2020, during the flowering period, in the foothills of the Trans-Ili Alatau, Almaty region.

An anatomical study was performed on the fixed material. Cross-sections of roots, stems and leaves were prepared manually and with the help of a microtome on the TOS-2 freezing device [24-26]. The object was covered with a cover glass, viewed from both sides under a microscope, first at a small (x 100), then at a large (x400) magnification using an Olympus BX41 microscope. Photography was carried out using the LOMO DCM 800 camera using the technique of microscopic examination of medicinal plant raw materials at the laboratory of Plant Anatomy and Morphology, Al-Farabi Kazakh National University [27].

In the manufacture and description of the preparations, the methods generally accepted in plant anatomy were used. In the process of research methods were used freezing M. Prosimy and R. Barykina. Geometric calculations are obtained by the method of R. Barykina [28,29].

When analyzing the data obtained, statistical processing was used, using the Microsoft Office software package.

Results and discussion

The leaves of *C. maculatum* L. are arranged alternately, the lower leaves are three times pinnate (resemble a parsley leaf) and reach a length of 30-60 cm [30]. The flowers are small, white, with the inner side collected in bundles of about 12-20 flowers. The seed is ovate, light brown dioecious, slightly compressed from the side. The stem is 60-180 cm high, branched, curved, hollow, with some places bluish, the lower part is covered with reddish-brown spots, because of these spots and is called «spotted» (Figure 1). In the first years of the growing season, the roots begin to develop well, from the second year the stem develops [31].

On the surface of the root of *C. maculatum* L. there is a 1-2-row layer of exoderm. The cells of the exoderm have an elongated rectangular shape, are tightly connected and strongly elongated in the radial direction. The parenchyma of the primary cortex is represented by several layers (4-6) of round-elongated cells with slightly thickened walls without intercellular cells. In the cells of the primary cortex, there are multiple inclusions that give the section a certain granularity of this topographic zone. The phloem is located in small areas between the central vessels of the xylem. The cambium is represented by a single-row layer of rather small cells. The xylem is represented by numerous broad-colored vessels converging to the center, as well as fibers and small cells of the parenchyma (Figure 2). The morphometric parameters of the roots are presented in Table 1.

a b

Figure 1 – The general appearance of cultivated specimens. Note: a-the upper part of the inflorescence during flowering; b-the upper part of the inflorescence in the phase of the beginning of fruiting

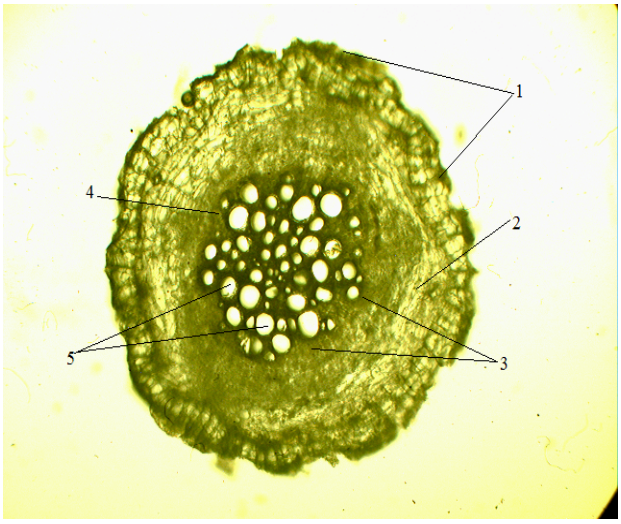

Figure 2 – Anatomical structure of the root of *C. maculatum* L. (x100)
1-exoderm, 2-primary cortex, 3-phloem, 4-cambium, 5 – xylem vessels

Table 1 – Morphometric parameters of the roots of *C. maculatum* L.

Exoderm layer thickness, μm	Primary crust thickness, μm	Central cylinder diameter, μm	Area of xylem vessels, $x10^{-3}mm^2$
0,55±0,150	17, 84±2,215		0,29±0,170
0,63±0,290	17, 90±2,110		0,20±0,110
0,30±0,180	17,95±2,513	8,464±3,110	0,10±0,09
0,40±0,160	14,87±2,414		0,11±0,09
0,35±0,210	15,05±3,110		0,17±0,120
average values			
0,446±0,198	16,722±2,418	8,464±3,110	0,174±0,116

The thickness of the exoderm layer averaged 0,446±0,198 μm, the thickness of the primary cortex 16,722 ± 2.418 μm, the diameter of the central cylinder 8,464±3,110 μm, and the area of xylem vessels 0,174±0,116x10^{-3} mm^2.

When considering the cross-section of the stem of *C. maculatum* L. (Figure 3) on the surface, a fairly tightly closed layer of epidermal cells is visible. The primary cortex is externally bounded by a 1-2-ply epidermis, followed by the angular collenchyme (the stem morphologically has significant surface ribbing) and the parenchyme.

As can be seen from the Figure 3, the collenchyme is mainly located in the ribs (5-7 rows), and the cells of the cortical parenchyma are located in 2-3 rows. Parenchymal cells have a rounded shape, thin-walled. Conducting beams of medium size. The primary phloem consists of thin-walled sieve-like elements and accompanying cells. The primary xylem occupies the inner part of the bundle, represented by 7-15 medium-and wide-light vessels. Along the entire circumference of the stem, a pronounced sclerenchymal lining is located above the launches. The xylem is surrounded in some places by tightly closed sclerenchyma cells. The cells of the heart-shaped parenchyma are numerous, have a rounded shape, and are thin-walled. In the stem, inclusions are noted in the areas of the conducting bundles and the primary cortex. The core is gradually destroyed, and an air-bearing cavity is formed in its place.

The morphometric parameters of the stem are presented in Table 2.

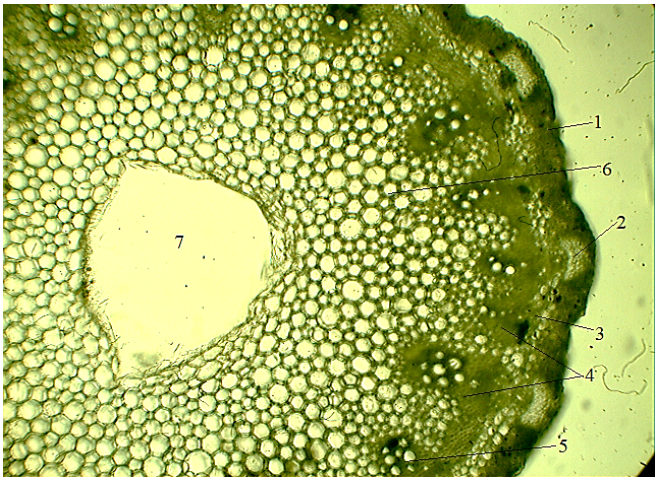

Figure 3 – Anatomical structure of the stem (x100).
Note: 1-epidermis, 2-collenchyma, 3-chlorophyll-bearing parenchyma, 4-sclerenchyma, 5-xylem vessels, 6-core parenchyma, 7-air-bearing cavity

Table 2 – Morphometric parameters of the stem *C. maculatum* L.

Thickness of the epidermis, μm	The thickness of the primary cortex, μm	Thickness of the sclerenchyma layer, μm	Diameter of the central cylinder, μm
0,68±0,265 0,55±0,314 0,82±0,221 0,90±0,317 0,110±0,289	1,386±0,902 1,381±0,874 1,436±0,800 1,385±0,599 1,276±0,562	0,674±0,102 0,773±0,147 0,942±0,196 0,778±0,152 0,805±0,143	24,173±2,265
average values			
0,612±0,281	1,373±0,747	0,794±0,148	24,173±2,265

From Table 2, it can be seen that the thickness of the epidermis layer on average was 0,612±0,281 μm, the thickness of the primary cortex was 1,373±0,747 μm, the diameter of the central cylinder was 24,173±2,265 μm, and the thickness of the sclerenchyma layer was 0,794±0,148 μm.

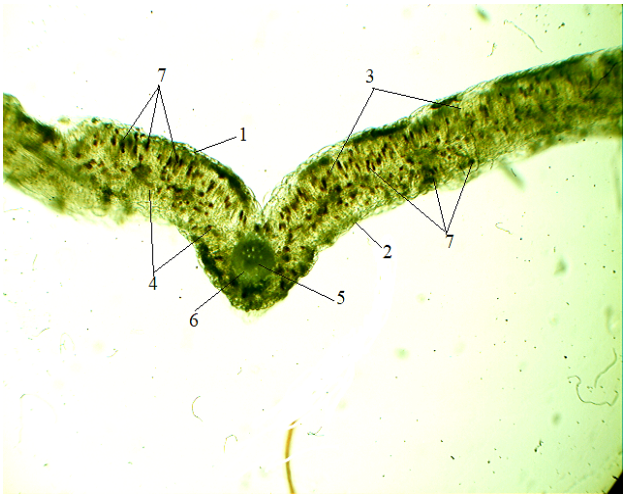

Figure 4 – Anatomical structure of the leaf *C. maculatum* L. (sw.x100).
Note: 1-upper epidermis, 2-lower epidermis, 3-chlorophyll-bearing columnar parenchyma, 4-spongy parenchyma, 5-conducting bundle, 6-sclerenchyma cells, 7-inclusions

Table 3 – Morphometric parameters of the leaves *C. maculatum* L.

Thickness of the epidermis, μm	Thickness of the mesophyll layer, μm	The thickness of the columnar mesophyll,μm	The thickness of the spongy mesophyll,μm	The area of the conducting bundles, x10^{3}мм^2
0,063± 0,05	0,780± 0,12	0,482± 0,15	0,296± 0,13	0,357± 0,20
0,050± 0,06	0,926± 0,15	0,475± 0,15	0,519± 0,1	0,310± 0,18
0,070± 0,02	0,955± 0,18	0,325± 0,19	0,305± 0,11	0,248± 0,11
0,090± 0,03	0,970± 0,17	0,494± 0,09	0,410± 0,14	0,470± 0,20
0,131± 0,03	0,982± 0,22	0,536± 0,10	0,407± 0,14	0,260± 0,16
average values				
0,081± 0,038	0,922± 0,168	0,462± 0,136	0,387± 0,124	0,329± 0,17

From the surface, the leaf blade of *Conium maculatum* L. is covered with a thin layer of cuticle. Weak wrinkling is visible on both sides of the sheet. The cells of the upper epidermis have a lesser degree of tortuosity than the cells of the lower epidermis. The cells have thin walls. Columnar chlorophyll-bearing parenchyma is represented by two rows of densely spaced oblong cells with numerous inclusions. The lower part of the mesophyll is represented by 2-3 layers of cells and consists of a loose spongy parenchyma, and numerous inclusions are also noted. The cells of the columnar mesophyll have an average size of 0,462±0,136 microns, and the spongy mesophyll 0,387± 0,124 microns. The median vein of the leaf has a sclerenchymal lining. Smaller conducting bundles of the leaf in the number 2-4 of the collateral are closed. The area of the conducting beams is 0,329=0,17x10^3 mm^2. There is one secretory channel between the sclerenchyma and the corresponding conducting beam (Figure 4). The morphometric parameters of the leaves are presented in Table 3. Thus, on the basis of the morphological and anatomical study, basic structural features of *C. maculatum* L. were revealed.

Conclusion

Work on the definition of the anatomical structure of the species *Conuim Maculatum* L. conducted in the research center of medicinal plants of the Al-Farabi Kazakh National University. According to the purpose of the work, by studying the anatomical structure of the plant hemlock spotted (*Conium maculatum* L.) belonging to the family *Apiaceae* Lindl. diagnostic signs were identified, the place of biologically active components in the cell was determined. As a result of studying the anatomical structure of the plant, it was found that the plant leaf is covered with thin cuticles, and the lower part of the mesophyll consists of a loose spongy parenchyma and a 2-3-layer cell. On a cross-section of the stem of the plant *Conium maculatum* L. clearly visible, tightly closed layer of epidermis cells. The presence of a 1-2-row layer of rectangular ectoderm in the root bundle was established, the parenchyma of the first root bundle cortex consists of several layers (4-6).

Acknowledgment

Authors thank Prof. Samir Anis Ross (University of Mississippi, USA) for improvements introduced to the text.

References

1 Gemedzhieva N.G. (2009) Izuchenie i sohranenie bioraznoobraziya alkaloidonosnyh rastenij Kazahstana [Study and conservation of the biodiversity of alkaloid-bearing plants in Kazakhstan] // Vestnik KazNU. Seriya biologicheskaya, no. 1, pp. 5-14. https://bb.kaznu.kz/index.php/biology/article/view/31

2 Vetter J. (2004) Poison hemlock (Conium maculatum L.) // Food and Chemical Toxicology, vol 43, issue 9, September, pp. 1373-1382 https://doi.org/10.1016/j.fct.2004.04.009

3 Holm L., Doll J., Holm E., Pancho J., Herberger J. (1997) World weeds, natural histories and distribution. New York, 1152 p. ISBN 978-0-471-04701-8

4 Vickery M. (2010) Plant poisons: their occurrence, biochemistry and physiological properties // Science Progress, 93(2), pp. 181–221 https://doi.org/10.3184/003685010X12729948220326

5 Saeedeh Nury, Ahmad Hosseini, Adrian J. Gibbs, Musa Mohammadi (2020) Poison hemlock virus Y (PHVY), a novel potyvirus from Iranian Conium maculatum L. (Apiaceae Lindl.) // Australasian Plant Pathology, 17 January, pp. 119-126 https://doi.org/10.1007/s13313-020-00681-0

6 Budancev A.L., Lesiovskaya E.E. (2001) Dikorastushchie poleznye rasteniya Rossii [Wild-growing useful plants of Russia]. SPb., 663 p. ISBN 5-8085-0124-5

7 Brtalik D., Stopyra J., Hannum J. (2017) Intravenous poison hemlock injection resulting in prolonged respiratory failure and encephalopathy // Journal of Medical Toxicology, vol. 13, pp. 180-182 https://doi.org/10.1007/s13181-017-0601-0

8 Seegmiller W.H., Graves J., Robertson D.J. (2020) A novel rind puncture technique to measure rind thickness and diameter in plant stalks // Plant Methods, vol. 16, pp. 43-45 https://doi.org/10.1186/s13007-020-00587-4

9 Madaan R., Kumar S. (2012) Screening of alkaloidal fraction of Conium maculatum L. aerial parts for analgesic and antiinflammatory activity // Indian J. Pharm Sci, vol. 74, issue 5, September, pp. 457-460 https://doi.org/10.4103/0250-474X.108423

10 Zholondz M.Y. (2001) Rak: praktika iscelenie [Cancer: practice and healing]. SPb., 192 p. ISBN 978-5-49807-564-8

11 Mahlayuk V.P. (1993) Lekarstvennye rasteniya v narodnoj medicine [Medicinal plants in folk medicine]. Saratov, 544 p. ISBN 5-7633-0743-7

12 Chevallier A. (1996) The Encyclopedia of Medicinal Plants. DK Pub, 336 p. ISBN 0789410672

13 Mitich W.L. (1998) Poison-hemlock (Conium maculatum L.) // Weed Technology, vol.12, is. 1, March, pp. 194-197 https://doi.org/10.1017/S0890037X00042792

14 Kingsbury J. M. (1964) Poisonous plants of the United States and Canada// Science, 25 September, vol. 145, issue 3639, pp. 1425-1426 https://doi.org/10.1126/science.145.3639.1425-a

15 Cromwell B. T. (1956) The separation, micro-estimation and distribution of the alkaloids of hemlock (Conium maculatum L.)// Biochem, 64(2), pp. 259–266 https://doi.org/10.1042/bj0640259

16 Flora SSSR (1950). Tom 16 [Flora of the USSR. Vol. 16]. Moskva, pp. 225-229 ISBN 978-5458419918

17 Flora, rastitel'nost' i rastitel'nye resursy Kazahstana (2006) [Flora, vegetation and plant resources of Kazakhstan]. Almaty, 217 p. ISBN 9965-473-87-0

18 Atlas arealov i resursov lekarstvennyh rastenij SSSR (1983) [Atlas of areas and resources of medicinal plants of the USSR]. Moskva, 268 p. ISBN ВВН 0531-БН2-020818-07

19 Gemedzhieva N.G. (2012) Alkaloidonosnye rasteniya Kazahstana i perspektivy ih ispol'zovaniya

(na primere Dzhungaro-Severotyan'shan'skoj provincii) [Alkaloid-bearing plants of Kazakhstan and prospects of their use (on the example of the Dzungaro-North Tianshan province)]. Almaty, 312 p. ISBN 978-601-80287-0-0

20 Gemedzhieva N.G. (2009) Osobennosti biologii Conium maculatum L. v predgor'yah Zailijskogo Alatau [Biological features of Conium maculatum L. in the foothills of the trans-Ili Alatau] // Izvestiya NAN RK. Ser. biol. i med, Almaty, no. 2, pp. 24-27 http://library.kz/ru/menuvse/119-journalsnanrk/2010-10-03-11-53-53/484-2009-2

21 Bowman C., Snaghvi S. (1963) Pharmacological actions of hemlock (Conium maculatum L.) alkaloids // Journal of Pharmacy and Pharmacology, vol. 15, pp. 1–25 https://doi.org/10.1111/j.2042-7158.1963.tb12738.x

22 Karzhaubekova Zh. Zh., Gemejyieva N. G., Arisbaeva R. B. (2016) K soderzhaniyu efirnyh masel u dikorastushchih vidov gornyh hrebtov Yugo-Vostoka Kazahstana [The content of essential oils in wild species of mountain ranges in the South-East of Kazakhstan], vol. 65, no. 3, sep., pp. 34-39 https://bb.kaznu.kz/index.php/biology/article/view/1093

23 Isachenko A.G. (1998) Metody polevyh landshaftnyh issledovanij i landshaftno- ekologicheskoe kartografirovanie [Methods of field landscape research and landscape-ecological mapping]. SPb., 112 p. ISBN 5-288-02079-5

24 Bar'kina R.P., Veselova T.D., Devyatov A.G., Dzhalilova H.H. (2004) Spravochnik po botanicheskoj mikrotekhnike. Osnovy i metody [Reference book on Botanical micro-technology. Basics and methods]. M:. MGU, 312 p. ISBN 5-211-06103-9

25 Biryuzova V.I., Borovyagin V.L., Gilev V.P. (1963) Elektronnomikroskopicheskie metody issledovaniya biologicheskih ob"ektov [Electron microscopic methods for studying biological objects]. M.: Izd-vo AN SSSR, 204 p. ISBN KAE 122-08022019-24

26 Vasnecova O. A. (2009) Medicinskoe i farmacevticheskoe tovarovedenie. Tom 2 [Medical and pharmaceutical commodity science. Vol. 2]. M. : Geotar-Media, 608 p. ISBN 978-5-9704-1106-3

27 Polevoj V.V. (1989) Fiziologiya rastenij [Plant physiology]. M.: Vysshaya shkola, 484 p. ISBN 5-06-001604-8

28 Bajtenov M.S. (2001) Flora Kazahstana. Tom 2 [Flora of Kazakhstan. Vol. 2]. Almaty: Gylym. ISBN 9965-07-036-9

29 Da Cheng Hao, Xiao-Jie Gu, Pei Gen Xiao (2015) Medicinal Plants. Woodhead Publishing, 694 p. ISBN 978-0-08-100085-4

30 Tahaeva M., Amankulova B. (2006) Flora, rastitel'nost' i rastitel'nye resursy Kazahstana [Flora, vegetation and plant resources of Kazakhstan]. Almaty, 217 p. ISBN 9965-473-87-0

31 Dodd-Butera T., Broderick M. (2005) Plants, Poisonous // Encyclopedia of Toxicology, pp. 443-448 https://doi.org/10.1016/B0-12-369400-0/00771-7

IRSTI 34.19.21 https://doi.org/10.26577/ijbch.2021.v14.i2.04

A. Sekenova[1,2], Y. Li[1], A. Saparov[3], B. Mambetpayeva[4], N. Kulmaganbetova[4], Y. Ramankulov[1,3], V. Ogay[1*]

[1]Stem Cell Laboratory, National Center for Biotechnology, Nur-Sultan, Kazakhstan
[2]Department of General Biology and Genomics, School of Natural Sciences, L.N. Gumilyov Eurasian National University, Nur-Sultan, Kazakhstan
[3]Nazarbayev University, Nur-Sultan, Kazakhstan
[4]Astana Medical University, Nur-Sultan, Kazakhstan
*e-mail: ogay@biocenter.kz

Immunomodulatory properties of cytokine-preconditioned compact-bone derived mesenchymal stem cells cultured in 2D and 3D culture conditions

Abstract. Mesenchymal stem cells (MSCs) possess potent immunomodulatory properties and therefore represent a promising therapeutic tool for the treatment of immune-related diseases. Recently, preconditioning has been proposed as a strategy to improve the immunomodulatory activity of MSCs. In this study, we focused to investigate the effects of preconditioning with pro-inflammatory cytokines (TNF-α and IFN-γ) on immunomodulatory activity of mouse compact bone-derived MSCs (CB MSCs) in 2D and 3D culture conditions. Mouse CB MSCs for the 2D condition were cultured in a standard tissue culture plate. 3D spheroid MSCs were formed by enforced composing in Nunclon Sphera 96-well U-bottom plate. MSCs in 2D and 3D spheroid cultures were preconditioned with TNF-α and IFN-γ alone and in combination for 24 hours. The levels of immunomodulatory factors (PGE2, IL-6, IL-10, TNF-α, IFN-γ) were measured by ELISA. The immunomodulatory properties of MSCs were examined by macrophage inflammation and lymphocyte co-culture assays. Our results showed that TNF-α and IFN-γ more effectively increased the secretion of PGE2 and IL-6 by 3D spheroid MSCs compared with 2D MSCs culture. Cytokine-preconditioned 3D spheroid MSCs significantly decreased the production of TNF-α, IFN-γ, IL-10 in splenic lymphocytes and TNF-α and IL-6 in macrophages. Cytokine-preconditioned 3D spheroid MSCs increased IL-6 and IL-10 levels in lymphocytes and macrophages respectively. It was found that 3D spheroid MSCs more effectively suppressed the proliferation of T cells compared with 2D MSCs culture. Moreover, preconditioning of 3D spheroid MSCs using TNF-α suppressed more effectively in vitro immune response than preconditioning with IFN-γ or with the combination of two cytokines. Thus, our data suggest that preconditioning with pro-inflammatory cytokines more effectively increases the immunomodulatory activity of 3D MSC spheroids compared to 2D MSC culture.

Key words: Cytokines, immunomodulation, MSCs, preconditioning, 3D spheroids.

Introduction

Mesenchymal stem cells (MSCs) are a heterogeneous population of adult multipotent stromal cells that can be isolated from almost all mammalian tissues, including compact bone [1]. MSCs are characterized by their self-renewal capacity, immune tolerance and high multilineage differentiation potential. In addition, MSCs exert immunomodulatory effects on a wide range of immune cells, which is mediated by both cell-cell contacts and the secretion of various factors of immune regulation such as prostaglandin E2 (PGE2), indoleamine-2,3-dioxygenase (IDO), transforming growth factor β (TGF-β), hepatocyte growth factor (HGF), galectin-1, interleukin 6 (IL-6) and interleukin 10 (IL-10) [2]. Due to their immunomodulatory and regenerative abilities, MSCs are considered a new therapeutic tool for the treatment of many diseases, especially those of an inflammatory nature [3]. Several clinical studies have shown the beneficial effects of MSCs transplantation for the treatment of autoimmune diseases, such as graft-versus-host disease (GVHD), rheumatoid arthritis, Crohn's disease, type 1 diabetes mellitus and multiple sclerosis [4,5]. However, the effectiveness of MSC-based therapy in clinical trials is often insufficient due to allow survival rate and engraftment

of the transplanted MSCs in a severe hypoxic and inflammatory microenvironment.

To increase the therapeutic efficiency of MSCs, several approaches have been proposed to increase the survival and immunomodulatory or anti-inflammatory properties of transplanted MSCs. These approaches are based on *in vitro* preconditioning of MSCs with a high concentration of pro-inflammatory cytokines, hypoxia, heat shock or oxidative stress [6]. Many studies have demonstrated that preconditioned MSCs showed a sufficient survival rate and enhanced regenerative and immunomodulatory effects in damaged sites [7-10]. For example, it has been shown that preconditioning with interferon-γ (IFN-γ) and interleukin-1β (IL-1β) significantly increased the immunosuppressive properties of MSCs. MSCs preconditioned with IFN-γ and IL-1β significantly decreased the proliferation of peripheral blood mononuclear cells, inhibited T cell differentiation into T helper 1 (Th1) cells, induced T regulatory cells (Tregs) differentiation and increased secretion of PGE2 and IDO more than that of single treatments. Also, the *in vivo* study has demonstrated that preconditioning of MSCs with IFN-γ and IL-1β showed a significant improvement in the condition of the damaged mucous membrane and a decrease in serum level of IL-6 of acute experimental colitis in mice as compared to untreated MSCs [11]. In another study, mouse MSCs, preconditioned with IFN-γ and IL-1β, when compared with untreated MSCs, secreted high levels of immunosuppressive mediators (nitric oxide (NO), IL-6, and PGE2) and promoted macrophage polarization toward the anti-inflammatory alternatively activated macrophages (M2b phenotype or M2), which is mainly mediated by IL-6 cytokine. Furthermore, M2b macrophages highly produced IL-10 and significantly inhibited IFN-γ expression in CD4 T lymphocytes [12]. Similar results were also observed in human MSCs treated with IFN-γ and tumor necrosis factor-alpha (TNF-α). François and colleagues have reported that preconditioned human MSCs upregulated IDO, more effectively suppressed T cell proliferation and promoted the differentiation of monocytes into IL-10-producing M2 anti-inflammatory macrophages [13]. Moreover, preconditioning with both IFN-γ and TNF-α significantly increased the expression of several chemokine molecules and receptors such as chemokine (C-X-C) motif) ligand 9 (CXCL9), chemokine (C-X-C) motif) ligand 10 (CXCL10), C-X-C chemokine receptor type 3 (CXCR3) and C-C chemokine receptor type 3 (CCR5) in MSCs, which are involved in the chemotaxis and the inhibition of the proliferation of activated leukocytes [14].

Recently, it has been shown that the aggregation of human MSCs into three-dimensional spheroids (3D-spheroid MSCs) increases immunomodulatory properties, stemness and survival of MSCs after administration [15]. It has been established that culturing MSCs in a 3D microenvironment significantly enhances the expression of anti-inflammatory genes such as TNF-α-stimulated gene 6 (TSG-6), cyclooxygenase-2 (COX-2) and stanniocalcin-1 (STC-1) [16]. Moreover, 3D spheroid culture enhanced immunosuppressive properties of MSCs and increased PGE2, transforming growth factor β1 (TGF-β1) and IL-6 levels compared with two-dimensional culture of MSCs (2D MSCs) [17]. Although most studies have been conducted using human MSCs, no reports were comparing the immunomodulatory properties of 2D and 3D cultures of mouse compact bone-derived MSCs (CB-MSCs) after preconditioning with pro-inflammatory cytokines TNF-α and IFN-γ. Thus, we hypothesize that the preconditioning with pro-inflammatory cytokines would modify the immunomodulatory properties of mouse CB-MSCs cultured under a 3D microenvironment. To test this hypothesis, we have compared the immunomodulatory properties of cytokine-preconditioned mouse CB MSCs cultured as a monolayer and 3D spheroids.

Materials and methods

Animals. Male C57BL/6 mice of 2-3-week-old were obtained from SPF-vivarium of M. Aikimbayev's Kazakh Scientific Centre for Quarantine & Zoonotic Diseases (Almaty, Kazakhstan). The animals were kept in a temperature-controlled environment (23°C) with 60% relative humidity applying a 12 h light/dark cycle. The animals had *ad libitum* access to food and water. Experimental procedures involving animals were in full compliance with the European Convention for the Protection of Vertebrate Animals Used for Experimental and other Scientific Purposes and were approved by the Local Ethics Committee for Animal Use of the National Center for Biotechnology (Nur-Sultan, Kazakhstan).

Isolation and culture of CB MSCs. Isolation of MSCs from mouse compact bones was conducted according to the protocol described previously by Zhu and colleagues [1]. Briefly, the tibia and femur were dissected from the hind limbs of mice. After removing muscles, both ends of the femur and tibia were cut by sterile scissors and the bone marrow was flushed

out with α-MEM medium by inserting a 0.45-mm syringe needle into the bone cavity. Femur and tibia were cut into small chips by scissors and treated by α-MEM medium containing 10% fetal bovine serum (FBS) and 0.1% collagenase II for 2 h in a shaking incubator at 37°C and 200 rpm. The enzyme-treated bone chips were washed with α-MEM medium and seeded into a T25 culture flask in the presence of α-MEM medium containing 10% FBS. After incubation for 3 days, non-adherent cells and tissue debris were removed, and bone chips were incubated additional 2 days in α-MEM medium containing 10% FBS at 37°C and 5% CO_2. After 5 days in culture, adherent cells were harvested with TrypLE Express (Gibco, USA) and reseeded at a split ratio of 1:3. The culture medium was changed every 2 days. The passage was conducted twice per week at a split ratio of 1:3. The cells at passages 3-6 were used for the study.

Colony-forming unit-fibroblast assay. CB MSCs (passage 3) were harvested using TrypLE Express, and the total cell number was determined by using an automatic cell counter Bio Rad TC20. Harvested cells were seeded into T25 culture flasks at a density of 1000 cells/flask. After 14 days, cell cultures were washed with phosphate-buffered saline (PBS) and stained with 0.5% crystal violet in methanol for 10 minutes at room temperature. After staining, flasks were washed with PBS, allowed to dry, and colonies were counted and analyzed by using a stereomicroscope SZ61 (Olympus, Hamburg, Germany).

Multilineage differentiation assay. For adipogenic differentiation, 1×10^4 cells/cm^2 were plated in a 6-well culture plate and cultivated in an adipogenic differentiation medium composed of high glucose DMEM supplemented with 15% FBS, 0.2 mM L-glutamine, 100 μM L-ascorbic acid, 200 μM indomethacin, and 100 nM dexamethasone. The medium was changed twice a week. After 21 days, the cells were fixed with 4% paraformaldehyde solution (PFA) and stained with Oil red O. For osteogenic differentiation, the cells at 90% confluence were cultivated in an osteogenic differentiation medium composed of low glucose DMEM supplemented with 15% FBS, 200 μM L-ascorbic acid, 10 mM glycerolphosphate, and 100 nM dexamethasone. The medium was changed twice a week for 3 weeks. Osteogenic differentiation was evaluated using Alizarin red staining. For chondrogenic differentiation, the cells were resuspended at 1.25×10^6 cells/ml in a chondrogenic differentiation medium composed of high-glucose DMEM supplemented with 1% ITS+Premix, 100 μmol/L ascorbate-2 phosphate, 0.1 μm dexamethasone, and 10 ng/ml TGF-β1. To create chondrogenic micromass pellets, 2.5×10^5cells from this cell solution were placed in a 96-well polypropylene plate, centrifuged at 500×*g*, and placed in an incubator at 37°C and 5% CO_2. The medium was changed twice a week. After 3 weeks, the cell pellets were harvested, fixed with 10% neutral-buffered formalin, paraffin-embedded, sectioned at 5 μm, and stained with Toluidine blue.

Flow cytometry analysis. 5×10^5cells per sample were stained by appropriate antibodies for phenotyping of MSCs and T cells. For MSCs the following antibodies were used: CD29-PE (clone HM β1-1), CD31-PE (clone MEC 13.3), CD44-FITC (clone IM7), CD45-FITC (clone 30-F11), CD90-FITC (clone 53-2.1), CD105-PE (clone MJ7/18). T cells were stained by CD4-PE (clone RM4-5), CD8-PE (clone 53-6.7), FoxP3-Alexa Fluor 488 (clone MF23) and Ki-67-Alexa Fluor 647 (clone B56). As negative controls following isotypes match antibodies were used: IgG2a-PE, IgG2b-FITC, and IgG1-Alexa Fluor 647. All antibodies were obtained from BD Biosciences. Flow cytometry analysis was performed on Attune NxT Acoustic Focusing Flow Cytometer (Thermo Fisher Scientific, UK). Obtained data were analyzed using the FlowJo software (FlowJo LLC, USA).

Spheroid formation. Formation of 3D MSCs spheroids was performed using "3D cell culture handbook" [18]. MSCs (passage 5) were harvested by TrypLE Express and resuspended in α-MEM medium containing 10% FBS. For spheroid formation, 2×10^4 MSCs were added into each well of Nunclon Sphera 96-well U-bottom plate (Nunc, USA) and incubated in a rotary orbital shaker (Biosan, Latvia) at 25 rpm, 37°C and 5% CO_2 for 48 hours [19]. Formed spheroids were collected and used for morphometric analysis and immunomodulatory factor quantification.

Immunofluorescence staining of spheroids. Spheroids were fixed with 4% PFA containing 1% Triton X-100 for 20 min at 37°C. After washing with 0,1% Triton X-100 in PBS, spheroids were incubated in 1% bovine serum albumin for 30 min at 37°C. For immunofluorescence staining [20], spheroids were incubated with monoclonal anti-CD90-FITC antibody (1:100) (BD Biosciences, USA) for 12 h at 4°C, washed three times in 0.1% Triton X-100 and stained with propidium iodide (Gibco, USA). After washing in PBS, stained spheroids were transferred in a glass-bottom dish (Nunc, USA) and immersed in Prolong Live antifade reagent (Thermo Fisher Scientific, USA) and imaged with a confocal laser scanning microscope LSM 780 (Carl Zeiss, Ger-

many). Image processing was conducted with the Image J software.

Cytokine preconditioning of MSCs. For preconditioning of 2D MSCs, 2×10^5cells were plated in T25 culture flasks and cultured in complete culture media for 2 days at 37°C and 5% CO_2. For preconditioning of 3D spheroid MSCs, 2×10^4 cells/well were incubated in a 96-well U-bottom 3D cell culture plate on the rotary orbital shaker for 2 days at 25 rpm, 37°C and 5% CO_2. After 2 days of culture, 2D MSCs and 3D-spheroid MSCs were treated with 20 ng/ml recombinant mouse TNF-α, 20 ng/ml of recombinant mouse IFN-γ individually and in combination for 24 h at 37°C and 5% CO_2. 2D MSCs and 3D-spheroid MSCs cultures without cytokine treatment served as controls. The dosage of cytokines was selected according to previously published data [21-23]. After cytokine preconditioning, 2D MSCs and 3D-spheroid MSCs and supernatants were collected for the measurement of immunomodulatory factors and co-culture with lymphocytes and macrophages.

Enzyme-linked immunosorbent assay. Cell culture supernatants were collected from co-culture of MSCs with T cells or macrophages, and concentrations of IL-6, IL-10, TNF-α and IFN-γ were measured by enzyme-linked immunosorbent assay (ELISA) kits (BD Biosciences, USA) according to the manufacturer's instruction. PGE2 levels in cellular supernatants were determined by competitive ELISA technique using PGE2 ELISA kit (Cusabio, China) according to the manufacturer's instruction.

Lymphocyte co-culture assay. Murine splenocytes were isolated from the spleen of 8-week old C57BL/6 males. To obtain a single-cell suspension, freshly isolated spleens were placed in a chilled RPMI-1640 medium containing 1% antibiotic-antimycotic solution and crushed through a 70-μm nylon cell strainer (Corning, USA). Erythrocytes were lysed with BD Pharm Lyse lysing buffer (BD Biosciences, USA). CD4□T cells (>95% purity) purification was performed by negative immunomagnetic selection using BD IMag Mouse CD4 T Lymphocyte Enrichment Set (BD Biosciences, USA). T cells were activated with 5 μg/ml concanavalin A (ConA) (Sigma, USA). The ratio of T lymphocytes and MSCs was 1:50, respectively [24]. T cell/MSC co-cultures were incubated in a 96-well round-bottom plate for 72 h in RPMI 1640 supplemented with 10% FBS, 2 mM L-glutamine, and 20 μM β-mercaptoethanol (Gibco, USA) at 37°C and 5% CO_2. Three independent experiments were done in quintuplicate. T cell proliferation was measured by Ki-67 expression using flow cytometry.

Macrophage inflammation assay. Peritoneal macrophages were isolated from the peritoneal cavity of C57BL/6 mice and resuspended in α-MEM supplemented with 10 % FBS, 2 mM L-glutamine and 1% antibiotic-antimycotic solution. Before co-culture assay, macrophages were stimulated with 500 ng/ml of lipopolysaccharide (LPS) for 24 h to determine cytokine responses [16]. Stimulated macrophages (5×10^5) and cytokine preconditioned MSCs (2×10^5) were co-cultured for 18 h in 24-well tissue culture-treated plate at 37 °C and 5% CO_2. 3D spheroids were taken based on that 1 spheroid had 2×10^4 cells. LPS-stimulated and non-stimulated macrophages without MSCs served as controls. Three independent experiments were done in triplicate. The supernatants from macrophage/MSCs co-culture were collected for the measurement of cytokine levels.

Statistical analysis. All data obtained are presented as mean ± standard deviation (SD). The statistical significance was calculated using two-way ANOVA and Student's t-test. $P < 0.05$ was considered statistically significant. Statistical analysis was performed using GraphPad Prism 9.1.0 software (USA).

Results and discussion

Characterization of mouse CB MSCs. Mouse MSCs from compact bone were spindle-shaped (Figure 1A), expanded rapidly in culture and reached confluence within 4-5 days (Figure 1B). Further analysis showed that MSCs have the capacity to form fibroblastic colonies (Figure 1C) and can differentiate into adipocytes, osteoblasts and chondrocytes (Figure 1 D-F), indicating that they have self-renewal and multipotent potential. In addition, MSCs expressed CD29, CD44, CD90, CD105, but not CD31 and CD45 (Figure 1G).

*Characterization of 3D-spheroid MSCs.*MSCs (passage ≤3) was aggregated into spheroids in microwells of a low-binding plate within three days (Figure 2A). 3D-spheroid MSCs had an average diameter of approximately 65 μm and had 2×10^4 cells (Figure 2A, B). Morphologically, they had spherical or slightly oblong shapes. CLSM imaging revealed that spheroids appeared as compact cellular structures without any cavities (Fig 2C). In addition, spheroids highly expressed CD90 – one of the surface markers of MSCs.

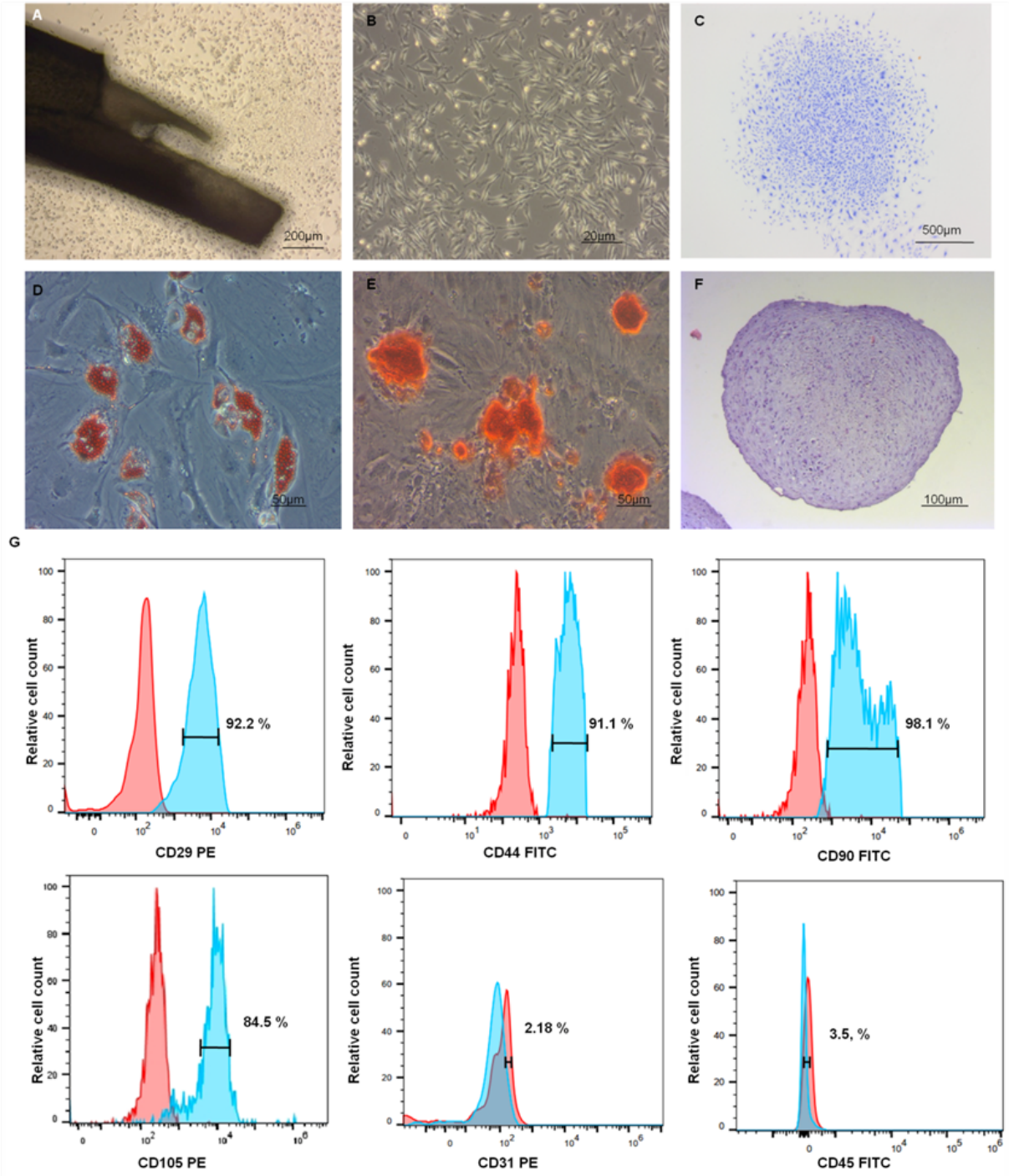

Figure 1 – Characterization of mouse CB MSCs. (A) On the 4th day after initial culture, fibroblast-like cells migrated from compact bone chips.
(B) A phase-contrast image of the monolayer culture of MSCs (passage 2) showing typical spindle-shaped morphology.
(C) A representative image of the fibroblastic colony of MSCs stained with crystal violet.
(D) Phase-contrast image of MSCs culture after adipogenic differentiation.
The cells contain orange lipid droplets stained with oil red O.
(E) Phase-contrast image of MSCs culture after osteogenic differentiation.
The cells contain orange depositions of calcium stained with alizarin red S.
(F) Chondrogenic differentiation of MSCs pellet culture. Cross-section of chondrogenic pellet stained with a toluidine blue.
(G) Flow cytometry analysis of MSCs markers (CD29, CD44, CD90, CD105),
hematopoietic, and endothelial cell markers (CD45 and CD31)

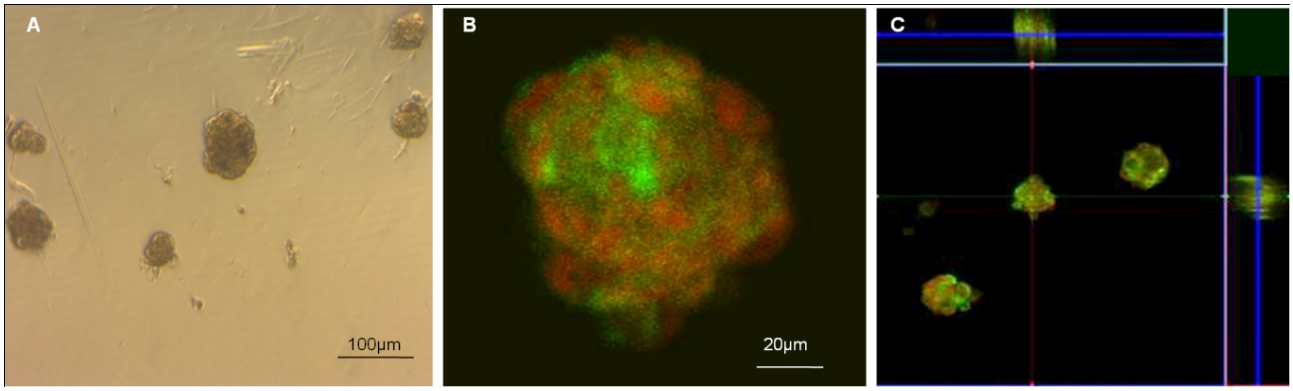

Figure 2 – Characterization of 3D-spheroid MSCs. A) 3D-spheroid MSCs formed after 72 h aggregation. B) A representative CLSM image of 3D-spheroid MSCs stained by CD90-FITC antibodies (green). The cell nuclei were stained with propidium iodide (red). (C) Orthogonal view of 3D-spheroid MSCs by CLSM

Characterization of TNF-α of and IFN-γ preconditioned 2D MSCs and 3D spheroid MSCs cultures. To evaluate the secretion of immunomodulatory factors in cytokine preconditioned MSCs, levels of PGE2 and IL-6 secretion were analyzed with ELISA. Evaluation by ELISA revealed that the PGE2 level in 3D-spheroid MSCs was significantly greater compared with 2D MSCs (Figure 3 A). Preconditioning of 3D-spheroid MSCs with TNF-α or IFN-γ resulted in approximately a 1.3-fold increase in PGE2 levels compared with either TNF-α-preconditioned or INF-γ-preconditioned 2D MSCs cultures. PGE2 level in 3D-spheroid MSCs preconditioned with the TNF-α and IFN-γ in combination was 1.4-fold higher compared with those cytokines preconditioned in 2D MSCs culture. IL-6 secretion by 2D MSCs and 3D-spheroid MSCs was significantly increased by both individual preconditioning with TNF-α, INF-γ and their combination (Figure 3 B). Preconditioning with TNF-α and IFN-γ in combination appeared to increase IL-6 secretion by 3D-spheroid MSCs synergistically, as the greatest IL-6 secretion was observed in spheroids treated with the combination of both cytokines (Figure 3 B).

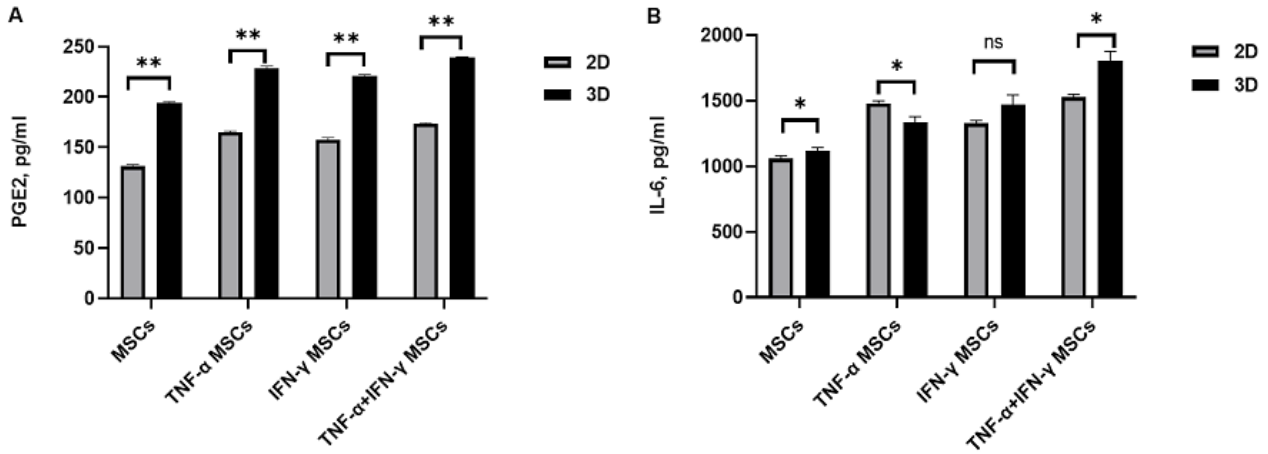

Figure 3 – Characterization of cytokine preconditioned 2D MSCs and 3D-spheroid MSCs. MSCs were incubated in the presence of 20 ng/ml TNF-α and 20 ng/ml IFN-γ for 24 h. IL-6 (A) and PGE2 (B) levels in culture supernatants were measured by ELISA. Statistical significance (*p < 0.05; **p < 0.01)

Analysis of cytokine profile in the lymphocyte co-culture assay. Since MSCs are able to exert their immunomodulatory effects on the functional activity of T cell populations, we measured the levels of cytokine production after the co-culturing of untreated and cytokine preconditioned 2D MSCs and 3D-spheroid MSCs with activated lymphocytes in ELISA (Figure4). The results demonstrated that the production levels of TNF-α, IFN-γ and IL-10 in 3D-spheroid MSCs were low and the level of IL-6 was high compared with 2D MSCs (Figure 4). Preconditioning of 3D-spheroid MSCs with TNF-α alone led to an approximate 0.5-fold decrease in TNF-α and IFN-γ levels, and also the 2-fold decrease in IL-10 levels compared to the same group in 2D MSCs (Figure 4 A, B, C). Preconditioning of 3D-spheroid MSCs with IFN-γ alone resulted in an approximate 0.3-fold decrease in TNF-α and IFN-γ levels (Figure 4 A, B). In contrast, an about 0.2-fold increase in IL-6 level compared to the same group in 2D MSCs was observed (Figure 4 D). The production levels of IL-10 were similar in IFN-γ treated and in combination (TNF-α + INF-γ) treated 2D and 3D-spheroid MSCs (Figure 4 C). Preconditioning of 3D-spheroid MSCs with the combination of the two cytokines contributed to the near 0.4-time decrease in IFN-γ levels, in comparison with similarly treated 2D MSCs cultures (Figure 4B).

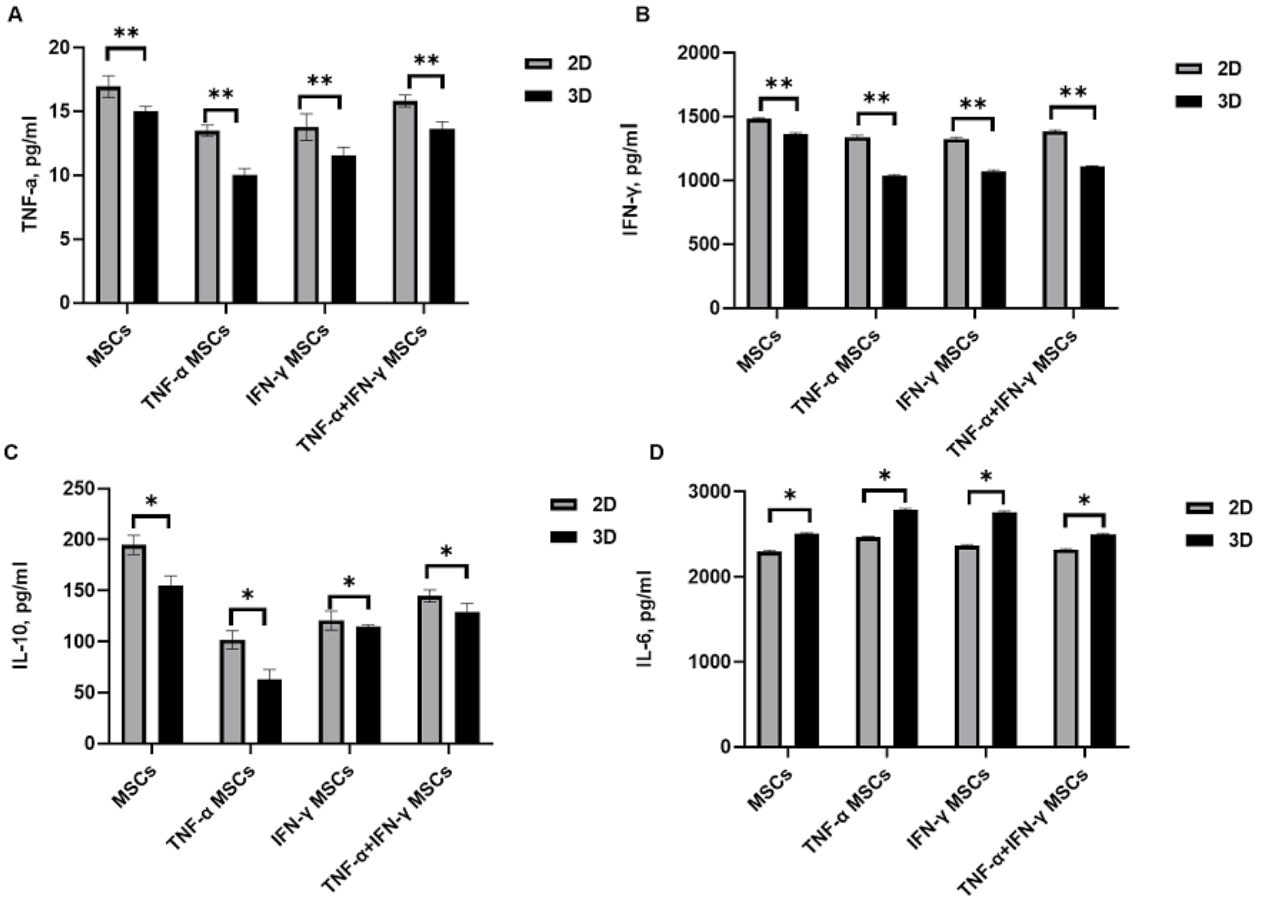

Figure 4 – The effect of cytokine preconditioned 2D MSCs and 3D-spheroid MSCs on the secretion of TNF-α (A), IFN-γ (B), IL-10 (C) and IL-6 (D) by splenic lymphocytes (ConA-activated T cells were co-cultured with preconditioned 2D MSCs and 3D-spheroid MSC). Cytokine levels in culture supernatants were measured by ELISA. Data are illustrated as mean ±SD (*p < 0.05; **p < 0.01, ***p < 0.001)

Analysis of T cell subpopulations using FACS. The effect of cytokine preconditioned 2D and 3D-spheroid MSCs on functional activity of CD4□ T cells, CD8□ T cells and Tregs are presented in Figure 5. Flow cytometry analysis showed that values of CD4□ T cells, CD8□ T cells, Foxp3□ CD4□Tregs were significantly reduced in 3D-spheroid MSCs compared with 2D MSCs. Preconditioning of 3D-spheroid MSCs with TNF-α alone resulted in a decrease in approximately 2-fold in CD4□ T cells, and 0.4-fold in CD8□ T cells and Tregs, compared with the identically treated 2D MSC cultures (Figure 5). Preconditioning of 3D-spheroid MSCs with INF-γ alone promoted a near 2 times drop of CD4□ T cells and CD8□ T cells percentage (Figure 5 A, B). Also, there was a 2.6-fold drop in the percentage of Tregs at IFN-γ treated 3D-spheroid MSCs compared to the same group of 2D MSC cultures (Figure 5 C). Preconditioning of 3D-spheroid MSCs with the combination of two cytokines led to a 2.5 times reduction in CD4□ T cells and CD8□ T cells percentage and also the 3-fold decline in the percentage of Tregs, in comparison with identically treated 2D MSCs cultures (Figure 5). The next analysis was assessed in comparison with untreated 3D spheroid MSCs. 3D spheroid MSCs preconditioned using TNF-α promoted the increase of CD4□ T and CD8□ T cells, nevertheless the decrease in Foxp3□ CD4□Tregs. The levels of CD4□ T cells, CD4□ T cells and Tregs were raised by the effect of 3D spheroid MSCs preconditioned using IFN-γ. Preconditioning with the combination of two cytokines resulted in moderate growth in CD4□ T and CD8□ T cells, however, the decline in Tregs numbers.

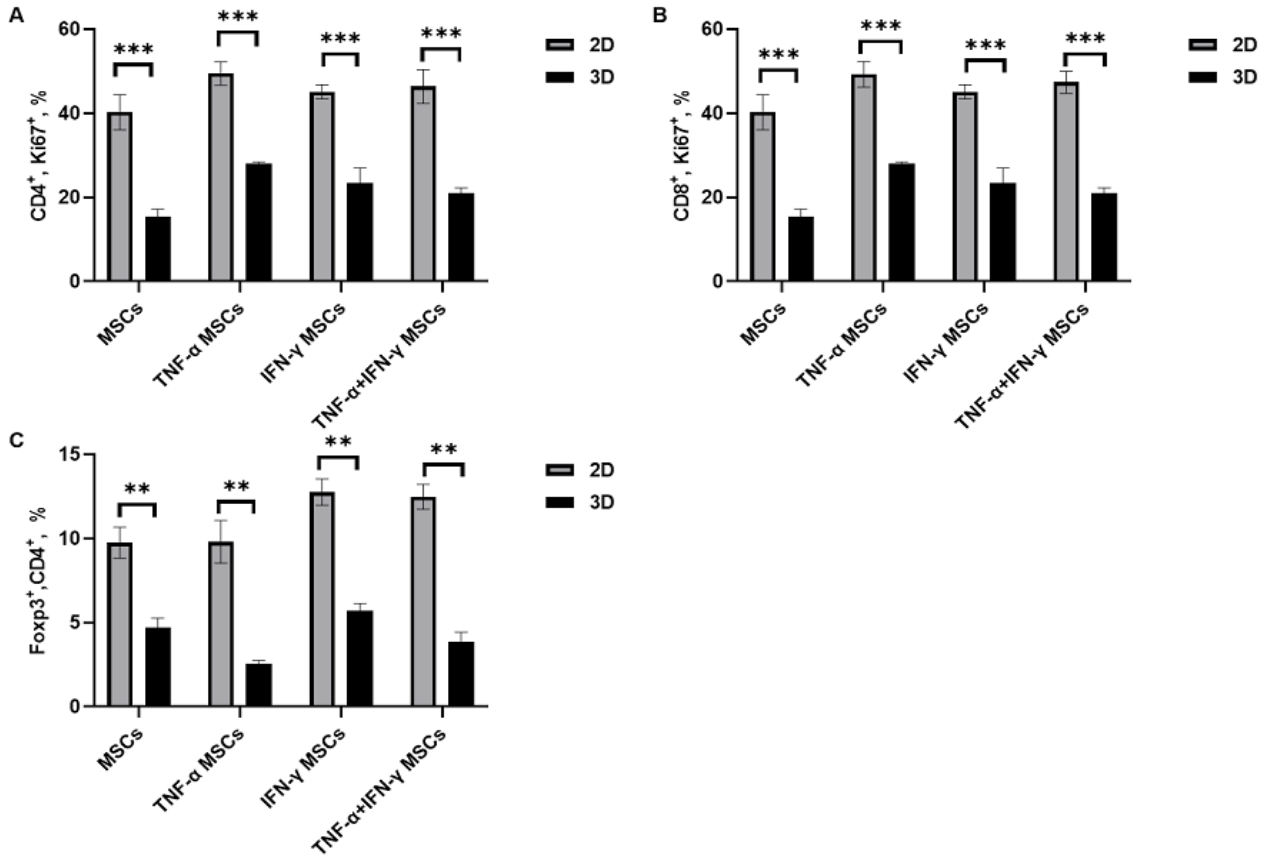

Figure 5 – The effect of cytokine preconditioned 2D MSCs and 3D-spheroid MSCs on the proliferation of T cells. Concanavalin A activated T cells were co-cultured with preconditioned 2D MSCs and 3D-spheroid MSC. The percentage of CD4□T cells (A), CD8□T cells (B) and FoxP3□ regulatory Tregs (C) examined by flow cytometry All values are expressed as mean ± SD and representative of triplicate experiments (*p < 0.05, **p < 0.01, ***p < 0.001)

Analysis of cytokine profile in macrophage inflammation assay. The investigation of the cytokine profile after co-culture of untreated and cytokine preconditioned 2D and 3D-spheroid MSCs with macrophage was evaluated by ELISA (Figure 6). The results of ELISA demonstrated that the production of TNF-α and IL-6 was low, and the production of IL-10 was significant only in TNF- α treated 3D-spheroid MSCs compared with 2D MSCs. Preconditioning of 3D-spheroid MSCs with TNF-α alone promoted the 4.5-fold and 3-fold decline in the secretion of TNF-α and IL-6 levels, respectively, compared with 2D MSCs (Figure 6 A, C). The levels of IL-10 were similar in both 2D and 3D-spheroid MSCs treated with TNF-α (Figure 6B). Preconditioning of 3D-spheroid MSCs with INF-γ alone resulted in nearly equal levels of TNF-α and, unexpectedly, the 4-fold drop in IL-6, while the value for IL-10 increased 0.3 times compared with 2D MSCs (Figure 6). Preconditioning of 3D-spheroid MSCs with the combination of two cytokines contributed to the 1.4-fold rise in TNF-α, however, values for IL-10 levels were found as not significant (Figure 6 A, B). In contrast, the 2-times decline in IL-6 production levels, in comparison with identically treated 2D MSCs cultures, was determined (Figure 6 C).

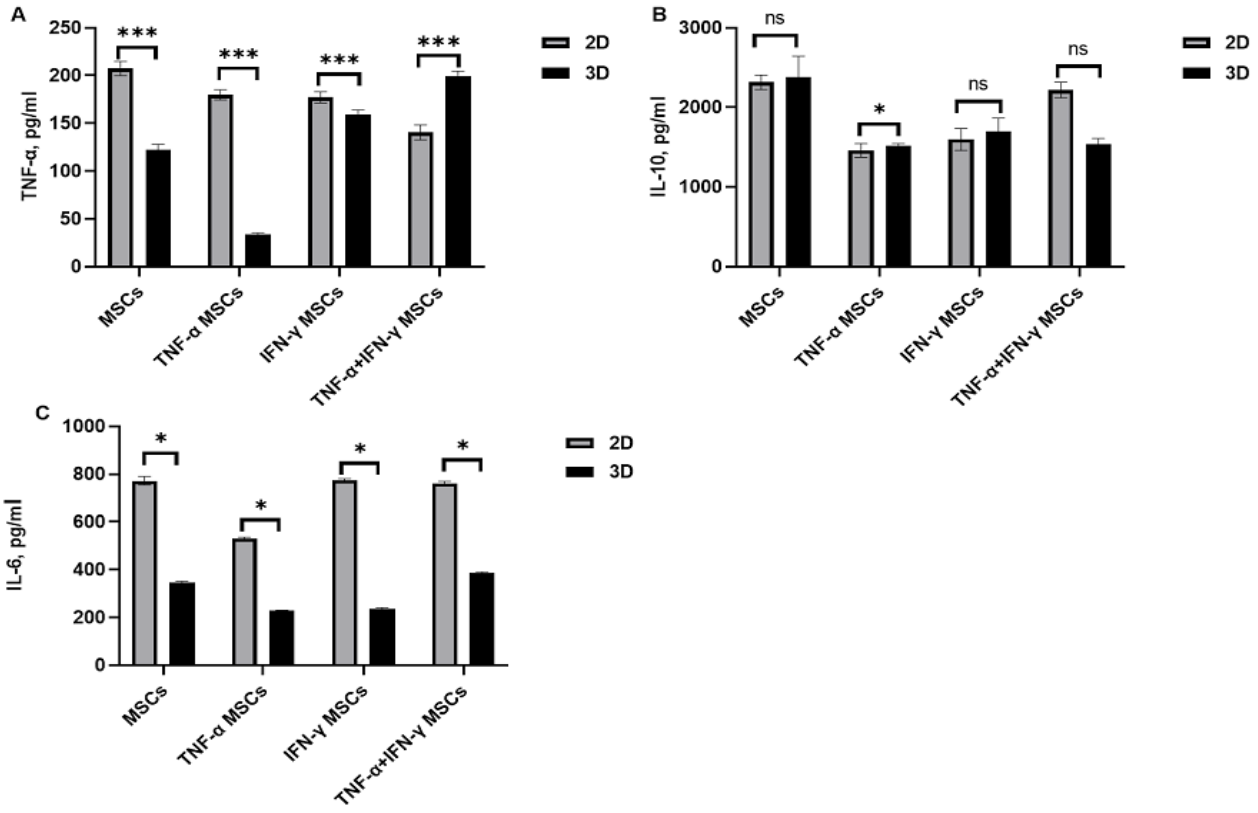

Figure 6 – The effect of cytokine preconditioned 2D MSCs and 3D-spheroid MSCs on the secretion of TNF-α (A), IL-10 (B) and IL-6 (C) by peritoneal macrophages (LPS activated mouse macrophages were co-cultured with preconditioned 2D MSCs and 3D-spheroid MSC). Cytokines' degree in culture supernatants are measured by ELISA. Data is illustrated as mean ± a (SD) (*p < 0.05; **p <0.01; ***p < 0.001, ns – non-significant)

The results of our study demonstrated that the immunomodulatory properties of mouse CB MSCs preconditioned with pro-inflammatory cytokines were improved at 3D spheroids culture. It is known that the cytokines TNF-α and INF-γ are present in an inflammatory environment; therefore, preconditioning with these cytokines provides normal physiological conditions for MSCs in comparison with other approaches [21,25]. Furthermore, the 3D culture can be considered another approach for preconditioning MSCs, which is close to normal physiological conditions. It was reported that preconditioning with in-

flammatory cytokines significantly improved the immunotherapeutic properties of hMSC, which already possessed these properties due to 3D culture [17]. We revealed that the production of immunomodulatory factors PGE2 and IL-6 in 3D-spheroid MSCs was higher than in 2D MSCs. The secretion of PGE2 and IL-6 increased when cytokine-preconditioned CB MSCs were cultured as 2D state and 3D spheroids. The formation of 3D spheroids from mouse CB MSCs improved the secretion of immunomodulatory factors, especially PGE2, as previously reported [26,16,2]. Ferreira and colleagues have reported that pro-inflammatory factors such as TNF-α, INF-γ, IL-1β and LPS can activate MSCs to secrete these mediators [27]. Moreover, the secretion of PGE2 and NO in murine MSCs is controlled by IL-6 [12], and PGE2 also have strong anti-inflammatory properties [28]. Interestingly, the use of 3D-spheroid MSCs in *in vivo* studies after injection into the inflamed area also increased the level of PGE2, IL-6, and IDO [26, 28]. It was reported that the reprogramming of macrophages from pro-inflammatory to anti-inflammatory phenotype can occur under the action of PGE2 obtained using the 3D-spheroid MSCs culture, along with other known methods, such as a NO-dependent mechanism [28]. It has been suggested that the secretion of PGE2 in 3D-MSCs is controlled by activation of the macrophage receptor EP4, by caspase pathway, NF/kB, IL-1 signaling, and intercellular contact mechanisms [28,17].

According to our results, preconditioning with pro-inflammatory cytokines TNF-α and IFN-γ altered the immunomodulatory capacity of 3D-spheroid MSCs in co-cultures with activated T cells as compared to untreated 3D-spheroid MSCs. It was reported that murine 3D-spheroid MSCs reduced the levels of TNF-α, INF-γ, and IL-6 in mice with colitis [29]. From our results, preconditioning of 3D-spheroid MSCs with a single pro-inflammatory cytokine TNF-α increased the suppression of TNF-α, IFN-γ, IL-10 production by lymphocytes compared to 2D MSCs. Moreover, preconditioning of 3D-spheroid MSCs with another pro-inflammatory cytokine IFN-γ also increased the suppression of cytokine production, but only TNF-α and IFN-γ by lymphocytes compared to 2D MSCs. Furthermore, preconditioning of 3D-spheroid MSCs with the combination of these cytokines also increased the suppression of IFN-γ and IL-10 production by lymphocytes compared to 2D MSCs. Our results on the cytokine profile obtained from co-culturing of 2D MSCs (untreated and pretreated) with lymphocytes are consistent with the data of Frodermann and colleagues, who studied the effects of MSCs *in vitro* and in animal models of atherosclerosis [24]. We also observed that the levels of IFN-γ and TNF-α production decreased in the co-culture of 2D MSCs with T cells, which is consistent with previously published data [30]. We showed that preconditioning of 3D-spheroid MSCs with only one pro-inflammatory cytokine IFN-γ decreased the suppression of IL-6 production by lymphocytes when compared to the same group of 2D MSCs. Our results indicate the level of IL-10 production by activated lymphocytes was similar in both groups after the addition of TNF-α treated 3D-spheroid MSCs and 2D MSCs. Moreover, co-culturing of untreated 2D MSCs with lymphocytes decreased IL-10 production, which is consistent with previously published data [31]. However, data published by another group did not confirm this [21].

We observed from our results that MSCs cultured as 3D spheroids can have increased paracrine activity and effectively suppress T cells. The level of CD4 and CD8 T cells decreased under the influence of 3D-spheroid MSCs pretreated with TNF-α and IFN-γ separately as well as in combination as compared to 2D MSCs. It was reported that the mechanism of suppression of T cells by 2D MSCs preconditioned with the cytokine INF-γis mediated via JAK-STAT1 signaling, in which IDO, in particular, reduces the level of tryptophan required for T-cell proliferation, as demonstrated in a GVHD mouse model [32]. Our data showed a decrease in the level of CD8 T cells and an increase in Tregs in the group of 2D MSCs pretreated with TNF-α, as compared with untreated 2D MSCs, similar to other studies [33, 31]. Moreover, cytokine preconditioning of 3D-spheroid MSCs resulted in a decreased number of Tregs when compared to the same group of 2D MSCs. Previous studies have shown that MSCs isolated from different sources but preconditioned with the same cytokine, still have different effects on T-cell response [6,32].

MSCs cultured as 3D spheroids and preconditioned with cytokines can elevate their paracrine activity and effectively suppress macrophage functions [22]. According to our results, preconditioning with pro-inflammatory cytokines TNF-α and IFN-γ altered the immunomodulatory capacity of 3D-spheroid MSCs in co-cultures with activated macrophages as compared to non-treated 3D-spheroid MSCs. Preconditioning of 3D-spheroid MSCs with a single pro-inflammatory cytokine TNF-α increased the suppression of TNF-α and IL-6 secretion by macrophages compared to 2D MSCs, which was shown in our results. Moreover, preconditioning of 3D-spheroid MSCs with another pro-inflammatory cytokine

IFN-γ also increased the suppression of cytokine production, but only IL-6 by macrophages compared to 2D MSCs. Based on our data, preconditioning of 3D-spheroid MSCs with the combination of these cytokines also increased the suppression of IL-6 secretion by macrophages compared to 2D MSCs. Our data indicate that the level of TNF-α produced by macrophages decreased under the influence of cytokine-preconditioned 2D MSCs compared to untreated 2D MSCs, which is consistent with previously published data [34]. Moreover, 3D-spheroid MSCs preconditioned with TNF-α also reduced TNF-α production by macrophages. Similar results were reported by Zimmermann and colleagues [17]. Production of TNF-α and IL-6 by macrophages was low and IL-10 was high due to the effect of 3D MSCs, which is consistent with previously published data [28]. The authors concluded that MSCs activated by pro-inflammatory stimuli begin to secrete anti-inflammatory PGE2, which polarizes macrophages from type M1 (classically activated macrophages) to type M2 phenotype [28]. This ability of MSCs to polarize macrophage differentiation is one of the mechanisms of their contribution to the treatment of arthritis, sepsis and lesions of the cecum [28]. According to Ylostalo and colleagues, the polarization of macrophages from pro-inflammatory to anti-inflammatory phenotype by 3D-spheroid MSCs is mediated by PGE2 and NO-dependent mechanism [28].

Conclusion

The results of our investigations suggest that biological factors and micro-environmental conditions, including cytokine preconditioning and 3D spheroid culture, can regulate the production of anti-inflammatory mediators released by MSCs. It was noted that preconditioned MSCs had improved survival and possess promising potential in the treatment of myocardial infarction [35]. Previous studies suggest that cytokine preconditioned MSCs have an immunomodulatory and suppressive effect on lymphocytes and macrophages through mechanisms such as paracrine action, intercellular interaction and microenvironment [6,8,34,25,10]. Our data suggest that preconditioning with pro-inflammatory cytokines more effectively increases the immunomodulatory activity of 3D MSC spheroids compared to 2D MSC culture. Further work is required to elucidate the effect of cytokine-preconditioned 2D MSCs and 3D-spheroid MSCs in the *in vivo* studies.

Funding

This work was financially supported by the Ministry of Education and Science of the Republic of Kazakhstan (Grant no. AP0514447).

Acknowledgments

The authors thank Dr. Aidos Baumuratov and Aigul Kussanova (Core Facility of Nazarbayev University) for technical assistance in flow cytometry and confocal laser scanning microscopy.

References

1 Zhu H, Guo Z-K, Jiang X-X, Li H., et al. (2010) A protocol for isolation and culture of mesenchymal stem cells from mouse compact bone. Nature Protocols, vol. 5, no. 3, pp. 550-60. https://doi: 10.1038/nprot.2009.238.

2 Miceli V., Pampalone M., Vella S., Carreca A.P., et al. (2019) Comparison of immunosuppressive and angiogenic properties of human amnion-derived mesenchymal stem cells between 2D and 3D culture systems. Stem Cells Intern., pp. 7426279. https://doi: 10.1155/2019/7486279.

3 Ankrum J., Karp J.M. (2010) Mesenchymal stem cell therapy: Two steps forward, one step back. Trends in Mol Med., vol. 16, no. 5, pp. 203-9. https://doi: 10.1016/j.molmed.2010.02.005.

4 Leyendecker A. Jr., Gomes Pinheiro C.C., Amano M.T., Bueno D.F. (2018) The use of human mesenchymal stem cells as therapeutic agents for the in vivo treatment of immune-related diseases: a systematic review. Front in Immunol., no. 9, pp. 2056. https://doi: 10.3389/fimmu.2018.02056.

5 Gugliandolo A., Bramanti P., Mazzon E. (2020) Mesenchymal stem cells in multiple sclerosis: recent evidence from pre-clinical to clinical studies. Intern J of Mol Sci., vol. 21, no. 22, pp. 8662. https://doi: 10.3390/ijms21228662.

6 Saparov A., Ogay V., Nurgozhin T., Jumabay M., et al. (2016) Preconditioning of human mesenchymal stem cells to enhance their regulation of the immune response. Stem Cells Intern., pp. 3924858. https://doi: 10.1155/2016/3924858.

7 Baldari S., Di Rocco G., Piccoli M., Pozzobon M., et al. (2017) Challenges and strategies for improving the regenerative effects of mesenchymal stromal cell-based therapies. Intern J of Mol Sci., vol. 18, no. 10, pp. 2087. https://doi: 10.3390/ijms18102087.

8 Hu C., Li L. (2018) Preconditioning influences mesenchymal stem cell properties in vitro and in vivo. J of Cell and Mol Med., vol. 22, no. 3, pp. 1428-1442. https://doi: 10.1111/jcmm.13492.

9 Mansurov N., Chen W.C.W., Awada H., Huard J., et al. (2018) A controlled release system for simultaneous delivery of three human perivascular stem cell-derived factors for tissue repair and regeneration. J of Tiss Eng and Regen Med., vol. 12, no. 2, pp. e1164-e1172. https://doi: 10.1002/term.2451.

10 Noronha N., Mizukami A., Caliari-Oliveira C., Cominal J.G., et al. (2019) Priming approaches to improve the efficacy of mesenchymal stromal cell-based therapies. Stem Cell Res and Ther., no. 10, pp. 131. https://doi: 10.1186/s13287-019-1259-0.

11 Yu Y., Yo S.M., Park H.H., Baek S.Y., et al. (2019) Preconditioning with interleukin-1 beta and interferon-gamma enhances the efficacy of human umbilical cord blood-derived mesenchymal stem cells-based therapy via enhancing prostaglandin E2 secretion and indoleamine 2,3-dioxygenase activity in dextran sulfate sodium-induced colitis. J of Tiss Eng and Regen Med., vol. 13, no. 10, pp. 1792-1804. https://doi: 10.1002/term.2930.

12 Philipp D., Suhr L., Wahlers T., Choi Y-H, et al. (2018) Preconditioning of bone marrow-derived mesenchymal stem cells highly strengthens their potential to promote IL-6-dependent M2b polarization. Stem Cell Res and Therapy, no. 9, pp. 286. https://doi: 10.1186/s13287-018-1039-2.

13 Francois M., Romieu-Mourez R., Li M., Galipeau J. (2012) Human MSC suppression correlates with cytokine induction of indoleamine 2,3-dioxygenase and bystander M2 macrophage differentiation. Mol Ther., vol. 20, no. 1, pp. 187-95. https://doi: 10.1038/mt.2011.189.

14 Ren G., Zhang L., Zhao X., Xu G., et al. (2008) Mesenchymal stem cell-mediated immunosuppression occurs via concerted action of chemokines and nitric oxide. Cell Stem Cell, vol. 2, no. 2, pp. 141-50. https://doi: 10.1016/j.stem.2007.11.014.

15 Petrenko Y., Sykova E., Kubinova S. (2017) The therapeutic potential of three-dimensional multipotent mesenchymal stromal cell spheroids. Stem Cell Res and Ther., vol. 8, no. 1, pp. 94. https://doi: 10.1186/s13287-017-0558-6.

16 Bartosh T.J., Ylostalo J.H. (2019) Efficacy of 3D culture priming is maintained in human mesenchymal stem cells after extensive expansion of the cells. Cells, vol. 8, no. 9, pp. 1031. https://doi: 10.1002/9780470151808.sc02b06s28.

17 Zimmermann J.A, McDevitt T.C. (2014) Preconditioning mesenchymal stromal cell spheroids for immunomodulatory paracrine factor secretion. Cytother., vol. 16, no. 3, pp. 331-45. https://doi: 10.1016/j.jcyt.2013.09.004.

18 Protocols and Applications (accessed on June 18, 2021). 3D cell culture handbook. Thermofisher website. https://assets.thermofisher.com/TFS-Assets/BID/Handbooks/3d-cell-culture-handbook.pdf.

19 Sekenova A.Y., Rakhymzhanova A.K., Li E.A., Ogay V.B. (2019) Generation of three-dimensional spheroids from mouse mesenchymal stem cell. Euras J of Appl Biotech., no, 2, pp. 41–50.

20 Prockop D.J., Phinney D.G., Bunnell B.A. (2008) Methods and protocols. Preface. Methods in Molbiol. (Clifton, NJ), no. 449, pp. v-vii. PubMed PMID: MEDLINE:18453071.

21 Lin T.H., Pajarinen J., Nabeshima A., Lu L., et al. (2017) Preconditioning of murine mesenchymal stem cells synergistically enhanced immunomodulation and osteogenesis. Stem Cell Res and Ther., vol. 8, no. 1, pp. 277. https://doi: 10.1186/s13287-017-0730-z.

22 Sivanathan K.N., Gronthos S., Grey S.T., Rojas-Canales D., et al (2017). Immunodepletion and hypoxia preconditioning of mouse compact bone cells as a novel protocol to isolate highly immunosuppressive mesenchymal stem cells. Stem Cells and Devel., vol. 26, no. 7, pp. 512-527. https://doi: 10.1089/scd.2016.0180.

23 Yan L., Zheng D., Xu R-H. (2018) Critical Role of tumor necrosis factor signaling in mesenchymal stem cell-based therapy for autoimmune and inflammatory diseases. Front in Immunol., no. 9, pp. 1658. https://doi: 10.3389/fimmu.2018.01658.

24 Frodermann V., Duijn J. van, Pel M. van, van Santbrink P.J., et al. (2015) Mesenchymal stem cells reduce murine atherosclerosis development. Scient Rep., no. 5, pp. 15559. https://doi: 10.3389/fimmu.2018.01658.

25 Ogay V.B., Sekenova A.Y. (2019) Precondicionirovaniye kak novyi sposob povisheniya terapevticheskoy effektivnosti mezenchimalnuyh stvolovyuh kletok. [Preconditioning as a new method of the enhancement of the therapeutic effectiveness of mesenchymal stem cells]. Aktual'n bioteh., vol. 3, no. 30, pp. 423-424.

26 Ylostalo J.H., Bazhanov N., Mohammadipoor A., Bartosh T.J. (2017) Production and administration of therapeutic mesenchymal stem/stromal cell (MSC) spheroids primed in 3-D cultures under xeno-free conditions. J of Visual Exper., no. 121, pp. 55126. https://doi: 10.3791/55126.

27 Ferreira J.R., Teixeira G.Q., Santos S.G., Barbosa M.A., et al. (2018) Mesenchymal stro-

mal cell secretome: influencing therapeutic potential by cellular pre-conditioning. Front in Immunol., no. 9, pp. 2837. https://doi: 10.3389/fimmu.2018.02837.

28 Ylostalo J.H., Bartosh T.J., Coble K, Prockop DJ. (2012) Human mesenchymal stem/stromal cells cultured as spheroids are self-activated to produce prostaglandin E2 that directs stimulated macrophages into an anti-inflammatory phenotype. Stem Cells., vol. 30, no. 10, pp. 2283-96. https://doi: 10.1002/stem.1191.

29 Oishi Y., Manabe I.. (2018) Macrophages in inflammation, repair and regeneration. Intern Immunol., vol. 30, no. 11, pp. 511-528. https://doi: 10.1093/intimm/dxy054.

30 Wang A.Y.L., Loh C.Y.Y., Shen H-H, Hsieh S-Y, et al. (2020) Human wharton's jelly mesenchymal stem cell-mediated sciatic nerve recovery is associated with the upregulation of regulatory T cells. Intern J of Mol Sci., vol. 21, no.17, pp. 6310. https://doi: 10.3390/ijms21176310.

31 Molendijk I., Barnhoorn M.C., de Jonge-Muller E.S.M., Mieremet-Ooms M.A.C., et al. (2016) Intraluminal injection of mesenchymal stromal cells in spheroids attenuates experimental colitis. J of Crohn's and Colitis., vol. 10, no. 8, pp. 953-64. https://doi: 10.1093/ecco-jcc/jjw047.

32 Kim D.S., Jang I.K., Lee M.W., Ko Y.J., et. el. (2018) Enhanced immunosuppressive properties of human mesenchymal stem cells primed by interferon-gamma. EBio Med., no. 28, pp. 261-73. https://doi: 10.1016/j.ebiom.2018.01.002.

33 Li H., Wang W., Wang G., Hou Y., et al. (2015) Interferon-gamma and tumor necrosis factor-alpha promote the ability of human placenta-derived mesenchymal stromal cells to express programmed death ligand-2 and induce the differentiation of CD4(+) interleukin-10(+) and CD8(+) interleukin-10 (+)Treg subsets. Cytother., vol. 17, no. 11, pp. 1560-71. https://doi: 10.1016/j.jcyt.2015.07.018.

34 Saeedi P., Halabian R., Imani Fooladi A.A. (2019) A revealing review of mesenchymal stem cells therapy, clinical perspectives and modification strategies. Stem Cell Investig., no. 6, pp. 34. https://doi: 10.21037/sci.2019.08.11.

35 Raziyeva K., Smagulova A., Kim Y., Smagul S., et al. (2020) Preconditioned and genetically modified stem cells for myocardial infarction treatment. Intern J of Mol Sci., vol. 21, no. 19, pp. 7301. https://doi: 10.3390/ijms21197301.

IRSTI 68.35.47 https://doi.org/10.26577/ijbch.2021.v14.i2.05

D. Jabborova[1*], T. Bozorov[1], L. Li[2], A. Kistaubayeva[3], D. Egamberdieva[4]

[1] Institute of Genetics and Plant Experimental Biology, Academy of Sciences of Uzbekistan, Tashkent, Uzbekistan
[2]Xinjiang Institute of Ecology and Geography, Chinese Academy of Sciences, Urumqi, China
[3]Al-Farabi Kazakh National University, Almaty, Kazakhstan
[4]Leibniz Centre for Agricultural Landscape Research (ZALF), Müncheberg, Germany
*e-mail: dilfuzajabborova@yahoo.com

Identification and characterization of endophytic bacteria isolated from root nodules of lentil (*Lens culinaris* L.) grown on saline soils

Abstract. In this study the endophytic bacteria from the root nodules of lentil (*Lens culinaris* L.) grown on saline soils were isolated and their beneficial properties for plants were characterized. A total of 12 isolates were isolated from nodules and four isolates (L2, L6, L9, L10) were able to produce lipase, protease and cellulose enzymes. All bacterial isolates were positive to glucanase activity. Eleven isolates did not show antagonistic activity against fungal strains *Fusarium (F.) oxysporum*, *F. equiseti* and *Verticillium (V.) dahliae*. One isolate (L10) appeared to have the highest antifungal activity against *F. oxysporum*, *F. equiset* and *V. dahlia*. The effect of bacterial isolates of plant growth promoting rhizobacteria (PGPR) on root and shoot growth of lentils were studied in pot experiments. The result revealed that among twelve isolates only five bacteria (L2, L4, L5, L9 and L10) increased significantly the fresh weight of lentil. The 16S rRNA sequencing data showed that five bacterial isolates, which showed the positive effect on plant growth, belong to *Bacillus (B.) subtilis* L2, *Rhizobium* sp. L4, *Enterobacter tabaci* L4, *B. cereus* L9, and *B. velezensis* L10. They can possibly be suggested as microbial inoculants for lentil under saline soil conditions. Among bacterial isolates *B. velezensis* L10 could be used as a biological control agent to protect lentil from fungal pathogens.
Key words: nitrogen fixation, plant growth promoting rhizobacteria (PGPR), phosphate solubilization, siderophore production, 16S rRNA.

Introduction

Lentil is an important pulse crop and plays major role both in human and animal feeding as a protein source, fiber, and various minerals, such as iron and zinc. It is grown worldwide in Europe, North America, and Asian regions, and its production reached 6.3 million tons in a 6.1 million ha area across more than 50 countries in 2018 [1,2]. Endophytes living inside the plant cells are essential for them [3,4]. There are many reports indicating beneficial effects of endophytes, such as *Rhizobium*, *Bacillus*, *Pseudomonas*, *Stenotrophomonas* as well as others [5-7]. Endophytes promote plant growth [8,9], tolerance to abiotic stresses [10], and control plant pathogens [11,12]. Several reports have shown that rhizobia inoculants improved nodulation, nitrogenase activity, plant biomass and productivity [13,14]. They stimulate the production of phytohormones like auxins and gibberellins [15-17], production of low molecular weight organic acids and exopolysaccharides [18], 1-aminocyclopropane-1-carboxylate (ACC) deaminase [19,20], antagonism against phytopathogens [21] and synthesizing cell wall degrading enzymes, including pectinase, β-1,3-glucanase, and chitinase [22]. Several endophytic bacteria were isolated from chickpea grown on saline soils and identified as *B. cereus* NUU1, *Achromobacter xylosoxidans* NUU2, *B. thuringiensis* NUU3, and *B. subtilis* NUU4 [23]. They were able to produce phytohormones, cell wall degrading enzymes, hydrogen cyanide, and stimulated plant growth of chickpea under the salt stress [23].

We aim to isolate endophytic bacteria from the nodules of lentil (*Lens culinaris* L.) grown on saline soils and examine their beneficial properties for plants growing in saline conditions. This will improve our understanding of diversity of microorganisms associated with leguminous plants and their interaction with host plants under extreme conditions

This paper reports the results of the first isolation of endophytic bacteria from a lentil grown in extreme environment.

Materials and methods

Isolation of endophytic bacteria. Four lentil plants were collected from salt affected lands in Syrdarya region, Uzbekistan (41000′N, 64000′E) in July 2018. For the last 50-60 years, the soils have been cropped to cotton monoculture under flood irrigation without proper drainage facilities using the natural flow system and soil electrical conductivity is 5.6±0.6 dS m^{-1}. Plant samples were transferred to laboratory in plastic seal bags and stored at +4 °C. A total of 10 healthy and undamaged root nodules were collected from lentil plants. The nodules were washed under tap water to remove soil particles, surface sterilized in 5% sodium hypochlorite solution for 5 min and washed 5–6 times in sterile distilled water. Surface sterilized nodules were crushed as described by Muthini et al. [24], and loopful of suspension plated onto Yeast Extract Mannitol Agar (YEMA). The plates were incubated in the dark at 28 °C for 3–5 days. A total of 12 bacterial isolates were obtained and stored in the nutrient broth with 20% glycerol at 80 °C.

DNA extraction from cultured bacteria and sequencing. Bacterial colonies were selected at random and incubated in 3 mL Luria-Bertani Broth (10 g/L Bacto Tryptone (Oxoid, Canada), 5 g/L Bacto-Yeast Extract (Oxoid, Canada), 5 g/L NaCl, pH 7.0) on a rotary shaker at 250 rpm at 28 °C overnight. Suspensions were centrifuged at 8,000 rpm for 1 min and bacterial pellets were treated with proteinase K. Bacterial DNA was extracted using a TIANamp Bacteria DNA Kit (Tiangen, China) according to the manufacturer protocol. DNA was diluted based on concentration and used for polymerase chain reaction (PCR) on a Veriti™ thermal cycler (Applied Biosystems, USA). Forward primer 27F 5'-AGAGTTTGATCATGGCTCAG-3' and reverse primer 1492R 5'-TACGGCTACCTTGTTACGACTT-3' were used for PCR amplification. Briefly, in a total volume of 50 µL containing 10 µL of PrimeSTAR HS (Premix) (Takara, Japan) containing an appropriate concentration of dNTPs (0.2 mM) and Taq polymerase (5 U), 1 µL (0.2 µM) of each primer, and 2 µL of diluted DNA. The PCR conditions included 5 min at 95 °C for the initial step followed by 35 cycles at 94 °C for 15 s (denaturation), 55 °C for 30 s (annealing), and 72 °C for 2 min (elongation), with a final extension at 72 °C for 10 min. PCR products were visualized on a 1.5% agarose gel. PCR products were triplicated and sent to Quintara Biosicences (China) for further purification and Sanger sequencing. SeqMan (in a LaserGene software version 7.0 (DNAStar, Madison, WI, USA) was used for assembling the sequences. Sequences of approximately 1400 bp were compared with other 16S RNAs deposited in GenBank nucleotide collection using the NCBI BLAST algorithm. Alignment of sequences obtained by Sanger method and retrieved bacterial sequences was performed using the ClustalW algorithm of the AlignX program of the Vector NTI software. A phylogenetic tree was constructed based on the UPGMA algorithm following the Kimura's two-parameter method with 1,000 bootstrap replicates in MEGA7 [25].

Cell wall degrading enzymes. Confirmation of cellulose-degrading ability of bacterial isolates was performed by streaking on the cellulose Congo-Red agar media with the following composition: KH_2PO_4 0.5 g, $MgSO_4$ 0.25 g, cellulose 2 g, agar 15 g, Congo-Red 0.2 g, and gelatin 2 g; distilled water 1 L and at pH 6.8–7.2. Clearance halos around and beneath the colony were observed around the bacterial colonies indicating the enzymatic degradation of cellulose [26].

Protease enzyme assay was performed on sterile skim milk agar plates (with Pancreatic digest of casein 5.0, Yeast extract 2.5, Glucose 1.0, Agar 15.0, Distilled water 1000 mL, Skim milk 7% added as inducer). Isolates were spot inoculated and incubated at 30 °C; appearance of clearance zone around the colony indicated the enzymatic degradation of protease.

For determination of lipase enzyme, the following medium was used: peptone 10 g, calcium chloride 0.1 g, sodium chloride 5 g, agar 15 g, distilled water 1 L, 10 mL sterile Tween 20. All bacterial isolates were streaked on this medium and incubated at 27 °C for 48 h. Depositions around the bacterial colonies indicated lipase activity.

Antagonistic activity against plant pathogenic fungi. The bacterial isolates were tested *in vitro* to select those with inhibitory effects against *Fusarium oxysporum, Fusarium equiseti*, *Eurotium heterocaryoticum, Verticillium dahlia,* and *Thorybes diversus* using a plate with ISP2 agar. Fungal strains were grown on agar at 28ºC for 5 days. Antifungal activity was recorded as the width of the zone of growth inhibition between the fungus and examined bacteria. All samples were tested in triplicate.

Production of indole-3-acetic acid. The production of indole 3-acetic acid (IAA) was determined according to the method of Bano and Musarrat [27]. Bacterial isolates were grown on LC medium with and without tryptophan (500 µl/ml) and incubated at 28 °C. After 3 days of cultivation, aliquots of bacterial cultures were centrifuged at 13,000 g for 10 min.

1 mL of supernatant was transferred to a fresh tube to which 100 µl of 10 mM orthophosphoric acid and 2 mL of reagent (1 ml of 0.5 M $FeCl_3$ in 50 ml of 35% $HClO_4$) were added. After 25 min, the absorbance of the developed pink color was read at 530 nm. The IAA concentration in culture was calculated using a calibration curve of pure IAA as a standard.

Plant growth promotion assay. Lentil (*Lens culinaris* L.) seeds were used for plant growth experiments. Seeds were sorted to eliminate broken, small and infected seeds and sterilized for washing in 95% ethanol for 15 min and 10% sodium hypochlorite (NaOCl) for 5 min. Strains were used for inoculation of sterile seeds. 1 mL of each culture were pelleted by centrifugation and cell pellets were washed with 1 ml phosphate buffered saline (PBS; 20 mM sodium phosphate, 150 mM NaCl, pH 7.4) and resuspended into PBS. The suspension was used for the inoculation was adjusted to the final concentration of approximately 10^8 cells/mL. Uniform seeds were first placed with sterile forceps into bacterial suspension for 10 minutes and then were cultivated into plastic pots of soil. Plants were grown for 30 days. At harvest, after 30 days, plant height, root length, root dry weight, shoot dry weight and nodule number will be determined.

Statistical analysis. StatView® Software issued by SAS Institute Inc., USA was used to perform Fisher's LSD test following ANOVA.

Results and discussion

Production of cell wall degrading enzymes. In the present study, we studied twelve endophytic bacteria isolated from root nodules of lentil grown in saline soils. The results of lipase, protease and cellulase activity assays revealed that eight isolates did not produce lipase, protease or cellulase enzymes. Five isolates were able to produce protease and cellulase enzymes. The maximum production of lipase by *B. cereus* isolate L9 was equivalent to 32 mm (Table 1).

Table 1 – Overview of the production cell wall degrading enzymes by isolated bacteria

Bacterial isolates	Enzymes					IAA
	Lipase[a]	Protease[b]	Cellulase[c]	Xylanase	Glucanase	
Rhizobium sp. L1	-	-	-	-	+	-
Bacillus subtilis L2	26	18	32	-	+	+
Bacillus cereus L3	-	16	12	-	+	-
Enterobacter tabaci L4	-	-	-	+	+	-
Rhizobium sp. L5	-	-	-	-	+	+
Bacillus subtilis L6	30	16	24	-	+	-
Rhizobium sp. L7	-	-	-	-	+	-
Rhizobium sp. L8	-	-	-	-	+	-
Bacillus cereus L9	32	22	15	-	+	-
Bacillus velezensis L10	25	23	30	-	+	+
Rhizobium sp. L11	-	-	-	-	+	-
Rhizobium sp. L12	-	-	-	-	+	-

Note: [a, b, c] – enzyme activity assessed by the width of zone of growth inhibition (mm); "-" – negative, "+" – positive

As can be seen from the Table 1, *B. subtilis* isolate L2 produced the highest amount of cellulase enzyme compared to other isolates, while *B. velezensis* isolate L10 showed a maximum protease activity. Most of isolates did not show xylanase activities. Only bacterial isolate L4 produced the highest amount of xylanase and glucanase. About 8% of the isolates showed high, 25% medium and 58% low ability in producing glucanase. Li et al. [9] have also shown that among lipase producing bacteria *Bacillus* species produced the highest amount of lipase. Cell wall-degrading enzymes are key factors on biological control of plant pathogens by plant associated bacteria, therefore they might be promising candidates for the biological control agents.

The bacterial isolates L2, L5 and L10 appeared to produce IAA in media containing 1.5% NaCl (Table 1). Plant hormones play an important role in processes of plant physiology, including seed germination, root formation, root elongation, and blossom formation. IAA is the most abundant naturally occurring auxin with a well-documented ability to regulate many aspects of plant development [28,29].

Antifungal activity of entophytic bacteria against fungal strains. Plants are more susceptible to plant fungal pathogens, such as *Fusarium*, *Verticillum*, *Rhizoctonia*, under abiotic stress conditions. Root associated beneficial microbes with antifungal activity are able to control plant fungal diseases [30,31]. In our study eleven isolates did not show antagonistic activity against fungal strains *F. oxysporum, F. equiseti* and *V. dahlia*. Only B. *velezensis* isolate L10 displayed antimicrobial activity against fungal strains *F. oxysporum, F. equiseti* and *V. dahlia* except *E. heterocaryoticum.* Similar works have been reported in other studies, where plant associated endophytic bacteria *B. xiamenensis* isolated from the sugarcane rhizosphere showed strong antagonistic activity against fungal pathogens *Colletotrichum falcatum*, *F. oxysporum*, *F. moniliforme*, *Rhizoctonia solani*, *Macrophomina phaseolina* and *Pythium splendens*. The bacterial isolates were able to control sugarcane red rot and enhanced plant growth in saline conditions [32].

Evaluation of plant growth promoting ability of endophytic bacteria. In the present study seed inoculation with entophytic bacteria enhanced various growth parameters of lentil, including plant height, root length, root dry weight, shoot dry weight and nodule number of lentil (Figure 1). Significant increase in root length was observed with *Rhizobium* sp. L12 (76%), *Rhizobium* sp. L5 (59%), Enterobacter tabaci L4 (56%) *Rhizobium* sp. L1 (52%), *B. subtilis* L2 (41%), *Rhizobium* sp. L11 (40%), *Rhizobium* sp. L5 (39%) and *B. subtilis* L6 (35%) over control. Maximum rises in fresh weight of shoot were recorded with *B. velezensis* L10 (56%), *B.* cereus L9 (34%), *Rhizobium* sp. L5 (30%) and *Enterobacter tabaci* L4 (30%).

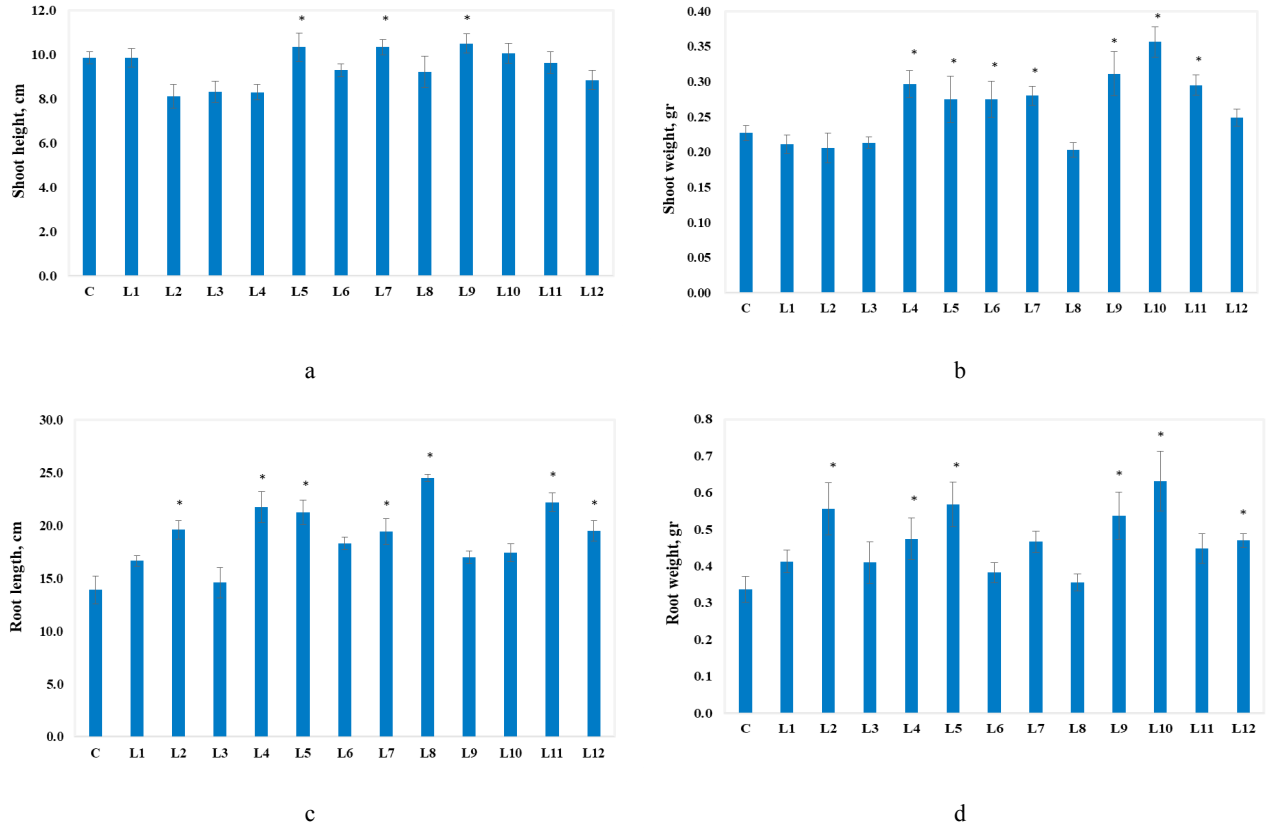

Figure 1 – Effect of endophytic bacteria on the plant height (A), plant length (B), shoot weight (C), and root weight (D). Plants were grown for 30 days under greenhouse conditions

The fresh weight of root significantly increases to 85%, 68%, 65%, 59%, 38, 38 and 38% when inoculated with *B. velezensis* L10, *Rhizobium* sp. L7, *B. subtilis* L2, *B. cereus* L9, *Rhizobium* sp. L1, *Rhizobium* sp. L8 and *Enterobacter tabaci* L4 compared to uninoculated control. Inoculation of lentil with *Rhizobium* sp. L12, *Rhizobium* sp. L11, *Rhizobium* sp. L7 and *Rhizobium* sp. L5 significantly increased the number of nodules compared to inoculation with *Rhizobium* sp. L1 and *Rhizobium* sp. L8. *Rhizobium* sp. L12 had a positive significant effect on the number of nodules per plant that the maximum the number of nodules per plant by 43 nodules that the number of nodules per plant increased by 43% as compared to Rhizobium sp. L1. Similar results were obtained by Raza et al. [33] in mungbean. *Rhizobium* sp. L5 improved nodule number in lentil. Similar findings were reported for chickpea [34], soybean [35] and mungbean [36]. An increased root and shoot biomass, nodule formation by rhizobial bacteria synthesizing auxins, cytokinins and abscisic acids were observed.

Molecular characterization identification of entophytic bacteria. The bacterial endophytes were identified by 16S rRNA gene sequence (Table 2, Figure 2). According 16S rRNA sequencing data, bacterial isolates L1, L5, L7, L8, L11 and L12 showed 99.93% similarity with the *Rhizobium* sp. The isolates L2, and L6 showed 100% similarity with *Bacillus subtilis* respectively. The isolate L10 showed 99.7% similarity with *B. velezensis*. L3 and L9 isolates showed 100% similarity with *Bacillus cereus*. The isolates L2 and L6 showed 100% similarity with *B. subtilis*, respectively. L4 isolate showed 99.30% similarity with *Enterobacter tabaci*.

Among isolates we also identified siblings, thus considered in further experiments. Species from genera, such as *Rhizobium*, *Bacillus* and *Enterobacter* have already isolated from legumes in several studies [37,38].

Table 2 – Bacteria isolated from lentil plants identified by 16S rRNA sequence analysis

isolate	Genus	Predicted species	Similarity (%)	GenBank accession
L10	*Bacillus*	*B. velezensis* strain FZB42	99.79%	NR_075005.2
	Bacillus	*B. amyloliquefaciens* strain NBRC 15535	99.72%	NR_041455.1
L2, L6	*Bacillus*	*B. subtilis* strain JCM 1465	100.00%	NR_113265.1
	Bacillus	*B. tequilensis* strain 10b	99.79%	NR_104919.1
L3, L 9	*Bacillus*	*B. cereus* ATCC 14579	100.00%	NR_074540.1
	Bacillus	*B. proteolyticus* strain MCCC 1A00365	99.93%	NR_157735.1
	Bacillus	*B. albus* strain MCCC 1A02146	99.93%	NR_157729.1
L4	*Enterobacter*	*E. tabaci* strain YIM Hb-3	99.30%	NR_146667.2
	Enterobacter	*E. asburiae* strain JCM6051	99.22%	NR_024640.1
L1,5,7,12	*Rhizobium*	*Rh. indigoferae* strain CCBAU 71042	99.93%	NR_115124.1
	Rhizobium	*Rh. laguerreae* strain FB206	99.93%	NR_118274.1
	Rhizobium	*Rh. leguminosarum* strain LMG 14904	99.93%	NR_114989.1
	Rhizobium	*Rh. indigoferae* strain CCBAU 71042	99.93%	NR_115124.1
L8, L11	*Rhizobium*	*Rh. laguerreae* strain FB206	99.93%	NR_118274.1
	Rhizobium	*Rh. leguminosarum* strain LMG 14904	99.93%	NR_114989.1

In previous work, the endophytic bacteria isolated from chickpea nodules with antagonistic activity against *F. solani* identified as *Bacillus cereus, Achromobacter xylosoxidans*, *B. thuringiensis*, and *B. subtilis*. They also demonstrated significant plant growth stimulating abilities under hostile environmental condition [39]. Other reports also confirmed that endophytic bacteria Bacillus subtilis isolated from leguminous plant stimulated root and shoot growth, nodulation and nutrient uptake of *Acacia gerrardii* under salt stress [40].

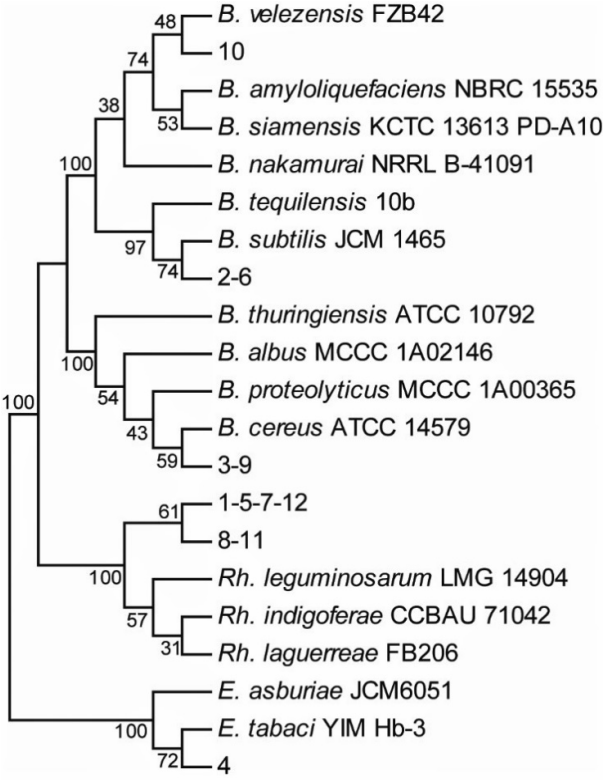

Figure 2 – Neighbor-joining phylogenetic tree based on 16S rRNA gene sequences isolated from endophytic bacteria of lentil (*Lens culinaris* L.), showing the relationship of isolated strains to their closest relatives in GenBank

Conclusion

In this study, we revealed the diversity of cultivable endophytic bacteria isolated from the nodules of lentil grown on saline soils of Uzbekistan. It is a first report on the characterization of endophytic bacteria identified as *Rhizobium* spp., *B. subtilis, B. cereus*, *B. velezensis* and *Enterobacter tabaci*. The endophytic bacteria produce phytohormone indole 3-acetic acid, and stimulated root and shoot growth lentil under saline soil. Among bacterial isolates *B. velezensis* L10 could be used as a biological control agent to protect lentil from fungal pathogens. Our findings suggest that plants grown in salt affected soils could be a source for the selection of microbes with antagonistic activity against plant fungal pathogens, and plant growth stimulators and might be considered as promising candidates for the improvement of plant health under saline soil conditions. However, these findings also show that further research is required in field experiments to confirm their plant beneficial effect under natural environmental conditions.

Funding

Research was supported by CPEA-LT-2016/10095 grant from the Eurasia program of the Norwegian Centre for Cooperation in Education and by the President of Chinese Academy of Sciences International Fellowship Initiative (Grant No. 2018VBA002S), both to Dilfuza Egamberdieva.

References

1 Urbano G., Porres J.M., Frias J., Vidal-Valverde C. (2007) Nutritional value. In: Yadav S S, McNeil, D L, Stevenson P C, eds., Lentil: An Ancient Crop for Modern Times. Springer, The Netherlands. pp. 47-93.

2 Cokkizgin A., Shtaya M.J.Y. (2013) Lentil: origin, cultivation techniques, utilization and advanced in transformation. Agricultural Sciences, 1(1), pp. 55-62.

3 Egamberdieva D., Berg G., Lindström K., Räsänen L.A. (2013) Alleviation of salt stress of symbiotic Galega officinalis L. (goat's rue) by co-inoculation of rhizobium with root colonising Pseudomonas. Plant Soil, 369(1), pp. 453-465. DOI:10.1007/s11104-013-1586-3

4 Yadegari M., Rahmani H.A. (2010) Evaluation of bean (Phaseolus vulgaris) seeds' inoculation with Rhizobium phaseoli and plant growth promoting Rhizobacteria (PGPR) on yield and yield components. Afr J Agric Res., vol. 5(9), pp. 792-799.

5 Egamberdieva D., Wirth S., Jabborova D., Räsänen L., Liao H. (2017) Coordination between Bradyrhizobium and Pseudomonas alleviates salt stress in soybean through altering root system architecture. J. Plant Interactions, vol. 12, pp. 100-107. DOI:10.1080/17429145.2017.1294212

6 Egamberdieva D., Jabborova D., Wirth S. (2013) Alleviation of salt stress in legumes by co-inoculation with Pseudomonas and Rhizobium. In: Arora N. (eds.) Plant Microbe Symbiosis: Fundamentals and Advances. Springer, New Delhi. DOI:10.1007/978-81-322-1287-4_11

7 Egamberdieva D., Jabborova D., Hashem A. (2015) Pseudomonas induces salinity tolerance in cotton (Gossypium hirsutum) and resistance to Fusarium root rot through the modulation of indole-3-acetic acid. Saudi J. Biol Sciences, vol. 22(6), pp. 773-779. DOI: 10.1016/j.sjbs.2015.04.019

8 Liu Y., Guo J., Li L., Asem M.D., Zhang Y. et al. (2017) Endophytic bacteria associated with endangered plant Ferula sinkiangensis KM Shen in

an arid land: diversity and plant growth-promoting traits. Journal of Arid Land, vol. 9(3), pp. 432-445. DOI: 10.1007/s40333-017-0015-5

9 Li L., Mohamad O.A.A., Ma J., Friel A.D. et al. (2018) Synergistic plant–microbe interactions between endophytic bacterial communities and the medicinal plant Glycyrrhiza uralensis F. Antonie van Leeuwenhoek, vol. 111, pp. 1735–1748. DOI: 10.1007/s10482-018-1062-4

10 Ahmad M., Zahir Z.A., Asghar H.N., Arshad M. (2012) The combined application of rhizobial strains and plant growth promoting rhizobacteria improves growth and productivity of mung bean (Vigna radiata L.) under salt-stressed conditions. Annals of Microbiology, vol. 62, pp. 1321–1330. DOI: 10.1007/s13213-011-0380-9

11 Gond S.K., Bergen M., Torres M.S., White J.F. (2015) E□ect of bacterial endophyte on expression of defense genes in Indian popcorn against Fusarium moniliforme. Symbiosis, vol. 66, pp. 133-140. DOI:10.1007/s13199-015-0348-9

12 Soares M.A., Li H., Bergen M., White J.F. (2015) Functional role of an endophytic Bacillus amyloliquefaciens in enhancing growth and disease protection of invasive english ivy (Hedera helix L.). Plant Soil, vol. 405, pp. 107-123. DOI:10.1007/s11104-015-2638-7

13 Kashem M.A., Mian M.H., Rahman M.F. (2000) Effect of Bradyrhizobium on the yield of mungbean (Vigna radiata L.) grown in Ganges tidal floodplain soil. J Agric Res, vol. 38, p. 407.

14 Youseif S.H., Abd El-Megeed F.H., Saleh S.A. (2017) Improvement of faba bean yield using rhizobium/agrobacterium inoculant in low-fertility sandy soil. Agronomy, vol. 7(1), pp. 1-12. DOI:10.3390/agronomy7010002

15 Egamberdieva D. (2012a). Pseudomonas chlororaphis: A salt tolerant bacterial inoculant for plant growth stimulation under saline soil conditions. Acta Physiologiae Plantarum, vol. 34, pp. 751-756.

16 Egamberdieva D. (2012b) Colonisation of Mycobacterium phlei in the rhizosphere of wheat grown under saline condition. Turkish J. Biology, vol. 36, pp. 487-492.

17 Liu Y., Mohamad O.A.A., Salam N. et al. (2019) Diversity, community distribution and growth promotion activities of endophytes associated with halophyte Lycium ruthenicum Murr. 3 Biotech, vol. 9, p. 144. DOI:10.1007/s13205-019-1678-8

18 Naseem H., Ahsan M., Shahid M.A., Khan N. (2018) Exopolysaccharides producing rhizobacteria and their role in plant growth and drought tolerance. J Basic Microbiol, vol. 58(12), pp. 1009-1022. DOI: 10.1371/journal.pone.0222302

19 Glick B.R. (2014) Bacteria with ACC deaminase can promote plant growth and help to feed the world. Microbiol Res., vol. 169, pp. 30–39. DOI:10.1016/j.micres.2013.09.009

20 Egamberdieva D,, Kucharova Z,, Davranov K, et al. (2011) Bacteria able to control foot and root rot and to promote growth of cucumber in salinated soils. Biol Fertil Soils, vol. 47, pp. 197-205. DOI:10.1007/s00374-010-0523-3

21 Abdullah A.S., Moffat C.S., Lopez□Ruiz F.J., et al. (2017) Host–multi–pathogen warfare: pathogen interactions in coinfected plants. Front Plant Sci, vol. 8, pp. 1-12, DOI:10.3389/fpls.2017.01806

22 Cho S.T., Chang H.H., Egamberdieva D., et al. (2015) Genome analysis of Pseudomonas fluorescens PCL1751: a rhizobacterium that controls root diseases and alleviates salt stress for its plant host. PLOS One, vol. 10(10): e0140231. DOI:10.1371/journal.pone.0140231

23 Egamberdieva D., Wirth S., Shurigin V., Hashem A., Abd_Allah E.F. (2017) Endophytic bacteria improve plant growth, symbiotic performance of chickpea (Cicer arietinum L.) and induce suppression of root rot caused by Fusarium solani under salt stress. Front Microbiol,vol. 28(8), 1887. DOI:10.3389/fmicb.2017.01887.

24 Muthini M., Maingi J.M., Muoma J.O., Amoding A., Mukaminega D., Osoro N. et al. (2014) Morphological assessment and effectiveness of indigenous rhizobia isolates that modulate P. vulgaris in water hyacinth compost testing field in Lake Victoria basin. British Journal of Applied Science & Technology, vol. 4(5), pp.718-738.

25 Kumar A., Singh R., Yadav A., Giri D.D., Singh P.K., Pandey K.D. (2016) Isolation and characterization of bacterial endophytes of Curcuma longa L. 3 Biotech, vol. 6(60), pp. 1-8. DOI: 10.1007/s13205-016-0393-y

26 Gupta P., Samant K., Sahu A. (2012) Isolation of cellulose-degrading bacteria and determination of their cellulolytic potential. Int. J. Microbiology, pp. 1-5. DOI:10.1155/2012/578925

27 Bano N., Musarrat J. (2003) Characterization of a new Pseudomonas aeruginosa strain NJ-15 as a potential biocontrol agent. Curent microbiology, vol. 46, pp. 324–328, DOI: 10.1007/s00284-002-3857-8

28 Egamberdiyeva D., Hoflich G. (2002) Root colonization and growth promotion of winter wheat and pea by Cellulomonas spp. at different temperatures. J. Plant Growth Regulation, vol. 38, pp. 219-224. DOI:10.1023/A:1021538226573

29 Egamberdiyeva D., Hoflich G. (2003) Influence of growth promoting bacteria on the growth of wheat at different soils and temperatures. Soil Biol. Biochem,vol. 35, pp. 973-978, DOI:10.1016/S0038-0717(03)00158-5

30 Deketelaere S., Tyvaert L, França S.C. et al. (2017) Desirable traits of a good biocontrol agent against Verticillium wilt. Front Microbiol, vol. 8, pp. 1-23. DOI: 10.3389/fmicb.2017.01186

31 Egamberdieva D., Kamilova F., Validov S., Gafurova L, Kucharova Z, Lugtenberg B. (2008) High incidence of plant growth-stimulating bacteria associated with the rhizosphere of wheat grown in salinated soil in Uzbekistan. Environ. Microbiology, vol. 19, pp. 1-9, DOI:10.1111/j.1462-2920.2007.01424.x

32 Amna Xi.Y., Farooq M.A., Javed N.T. (2020) Multi-stress tolerant PGPR Bacillus xiamenensis PM14 activating sugarcane (Saccharum officinarum L.) red rot disease resistance. Plant Physiol Biochem, vol. 151, pp. 640-649.

33 Raza W., Akhtar M, Arshad M., Yousaf S. (2004) Growth, nodulation and yield of mungbean (Vigna radiata L.) as influenced by coinoculation with rhizobium and plant growth promoting rhizobacteria. Pakistan J. Agricultural Sciences, vol. 41(3-4), pp.125-130.

34 Ben Romdhane S., Tajini F., Trabelsi M., Aouani M., Mhamdi R. (2007) Competition for nodule formation between introduced strains of Mesorhizobium ciceri and the native populations of rhizobia nodulating chickpea (Cicer arietinum) in Tunisia. World J Microbiol Biotechnology, vol. 23, pp. 1195-1201. DOI:10.1007/s11274-006-9325-z

35 Zhang H., Prithiviraj B., Charles T.C., Driscoll B.T., Smith D.L. (2003) Low temperature tolerant Bradyrhizobium japonicum strains allowing improved nodulation and nitrogen fixation of soybean in a short season (cool spring) area. Eur. J. Agronomy, vol. 19(2), pp. 205-213. DOI:10.1016/S1161-0301(02)00038-2

36 Hafeez F.Y., Hameed S., Ahmad T., Malik K.A. (2001). Competition between effective and less effective strains of Bradyrhizobium spp. for nodulation on Vigna radiata. Biology Fertility Soils, vol. 33, pp. 382-386. DOI: 10.1007/s003740000337

37 Nushair A.M., Saha A.K., Rahman M.A., Mohanta M.K., Haque M.F. (2017) Characterization of indigenous Rhizobium strain isolated from lentil in Rajshahi, Bangladesh. Asian J. Advanced Basic Sciences. vol. 5(1), pp. 21-25.

38 Li L., Sinkko H., Montonen L., Wei G.H., Lindstrom K., Rasanen L.A. (2012) Biogeography of symbiotic and other endophytic bacteria isolated from medicinal Glycyrrhiza species in China. FEMS Microbiology Ecology, vol. 79(1), pp. 46-68. DOI:10.1111/j.1574-6941.2011.01198.x

39 Egamberdieva D., Wirth S., Shurigin V., Hashem A., Abd_Allah E.F. (2017) Endophytic bacteria improve plant growth, symbiotic performance of chickpea (Cicer arietinum L.) and induce suppression of root rot caused by Fusarium solani under salt stress. Front Microbiol. 28;8:1887. DOI:10.3389/fmicb.2017.01887

40 Hashem A., Abd_Allah E.F., Alqarawi A., Al-Huqail A.A., Wirth S., Egamberdieva D. (2016) The nteraction between arbuscular mycorrhizal fungi and endophytic bacteria enhances plant growth of Acacia gerrardii under salt stress. Frontiers in Plant Science, 7:1089, DOI:10.3389/fmicb.2016.01089

IRSTI 05.16.08; 65.01 https://doi.org/10.26577/ijbch.2021.v14.i2.06

N.M. Kerimbek[1], S.G. Sabitova[1],
A.B. Issayeva[2,3], M.A. Nurseitova[1,2*]

[1]Al-Farabi Kazakh National University, Almaty, Kazakhstan
[2]ANTIGEN Co. LTD, Almaty region, Kazakhstan
[3]Satbayev University, Almaty, Kazakhstan
*e-mail: mnurseitova2@gmail.com

Use and production of nanofoods in Kazakhstan

Abstract. With more than 8982 nanoproducts worldwide, nanotechnology is the basis of a new industrial revolution, which lead to the emergence of many products that are fundamentally new in their capabilities and properties. One of these new products is nanofood. It incorporates the use of nanoparticles and/or nanotechnology techniques and tools during the growing, manufacturing, farming processing and/or packaging of food and also in the foods themselves. As is, the global market of nano-packaging used in food industry in 2013 estimated to be $6.5 billion and around $15.0 billion in 2020. Currently in Kazakhstan research in the field of nanotechnology has been carried out to obtain nanostructured carbon materials, nanocarbon sorbents for the mining and metallurgical complex and medical purposes, metal-carbon catalysts for obtaining petrochemical products. In this paper authors monitored the market of Kazakhstan on the availability of nanoproducts, providing analysis of the recent studies on the use of nanoproducts in other countries and tried to describe the possibilities of their usage and production in Kazakhstan.
Key words: Nanofoods, nanomaterials, nanotechnology, nanoencapsulation, Kazakhstan.

Introduction

Nanofood products are new generation products. Nanofoods could be obtained by coating with nanoparticles and nanomaterials. During the digestion a lot of bioactive compounds and nutrients are deformed or destructed by a gastric intestinal juice and other factors. Nanodelivery systems are deal with the problem [1]. For example, nanoencapsulation are provided by nano capsules, which include in itself liquid of biologically active compound and is protected from the different harsh conditions that can cause diffusion or breakdown of coated component. It mainly maintains to have stability, control of release, which must be under specific environmental conditions, provide the protection from biological and chemical degradation, especially from oxidation etc. [1,2]. Nanoencapsulation used to deliver certain compounds and covering an unwanted odor, thus transporting them through gastrointestinal tract [3].

Nowadays in the world 8982 nanoproducts are produced in 2520 companies in 63 countries [4]. From this data, about 339 food-related nanoproducts of 50 various types. These products are introduced into global markets by 131 companies, the headquarters of which are located in 23 different countries. The products are classified into supplements, packaging, meal, sports nutrition, and food sensors sub-industrial sectors [4]. The global market of nano-packaging used in food industry in 2013 estimated to be $6.5 billion and around $15.0 billion in 2020 [5]. The most active countries in promoting nanotechnology in the food industrial sector are USA, Australia, Iran, China, Russia, South Korea, Germany, the Netherlands, Switzerland, and Indonesia.

Recently, nanotechnologies have been gaining popularity in Kazakhstan. Since 2003, research on nanostructures in certain areas has been carried out under the programs of fundamental research of the Ministry of education and science of the Republic of Kazakhstan.

Since 2006, applied research on nanomaterials and nanotechnologies has been funded by the Ministry of industry and trade under the program "Development of promising new materials for various purposes for 2006-2008" [6].

The country has 5 development institutes and 9 technology parks. In the regions of the country, 5 national scientific and 15 University laboratories of engineering profile were opened in priority areas of scientific and technological development, including the development of nanotechnologies. Among them,

there is the national nanotechnology laboratory at the al-Farabi Kazakh National University that engaged in fundamental and applied research in the field of nanoscience and nanotechnology, nano-engineering and nanomaterials and the creation of new techniques, technologies and nanomaterials using various physical, chemical and biological processes [7]. The NANOFAB scientific and technological center has been established in Shymkent, one of the main tasks of which is to create promising nanomaterials based on the raw materials of Kazakhstan.

According to the experts, there are some weaknesses in the development of nanotechnology in Kazakhstan, in particular there is no tradition of creating and developing nanotechnology; no Coordinating Center for the implementation of state policy in the field of nanotechnology, the development of innovative infrastructure in the field of nanotechnology, the implementation of projects for the creation of promising nanotechnologies and nano industry; insufficient funding for research and development in the field of nanotechnology; lack of long-term scientific and technical programs; laboratories are practically not provided with modern technological equipment for the production of nanomaterials; lack of qualified personnel to support the industry; there are no permanent large-scale nanotechnology forums and world-class conferences; low level of information support on nanotechnology issues, lack of information in the state language; low share of production of high-tech and knowledge-intensive types of products [8].

According to KazDATA [9] at the end of 2020 most food products are imported from Russia, Ukraine, Belarus, China and Germany. But there is no information about imported nanofood.

In this regard, we conducted a monitoring analysis of the development, application of Nanotechnology in food processing, in food packaging, Nanotechnology in Dairy Industry, in Agri-food production, Nanotechnology for aquaculture and fisheries, Nanotechnology in poultry production.

Nanotechnology in food industry and food processing

The science related to nanotechnology is new compared with other sciences. However, nanosized devices and objects have existed on earth as long as life. The exceptional mechanical performance of biomaterials, such as bones or mollusk shells, is due to the presence of nanocrystals of calcium compounds [10].

Nanotechnologies can be used in various industries, including the applications in food production such as pesticide delivery systems through bioactive nanoencapsulation, biosensors to detect and quantify pathogens, organic compounds, other chemicals and food composition alteration, high-performance sensors (electronic tongue and nose) and edible thin films to preserve fruit. The discovery of nanotubes was announced by Japanese scientist Sumio Iijima in 1991, he said that there are very thin special cylindrical formations of carbon [11]. These nanotubes made from milk proteins (for example, α-lactalbumin) will be effective as viscosifying agent and then can be used in food processing. At the same time nanotechnology has improved food packaging by offering improvements in the functional components of packaging materials, such as antimicrobial activity, ensure a long shelf life of food products. It is also involved in the detection of food toxins, favor production, and color formation [12].

Nanotechnology is highly demanded in food industry in following ways: encapsulation and delivery system of biologically active compounds, antimicrobial activity of some nanomaterials, tracking and tracing of food products, food sensory evaluation, production of functional foods [13]. Application of nanotechnology in food processing begins with the extending shelf-life of food products. Another application of nanotechnology is the identification of spoiled food. Detection of the pathogens is one of the tasks in food quality and safety assessment. Critical point of each food industry is the identification of pathogen. Thus, nanosensors are used to determine possible pathogens [14]. Furthermore, nanocarriers are widely use as delivery systems to carry certain bioactive compound to target place in the human body [13]. There are some criteria for choice of excellent nanocarrier: (1) able to carry to certain target; (2) provide high protection during transfer; (3) ensure high rate [15].

Nanotechnology used in food processing for production of functional foods such as dairy products, ice-cream, chocolate that can be treated as healthier and more beneficial for consumption. The treatment is provided by a reduction of fat composition and increasing vital nutrients percentage in food. These include increasing the number of proteins, amino acids, macronutrients and micronutrients, also vitamins [16,2].

Keeping the food fresh and ensuring the safety by prevention of product contamination by microorganisms or chemicals is one of the most important tasks during food production. Because of these factors up until now the main application area for nanotechnol-

ogy in food industry remains food packaging. The application of nanotechnology allowed producers to overcome food allergies, eliminating pesticide use, food packaging, restoring food damage and sensory evaluation to processes [17]. Principal advantages of packaging produced with application of nanotechnology is ability to actively response on threads. There are 4 main types of packaging systems. They are biodegradable, improved, active and smart packaging [18-20].

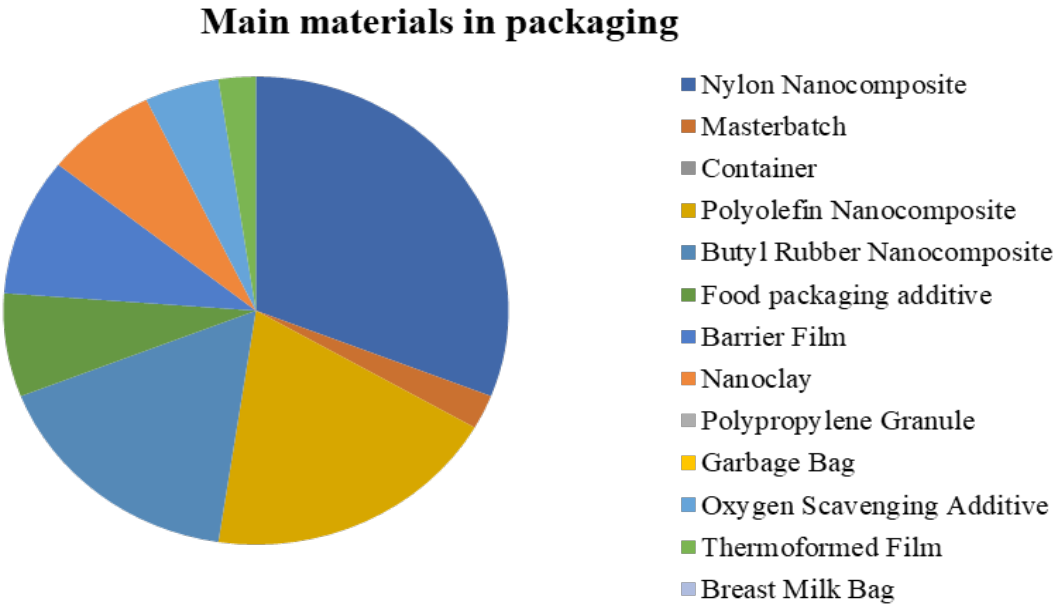

Figure 1 – Various product types used in food packaging

According to the Nanotechnology products database [4], in the world nanopackaging are using in 104 products, in 48 companies, 12 countries. The main nanomaterials, which are using in food packaging are clay, silver, and titanium dioxide (Figure 1).

Nanotechnology in dairy industry

The development of nanotechnology in the dairy industry makes it possible to improve the nutritional quality of products, thereby having a beneficial effect on the health of consumers [21,22]. Dairy nutrients have an impact on body health, metabolism, and inflammation by altering mitochondrial function and the composition of the gut microbiota [23]. These effects can be affected at the nanoscale, throughout the so-called nanoeffect, where increased physical properties, reactivity, or biological interactions occur below 100 nm [22].

Nanotechnology can also be used to improve the texture of food (for example, to improve the consistency of dairy products such as yogurt and ice cream) [24,25]. Furthermore, nanotechnologies are used to improve the nutritional quality of milk, as milk contains nanostructures because some of its proteins (such as casein) form nanoscale clusters to stabilize the oil-in-water emulsion [26, 27].

The oral delivery of anti-cancer macromolecules by using new nanoplatforms can help to administrate this type of therapeutic molecules by encapsulated in food products even dairy foods. For this chitosan coated ceramic nanocarriers by using alginate enclosed can be loaded with anticancer bovine lactoferrin- natural protein of milk [28].

Micro- and nanoencapsulation of probiotics in dairy products is an excellent solution to protect them from stomach acidity and high levels of bile in the intestinal cavity [29]. One of the latest applications of nanoencapsulation or by using other nanocarriers is the incorporation of bioactive molecules into novel functional foods [30].

In Kazakhstan ready dairy products are being imported, as is obvious from their availability in shops. According to the data of CEIC Data, an ISI Emerging Markets Group the Import of Milk and Milk products was reported at 36,700 tons in 2017 [31]. The main percent of the national market for packaged dairy products are imported. But there is no data about nano milk products.

Nanotechnology in agri-food production

Agriculture as a main source of raw food product. Thus, nanotechnology used to increase productivity and decrease the number of pesticides that used to treat crops, in the production of agriculturally derived food and to ensure the delivery of veterinary drugs to fish feed [32]. It can be nanofertilizers that are used to improve soil in which will grow potential agro-product. Nanotechnology has recent advantages in agri-food production [33]. The technology is (1) develop and improve productivity, (2) able to monitor and analyze, (3) provide protection [33]

Nutritional animal feeding and diagnosing diseases and providing efficient treatment methods are functions of nanotools used in the agri-food sector. Nanosensors can identify pathogens in animal feed and gastrointestinal tract. Coliform bacteria as *Escherichia coli* are a potential pathogen in the intestine. The active growth of the *Escherichia coli* in the intestine can cause several diseases. Aquaculture is another important direction in the agri-food sector.

Another direction that uses nanotechnologically derived products is plant agriculture. Pesticides are used to protect crops, vegetables and fruits from pests. However, side effects of pesticides among human are significant. Because of toxicity of chemical compounds in the composition of pesticides, it is better to find safe alternative. Fabrication of nanoderived chemical compounds allow to solve problem and to increase efficacy of pest control [32].

Proper entrapment plant treating agrochemicals is made due to nanoparticles. Nanoencapsulation process give ability to deliver pesticides, herbicides to target site and to save time and unnecessary waste of material. In addition, nanoencapsulated agrochemicals will be protected from pH, pressure and temperature alteration [32].

Nanotechnology for aquaculture and fisheries

In aquaculture and fisheries nanotechnology found its application in multiple spheres of industry such as fish health and growth control, delivery of drugs, nutrients, biologically active compounds as well as water purification. Including water treatment, detection, and control of aquatic pathogens, efficient delivery of biologically active compounds (including hormones and vaccines) and enhancement of its bioavailability [34,35].

Introduction of nano-selenium shown a significant effect on growth and antioxidant defence system in common carp [34]. Addition of nano selenium, zinc and manganese promoted the stress resistance and bone mineralization of gilthead seabream (*Sparus aurata*) [34]. Combination of nano-iron and *Lactobacillus casei* had significantly improved growth parameters in rainbow trout. Addition of manganese-oxide nanoparticles into diet significantly promoted growth and antioxidant defence system of freshwater prawn [34].

Also, the delivery of the compounds to fish is one of the most important tasks in aquaculture. This way the control over the aquaculture is maintained. This way a wide variety of compounds may be delivered. For example, pathogenic antigen, antibiotics, hormones, probiotics, pharmaceuticals, and nutraceuticals. These compounds are delivered by either oral administration or injection and are biodegradable and safe for fish and human health. The most popular nano materials used for encapsulation are alginate, chitosan, Poly (D, L-lactic-co-glycolic acid), liposomes. The encapsulation of compounds increases bioavailability, increases its stability in water and in body of a fish, maintains the controlled release of the drugs [34,36].

Nanotechnology in poultry production

In the poultry, foodborne pathogens are *Salmonella* and *Campylobacter* [39], which may be present in the intestinal flora or skin of healthy birds [40]. Fortunately, *Salmonella* and *Campylobacter* are sensitive to heat and should not be transmitted to humans if the meat has been properly heat treated [40]. There are several ways to take advantage of nanotechnology at various stages of the food chain to improve the microbiological quality of food during production and processing. For example, it has been reported the potential benefits of applications of nanoparticles as a poultry feed additive [41] and described the biocidal properties and usage of nanosilver to disinfect chicken hatcheries [42].

The most of foodborne disease outbursts can be related to crosscontamination through contact with infected food contact surfaces [43]. Nanoengineered surfaces can be used in developing antimicrobial coatings to prevent the growth of biofilms and enhance food safety [43]. Nanoscale metals such as silver, and photocatalytic metal oxide nanoparticles (such as titanium dioxide and zinc oxide) can be used in these antimicrobial surfaces [44].

Undoubtedly, the largest active area of application of nanotechnology is in food packaging. The suitable packaging of poultry meat products is important for food safety and expanding prod-

uct shelf-life [45]. It was reported that in challenge study active packaging of ready-to-eat poultry meat sausages by using zinc oxide nanoparticles showed a substantial reduction in the number of inoculated *Salmonella typhimurium* and *Staphylococcus aureus* [46].

Smart packaging that includes nanosensors can inform consumers about food or respond to this information and change the conditions inside the package to delay spoilage/contamination [47]. An example of such packaging is a label made of a layer of nanosilver, which reacts to sulfur compounds formed as a result of spoilage of poultry meat.

In poultry industry nanosensors have been designed to detect antibiotics in chicken tissue and foodborne pathogens. Nanosensors also has been used in detection of biogenic amines such as putrescine, cadaverine during the monitoring of deterioration of raw chicken meat [48].

The numerous possibilities of application of nanotechnology in poultry industry, in poultry processing chain to improve quality and safety of foods are existing with promising results.

Conclusion

We monitored the availability of nanoproducts on the market of Kazakhstan. According to the analysis for the presence of inscriptions and the label "Nano" in the packaging/labeling of dairy products, bread and bakery products and wine and vodka products. As a result, out of the studied 25 dairy products, 17 confectionery products, 20 wine and vodka products on the market of Kazakhstan, there is no accurate information that we use nanoproducts. But according to some data from scientists [49], we are already using. In view of the fact that the use of nanotechnology can enhance food processing, packaging, and safety; increase taste and nutrition; and can increase food production and economic efficiency. For example, titanium dioxide is added to a huge number of products in nano-form, including paints, paper, and plastics, but also gives a white pigment to most toothpastes and many processed foods, including Mentos, Trident and Dentyne gum, M & Ms, Betty Crocker Whipped Cream Frosting, Jello Banana Cream Pudding, Vanilla milkshake pies, and original Nestlé coffee cream. To date, no one denies that the above-mentioned products are consumed in Kazakhstan. Thus, imported nanoproducts are used in Kazakhstan.

References

1 Marsh K., Bugusu B. Food packaging—roles, materials, and environmental issues: Scientific status summary // Journal of Food Science. – 2007. – Vol. 72, No 3. – P. 39-55

2 Pradhan N., Singh S., Ojha N., Srivastava A., Barla A., Rai V. Facets of nanotechnology as seen in food processing, packaging, and preservation industry // Biomed Res Int. – 2015. – P. 1–17.

3 Ravichandran R. Nanotechnology Applications in Food and Food Processing: Innovative Green Approaches, Opportunities and Uncertainties for Global Market // Int. J. Green Nanotechnol. Phys. Chem. – 2010. – Vol. 1, No 2. – P. 72-96.

4 Available at https://product.statnano.com/ (accessed on 16/04/2021)

5 Bumbudsanpharoke N., Ko S. Nano-Food Packaging: An Overview of Market, Migration Research, and Safety Regulations // Journal of Food Science – 2015. – Vol.80 – (5), R910–R923. doi:10.1111/1750-3841.12861

6 Amanzhol I. Nanotechnology in Kazakhstan: a PR campaign or a lifeline for the economy? // Business Week, November 13. – 2009.

7 Kitaygorodtseva T. Nanomaterials and nanotechnologies in Kazakhstan // G-Global, International virtual Platform at the Astana Economic Forum. – 2013.

8 Yerbolatuly D. State and prospects of nanotechnology development in Kazakhstan // In the collection of materials from the conference "The contribution of young researchers to the industrial and innovative development of Kazakhstan" Ust-Kamenogorsk. – 2011.

9 Available at https://blog.kazdata.kz/import-export/rejting-produktov-pitaniya-import-i-eksport-2.html (accessed on 16/04/2021)

10 Atkinson, William Illsey // Nanocosm: Nanotechnology and the big changes coming from the inconceivably small // AMACOM Div American Mgmt Assn. -2003. – Vol. 80(12).

11 Ahmad A. Kholoud M. Carbon nanotubes, science and technology part (I) structure, synthesis and characterisation // Arabian Journal of Chemistry// -2010. -Vol.5 -P.1-23

12 B.S. Sekhon. Food nanotechnology—an overview // Nanotechnol. Sci. Appl. // -2010. – Vol.3 –P. 1–15.

13 Singh, T., Shukla, S., Kumar, P., Wahla, V., & Bajpai, V. K. Application of Nanotechnology in Food

Science: Perception and Overview // Frontiers in microbiology. -2017. – Vol. 8. – P. 1501.

14 Kumar V., Guleria P., Mehta S.K. Nanosensors for food quality and safety assessment // Environ Chem Lett. -2017. – Vol.15. – P. 165-177.

15 Bratovčić A., Odobašić A., Ćatić S., Šestan I. Application of polymer nanocomposite materials in food packaging// Croat. J. Food Sci. Technol. -2015. -Vol.7, No 2. -P. 86-94.

16 Alfadul, Sulaiman & Elneshwy, A.A.. Use of nanotechnology in food processing, packaging and safety review // African Journal of Food, Agriculture, Nutrition and Development. – 2010. – Vol. 10, No 6. – P. 2179-2731.

17 Mandal P. K., Choi K., Sang-Gi Min, and Chi-Ho Lee. Application of Nanotechnology in Food Packaging: An Overview // Korean J. Food Sci. Ani. Resour. – 2009. – Vol. 29. – No. 4. – P. 403-408.

18 Duncan T. V. Applications of nanotechnology in food packaging and food safety: barrier materials, antimicrobials and sensors // J Colloid Interface Sci. – 2011. – 363. – P.1-24.

19 Jampílek J., Kráľová K. Nanomaterials Applicable in Food Protection // Nanotechnology Applications in the Food Industry. Taylor & Francis Group. – 2018. – Vol. . – P. 75-89.

20 Pal M. Nanotechnology: A New Approach in Food Packaging // Food Microbial Saf Hyg. – 2017. – Vol. 2. – No. 4. – P. 1-2.

21 Playne M., Bennett L. Functional dairy foods and ingredients // Aust. J. Dairy Technol.//-2003.-Vol.58-P.242-264.

22 Riviere J.E. Nanotechnology in the Food, Beverage and Nutraceutical Industries //Woodhead Publishing// -2012. -P. 40–52.

23 Trinchese G., Cavaliere G. Human, donkey and cow milk differently affects energy efficiency and inflammatory state by modulating mitochondrial function and gut microbiota //J. Nutr. Biochem// -2015.

24 Imran M., Revol-Junelles A.M. Active food packaging evolution: transformation from micro to nanotechnology // Crit. Rev. Food Sci. Nutr.// -2010.-Vol. 50 -P.799–821.

25 Coles D., Frewer L.J.Nanotechnology applied to European food production. A review of ethical and regulatory issues //Trends Food Sci. Tech //-2013. – Vol. 34 –P. 32-43.

26 Park H. S., Ahn J. Effect of nano-calcium enriched milk on calcium metabolism in ovariectomized rats// J. Med. Food// -2008. –Vol. 11 – P.454-459.

27 Semo E., Kesselman E. Casein micelle as a natural nano-capsular vehicle for nutraceuticals // Food Hydrocolloid// -2007. –Vol. 21 – P.936-942.

28 Mahidhara G., Kanwar R. K. Novel nanoplatmform for oral delivery of anti-cancer biomacromolecules //Int. J. Nanotechnol // – 2012. –Vol. 9 – P. 942-960.

29 Kailasapathy K., Champagne C. P. Trends in the microencapsulation of probiotics for application in dairy products // Agro Food Ind. Hi Tech // – 2011. – Vol.22 –P.25-27.

30 Kaya-Celiker H., Mallikarjunan K., Better nutrients and therapeutics delivery in food through nanotechnology // Food Eng. Rev// -2012. –Vol.4 – P. 114-123.

31 Available at https://www.ceicdata.com/en/russia/trade-by-product-kazakhstan/imports-kazakhstan-volume-milk--milk-products (accessed on 20/04/2021)

32 Handford C. E., Dean M., Henchion M., Spence M., Elliott C. T., & Campbell, K. Implications of nanotechnology for the agri-food industry: Opportunities, benefits and risks // Trends in Food Science & Technology. – 2014. – Vol. 40, No 2. – P. 226–241.

33 Sekhon B. S. Nanotechnology in agri-food production: an overview // Nanotechnology, science and applications. – 2014. – Vol. 7. – P. 1–53.

34 Shah, B.R. and Mraz, J. (2020), Advances in nanotechnology for sustainable aquaculture and fisheries. Rev Aquacult, 12: 925-942

35 Rather, Ma & Sharma, Rupam & Aklakur, Md & Ahmad, S & Kumar, Neeraj & Khan, Mohammad & V L, Ramya. (2011). Nanotechnology: A Novel Tool for Aquaculture and Fisheries Development. A Prospective Mini-Review. Fish Aqua. 2011.

36 Oluwatosin Abidemi OGUNKALU. Utilization of Nanotechnology in Aquaculture and Seafood Sectors. Eurasian Journal of FOOD SCIENCE AND TECHNOLOGY // 2019

37 Huang, S., Wang, L., Liu, L. et al. Nanotechnology in agriculture, livestock, and aquaculture in China. A review. Agron. Sustain. Dev. 35, 369–400 (2015).

38 OECD/FAO (2016). OECD-FAO agricultural outlook 2016-2025.

39 Furukawa I., Ishihara T. Prevalence and characteristics of Salmonella and Campylobacter in retail poultry meat in Japan // Japanese Journal of Infectious Diseases // -2017. – Vol. 70(3) – P.239–247.

40 Barbut S. Microbiology and sanitation poultry products processing // CRC Press // -2001.

41 Gangadoo S., Stanley D. Nanoparticles in feed: Progress and prospects in poultry research // Trends in Food Science & Technology // -2016. –Vol. 58 – P.115–126.

42 Banach M., Tymczyna L. Nanosilver biocidal properties and their application in disinfection of hatchers in poultry processing plants // Bioinorganic Chemistry and Applications //- 2016. –Vol.15.

43 Griffith A., Neethirajan S. Development and evaluation of silver zeolite antifouling coatings on stainless steel for food contact surfaces // Journal of Food Safety // -2015. – Vol. 35(3) – P.345–354.

44 Eleftheriadou M., Pyrgiotakis G. Nanotechnology to the rescue: Using nano-enabled approaches in microbiological food safety and quality // Current Opinion in Biotechnology// -2017. –Vol.44 –P.87–93.

45 Panea B., Ripoll G. Effect of nanocomposite packaging containing different proportions of ZnO and Ag on chicken breast meat quality // Journal of Food Engineering// -2014. – Vol.123 –P.104–112.

46 Akbar A. Zinc oxide nanoparticles loaded active packaging, a challenge study against Salmonella typhimurium and Staphylococcus aureus in ready-toeat poultry meat //Food Control // -2014. – Vol.38 – P. 88–95.

47 Cushen M., Kerry J. Nanotechnologies in the food industry – recent developments, risks and regulation //Trends in Food Science & Technology // -2012. –Vol. 24(1) –P.30–46.

48 Liu S. F., Petty A. R. Single-Walled carbon nanotube/metalloporphyrin composites for the chemiresistive detection of amines and meat spoilage // Angewandte Chemie International Edition// -2015. –Vol. 54(22) –P.6554–6557.

49 A. Weir, P.Westerhoff, L. Fabricius, N. V. Goetz Titanium Dioxide Nanoparticles in Food and Personal Care Products//, Environ Sci Technol. 2012. Vol.21-46(4). – P. 2242–2250.

IRSTI 34.15.51 https://doi.org/10.26577/ijbch.2021.v14.i2.07

A. Ahsan[1*], A.T. Mansharipova[2]

[1]Lynx Eurasia LLC, Almaty, Kazakhstan
[2]Kazakh Russian Medical University, Almaty, Kazakhstan
*e-mail: drahsanali@yahoo.com

Molecular mechanisms of apoptosis

Abstract. Apoptosis is a regulated process of programmed cell death, as a result of which the cell breaks down into separate apoptotic bodies, limited by the plasma membrane. Fragments of a dead cell are usually very quickly phagocytosed by macrophages or neighboring cells, bypassing the development of an inflammatory reaction. One of the main functions of apoptosis is the destruction of defective (damaged, mutant, infected) cells. In multicellular organisms, apoptosis is also involved in the processes of differentiation and morphogenesis, in maintaining cellular homeostasis, in providing important aspects of the development and functioning of the immune system. Research on programmed cell death has been underway since the late 1960s. It is now known that the main trigger factors for triggering cell apoptosis are the imbalance of free radical, hormonal reactions. However, there are very few works on the study of the most toxic free radicals, such as hydroxyl radical, peroxynitrite, superoxide anion, as well as stress hormones on the development of the apoptosis process, in particular, cardiomyocytes. In this review, we decided to present a brief analysis of the key molecular mechanisms of apoptosis in this direction.
Key words: apoptosis, caspase, p53, TNF, cytokine, DNA damage.

Introduction

In the past 3 decades, 2 distinct forms of cell death, necrosis and apoptosis, have been defined in terms of mechanism, sequence of events, biochemistry, and morphology. Necrosis refers to a range of morphological changes resulting from the enzymatic digestion of the cell, the disruption of cellular membranes, and the denaturing of proteins that accompanies cell death [1]. Apoptosis, in contrast, is a programmed, active, highly selective mechanism of cell death allowing for the removal of cells that are redundant or excessively damaged [2]. Apoptosis is initiated by a number of different stimuli, including DNA damage, intracellular damage, toxins, and extra cellular signals [3]. In multicellular organisms' it is an essential component of development and cellular regulation [4].

Caspases and their subfamilies

One of the basic stages of apoptosis is the reception of signal, a precursor of destruction in the form of information to the cell, either external or arising inside the cell. The signal is perceived by the receptors and is analyzed. Further through receptors or their combinations the received signal is consistently transferred to the intermediate molecules (messengers) through the various ways and finally reaches the nucleus where the activation of cellular suicide program takes place by the activation of lethal and/or repression of antilethal genes. With regard to human cells apoptosis, in most cases is linked to the proteolytic activation of caspase cascade – a family of evolutionarily conservative cystein protease, which specifically split proteins after aspartic acid residues [5]. On the basis of the structural homology caspase are further subdivided into the subfamily) caspase-1 (caspase 1, 4, 5), b) caspase-2 (caspase-2) and c) caspase-3 (caspase 3, 6-10) [6]. However, apoptosis is also possible without the involvement of caspase: super synthesis-promoters of apoptotic proteins Bax and Bak induced apoptosis in the presence of caspase inhibitors [7]. Molecular targets of caspase – effectors are many proteins, degradation of which causes the development of irreversible processes that are characterized for apoptosis. These anti apoptotic proteins are of Bcl-2 family, DNAse inhibitor, DFF (DNA fragmentation factor), lamin proteins, cytoskeleton proteins, proteins involved in DNA reparation, mRNA splicing, DNA replication and others [8].

Caspases, in the form of less active pro enzyme, are present in the cell, constitutionally, that allows inducing apoptosis rapidly. One of the pathways to

activate caspase is linked to the interaction of apoptosis inducers with the specific receptors (Fas, TNF, ARO3). Another way of the activation of caspase 9 occurs as a result of hetrodimer proteins of Bcl-2 family. Third way of caspase activation is with the help of granzyme in the poreconstituent proteins [9].

DNA fragmentation and accompanying molecules

One of the important events in the process of apoptosis is the fragmentation of DNA. In the terminal phase of apoptosis, caspase splits specific protein topoisomerase II, which is involved in the formation of higher-order DNA structures, and histone H1, protecting DNA from the action of endonuclease at internuleosomal level. As a result of this, splitting of DNA molecules into fragments of certain sizes takes place: large – about 50 and 300 thousand bp and small – 180 bp (and multiples of them).

Fragmentation of DNA is carried out near different endonuclease. In particular, splitting into fragments of 180 bp provides activation of Ca^{2+}, Mg^{2+} dependent endonuclease [10]. There are regulators that block or, conversely, encourage the devastating effect of CASPASE. These include the proteins of Bcl-2 family (inhibitors of apoptosis: A1, Bcl-2, Bcl-W, Bcl-X_L, Brag-1, Mcl-1 and NR 13) and the proteins of Bax family (promoters of apoptosis: Bad, Bak, Bax, Bcl-X_s, Bid, Bik, Bim, Hrk, Mtd) [11]. Important role in the induction of apoptosis play genes – tumor growth suppressors: p53, Rb, p21, p33, etc. They are involved in stopping the cell cycle and launching the programmed cell death in incorrigibility violated structure of DNA.

This prevents the survival and reproduction of the cells with transforming genome. One of apoptotic events is realized in the cell nucleus and is the fragmentation of DNA. The degradation of DNA is the terminal phase of apoptosis. During the degradation of DNA initially formation of large fragments containing approximately 300 thousand bp takes place, later some – 30-50 thousand bp.

Then comes the next phase of the fragmentation of DNA – its internucleosomal degradation, with the formation of fragments containing 180 bp (lengthening of DNA threads in nucleosome), or multiples of them in length. Specifically, these fragments appeared as "ladders" during the DNA electrophoresis of apoptotic cells lysates, which are widely used for the identification of apoptosis. Such fragmentation of DNA is linked to the proteolytic splitting of specific protein topoisomerase II.

This protein accomplishes the structural and enzymatic function and is involved in the formation of higher-order DNA structures – super spiral hinges. They contain 50 thousand bp. Six loops united into a single disc like outlet forming even more complex structure and have 300 thousand bp in their composition, respectively. It should be remembered that fragments of 50 and 300 thousand bp split the DNA in the initial stage of degradation during apoptosis.

Degradation of topoisomerase II caspases are one of the reasons for the fragmentation of DNA. Likewise, substrate of protease during apoptosis is histone H1, which protects DNA from the endonuclease at the internucleosomal level. As a result of this splitting, the degradation of DNA into fragments takes place of approximately 180 bp and multiple of them.

In order to constantly hinder the process of programmed cell death in certain physiological framework in biological systems, there are a number of factors acting as either inducers or inhibitors of apoptosis. Some of them, depending on conditions, have both pro and anti apoptotic action.

p53 transcription factor

Until present it was believed that non reparative DNA damage leads to cell death as a result of the functional disorders of all biochemical systems due to the impossibility of an adequate transcription of genes having defect in the DNA matrix. Studies in recent years have led to the formation of absolutely new understanding of the cell death mechanism, having DNA damage, as the process, carried out in accordance with a specific genetic program. In induction of this program having damage to the DNA of cells, important role plays p53 protein. This protein with a molecular weight of 53 kDa localized in the cell nucleus is known as one of the transcription factors, the increased expression of which leads to repression of number of genes regulating transcription and involved in the delay of cells in cell cycle phase G1. In DNA damage under the influence of ionizing radiation, or UV radiation, topoisomerase II inhibitors and some other impacts, activation of p53 gene expression takes place. Block of the cell cycle in the phases of G1 and G2 till DNA replication and mitosis, respectively, makes possible reparation of damaged DNA and prevents thus the emergence of the mutant cells. If the activity of reparation system is insufficient and DNA damage persisted, then in such cells programmed cell death or apoptosis is induced, which leads to the protection of body from the presence of cells with damaged DNA. At the level of transcription p53 regulates the expression of genes involved

in the blockade of the cell cycle – p21 (inhibitor of majority cyclin – dependent kinase, either interacts with the complexes, determining DNA synthesis and reparation, or with the proteins, modulating apoptosis – Bax. Mutation of p53 gene allows such cells to maintain viability in mitosis, which lead to survival of cells subjected to transformation. Indeed, in transformation significant numbers of mutations are found in p53 gene. Thus, under the influence of p53 genotoxic agents not only increases the time of DNA reparation, but in this way also protect the body from cells with dangerous mutations. Blocking the process of apoptosis may reduce the ability of transformed cells to activate the program cell death.

Bcl-2 proteins

It is known that process regulating cell death can be conditionally divided into several different phases: initiating phase of apoptosis, signal activation of caspase, endonuclease activation and specific degradation of the DNA, resulting in the cell death. If the initial phase varies depending on the type of the cells and apoptosis induction signal, then degradation stage of the DNA is universal for most of the cells. This phase is transitional to the irreversible – terminal phase of apoptosis, which is controlled by the family of Bc1-2 proteins. In this regard, clarifying the role of Bc1-2 proteins family plays the central role in studying the regulation of apoptotic process. Proteins of this family are either inducer of apoptosis (Bad, Bax, Bcl-Xs, Bik, Bid, Bak), or inhibitors (Bcl-2, Bcl-XL). Proteins of Bcl-2 family are in constant dynamic equilibrium, forming a homo – and hetrodimers that, ultimately, affect in the development of cell apoptosis. Therefore, it is believed that the ratio of the active forms of these proteins determine the rheostat of life and death of the cells. The regulation mechanism of this process should be considered in the position structurally – the functional relationship between proteins of this family that allow them to merge into one family – a family of Bcl-2 proteins [12]

Fas-L cytokine

The best studied are the sequence of events that lead a cell to apoptosis as a result of the interaction of TNF family proteins with specific receptors. A striking representative of this group of proteins is the system of Fas/Fas-L (ligand) [13]. It should be noted that other functions are still unclear for this system, except induction of cell apoptosis. Fas/APO-l/CD-95- receptor, as per structure are related to the receptors of TNF family. Interaction with Fas Fas-L or with monoclonal antibodies leads to the apoptosis of cells. Fas is constitutively expressed on the surface of many cell types: on thymocytes, lymphoblastoid cell lines, activated T and B lymphocytes, as well as fibroblasts, hepatocytes, keratinocytes, mieloid cells, cardiomyocytes. The human Fas consists of 325 amino acid residues and refers to the membrane of the type I proteins, that is, in its structure could be extracellular, transmembrane and cytoplasmic domains. Homology of the amino acid sequence among the family of TNF receptors is high. About 80 amino acid residues form a death domain (DD), which is involved in protein-protein interactions with cytoplasmic proteins, generating the signal of death. Gene Fas in humans is localized at the long shoulder chromosome 10 and consists of 9 axons.

Fas-L is a cytokine and belongs to the family of cytokines of TNF. Fas-L is expressed in activated T-lymphocytes, natural killers, as well as Sertoli cells, parenchymal cells of the anterior eye chamber that allow these cells to kill any Fas-expressing cell, including the activated T-lymphocyte. This mechanism determines the presence of protected places from the immune system. Fas-L exists in two forms – insoluble or membranecombined and soluble, split able from the cells with the help of metalloproteinkinases. Soluble form of human Fas-L retains their activity. Like other ligand receptor of the TNF family, Fas L-homotrimer attached with 3 molecules of Fas. In attachment with ligand receptors oligomerization of cytoplasmic proteins occurs: DD (domain death) is related to the receptor of adaptor protein – FADD (Fas-associated death domain) containing DED – effectors death domain and procaspase-8. As a result of this process, the activation of apoptosis specific protease – caspase-8 happens and develops the characteristic of apoptotic processes [14].

Apoptosis and autophagy

Autophagy and apoptosis are extensively focused areas of research in the context of tumor suppression, where autophagy is responsible for degradation and elimination of misfolded proteins and damaged organelles, at the same time enhancing cancer cell survival in response to stress conditions like hypoxia, thereby promoting chemoresistance to the tumor cells (Figure 1). The importance of inhibition of cytoprotective autophagy and deletion of the intermediate pathways involved to facilitate tumor cell death is impossible to be underestimated, as this gives possibilities for future prospects in designing drug combinations facilitating the synergistic effect of autophagy and apoptosis in achieving cancer cell death [15].

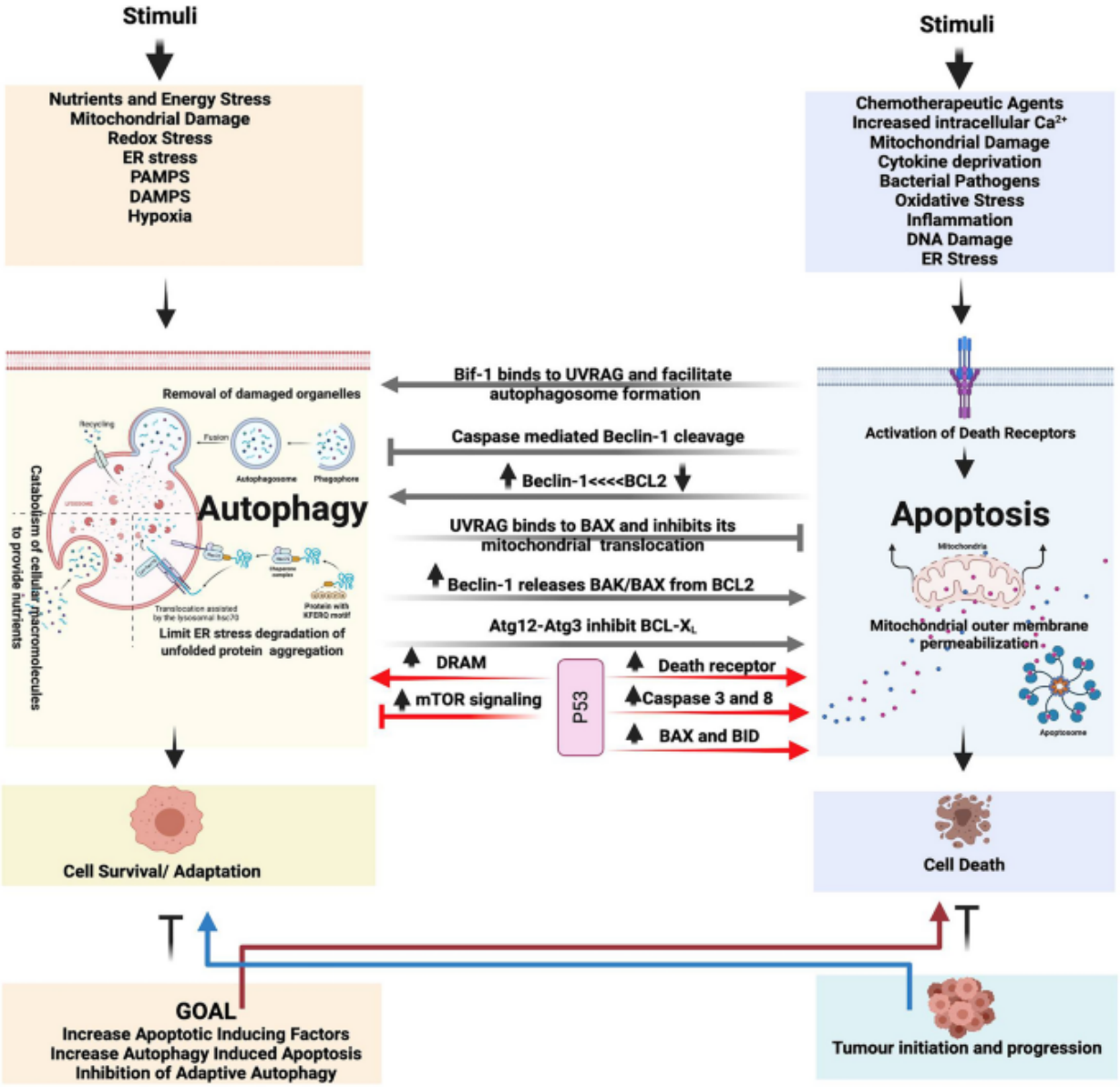

Figure 1 – Autophagy vs apoptosis [15]

PANoptosis

Pyroptosis, apoptosis and necroptosis are the most genetically well-defined programmed cell death intricately involved in both homeostasis and disease. Although the identification of key initiators, effectors and executioners in each of these pathways has historically delineated them as distinct, growing evidence has highlighted extensive crosstalk among them. These observations have led to the establishment of the concept of PANoptosis, defined as an inflammatory programmed cell death pathway regulated by the PANoptosome complex (Figure 2), which holds potential to kill cancer cells, and thus could be targeted for therapeutic benefit [16].

And as once again was noted by Dr. Anthony Lemarié in his introduction for the special issue of (International journal of molecular sciences, 2022): Concerning apoptosis, several aspects must be addressed, such as the dependency on the caspase proteases, the involvement of extrinsic (death receptors) and intrinsic (mitochondrial) pathways, and the role of the endoplasmic reticulum pathway. Finally, it would be of great interest to focus on the pro-survival vs. pro-apoptotic regulation in tumor cells and during anticancer treatments (either chemo or radiotherapy), particularly toward several emerging targets, such as cancer stem cells or circulating cancer cells.

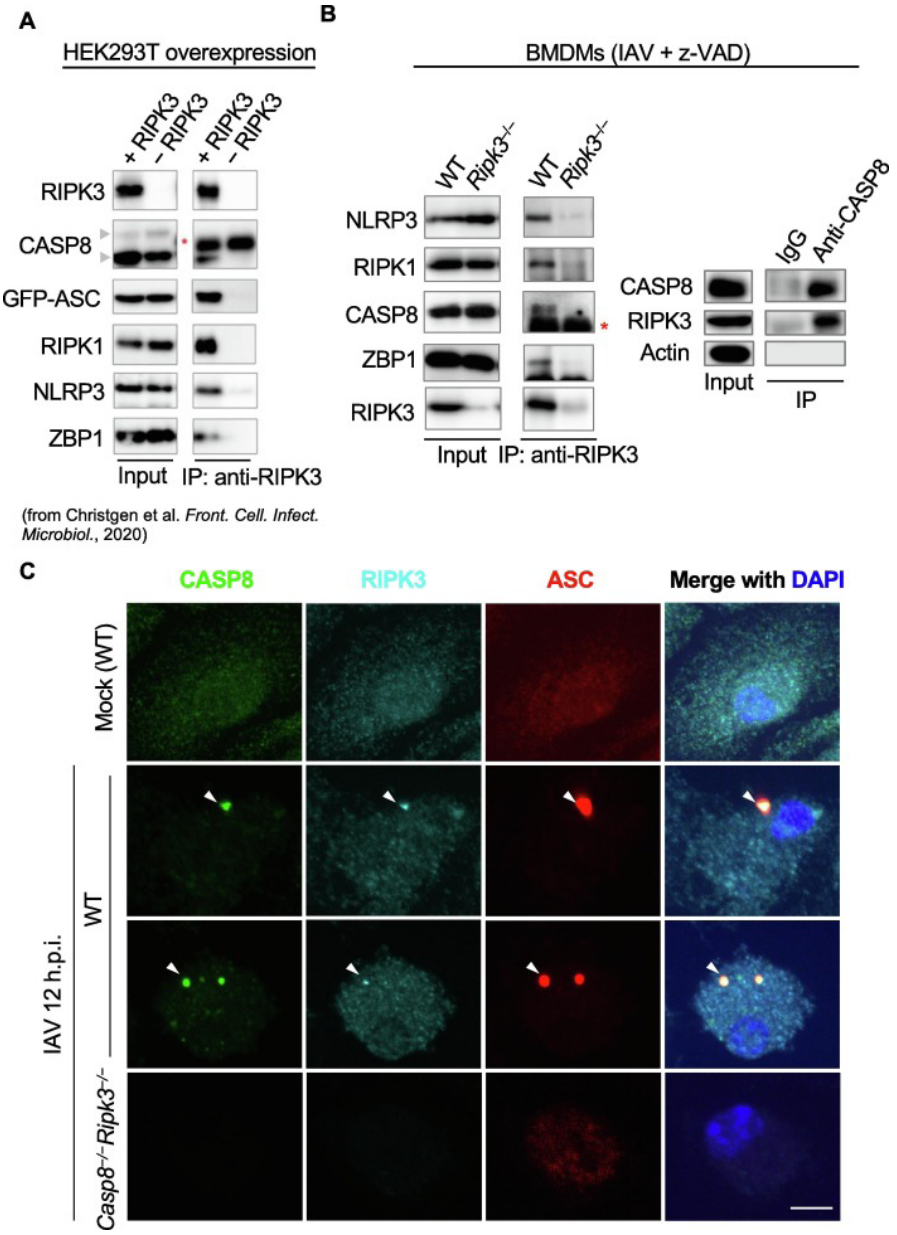

Figure 4 – Experimental evidence of PANoptosome formation.
(A) Immunoprecipitation of RIPK3 in HEK293T cells overexpressing PANoptosome components (published data from Christgen, S., et al. Front. Cell. Infect. Microbiol., 2020).
(B) Immunoprecipitation of RIPK3 in IAV-infected WT and *Ripk3*−/− BMDMs (left) and immunoprecipitation of CASP8 in WT cells showing the interaction among key components of the PANoptosome. (C) Immunofluorescence staining of indicated molecules in IAV-infected BMDMs showing the colocalization of principle components of the PANoptosome. BMDMs infected with IAV (PR8) at MOI = 20 for 12 h and stained with anti-ASC (2EI-7, Millipore), anti-CASP8 (1G12, Enzo) and anti-RIPK3 (B-2, Santa Cruz, pre-conjugated). Scale = 5 μm. Asterisks indicate non-specific bands [16]

Conclusion

Implementation of the various phases of DNA degradation is associated with appearance of activity of various endonuclease. There is not enough information about the characteristics of endonulease which determine the appearance of large DNA fragments. Slightly more information is available about the processes of internucleosomal degradation of DNA, which results in the formation of DNA frag-

ments of 180 bp. It is believed that this type of degradation is provided by the activation of Ca^{2+}, Mg^{2+}-dependent endonuclease [17]. The decisive moment in the launch of apoptosis plays hetrodimerization of the protein of Bcl-2 family – inducers and inhibitors of apoptosis. In what way proteins of Bcl-2 family receive the signal to the regulation of apoptosis from these receptors? At present, the ability to modulate the state of the protein of Bcl-2 family has been studied, at least 3 different mechanisms – changing the structure of proteins Bad, Raf-1 and Bag-1. Probably, there are many ways to regulate the functional activity of the proteins of Bc1-2 family at the cellular level as inhibitors, and as well as inducers of apoptosis through certain signal-transmitting molecules and the ways of their activation. Considering the functional importance of the Bcl-2 family proteins in regulation of such a complex and multifaceted process, as apoptosis, it could be argued that these proteins are promising target for the purpose of manipulating the desired impact on the fate of cells.

References

1 Patricia J. M. Best; David Hasdai et.el. Apoptosis. Basic concepts and implications in coronary artery disease// atherosclerosis, thrombosis and vascular biology. 1999; 19:14-22

2 Kerr JFR, Wyllie AH, Currie AR. Apoptosis: a basic biologic phenomenon with wide-ranging implications in tissue kinetics. Br J Cancer. 1972; 26:239–257.

3 Rowan S, Fisher DE. Mechanisms of apoptotic cell death. Leukemia. 1997; 11:457–465.

4 Risau W, Flamme I. Vasculogenesis. Annu Rev Cell Dev Biol. 1995; 11:73–91.

5 Biidihardjo L., Oliver H., Liitter M. et al. Biochemical pathways of CASPASE activation during apoptosis //Ann. Rev. Cell Dev. Biol. – 1999. – Vol. 15.- P. 269-290.

6 Fadeel B., Zhivotovsky B., Orrenius S. All along the watchtower: on the regulation of apoptosis regulators //The FASEB Journal. – 1999. – Vol. 13. – P. 1647-1657.

7 Pinto M., Perez J.J., Rubio-Martinez J. Molecular dynamics study of peptide segments of the BH3 domain of the proapoptotic proteins Bak, Bax, Bid and Hrk bound to the Bcl-xL and Bcl-2 proteins //J. Comput. Aided. Mol. Des. – 2004. – Vol. 18. – P. 13-22.

8 Mayr M., Hu Y., Hainaut H., Xu Q. Mechanical stress-induced DNA damage and rac-p38MAPK signal pathways mediate p53-dependent apoptosis in vascular smooth muscle cells //FASEB J. – 2002. – Vol. 16. – P. 1423-1425.

9 Decker T., Kovarik P. Transcription factor activity of STAT proteins: structural requirements and regulation by phosphorylation and interacting proteins //Cell. Mol. Life Sci. – 1999. – Vol. 55. – P. 1535 – 1546.

10 Zhivotovsky, B., Burgess, D. H., Vanags, D. M., Orrenius, S. Involvement of cellular proteolytic machinery in apoptosis //Biochem. Biophys. Res. Commun. – 1997. – Vol. 230.- P. 481- 488.

11 Belushkina N.N. Control of the apoptotic process by the proteins of Bcl-2 //Vopr.biol.med. pharm.chemistry. – 2000. – № 3.- C. 9-16.

12 Reed J.C. Bcl 2 and regulation of programmed cell death //J/Cell Biol.-1994.-Vol.124.-P.1-6.

13 Ohtsuka T., Hamada M., Sasaki O. et al. Clinical implications of circulating soluble Fas and Fas ligand in patients with acute myocardial infarction //Coron. Artery Dis. – 1999. – Vol. 10. – P. 221–225.

14 Earnshaw W. C., Martins L. M., Kaufmann S. H. Mammalian CASPASEs: structure, activation, substrates, and functions during apoptosis //Ann. Rev. Biochem. – 1999. – Vol. 68. – P. 383-424.

15 Das S, Shukla N, Singh SS, Kushwaha S, Shrivastava R. Mechanism of interaction between autophagy and apoptosis in cancer. Apoptosis. 2021;26(9-10):512-533. doi: 10.1007/s10495-021-01687-9. Epub 2021. PMID: 34510317.

16 Yaqiu Wang, Thirumala-Devi Kanneganti. From pyroptosis, apoptosis and necroptosis to PANoptosis: A mechanistic compendium of programmed cell death pathways, Comput Struct Biotechnol J. 2021, Vol. 19, P. s 4641-4657, https://doi.org/10.1016/j.csbj.2021.07.038.

17 Eastman A. Assays for DNA fragmentation, endonucleases, and intracellular pH and Ca2+ associated with apoptosis //Methods of Cell Biology. – 1995. – Vol. 46. – P. 41-55.

IRSTI 34.29.25 https://doi.org/10.26577/ijbch.2021.v14.i2.08

E.M. Oleynikova

Voronezh State Agrarian University named after Emperor Peter the Great, Voronezh, Russia
e-mail: cichor@agronomy.vsau.ru

Population biology of the endemic species *Pimpinella tragium* Vill.

Abstract. For the first time for the European part of Russia, a study of the population biology of the endemic species of chalk and limestone *Pimpinella tragium* Vill. in natural habitats of the Voronezh region was carried out. The species is an obligate calcephyte, prefers open chalk substrates. Biomorphological analysis made it possible to classify *Pimpinella tragium* as a herbaceous polycarpic taproot plant. Due to the presence of a powerful taproot, the species promotes the fixation of weak chalky substrates. In the future, open groups of calciphilic vegetation with the participation of *Pimpinella* may appear on the Cretaceous substrate. Six-year monitoring of the main stages of development of *Pimpinella tragium* made it possible to identify 4 ontogenetic periods and 9 age states: latent (seeds), pregenerative (seedlings, juvenile, immature and virginal individuals), generative (young, middle-aged, old generative individuals), postgenerative (senile individuals). The paper presents the morphometric characteristics of individuals of different age groups. The ontogenetic structure of *Pimpinella tragium* cenopopulations was studied, the type of the basic spectrum was revealed. Most cenopopulations have a left-sided spectrum; the absolute maximum is more often represented by young individuals, the local maximum – by middle-aged individuals. For some populations, a centered ontogenetic spectrum was noted with maxima on middle-aged generative individuals. The formation of the ontogenetic structure of *Pimpinella tragium* cenopopulations is significantly influenced by the physical characteristics of the Cretaceous substrate, and hence the physiological characteristics of this species. The ability of the species to reproduce only by seed is of great importance, since in different years the germination and survival rate of seedlings can differ sharply.

Key words: *Pimpinella tragium* Vill., population biology, ontogenesis, coenopopulations (CP), Cretaceous substrate, endemic species, Voronezh region.

Introduction

The problem of studying and effectively preserving the biodiversity of the vegetation cover is one of the most pressing problems of our time. In this regard, the study of the unique flora of the Cretaceous outcrops, which includes a number of endemic, rare and endangered species, is of undoubted interest [1-4].

The aim of this work was to study the ontogeny and structure of populations of endemic species of chalk and limestone *Pimpinella tragium* Vill from the Apiaceae family. The studies were carried out in the Voronezh region.

Voronezh region is located in the south-west of the European part of Russia between 49° 34’ and 52° 06’ north latitude and 38° 09’ and 42° 55’ east longitude. It is located in the central part of the East European (Russian) plain, at the junction of the Central Russian and Kalach uplands and the Oka-Don Plain, the region stretching from north to south for 277.5 km, and from west to east for 352 km, its area is 52.4 thousand km^2. Voronezh region in the north and northeast borders with Lipetsk and Tambov, in the west – with Belgorod and Kursk, in the east – with Saratov and Volgograd, in the southeast – with Rostov and in the south-west – with the Luhansk region of Ukraine (Figure 1) [5]. Voronezh region is located at the border of two botanical-geographical zones – forest-steppe and steppe, which provides a rich floristic composition and heterogeneity of landscape-ecological conditions.

The territory of the Voronezh region has passed a long and difficult path of geological development, which is reflected in its modern landscape and ecological features, in turn, leaving an imprint on the vegetation cover. Along with the covers of Quaternary sediments, the Cretaceous system rocks are most widespread in the region. Cretaceous deposits are represented by Lower Cretaceous and Upper Cretaceous rocks, which in a fairly large part of the region can come to the surface along the slopes of river valleys, gullies and ravines [6]. The most fre-

quently noted outcrops of Upper Cretaceous rocks in the northwestern, southwestern, southern and southeastern parts of the region. V. Mikhno [7], based on long-term field observations and analysis of literature data, comes to the conclusion that the time of appearance of calciphilous vegetation in different regions of the East European Plain is asynchronous, since the territory was populated with relict plant species both autochthonously and by migrations from mountainous regions of the Mediterranean, the Caucasus, Central Asia and other regions. The main prerequisite for the convergence of relics of different eras was the physicochemical properties of the Cretaceous rocks, the originality of their denudation, as well as specific microclimatic conditions. The most important environmental factors affecting the spread of chalk plants are [7,8] temperature, humidity and chemical composition of the nutrient substrate. So, D. Sakalo [8] indicates that the main typomorphic element of chalk substrates is calcium, the need for which determines the peculiarities of the ecology and physiology of calcephilous species, in particular, their ability to use for photosynthesis the carbon dioxide of calcium bicarbonates entering through the root system has been shown. There is also information in the literature [9] that representatives of the Cretaceous flora are very selective about the chemical purity of carbonate soils, preferring pure chalk substrates to contaminated chalk, where calcium is readily available for plants and is absorbed in the required amount by the calciphilic flora.

The material for the analysis was collected in Ostrogozhsky, Liskinsky, Kamensky, Podgorensky, Rossoshansky, Olhovatsky and Kantemirovsky districts (Figure 1, the author indicates the approximate location of the studied habitats). Route and stationary expeditions have been carried out annually since 2008.

Figure 1 – Voronezh region map. From: https://www.shutterstock.com/es/image-vector/detailed-map-voronezh-region-russia-175714598

The study of the unique flora of chalky outcrops is of great interest since it is composed of many endemic species of plants. In Voronezh region, the outputs of chalk and marl are confined to the riverine slopes and slopes of hills composed of chalk (North-Western, Southern, South-Western and South-Eastern areas). Chalk landscape – specific natural-territorial complexes, where the main role is played by chalk-loamy rocks. Natural specificity is determined by the erodibility of the terrain, high reflectivity, lack of the developed soil, predominance of sparse vegetation of calciphyte groups. By the flora of the cretaceous outcrops a set of species associated in its distribution with the chalk substrate are understood.

According to modern reports more than 500 species of angiosperms growing on the outputs of chalk and marl are marked in Voronezh region [10]. A significant portion of them belongs to endemic and relict species which existed in pre-glacial period. Depending on the degree of adaptation they can be divided into four groups: obligate calciphyte, optional calciphyte, insensitive to calcium content types, calciphobous species.

Cretaceous outcrops have a number of common features such as lack or weak development of soils, the mobility of the Cretaceous rocks, specific microclimate, physical and chemical properties of chalk as a substrate on which the plants grow. In this regard in the composition of the Cretaceous flora species certain life forms dominate such as subshrubs and perennial herbaceous plants with a powerful taproot penetrating to the depth of 50 cm to 2 m and more. It was repeatedly noted that such plants strengthen chalks [11].

Our interest in *Pimpinella tragium* as an object of population monitoring was caused by a number of factors: endemism, confinement to Cretaceous substrates of various genesis, the ability to dominate both in primary groups of vegetation and in stable communities. A comprehensive study of ontogenesis, structure and dynamics of cenopopulations (CP) of the species has not been previously carried out, we only studied the features of development and ontogenetic structure of CP of *Pimpinella tragium* [12].

Materials and methods

In carrying out this work, studies were carried out at various levels of the organization of plant systems: organ, organismic, population and coenotic. The methods of modern biomorphology, population biology, phytocenology and statistics were used.

Organ level of the structural organization. To study the underground organs of individuals in expeditionary conditions, the methods of dry excavation along the roots and the method of horizontal excavation were used. [13,14].

Study of an individual as a separate organism. The life form of plants was characterized according to the concept of I. Serebryakova [15] for individuals of a mature generative ontogenetic state. To isolate the ontogenetic states of *Pimpinella*, the generally accepted methods of population biology were used [11]. On the basis of morphological changes in the ontogeny of individuals, the age periods are distinguished and the ontogenetic states are characterized, which are further indicated in the text by symbols: **se** – resting seeds, **p** (plantulae) – seedlings, **j** (plantae juveniles) – juvenile, **im** (plantae immaturae) – immature, **v** (plantae virginiles) – virginal, $\mathbf{g_1}$ – young generative, $\mathbf{g_2}$ – middle-aged generative, $\mathbf{g_3}$ – old generative (plantae generativae), **s** (plantae seniles) – senile individuals.

Study of Pimpinella tragium populations. The ontogenetic structure and abundance were analyzed on accounting plots of 1 m^2, laid out in a systematic way. A plant of seed origin was used as a counting unit. When analyzing the CP structure, the recovery index I_r and the aging index I_a [11] were calculated, which are important population parameters. I_r reflects the share of undergrowth participation in the CP (or how many offspring at a given time point per one generative individual), and I_a – the share of participation of the aged fraction in the total sample.

Study of phytocenoses with the participation of Pimpinella tragium. To characterize plant communities on Cretaceous substrates, geobotanical descriptions were made on stationary plots, each with an area of 100 m^2. Subsequent analysis made it possible to compile a complete floristic list of the study areas. The coenotic significance of each species was assessed on the scale of abundance by Braun-Blanquet [16].

The morphometric data obtained in the course of work were processed statistically using the EXCEL software package.

All photographs were taken by the author personally (Figure 2, photos 1 and 2 – Kuvshin tract, Podgorensky district, May 02, 2021 and June 03, 2020, respectively; photo 3 – Marki village, Kamensky district, July 31, 2013. Figure 3, photo 1 – Volokonovka village, Kantemirovsky district, July 23, 2008; photo 2 – Ezdochnoe village, Ostrogozhsky district, July 28, 2018. Figure 6, photo 1 – May 08, 2012, photo 2 – August 11, 2012, both photos made near a chalk quarry on the western outskirts of the regional center Podgorensky). Figure 4 is made by the author on the basis of the ontogenetic herbarium of *Pimpinella tragium*.

Results and discussion

The genus *Pimpinella* comprises 150 species, distributed in Eurasia and Africa, over 16 of which are present in Europe [17]. The species is confined to the valleys of Volga and Don, Black sea coast of Caucasus. For the Voronezh region (Figure 2) it is observed on the Northern border of the area.

Figure 2 – Cretaceous landscapes of the Voronezh region

Obligate calcephyte, on chalk outcrops of the South, West and North-West region occurs everywhere: on the moving screes, dense indigenous outcrops of chalk and plumes and cones and outcrops with a mixture of humus and fine-grained deposits (Figure 3) [6,10,12].

According to the literature data, the taxon *Pimpinella tragium* has significant morphological variability [18,19].

We found that, on all of the listed types of Cretaceous substrates, *Pimpinella tragium* is part of the primary groups of vegetation. As both loose and dense chalk outcrops become overgrown, the species strengthens its cenotic positions and often acts as a dominant. The composition of subdominants depends on the type of Cretaceous substrate: *Scrophularia cretacea* Fisch.ex Spreng., *Hyssopus cretaceus* Dubjan. (mobile chalk talus), *Linaria cretacea* Fisch. ex Spreng., *Matthiola fragrans* Bunge (dense chalk), *Teucrium polium* L., *Thymus calcareus* Klok. et Shost., *Onosma simplicissimum* L., *Gypsophyla altissima* L. (mixture of chalk crushed stone with fine earth), *Festuca valesiaca* Gaudin (areas with turf).

The life form of *Pimpinella tragium* was determined on the basis of the classification developed by us earlier for tap-root grasses [11]. The biomorph of this plant is a polycarpic tap-root species with semi-rosette shoots. The ontogeny of the species for European part of Russia was described for the first time (Figure 4).

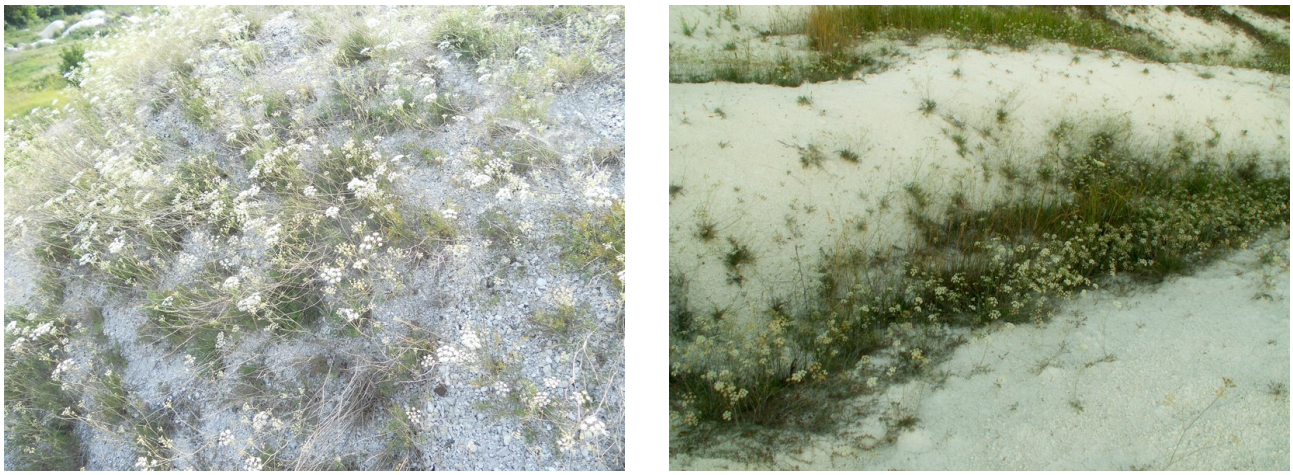

Figure 3 – Cenopolyulations on *Pimpinella tragium* on various chalk substrates

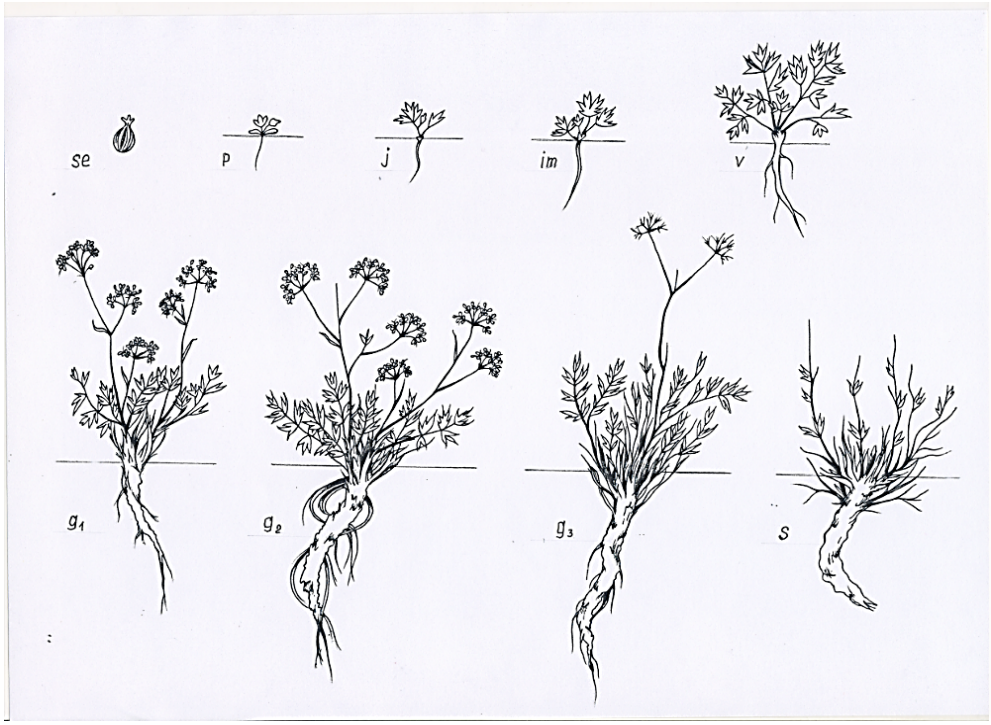

Figure 4 – Ontogenetic states of *Pimpinella tragium*. Developed by the author

The morphometric characteristics of individuals of different ontogenetic states are presented in Tables 1 and 2.

The embryonic period. Achenes (se) are dark brown, pear-shaped, with a wide base and a narrowed apex, on which an epispid disc is formed in the form of a thickened head. The surface is covered with thin threadlike ribs. Length and width – 1.5-2.5 cm.

The pregenerative period. Seedlings (p). Germination is aboveground. The hypocotyl is short. Cotyledons are oval-oblong, 10-15 mm long, 3-5 mm thick, on petioles fused at the bases. The first leaves are alternate, rounded, three-pentagonal in outline, with sharp teeth. Petioles up to 35-40 mm long, pink-violet at the base. The third leaf is weakly tripartite, with wide toothed lobes. Root length up to 30-50 mm, lateral roots are absent.

The author has found that the complete development cycle includes 4 periods and 9 age-related conditions, namely:

Table 1 – Morphometric characteristics of pregenerative and postgenerative individuals of *Pimpinella tragium*

Parameters	Ontogenetic states			
The number of vegetative rosette shoots	j	im	v	s
Total number of rosette leaves	1±0.00	1.56±0.02	2.65±0.24	3.12±0.46
Length of rosette leaves with petioles, cm	3.25±0.16	11.85±0.7	28.55±1.85	16.07±0.78
Rosette leaf width, cm	1.34±0.04	3.1±0.13	5.95±0.22	5.11±0.18
Caudex diameter, cm	0.51±0.02	0.99±0.05	1.55±0.08	1.34±0.05

Table 2 – Morphometric characteristics of generative individuals of *Pimpinella tragium*

Parameters	Ontogenetic states			
The number of axial generative shoots	g_1	g_2	g_3	g_1
Height of axial generative shoots	2.85±0.25	11.85±0.93	5.13±0.56	2.85±0.25
The number of lateral generative shoots	28.7±0.49	35.85±1.21	22.72±0.52	28.7±0.49
Number of inflorescences per individual	9.76±1.38	44.5±3.86	12.76±1.45	9.76±1.38
Number of stem leaves per individual	14.17±2.35	53.4±4.05	21.7±2.24	14.17±2.35
Caudex diameter, cm	13.18±1.76	46.22±3.12	17.33±1.98	13.18±1.76

Juvenile (j) plants have a rosette shoot with 3-5, rarely 7 leaves on petioles up to 4-6 mm long. The leaf plate is finger-dissected, the lobules are triangular. The length of the root is up to 15-20 cm, it is slightly tapering, lateral roots of the first order are formed in the lower third. Due to the contractile activity of the root, caudex appears and branches very early, and already in imature (im) individuals, the formation of 2-3 rosette shoots with 5-7 leaves and petioles from previously dead ones is possible.

The caudex diameter is 3-4 mm; transverse folds are clearly visible on it. The length of the petioles is up to 20 mm. The main root penetrates up to 20-25 cm, lateral skeletal roots up to 2 mm thick are formed at a depth of 2-5 cm.

Virginiles (v) plants have from 2 to several rosette shoots with numerous leaves, leaf plates without pubescence, oblong or ovoid in outline, with a petiole 3-8 cm long and 1-2.5 cm wide, twice pinnately dissected, primary lobes are ovoid in outline, 3-8 mm long and 1-4 mm wide. The caudex is branched, up to 20 mm in diameter, the height of individual heads is 10-15 mm, they are densely covered with stalks of dead leaves. As virginiles individuals develop, the root gradually deepens to 70 cm –1 m, along its entire length a few thin lateral roots of 1-3 orders of magnitude extend from it.

The generative period. Young generative (g_1) plants vary greatly in power, therefore they can have from 2-3 to 5 or more semi-rosette orthotropic shoots 15-40 cm high. Basal leaves are petiolar, completely coinciding in morphology with virginal-type leaves. Stem leaves are few in number, smaller. Umbrellas 2-4 cm in diameter, with 10-15 naked rays, almost equal in length, umbrellas 5-8 mm in diameter. Petals are white, about 1 mm long, shortly pubescent outside. One shoot has 1-3 umbrellas. The heads of the caudex are up to 25 mm in height, the main root is 1 m or more long, in the basal part it is densely speckled with transverse folds. The color of the root is very light, grayish-white. Young generative plants usually stay in the g1 state for 3-4 years. Middle-aged generative (g_2) plants, under optimal conditions of development, reach maximum power and can contain up to 15-20 semi-rosette orthotropic generative shoots, some shoots are only rosette. The number of umbrellas on one shoot increases on average to 5-7, the number of rays in each increase, which significantly increases the seed productivity of an individual. Caudex with a diameter of up to 20 cm, the height of the heads reaches 6 cm and more. Simultaneously with the transition of individuals to the g_2 state, a gradual partial destruction of caudex begins, associated with the transition of individual chapters to the secondary vegetation, and then death. However, in general, in middle-aged plants, the processes of neoplasm significantly exceed the dying off. This condition lasts for 5-8 years or more. On the contrary, in old genera-

tive (g_3) plants, the processes of withering become more and more important. Tissues die off not only in caudex, but also deeper, in the main root, in the formed cavities a chalk substrate is stuffed, mixed, depending on the type, with soil particles, fine gravel, etc. The confinement of the *Pimpinella tragium* to the slopes with a steepness of 10-50^0 and the mobility of the upper layer of the chalk substrate contribute to the mechanical detachment of weakly fixed caudex branches, its diameter decreases to 10-15 cm. An increasing number of shoots are no longer able to form flower-bearing stems, the number of fully ripening fruits is reduced. The bark of the root in some areas dies off and gradually sloughs off.

The postgenerative period. Senile (s) individuals are only capable of postgenerative vegetation. There are no more than 5 shoots, each rosette consists of 3-7 petiole leaves, which are morphologically similar to the leaves of imature individuals. The destruction of caudex, as well as the dying off of the main root, is accelerated. The caudex diameter does not exceed 5-8 cm. The total life span of senile individuals lasts no more than 3 years.

Simultaneously with the study of ontogeny, the ontogenetic structure CP was studied. Five communities with the participation of *Pimpinella tragium* were selected for observations: CP 1 and 3 were located on the southern and southwestern slopes and contained vast areas of hard chalk. CP 2, 4, and 5 were part of natural meadow phytocenoses on chalk rubble with an admixture of fine earth, chernozem-calcareous soil, or loose chalk outcrops. In CPs 2, 4, and 5, left-sided ontogenetic spectra were noted (Fig. 5) with maxima on imature or juvenile individuals, a local maximum on g_1 (CP 5) – or (CP 2, 4) g_2-individuals. These CP of the *Pimpinella* are part of sodded chalk communities with a relatively high projective cover (65-75%) and a slight steepness of the relief (5-15^0). Long-term observations allow us to talk about the optimal timing for the passage of each period of ontogenesis. The average density is 45.8 individuals per 1 m^2, I_r ranges from 1.17-1.58, I_a – 8.11-9.65. The left-sided nature of the spectra is primarily due to the seed type of self-maintenance of the species, while the dynamism of the pregenerative fraction is explained both by the short development of individuals of certain age groups and by the unevenness of seed reproduction and survival of seedlings.

Fluctuations in the number of age groups of the generative fraction depend on the duration of the young, middle-aged or old generative state in ontogenesis. At the same time, the presence and duration of development of individuals of all age groups are significantly influenced by the survival rate of seedlings during the years of research, the meteorological conditions of specific years, the compliance of ecological requirements with the conditions of the ecotope, anthropogenic factors, etc. In CP 1 and 3, centered age spectra (Figure 5) with a maximum at g_2 – individuals. We believe that this type of structure is formed primarily in connection with the physical properties of the chalk outcrops on which the *Pimpinella tragium* grows [20]. This is a hard, chalky substrate, so it is very difficult for the seed to gain a foothold and germinate. In addition, the top layer of chalk, due to seasonal changes in temperature and humidity, is gradually loosened and washed out by melting snow and precipitation.

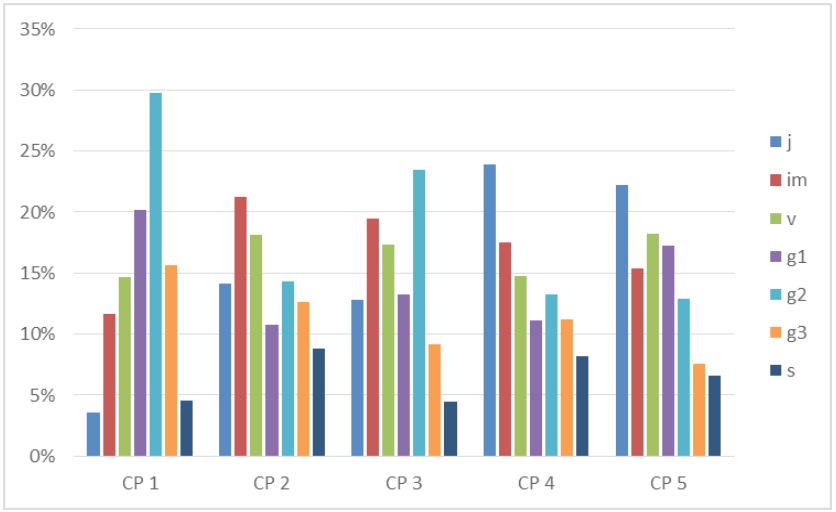

Figure 5 – Ontogenetic structure of *Pimpinella tragium* cenopopulations

The steepness of the slopes in some areas is 45-50^0 degrees. The projective cover of plants on chalk substrates does not exceed 55%, and in some loci – 5-20%. The gradual displacement of the upper layer of the chalk substrate leads to permanent death of individuals of all age groups. Individuals of the pregenerative fraction, small in size, are either washed out, or the chalky slurry curls the points of growth of the root rosette; in individuals of the generative fraction, both blocking of shoot growth points with chalk slurry and quite strong – up to 10 cm – exposure of caudex and root is observed, which significantly reduces the life of the plant. Postgenerative individuals (I_a – 4.63-4.76) die not only due to a decrease in the viability of the organism, but also because necrotic processes in caudex allow, with any mechanical effect (melt water, precipitation, wind, etc.), to come off as individual rosette shoots and heads of caudex. Among the selected CP of the *Pimpinella*, similar processes were most clearly manifested in CP 1 (density – 9.92 pcs/per 1 m^2, I_r – 0.45). Figure 6 shows the structure of the chalk substrate and the appearance of the plants after heavy rain.

Figure 6 – The state of juvenile (left) and middle-aged generative individuals (right) after the movement of water flows

Thus, the formation of the ontogenetic structure of the cenopopulations of *Pimpinella tragium*, along with the features of ontogenesis, is significantly imprinted by the physical properties of the substrate, and hence the physiological features of this species.

Conclusion

The need for a comprehensive study of the biology of rare and endangered plant species of Cretaceous outcrops is indisputable. An important aspect is the analysis of the features of ontogeny and the structure of populations of these species since these questions will help to gain an idea of the current state of phytocenoses growing on chalk and limestone substrates. This work presents the population and ontogenetic characteristics of one of the cenosis-forming species of the Cretaceous outcrops – *Pimpinella tragium*. In the Voronezh region, the species grows on the border of its range and is noted both in the forest-steppe and in the steppe parts of the region. *Pimpinella tragium* is a pioneer of overgrowing not only loose, but also dense chalk outcrops, as it tolerates compaction of the chalk substrate well. We have identified several types of phytocenoses with the dominance of this species, the subdominants are mainly tap-root perennial grasses and dwarf semishrubs, obligate calcephytes. It has been established that the species goes through all stages of ontogenesis and reproduces well enough by seed. However, the state of *Pimpinella tragium* cenopopulations is unstable and largely depends on the state of the Cretaceous substrate and the recreational load on it. In this regard, the industrial development of chalk, which has been actively developing in the Voronezh region in recent years, causes great concern. We believe that it is necessary to reduce the area of chalk quarries and prepare a program for the protection of plant communities of chalk outcrops at the regional level. Considering the ecological-cenotic and population characteristics of *Pimpinella tragium*, the species can be proposed as a model for the reclamation of significantly disturbed communities on

Cretaceous substrates. With regret, we have to state that the population biology of calcephytes for the entire territory of European Russia has been studied extremely poorly. This is all the more surprising, since the area of chalk substrates and plant communities on them is steadily decreasing under the influence of the increasing anthropogenic load. We believe that only joint efforts to study and protect calciphytic vegetation will allow preserving the unique Cretaceous landscapes and their floristic diversity.

References

1 Cancellieri L., Rosati L., Brunetti M., et al. (2020) The dry grasslands of Abruzzo National Park, the oldest protected area in the Apennines (Central Italy): overview of vegetation composition, syntaxonomy, ecology and diversity. Tuexenia, vol. 40, pp. 547-571. https://doi.org/ 10.14471/2020.40.019, available online at www.zobodat.at

2 Gusev A., Lisetskii F., Ermakova E. (2016) Principles and experience of justification of ecological representativeness of Emerald network potential sites. Research Journal of Pharmaceutical, Biological and Chemical Sciences, vol. 7, no. 2, pp.1178-1189.

3 Jeanneret P. (2015) From biodiversity conservation in agricultural landscapes to the promotion of functional biodiversity: shifting a paradigm? Ecological Modelling, vol.11, no. 316, pp.133–143. https://doi.org/10.1016/j.ecolmodel.2015.08.009.

4 Sluginova I.S. (2008) Semennaya produktivnost nekotorych redkich vidov rastenii melovych obnazheniy basseyna reki Polnoy [Seed productivity of some rare plant species of Cretaceous outcrops of the Polnaya river basin] Izvestiya vyzov. Severo-Kavkazskiy region. Estestvennye nauki, no. 4, p. 75-79.

5 Atlas Voronezhskoi oblasti (1994) [Atlas of the Voronezh region] Kiev: Ukrgeodezkartografiya, 48 p.

6 Khmelev K.F., Kunaeva T.I. (1999) Rastitelnyy pokrov melovych obnazheniy basseyna Srednego Dona [Vegetation cover of chalk outcrops in the Middle Don basin] Voronezh: VGAU, 214 p.

7 Mikhno V.B. (1992) Melovye landshafty Vostochno-Evropeyskoi ravniny [Cretaceous landscapes of the East European Plain] Voronezh: Petrovskyy skver, 232 p.

8 Sakalo D.I. (1963) Ekologicheskaya priroda stepnoy rastitelnosti Evrazii i ee proischozhdenie. Materialy po istorii flory i rastitelnosti SSSR [Ecological nature of the steppe vegetation of Eurasia and its origin. Materials on the history of flora and vegetation of the USSR] M.-L.: Izdatelstvo AN SSSR, vol. 4, pp. 407-425.

9 Dvurechenskiy V.N., Grigorevskaya A.Ya. (1985) O podvizhnosti kaltsefitnoy flory v predelakh Srednerusskoy vozvyshennosti [On the mobility of calciphyte flora within the Central Russian Upland] Biologicheskiye nauki, no. 1, pp. 69–72.

10 Agafonov V.A. (2006) Stepnye, kaltsefilnye, psammofilnye i galofilnye ekologo-floristicheskie komplekcy basseyna Srednego Dona: ich proischozhdenie i ochrana [Steppe, calciphilic, psammophilic and halophilic ecological-floristic complexes of the Middle Don basin: their origin and protection] Voronezh: VGU, 250 p.

11 Oleynikova E.M. (2014) Ontomorfogenes i struktura populyastiy sterzhnekornevych travyanistych rasteniy Voronezhskoy oblasti [Ontomorphogenesis and population structure of taproot herbaceous plants in the Voronezh region] Voronezh: VGAU, 367 p.

12 Oleynikova E.M. (2011) Endemichnyy kalstefit Pimpinella tragium (Apiaceae) na melach Srednego Dona [Endemic calcephyte Pimpinella tragium (Apiaceae) on the chalks of the Middle Don] Vestnik VGU. Seriya: Geografiya. Geoekologiya, no. 1, pp. 179-183.

13 Shalyt M.S. (1960) Metodika izucheniya morfologii i ekologii podzemnoi chasti otdelnych rastenii i rastitelnych soobshchestv [Methods for studying the morphology and ecology of the underground part of individual plants and plant communities] Polevaya geobotanica. M.-L.: Izdatelstvo AN SSSR, vol. 2, pp. 369-489.

14 Krasilnikov P.K. (1983) Metodika polevogo izucheniya podzemnych chastei rastenii [Method of field study of underground parts of plants] M.: Nauka, 208 p.

15 Serebryakov I.G. (1964) Zhiznennye formy vysshych rasteniy i ich izuchenie [Life forms of higher plants and their study] Polevaya geobotanica. M.-L.: Izdatelstvo AN SSSR, vol. 3, pp. 146-205.

16 Mirkin B.M., Naumova L.G., Solomeshch A.I. (2002) Sovremennaya nauka o rastitelnosti [Modern vegetation science] M.: Logos, 264 p.

17 Illicium, Pimpinella and Foeniculum (2004) (editor by M.M. Jodran). CRC Press: London, New York, Washington, 266 p.

18 Bogdanović S., Ruščić M. (2011) Pimpinella tragium Vill. subsp. lithophila (Schischk.) Tutin (Apiaceae), a new taxon in Croatian flora Acta Botanica Croatica, vol.70 (1), pp.115–120.

19 Yurtseva O.V., Tikhomirov V.N.(1998) Morphological diversity and taxonomy of the Pimpinella tragium Vill. group (Umbelliferae-Apioideae) in the Mediterranean. Feddes Repertorium, vol. 109, no. 7-8, pp. 479-500.

20 Oleynikova E.M. (2014) Biomorfologicheskiy analiz sterzhnekornevych katsefitov (na primere Voronezhskoy oblasti) [Biomorphological analysis of taproot calcephytes (on the example of the Voronezh region)] Problemy regionalnoy ekologii, no. 5, pp.140-145.

IRSTI 65.35.03 https://doi.org/10.26577/ijbch.2021.v14.i2.09

S. Javed , A. Safdar , A. Shoaib

University of the Punjab, Lahore, Pakistan
*e-mail: amna.iags@pu.edu.pk

Physical and chemical characterization of essential oils of *Rosa indica* and its application in hand sanitizer

Abstract. This research work documents the isolation, physical and chemical characterization of essential oil of *Rosa indica* L. and its application in hand sanitizer. *R. indica* essential oil (REO) extracted from freshly collected flower petals through hydro-distillation method showed 0.057% yield. Some of the physical and chemical properties of REO like density (0.92), refractive index (1.45), viscosity (9.46), specific gravity (0.92), optical rotation (optically active), acid number (14.10), ester number (28.19), consistency (solid), appearance (clear liquid), color (pale yellow), odor (floral, sweat rosaceous) and purity (100%) were determined in laboratory using standard protocols. GC-MS analysis of REO identified twenty-nine compounds belong to eight major groups. Monoterpene alcohol represented the main characterized group (59%) followed by sesquiterpenes hydrocarbons (21.20%), phthalate ester (9.99%), aldehyde hydrocarbon (1.41%), alkyne hydrocarbons (1.21%), aromatic hydrocarbons (1.21%) and pyrozole derivative (1.21%). However, among the monoterpene alcohol, the 1-phenylethyl alcohol (13.02%); citronellol (10.01%) and 6-octen-1-ol, 3,7-dimethyl (9.55%) were found in most abundant. Formulated hand sanitizer with REO exhibited physical and microbiological properties that were comparable with the market product. It also had pleasant scent, compatible with skin, easy to apply, and are acceptable to the users. The current study clearly shows that REO could be utilized as a potential ingredient in hand sanitizer formulation for giving the pleasant smell, acceptable physical and microbial quality parameters.
Key words: Rose essential oil, hand sanitizer, sweet smell, GCMS.

Introduction

Aromatic chemicals from medicinal aromatic plants generally belong to class of organic compounds (e.g., terpenes, phenolics and alkaloids), which have no direct function in plant's growth and metabolism, however, these compounds exhibit diverse biological activities being serve as important source in the agriculture, nutraceutical, and pharmaceutical industries [1]. Essential oils (EOs) are among the nonpolar aromatic organic plant compound's, which are composed of mixture of volatile lipophilic components (alkaloids, flavonoids, phenolic acids, monoterpenes, isoflavones, aldehydes, oxygen-containing, and non-oxygenated terpene hydrocarbons), and extensively used around the world in food, medicine, cosmetics, and beverages as environmentally friendly and cost-effective choice [2,3]. Many EOs have anti-inflammatory, and antiseptic features [4]. The bioactive components e.g., limonene, carvone, geranyl acetate etc. of EOs have been regarded as key components of sanitary products and toothpastes [5]. The unique aroma, flavors and natural antimicrobial contents have been incorporated in food packaging to extend the shelf-life and safety of perishable food [6]. Being antiviral, antimicrobial and anti-insectidal, application of EOs has also been explored as a natural preservative in many agricultural products [7]. The antimicrobial action of EOs has been reported to occur through targeting phospholipid bilayer, proton motive force, and quorum sensing [8].

Rosaceae is the 19th largest plant family, and Rosa is one of the biggest and most significant aromatic and medicinal genera of this family due to its essential oils and volatile products. Many of its species are native to Asia, Europe, North America, and Northwest Africa, where these are extensively utilized as a traditional medicine, in pharmaceutical products [9]. Its many species like *R. indica* [10], *R. alba* [9] and *R. damascena* [11] have been reported to produce essential oil, while *R. indica* producing essential oil are also being cultivated in Sindh province [12]. It has been stated that petal leaves generally deposit 93% (of the total content of the flower) of

the essential oil, and 0.035% is the average yield of oil content, however, it varies among varieties from 0.009% to 0.062% [13].

R. indica is a perennial flower shrub, contains trees, herbs or shrubs that are climbing, thorny or rhizomatous. Rose essential oil (REO) stimulate the brain to release endorphins, often called the "feel-good" hormone. REO use in aroma therapy to ease pain in patients who who've had surgery [14]. Rose oil also helps to decrease anxiety level of women during the pregnancy [15]. Furthermore, REO are being used as preservatives in food packaging due to their antibacterial, antioxidant, and anti-injury activities [16].

Literature indicates that EO could serve as a potential substitute to synthetic compounds, especially because of the resistance that has been increasingly developed by pathogenic microorganisms. Utilization of REO in hand sanitizer formulation could serve as beneficial alternative antimicrobial ingredient, especially for individuals who are sensitive to other commonly used compounds. In this study, the use of liquid hand sanitizer containing rose petal essential oil as an antimicrobial additive was investigated. REO addition in hand sanitizer has very wide application not only to give pleasant smell but also to treat particular mental and physical health issues. REO in hand sanitizer formulation helps skin to glow healthier and also lock the moisture of hands. Dinwiddie et al. [17] reported that addition of tea extract and lemongrass essential oil enhanced effectiveness of sanitizers against microbes and also offers additional benefit of free from toxic ingredients, which might be quite beneficial for health and environment as well. REO in hand sanitizer formulation aims to be both beneficial and sustainable without compromising efficacy or safety. The current study was conducted to characterize *R. indica* essential oil for its physic-chemical composition, to formulate it in hand sanitizer and to assess its physical, sensory and antimicrobial test.

Materials and methods

Extraction of rose essential oil (REO). Rose petals (10 kg) were hand-picked in the early hours during the flowering season (February-March 2021) from the Chaudhary Nursery, Near Ghelan bypass Pattoki (latitude: 31°01′00″ N, longitude: 73°50′59″ E, altitude: 194 m), Pakistan. Specimen number RP-1 were assigned to collected samples of rose. Hydrodistillation technique was performed for extraction of essential oil from fresh petals of *R. indica*. Briefly, the steam was passed through a glass pipe to the flask containing petals. The resultant vapors were condensed and collected in a receiver as a distillate. Oily layer was separated from aqueous layer by adding diethyl ether to the steam distillate. The mixture collected from collection assembly was poured into the separating funnel, shaken for 30 min, and allowed to stand for an hour to separate layers of water and organic layer (oil + solvent). Sodium sulphate was used as desiccant to remove water traces from organic layer. Oil and diethyl ether in the upper layer were heated at low temperature to evaporate solvent and to obtain pure oil. The oil sample were stored in sealed vials at 4 °C for further analysis.

Composition analysis of REO. Compositional analysis of essential oil had been performed by using gas chromatography coupled mass spectrometry (GC-MS), (Shimadzu GC-9A) equipped with capillary column (SPB-5) maintained with flame ionization detector at 220 ˚C. Carrier gas (N_2:1.0 mL min^{-1}) was adjusted at initial temperature at 50 °C for initial 5 min, followed by increase in temperature (5ºC min^{-1}) up to 235 ºC and finally sustained for 5 min. A column (HP-5 with dimensions: 25 m × 0.22 mm and 0.25 μm df) was used to complete analysis of the fraction

Physical and chemical analysis of REO. Physiochemical properties of REO like density, viscosity, specific gravity, optical rotation, acid number, ester number, consistency, appearance, odor, color, odor and purity were analyzed by the [18].

Preparation of hand sanitizer gel. Hand sanitizer was prepared following protocol described earlier with slight modification [19]. Carbopol (0.25 g) was dissolved in water (30 mL), and the mixture was stirred at 60 rpm for 30 minutes at 80 °C. Afterwards, 10 mL of ethanol was added into the mixture followed by further addition of ethanol (40 mL). Glycerin (0.8 mL) along with tri-ethanolamine (few drops) were also added into the mixture, and the mixture was homogenized. REO (0.5% v/v) was added drop wise with constant stirring to avoid air bubble formation and to obtain homogenous gel. The remainder of each formula was completed by distilled water. Control formulation was also prepared without adding REO (Table 1).

Product characterization. The hand sanitizer was analyzed for pH, density and viscosity using standard protocols. Sensory tests namely aroma, color, sticky and clarity were also performed to determine consumer response for the best treatment. Consumers response for the formulated hand sanitizer was assessed by observing sensory tests (aroma, color,

viscosity, sticky and clarity) involving 20 untrained respondents. The respondents rated the product by scoring 1 (strongly disliked) to 5 (strongly liked) after applying the sample to their palms.

Table 1 – Hand sanitizer formulation

Component (Purpose)	Concentration (v/v)
Carbopol (Thickening agent)	0.25%
Alcohol 100% (Antimicrobial)	50%
Glycerin (Emollient)	0.8%
Tri-ethanolamine (Solubilizing agent)	0.2%
Essential oil (Extract)	0.5%
Distilled water (Vehicle)	48.25%

Antimicrobial assays. Antimicrobial activity of REO was studied against gram positive bacteria *Escherichia coli* (FCBP-WB-0005). Microorganisms were collected from First Fungal Culture Bank of Pakistan (FCBP), Faculty of Agricultural Sciences, University of the Punjab, Lahore. Bacterial culture used was subcultured and maintained on LBA (Luria-Bertani agar).

Agar well diffusion method. Antimicrobial potential of REO and formulated hand sanitizer (with and without REO) was performed using agar diffusion method [20]. For antimicrobial assay, overnight nutrient agar derived cultures were used for preparation of inoculum suspension. Each sample of REO was tested at a 5 mg/mL concentration, and dimethylsulfoxide (DMSO) was used to dissolve essential oil. About 300 µL of colloidal suspension of bacterium was spread on the fresh LBA. Wells of 6 mm diameter were punched in the agar medium with the help of sterile cork-borer and filled with 100 µL of the sample. Inoculated plates were incubated overnight at 37 °C for 24 hours. The antibacterial activity was determined by measuring the diameter of zone of inhibition in millimeters (mm) around each well. The results are represented the mean of three replicates. Controls using DMSO and water were adequately prepared. The antimicrobial activity of REO, formulated hand sanitizer only, formulated hand sanitizer + REO was compared with two commercially available hand sanitizers.

Results and discussion

Yield of REO from 10 kg of petal was 0.057% on the petal fresh weight basis by hydro-distillation method (Table 2, 3).

Table 2 – Yield of essential oil of *Rosa indica* on petal fresh weight basis

Yield (%)	Values
Total flower used	10 Kg
Oil yield	0.057%

Table 3 – Physical properties of the essential oil from rose *(Rosa indica*) petal

Sr. No.	Property	Mean values ± S.D.
1	Density	0.92 ± 0.28
2	Refractive index (25°C)	1.45 ± 0.37
3	Viscosity (25°C)	9.46 mPa
4	Specific gravity (25°C)	0.92 ± 0.041
5	Optical rotation	Optically Active
6	Acid number	14.10 ± 0.78
7	Ester number	28.19 ± 0.46
8	Consistency	Solid
9	Appearance	Clear liquid
10	Color	Pale yellow
11	Odor	Floral, strong, and sweet rosaceous character
12	Purity	100% natural

The results are relevant with [21,22] as their findings revealed 0.042-0.045% and 0.07% yield of rose essential oil, respectively by hydro-distillation method. However, Khan and Shoaib-ul-Rehman [23] reported low yield 0.02% and 0.03% essential oil extracted from 20 kg of *Rosa centifolia* and *Rosa damascene* petal through Soxhlet extraction apparatus. It has been known that hydro-distillation product holds greater market value than the product from different extraction methods mostly due to procurement of greater number of essential oil components [24]. The physical quality parameters of REO including density (0.92 g/mL), refractive index (1.45), viscosity (9.46 mPa), specific gravity (0.92), optical rotation (optically active), acid number (14.1024), ester number (28.187), appearance (clear liquid), color (transparent), and odor (pleasant) are presented in Table 3. The results are comparable to [23], which demonstrates the color (brownish yellow and yellow color), refractive index (1.45 and 1.42), specific gravity (0.89 and 0.87) and acid number (12 and 15) for *R. centifolia* oil for *R. demascena* oil, respectively. Likewise, Shabbir et al. [25] reported yellowish brown color, 1.45 refractive index, 0.82 specific gravity, 14 acid number and 28 ester number in *R. centifolia* oil. Variations in the yield, physical and chemical compositions of REO oils may be related with the genetic background, biotic, and abiotic environmental factors, as well as the extraction methods and analytical conditions [26].

The GC chromatogram of *R. indica* essential oil (REO) is presented in Figure 1 and the structure of major compounds are shown in Figure 2.

Various chemical constituents, peak area and uses of isolated compounds are depicted in Table 4.

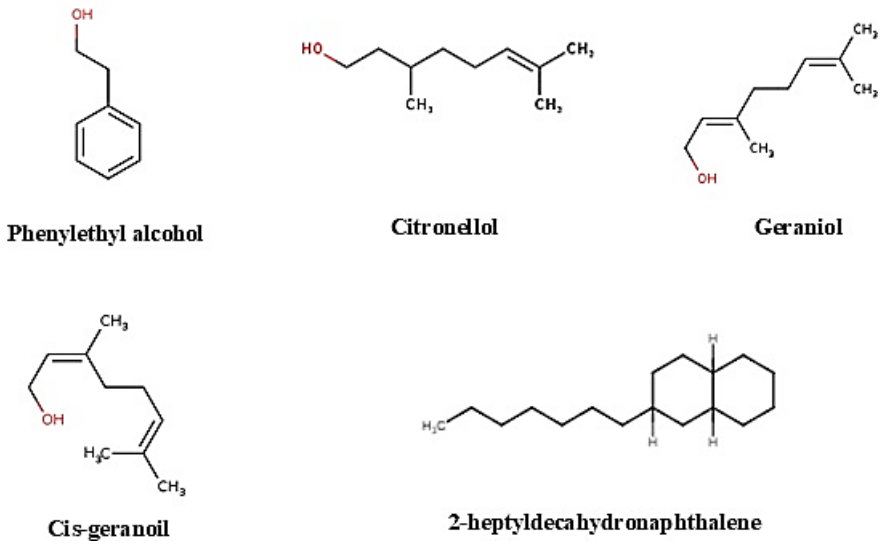

Figure 1 – Chromatogram of rose *(Rosa indica*) petal essential oil through GC-MS analysis

It was reported that these all compounds have multiple roles as antimicrobial, antiseptic, disinfectant, pharmaceutical, perfume, food and cosmetic ingredient. However, on the percentage occurrence of individual compound, the twenty-nine compounds representing 99.21% of the total content were grouped as most, moderately less and least abundant. Accordingly, three compounds, viz., 1-phenylethyl alcohol (13.02%); citronellol (10.01%) and 6-octen-1-ol, 3,7-dimethyl (9.55%) were found as most abundantly occurring compounds. However, three other compounds namely geraniol (7.11%); 2,6-octadien-1-ol, 3,7-dimethyl-(Z) (7.11%) and 2-heptyldecahydronaphthalene (5.35%) were documented as moderately abundant compounds. Six compounds namely bis(2-ethylhexyl) phthalate (3.41%); 1,4-benzenedicarboxylic acid, bis(2-ethylhexyl) ester (3.36%); diethyl phthalate (3.22%); 1-propanol, 2-(2hydroxypropoxy) (3.13%); phthalic acid, 7-bromoheptyl isobutyl ester (2.74%); cyclodecene, 3-bromo (2.66%) and 2-propanol, 1,1'-oxybis (2.27%) were reported as less abundant. Remaining fifteen compounds were among the least abundant group as their percentage of occurrence was in the range of 1-2%.

Besides, these twenty-nine compounds belong to eight major groups (Table 5).

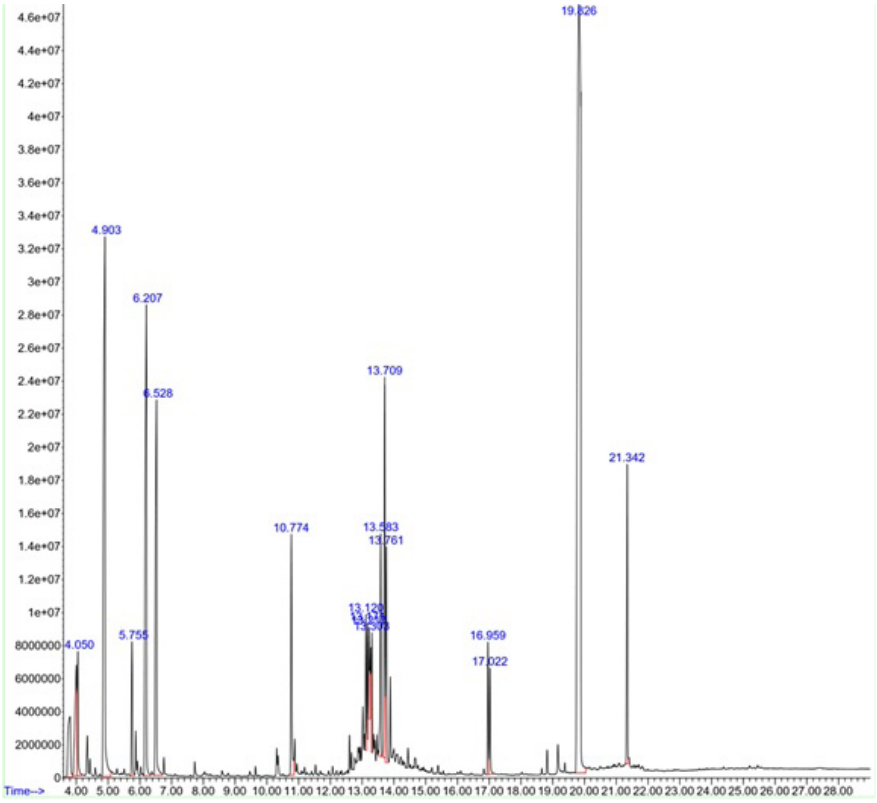

Figure 2 – Structures of compounds identified from major compounds identified from rose *(Rosa indica*) petal essential oil through GC-MS analysis

Table 4 – Biologically active compounds identified from rose *(Rosa indica*) petal essential oil through GC-MS analysis

Sr. No.	Compounds	Molecular Formula	Molecular weight (g/mol)	Retention time (min)	Peak area (%)	Uses
1	1-phenylethyl alcohol or methylphenyl carbinol	$C_8H_{10}O$	122.16	4.90	13.02	Antimicrobial, antiseptic, disinfectant, pharmacy, and perfumery [36]
2	Citronellol	$C_{10}H_{20}O$	156.26	6.20	10.01	Perfumes, insect repellents and mite attractant [37; 38]
3	6-octen-1-ol, 3,7-dimethyl or -β-Citronellol	$C_{10}H_{20}O$	156.26	6.20	9.55	
4	Geraniol	$C_{10}H_{18}O$	154.25	6.52	7.11	Food, fragrance, cosmetic, pharmacy, antimicrobial, anti-inflammatory, antioxidant, anti-cancer, and neuroprotective [39; 38]
5	2,6-octadien-1-ol, 3,7-dimethyl-,(Z) or cis-Geraniol	$C_{10}H_{18}O$	154.25	6.52	7.11	
6	2-heptyldecahydronaphthalene	$C_{18}H_{34}$	250.5	13.70	5.35	Antioxidant [40]
7	Bis(2-ethylhexyl) phthalate	$C_{24}H_{38}O_4$	390.56	19.82	3.41	Medicines, and perfumery [41]
8	1,4-benzenedicarboxylic acid, bis(2-ethylhexyl) ester	$C_{24}H_{38}O_4$	390.62	21.34	3.36	Cosmetics, plastics, medical devices, and pesticides [41]
9	Diethyl phthalate	$C_{12}H_{14}O_4$	222.24	10.77	3.22	Cosmetic, aspirin, medical tubes and antimicrobial activity [41]
10	1-propanol, 2-(2hydroxypropoxy)	$C_6H_{14}O_3$	134.17	4.00	3.13	Active surface agent, cosmetic, emollient and skin conditioning [42]

Table continuation

Sr. No.	Compounds	Molecular Formula	Molecular weight (g/mol)	Retention time (min)	Peak area (%)	Uses
11	Phthalic acid, 7-bromoheptyl isobutyl ester	$C_{19}H_2BrO_4$	399.3	13.76	2.74	Flavours, cosmetic and antimicrobial activity [43]
12	Cyclodecene, 3-bromo	$C_{10}H_{17}Br$	217.15	13.58	2.66	Antioxidant [40]
13	2-propanol, 1,1'-oxybis	$C_6H_{14}O_3$	134.17	3.80	2.27	Anti-germicidal, antifreeze, antimicrobial, intermediate for chemical reaction, and plasticizer [42]
14	Ethanol, 2-(dodecyloxy)-	$C_{14}H_{30}O_2$	230.39	5.75	1.70	Cosmetics, emulsifier, detergents, sclerosing agent and anesthetic [42]
15	1-octanol, 2,7-dimethyl	$C_{10}H_{22}O$	158.28	5.75	1.70	Perfumes, cosmetics, antiperspirant and shampoo [42]
16	1-octanol, 3,7-dimethyl	$C_{10}H_{22}O$	158.28	5.75	1.70	Perfumes, scents and dermatologist products [44]
17	3-eicosene, (E)	$C_{20}H_{40}$	280.5	16.95	1.57	Antimicrobial, antioxidant and food industry [40]
18	1-propanol, 2,2'-oxybis	$C_{20}H_{22}O_5$	342.4	4.05	1.50	Anti-germicidal, antifreeze, antimicrobial, intermediate for chemical reaction and plasticizer [42]
19	cis, cis-7,10,-hexadecadienal	$C_{16}H_{26}O$	234.38	13.12	1.43	Antioxidant [40]
20	Tricyclo[4.4.0.0(2,8)]decane	$C_{10}H_{16}$	136.23	13.12	1.43	Anti-fungal and anti-bacterial
21	Cyclohexanol, 2-methyl-5-(1 methylethenyl) or Carvomenthol	$C_{10}H_{18}O$	154.25	13.12	1.43	Detergents, plastics, resins and insecticides [42]
22	Bicyclopentylidene or cyclopentadiène	$C_{10}H_{16}$	136.23	13.21	1.40	Antifungal, insecticides and resins [45]
23	cis-(-)-1,2-epoxy-p-menth-8-ene or Limonene	$C_{10}H_{16}O$	152.23	13.21	1.40	Oviposition deterrent; insecticide; insect repellent; antimicrobial [46, 47]

Table 5 – Major groups of the bioactive compounds identified from rose *(Rosa indica*) petal essential oil through GC-MS analysis

Sr. No.	Compounds	Group	Percentage
1	1-phenylethyl alcohol or methylphenyl carbinol	Monoterpenes alcohol	59.03
2	Citronellol		
3	6-octen-1-ol, 3,7-dimethyl or -β-Citronellol		
4	Geraniol		
5	2,6-octadien-1-ol, 3,7-dimethyl-,(Z) or cis-Geraniol		
6	1-octanol, 2,7-dimethyl		
7	1-octanol, 3,7-dimethyl		
8	Cyclohexanemethanol, 2-(2 propenyl)-, trans-		
9	1-propanol, 2,2'-oxybis		
10	2-propanol, 1,1'-oxybis		
11	Ethanol, 2-(dodecyloxy)-		

Table continuation

Sr. No.	Compounds	Group	Percentage
12	2-heptyldecahydronaphthalene	Sesquiterpenes hydrocarbons	21.20
13	1-propanol, 2-(2hydroxypropoxy)		
14	Cyclodecene, 3-bromo		
15	3-eicosene, (E)		
16	cis, cis-7,10,13 -hexadecatrienal		
17	Tricyclo[4.4.0.0(2,8)]decane		
18	Cycloh hexanol, 2-methyl-5-(1 methylethenyl)		
19	Bicyclopentylidene		
20	cis-(-)-1,2-epoxy-p-menth-8-ene		
21	Bis(2-ethylhexyl) phthalate	Phthalate ester	9.99
22	1,4-benzenedicarboxylic acid, bis(2-ethylhexyl) ester		
23	Diethyl phthalate		
24	Phthalic acid, 7-bromoheptyl isobutyl ester	Acid ester	3.96
25	1,2-benzenedicarboxylic acid, butyl 2-ethylhexyl ester		
26	4-ethyl-2-hexynal	Aldehyde hydrocarbons	1.40
27	3-octyne, 2,2,7-trimethyl-	Alkyne hydrocarbons	1.21
28	1-methylbicyclo(4.4.0)decane(trans)	Aromatic hydrocarbons	1.21
29	3-(3,5-dimethyl-1H-pyrazol-4yl) propanamide	Pyrozol derivative	1.21
Total content			99.21

Among eight groups, monoterpene alcohol represented the main characterized class (59%) of the total oil content followed by sesquiterpenes hydrocarbons (21.20%), phthalate ester (9.99%), aldehyde hydrocarbon (1.41%), alkyne hydrocarbons (1.21%), aromatic hydrocarbons (1.21%) and pyrozole derivative (1.21%). Baydar et al. [27] also found occurrence of high percentage of the monoterpene alcohols (1-phenylethyl alcohol, citronellol and geraniol) in rose essential oil. Monoterpene alcohols especially 1-phenylethyl alcohol and citronella are anticipated for high rose oil quality and are responsible for perfumery value of rose oil [21]. Başer [28] also documented that greater proportion of the monoterpene alcohol components and less fractions of the sesquiterpene hydrocarbon in rose essential oil. Occurrence of hydrocarbons as the second highest components in rose oil following monoterpene are in accordance with report of [26]. In other studies, methyl eugenol was also reported in rose (*R. damascene*) essential oil [21,26,27]. However, in the current study, methyl eugenol was not present in REO, which might be ascribed that in those studies the flowers were from the late harvest of full-blown flowers or rose oils distilled from long-term fermented flowers [27]. Dobreva et al. [29] also enlighten the major volatile contents (citronellol, geraniol, nerol and nonadecane) of three oil-bearing genotypes of roses in Kazanluk. The occurrence of other class of volatile organic compounds contains acid ester and some derivative of phthalate ester were also reported by [30] in rose essential oil.

The organoleptic test of the formulated hand sanitizer (with or without REO) revealed that both gels were homogeneous, clear, easy to apply, light to spread, and had a consistent flow with the REO distinctive odor. The results were consistent with the previous findings [19]. Formulate hand sanitizer without REO (pH 4.80; viscosity 9910 cP and density 0.90 g/mL), and combination with REO (pH 4.51; viscosity 10340 cP and density 0.91 g/mL) exhibited acceptable levels (Table 6).

Table 6 – Physical properties of the formulated hand sanitizer (FHS) and along with rose essential oil (FHS-REO)

Sr. No.	Property	FHS Mean values ± S.D.	FHS-REO Mean values ± S.D.	FHS-REO Mean values ± S.D.	FHS-REO Mean values ± S.D.
1	Color	Transparent	Transparent	Transparent	Transparent
2	Odor	Alcoholic	Sweat rosaceous	Alcoholic	Alcoholic
3	Consistency	Clear gel	Clear gel	Clear gel	Clear gel
4	pH	4.80 ± 0.24	4.51 ± 0.33	4.92 ± 0.35	4.67 ± 0.13
5	Viscosity (cP)	9910 ± 0.19	10340 ± 0.14	9159 ± 0.34	10060± 0.14
6	Density (g/mL)	0.90 ± 0.31	0.91± 0.09	0.93± 0.15	0.98 ± 0.11

The results were comparable with the findings of [19] who also reported almost similar properties of the hand sanitizer prepared with addition of citrus peel essential oil. The results also revealed that formulated hand sanitizer with REO is safe for the skin as shown by its pH tolerant at 5.20-5.50 [31]. Generally, a pH range of 4 to7 avoids skin inflammation and irritation and is taken as safe range for broad range of skin. Moreover, recorded density of the product was lower than water, which indicated easy application of the product on the skin. The viscosity of the hand sanitizers was also accordance with the specification standard (2381-16893 cP) that may show ease with which the product can easily be poured and dripped on the palm [19].

The antimicrobial activity of formulated hand sanitizer against *Escherichia coli* seemed to be caused by the alcohol, as the alcohol-based hand sanitizers has been shown to kill gram-positive and negative bacteria [32]. WHO [33] also recommended utilization of alcohol-based hand sanitizers due to the broad and rapid action against microbes with the minimal risk of generating microbial resistance. REO also exhibited antimicrobial activity (61.71%), as indicated by the area of inhibition. High levels of citronellol and geraniol in the REO could be accountable for its antimicrobial potential. Similar investigations have been documented previously with the essential oil of *R. damascene* against human pathogenic fungi and bacteria [34] However, synergistic effects of many other components, may also contribute to antimicrobial activity of REO, which possibly have caused cell lysis by disturbing microbial cell permeability [34,35]. Besides, formulated hand sanitizer with REO showed more antimicrobial potential (87.81%) as compared to hand sanitizer without REO or REO alone. The antimicrobial activity of the formulated hand sanitizer was comparable with available hand sanitizer in the market (Table 7).

Table 7 – Antimicrobial assays against *Escherichia coli*

Sr. No.	Treatment	% Inhibition in growth
1	Control (water)	0
2	Control (DMSO)	15.00^{d}
3	Formulated hand sanitizer without REO	73.30^{b}
4	Formulated hand sanitizer with REO	87.81^{a}
5	REO	61.71^{c}
6	Market hand sanitizer 1	75.35^{b}
7	Market hand sanitizer 2	86.79^{a}

Letter in superscript indicate significant difference as showed by LSD test. The acceptability test study for formulated gel with REO was performed on 20 volunteers, and the results are presented in the Table 8.

It was revealed that the product felt nice in use since it is not sticky, does not produce any skin irritation, has delicate smell, liked by the prevailing number of users (≤ 65%).

Table 8 – Consumer response of formulated hand sanitizer with rose essential oil (FHS-REO).

Sr. No.	Property	Color	Clarity	Aroma	Thickness	Sticky
1	Score 1	0	0	0	0	0
2	Score 2	0	0	0	0	0
3	Score 3	20	10	0	10	10
4	Score 4	10	25	10	20	20
5	Score 5	70	65	90	70	70
Values are shown in %						

Conclusions

As was shown by our experiments. rose essential oil (REO) isolated from the fresh petal has a certain potential to be used as a supplementary component for improving the aroma of hand sanitizer with acceptable physical and microbiological quality parameters. Yield of REO from 10 kg of petal was 0.057% on the petal fresh weight when isolating with hydro-distillation method. The physical quality parameters of REO including density (0.92 g/mL), refractive index (1.45), viscosity (9.46 mPa), specific gravity (0.92), optical rotation (optically active), acid number (14.1024), ester number (28.187), appearance (clear liquid), color (transparent), and odor (floral, strong, and sweet rosaceous character) were established. Variations in the yield, physical and chemical compositions of REO oils may be related with the genetic background, biotic, and abiotic environmental factors, as well as the extraction methods and analytical conditions. Three compounds, viz, 1-phenylethyl alcohol (13.02%), citronellol (10.01%) and 6-octen-1-ol, 3,7-dimethyl (9.55%) were found as most abundantly occurring compounds. However, three other compounds namely geraniol (7.11%); 2,6-octadien-1-ol, 3,7-dimethyl-(Z) (7.11%) and 2-heptyldecahydronaphthalene (5.35%) were documented as moderately abundant compounds. Six compounds namely bis(2-ethylhexyl) phthalate (3.41%); 1,4-benzenedicarboxylic acid, bis(2-ethylhexyl) ester (3.36%); diethyl phthalate (3.22%); 1-propanol, 2-(2hydroxypropoxy) (3.13%); phthalic acid, 7-bromoheptyl isobutyl ester (2.74%); cyclodecene, 3-bromo (2.66%) and 2-propanol, 1,1'-oxybis (2.27%) were reported as less abundant. Remaining fifteen compounds were among the least abundant group as their percentage of occurrence was in the range of 1-2%. High levels of citronellol and geraniol in the REO could be accountable for its antimicrobial potential.

References

1 Mangalagiri N.P., Panditi S.K., Jeevigunta N.L.L. (2021) Antimicrobial activity of essential plant oils and their major components. Heliyon, vol. 7, no. 4, pp. e06835. https://doi.org/10.1016/j.heliyon.2021.e06835.

2 Bhavaniramya S., Vishnupriya S., SalehAl-Aboody M., Vijayakumar R., Baskaran D. (2019) Role of essential oils in food safety: Antimicrobial and antioxidant applications. Grain Oil Sci Technol., vol. 2, no. 2, pp. 49-55. https://doi.org/10.1016/j.gaost.2019.03.001.

3 Rehman A., Jafari S.M., Aadil R.M., Assadpour E., Randhawa M.A., Mahmood S. (2020) Development of active food packaging via incorporation of bio polymeric nano carriers containing essential oils. Trends Food Sci Technol., vol. 101, no. pp. 106-121. https://doi.org/10.1016/j.tifs.2020.05.001.

4 Anupama G., Netravathi D.K., Avinash M. (2019) Essential oils: A novel source for food preservation. J Pharmacog Phytochem., vol. 8, pp. 2098-2101.

5 Bakkali F., Averbeck S., Averbeck. D, Idaomar. M. (2018) Biological effects of essentialoils–a

review." Food Chemical Toxicol., vol. 46, no. 2, pp. 446-475. https://doi.org/10.1016/j.fct.2007.09.106.

6 Mei J., Ma X., Xie J. (2019) Review on natural preservatives for extending fish shelf life. Foods, vol. 8, no. 10, pp. 490. https://doi.org/10.3390/foods8100490.

7 Doost A.S., Nasrabadi M.N., Kassozi V., Nakisozi H., Meeren P.V.D. (2020) Recent advances in food colloidal delivery systems for essential oils and their main components. Trends Food Sci Technol., vol. 99, pp. 474-486. https://doi.org/10.1016/j.tifs.2020.03.037.

8 Gyawali R., Hayek S. A., Ibrahim S. A. (2015) Plant extracts as antimicrobials in food products: Mechanisms of action, extraction methods, and applications. Handbook of Natural Antimicrobials for Food Safety and Quality, vol. 49, pp. 49-62.

9 Verma A., Srivastava R., Sonar P.K., Yadav R. (2020) Traditional, phytochemical, and biological aspects of Rosa alba L.: A systematic review. Future J Pharmace Sci., vol. 6, no. 1, pp. 1-8. https://doi.org/10.1186/s43094-020-00132-z.

10 Rasheed H.M., Khan T., Wahid F., Khan R., Shah A.J. (2015) Chemical composition and vasorelaxant and antispasmodic effects of essential oil from Rosa indica L. petals. Evid-Based Complem Alter Med. vol. 2015, |Article ID 279247. https://doi.org/10.1155/2015/279247.

11 Androutsopoulou C., Christopoulou S.D., Hahalis P., Kotsalou C., Lamari F.N., Vantarakis A. (2021) Evaluation of essential oils and extracts of Rose geranium and rose petals as natural preservatives in terms of toxicity, antimicrobial, and antiviral activity. Pathogens, vol. 10, no. 4, pp. 494. https://doi.org/10.3390/pathogens10040494.

12 Farooq A., Khan M.A., Ali A., Riaz A. (2011) Diversity of morphology and oil content of Rosa damascene landraces and related Rosa species from Pakistan. Pak J Agri Sci., vol. 48, no. 3, pp. 177–183.

13 Georgiev E., Stoyanova A. (2006) A guide for the specialist in aromatic industry, Plovdiv Bulgaria.

14 Bhatia H., Sharma Y.P., Manhas R.K., Kumar K. (2015) Traditional Phyto remedies for the treatment of menstrual disorders in district Udhampur, J&K, India. J Ethnopharmacol., vol. 160, pp. 202-210. https://doi.org/10.1016/j.jep.2014.11.041

15 Khan J.A., Saurabh T. (2011) A study on antibacterial properties of Rosa indica against various pathogens. Elect J Environ Agric Food Chem., vol. 10, no. 9, pp. 2838-2846.

16 Bahrami A., Delshadi R., Jafari S.M, Williams L. (2019) Nanoencapsulated nisin: An engineered natural antimicrobial system for the food industry. Trends Foof Sci Technol., vol. 94, pp. 20-31. https://doi.org/10.1016/j.tifs.2019.10.002.

17 Dinwiddie M.T., Terry P.D., Chen J. (2014) Recent evidence regarding triclosan and cancer risk. Inter J Environ Res Pub Health, vol. 11, no. 2, pp. 2209-2217. https://doi.org/10.3390/ijerph110202209.

18 Lee J., Durst R.O.B.E.R.T., Wrolstad R.O.N.A. L.D. (2005) AOAC official method 2005.02: total monomeric anthocyanin pigment content of fruit juices, beverages, natural colorants, and wines by the pH differential method. Official methods of analysis of AOAC International.

19 Wijana S., Pratama E.P., Rahmah N.L., Arwani M. (2020) Hand sanitizer formulation using orange peel essential oil. In: IOP Conference Series. Earth Environ Sci., vol. 524, no. 1, p. 1-5. https://doi:10.1088/1755-1315/524/1/012021.

20 Elhawary E.A., Mostafa N.M., Labib R.M., Singab A.N. (2021) Metabolomic profiles of essential oils from selected rosa varieties and their antimicrobial activities. Plants, vol. 10, no. 8, pp. 1721. https://doi.org/10.3390/plants10081721.

21 Kara N., Erbaş S., Baydar H. (2017) The Effect of Seawater Used for Hydrodistillation on essential oil yield and composition of oil-bearing rose (Rosa damascena Mill.). Int J Secon Metabol., vol. 4, no. 3, pp. 423-428. https://doi.org/10.21448/ijsm.375120.

22 Oktavianawati K., Letisya N., Citra P., Utari D.P., AdiWinata I.N., Wuryanti Handayani W., Nugraha A.S (2019) Essential oil composition of rose flowers from karangpring village Jember district extracted by distillation and enfleurage. Jurnal Ilmu Dasar., vol. 20 no. 2, pp. 67-74. doi:https://doi.org/10.19184/jid.v20i2.8995

23 Khan M.A., Rehman S.U. (2005) Extraction and analysis of essential oil of Rosa species. Institute of Horticultural Sciences, University of Agri. Int J Agri Biol., 1560–8530/2005/07–6–973–974 http://www.ijab.org.

24 Pal P.K. (2013) Evaluation, genetic diversity, recent development of distillation method, challenges and opportunities of rosa damascene. J Essent Oil-Bear Plants, vol. 16, no. 1, pp.1-10. https://doi.org/10.1080/0972060X.2013.764176.

25 Shabbir M.K., Nadeem R., Mukhtar H., Anwar F., Mumtaz M.W. (2009) Physico-chemical analysis and determination of various chemical con-

stituents of essential oil in Rosa centifolia. Pak J Bot., vol. 41, no. 2, pp. 615-620.

26 Kazaz S., Baydar H., Erbas S. (2009) Variations in chemical compositions of Rosa damascena Mill. and Rosa canina L. fruits. Czech J Food Sci., vol. 27, no. 3, pp. 178-184. https://doi.org/10.17221/5/2009-CJFS.

27 Baydar H., Schulz H., Kruger H., Erbas S., Kineci S. (2008) Influences of fermentation time, hydro-distillation time and fractions on essential oil composition of Damask Rose (Rosa damascena Mill.). J Essenl Oil-Bear Plants., vol. 11, no. 3, pp. 224-232. https://doi.org/10.1080/0972060X.2008.10643624.

28 Baser K.H.C. (1992). Essential oils of Anatolian Labiatae: a profile. In WOCMAP I-Medicinal and Aromatic Plants Conference: part 1 of 4 33, pp. 217-238.

29 Dobreva A., Velcheva A., Bardarov V., Bardarov K. (2013) Chemical composition of different genotypes oil-bearing roses. Bulga J Agri Sci., vol. 19, no. 6, pp. 1213-1218.

30 Koksal N., Saribas R., Kafkas E., Aslancan H., Sadighazadi S. (2015) Determination of volatile compounds of the first rose oil and the first rose water by HS-SPME/GC/MS techniques. Afr J Tradit Complement Altern Med., vol. 12, no. 4, pp. 145. doi:10.4314/ajtcam.v12i4.21.

31 Milala A.S., Sofyan M., Wahjudi M. (2014) The formulation and antibacterial activity of hand sanitizer gels containing lampes (Ocimum sanctum L.) leaves extract as an active compound. In: International Symposium on Medicinal Plant and Traditional Medicine, 4-6 Jun 2014, Tawangmangu, Karanganyar, Indonesia, pp. 1-7. http://repository.ubaya.ac.id/id/eprint/24353.

32 Czerwinski S.E., Cozean J., Cozean C. (2014) Novel water-based antiseptic lotion demonstration rapid, broad-spectrum kill compared with alcohol antiseptic. J Infect Public Health., vol. 7, no. 3, pp. 199-204. https://doi.org/10.1016/j.jiph.2014.01.002.

33 Safety W.P., World Health Organization. (2009) WHO guidelines on hand hygiene in health care (No. WHO/IER/PSP/2009/01). World Health Organization.

34 Ghavam M., Afzali A., Manca M.L. (2021) Chemotype of damask rose with oleic acid (9 octadecenoic acid) and its antimicrobial effectiveness. Sci Rep., vol. 11, no. 1, pp. 1-7. https://doi.org/10.1038/s41598-021-87604-1.

35 Ghavam M., Manca M.L., Manconi M., Bachetta G. (2020) Chemical composition and antimicrobial activity of essential oils obtained from leaves and flowers of Salvia hydrangea DC. Ex Benth. Sci Rep., vol. 10, no. 1, pp. 15647. https://doi.org/10.1038/s41598-020-73193-y

36 Scognamiglio J., Jones L., Letizia C.S., Api A.M. (2012) Fragrance material review on phenylethyl alcohol. Food Chem Toxicol., vol. 50, no. 2, pp. 224–S239. https://doi.org/10.1016/j.fct.2011.10.028.

37 Yadav D.G., Lathi P.S. (2004) Synthesis of citronellol laurate in organic media catalyzed by immobilized lipases: kinetic studies. J. Mol. Catal. B Enzym., vol. 27, no.3, pp. 113-119. https://doi.org/10.1016/j.molcatb.2003.10.004.

38 Rihayat, T., Hasanah, U., Siregar, J. P., Jaafar, J., & Cionita, T. (2020, April). Geraniol quality improvement on citronella oil as raw material for making anti-bacterial perfumes. In: IOP Conference Series: Mater Sci Eng., vol. 788, no. 1, pp. 012028. IOP Publishing.

39 Mączka W., Wińska K., Grabarczyk M. (2020) One hundred faces of geraniol. Molecules, vol. 25, no. 14, pp. 3303. https://doi.org/10.3390/molecules25143303.

40 Assaeed A., Elshamy A., El Gendy A.E.N., Dar B., Al-Rowaily S., Abd-ElGawad A. (2020) Sesquiterpenes-rich essential oil from above ground parts of Pulicaria somalensis exhibited antioxidant activity and allelopathic effect on weeds. Agronomy, vol. 10, no. 3, pp. 399. https://doi.org/10.3390/agronomy10030399.

41 Jadhao M., Tsai E. M., Yang H.C., Chen Y.F., Liang S.S., Wang T.N., Teng Y.N., Huang H.W., Wang L.F., Chiu C.C. (2021) The long-term DEHP exposure confers multidrug resistance of triple-negative Breast Cancer Cells through ABC transporters and intracellular ROS. Antioxidants, vol. 10, no. 6, pp. 949. https://doi.org/10.3390/antiox10060949

42 Kozioł A, Stryjewska A, Librowski T, Sałat K, Gaweł M, Moniczewski A, Lochyński S. (2014) An overview of the pharmacological properties and potential applications of natural monoterpenes. Mini Rev Med Chem., vol. 14, no. 14, pp. 1156-68. DOI: 10.2174/1389557514666141127145820.

43 Baloyi N.D., Tekere M., Maphangwa K.W., Masindi V. (2021) Insights into the prevalence and impacts of Phthalate Esters in aquatic ecosystems. Front Environ Sci., vol. 9. https://doi.org/10.3389/fenvs.2021.684190.

44 Lapczynski S.P., Bhatia., C.S., Letizia A.M. (2008) Api, Fragrance material review on 3,7-dimethyl-octanol. Food Chem Toxicol., vol. 46, no. 11, pp. 139-141. doi: 10.1016/j.fct.2008.06.023.

45 Hudon J. (2009) Methodologies in organic chemistry and their applications to the synthesis of bioactive small molecules. Ph D thesis. McGill University Montreal, Quebec, Canada.

46 Aggarwal K.K., Khanuja S.P.S., Ahmad A., Santha Kumar T.R., Gupta V.K., Kumar S. (2002) Antimicrobial activity profiles of the two enantiomers of limonene and carvone isolated from the oils of Mentha spicata and Anethum sowa. Flavour Frag J., vol. 17, no. 1, pp. 59-63. https://doi.org/10.1002/ffj.1040.

47 Ibrahim M.A., Kainulainen P., Aflatuni A., Tiilikkala K., Holopainen J.K. (2001) Insecticidal, repellent, antimicrobial activity and phytotoxicity of essential oils: with special reference to limonene and its suitability for control of insect pests. Agr Food Sci Finland., vol. 10, no. 3, pp. 243-59. https://doi.org/10.23986/afsci.5697

IRSTI 31.25.19 https://doi.org/10.26577/ijbch.2021.v14.i2.011

U. Nakan[1*], B. Tolkyn[2], G.A. Mun[3],
G.Zh. Yeligbayeva[1], N.B. Tileubekov[1], N. Serikbay[1],
E.S. Negim[4]

[1]Satbayev University, Almaty, Kazakhstan
[2]A.B. Bekturov Institute of Chemical Sciences, Almaty, Kazakhstan
[3]Al-Farabi Kazakh National University, Almaty Kazakhstan
[4]Kazakh-British Technical University, Almaty, Kazakhstan
[*]e-mail: ulantaynakan@gmail.com

Swelling studies on poly(n, n-dimethyl acrylamide-co-acrylic acid) hydrogels

Abstract. Hydrogel copolymers based on N, N-dimethyl acrylamide (DMA) and acrylic acid (AAc) were synthesized with different molar composition ratios ([DMA:AAc] = 30:70, 50:50 and 70:30 mol. %) using ammonium peroxydisulfate as a free radical initiation system in the presence of various amounts of *N, N'*-methylene bis (acrylamide) as a crosslinker (0.05, 0.1 and 0.3 mol. %) and water as reactant medium. The swelling behavior of the obtained was characterized based on the amount of the by different amounts to added of the crosslinking agent. While the use of a large amount of crosslinking agent in the poly (DMA-co-AAc) hydrogels was reduced the swelling degree in the water medium, a smaller amount in the gel indicated the tendency of the gel to burst. Absorption studies were made using different concentrations of copper sulfate ($CuSO_4$). Poly(DMA-co-AAc) hydrogels absorption capacity is competitive when there are more N, N-dimethyl acrylamide content in copolymer than others. The swelling ratios of low concentration of Cu (II) ion are higher than those of higher concentration of Cu (II) ion. Hydrogel gave the highest swelling ratio for the solution containing the lowest Cu (II) ion concentration than for the solution containing the highest Cu (II) ion.

Key words: N, N-dimethyl acrylamide; acrylic acid; hydrogel; swelling degree; treating wastewater.

Introduction

Cross-linked polymers with various properties have been applied in industrial applications, including medicine, agriculture, electronics, biotechnology, engineering, food industry, etc. Polymers belong to the class of intelligent polymers because of their sensitivity to temperature [1-5].

N-isopropyl acrylamide hydrogels are widely studied as thermosensitive materials in different applications because of their excellent valuable properties. Phase transition of such polymers occurs at a fixed temperature interval. For poly-N-isopropyl acrylamide, its low critical solution temperature (LCST) is 32□. It noted that a person's change in body temperature from normal to elevated during diseases is within 36-41□. That is why the expansion of the thermal sensitivity range of the above-mentioned linear copolymers is significant. The task can be solved by adjusting the hydrophilic-hydrophobic balance of macro chains by copolymerizing these monomers with other comonomers [6-10].

Many authors studied the swelling kinetics based on DMA hydrogels with different monomers in different nature. Several monomers had been added to copolymer based on DMA to improve its special properties for applications, such as ion loading hydrogels. That the swelling kinetics of hydrogel had different properties depending on copolymer composition (hydrophobic/hydrophilic balance of copolymer), crosslink density, the degree of ionization and their interaction with ions are important [11-15].

The crucial application of hydrogel is a carrier of medicinal substances, such as drug delivery and high antibacterial activity. Poly(DMA-co-AAc) cross-linked copolymers have shown antimicrobial properties against both Grams (positive and negative) bacteria. Hydrogels' killing bacteria and drug delivery mechanisms have been proposed to improve Poly(DMA-co-AAc) [15].

In the present work, Poly(DMA-co-AAc) hydrogels were prepared using free radical polymerization in water media. The swelling properties of poly(DMA-co-AAc) hydrogel aqueous solution were investigated via the gravimetric method. Kinetics of sorption metal ions of Poly(DMA-co-AAc) hydrogel were studied

Materials and methods

Material. N, N-dimethyl acrylamide (DMA, 99%), ammonium persulfate (98%, APS, CAS 7727-54-0), *N, N'*-methylene-bis-acrylamide (99%, BIS, CAS 110-26-9), and Copper (II) salt ($CuSO_4$) (98%, CAS 7758-99-8) were purchased from Sigma Aldrich (Heidelberg, Germany). Oil emulsion was obtained from the Kyzylkiya field (Kazakhstan).

Synthesis of Poly(DMA-co-AAc) hydrogels. Hydrogels based on DMA and AAc were synthesized with different molar composition ratios (M1 (30:70), M2 (50:50), and M3 (70:30)), by free radical polymerization in water in presence of ammonium persulfate (2×10^{-2} M) as the radical initiator and *N,N'*-methylene bis (acrylamide) (0.05, 0.1 and 0.3 mol. %) as the cross-linking agent. Monomer mixture accounts 30% of the total volume, and the rest belongs to the solvent. The whole volume of reagents and solvent mixture was retained at 10 mL for all the compositions.

After degassing with argon for about 10 min to remove oxygen, the glass ampoule containing the reaction mixture was hermetically sealed and placed in the water bath at 60□ for various times (10, 20 and 40 minutes).

The obtained hydrogels were washed with distilled water for 10 days to purify the samples from unreacted monomers. Then, the hydrogel samples were dehydrated at room temperature and in a vacuum oven until the weight was kept constant [14].

Swelling study. Hydrogels were taken out after a reaction was cleaned by using distilled water for several days from unreacted monomers. The cleaned hydrogels were cut into small pieces of about 0.5 cm in height and dehydrated. The drying sample was in a vacuum oven at 25 □ until the weight was constant.

The swelling degree (g/g) was calculated from the formula:

$$\alpha=(m-m_0)/m_0$$

Where m is the mass of the swollen hydrogel (g); m_0 is the gel specimens' weight in dried (g); and α is the – degree of swelling.

Gel (**G**) and sol (**S**) fractions yield were calculated according to the formulas:

$$G = m_0/m_s * 100\%$$
$$S=100-G$$

where S is the sol fraction.

m_0 is the weight of the dry sample, g;

m_s is the weight of the synthesized sample, g.

The cross-linking density (j) calculated from formula:

$$J=1/(S+S^{1/2})$$

Results and discussion

The application of hydrogels in many fields is dependent on their swelling behavior in aqueous media. Therefore, studying the swelling kinetics of hydrogels are very important. The swelling ability of Poly(DMA-co-AAc) hydrogels aqueous solution were investigated via the gravimetric method. Figure 1 depicts the degree of swelling and time for the hydrogels based on different ratio monomers DMA and AAc. Water absorbability of Poly(DMA-co-AAc) hydrogels was determined. After two days, water absorption of the gel slows downed and further saturated and striving for balance. The swelling ability of Poly(DMA-co-AAc) was dependent on the copolymer composition. Thus, this process increases with decreasing the ratio of DMA in the hydrogel. The hydrogel showed the highest degree of swelling when more acrylic acid content was in copolymer than others. The work of many researchers reported swelling properties of hydrogels to depend on many factors, such as network density, monomer and solvent nature, polymer-solvent interaction parameter and more [16,17]. The swelling of these Poly(DMA-co-AAc) hydrogels relies on monomers' nature and parameters of synthesis. Although these hydrogels were synthesized under the same conditions, they showed different degrees of swelling, depending on the monomers nature. Comparing samples M1 and M3, the swelling degree decreased due to increasing the AAc ratio in the copolymer, suggesting.

Synthesis-time and crosslinking content are essential parameters in the preparation of three-dimensional copolymers. If the crosslinking agent in hydrogel synthesis is large, it can be crosslinking tightly and retain only a small amount of solvent. This is inefficient for polymers used as carriers of

our solution. The low content of binders leads to the fact that the hydrogel is rarely meshed, absorbs a considerable amount of solvents, and has difficulties in application. Therefore, it is essential to choose the optimal amount of sewing agent.

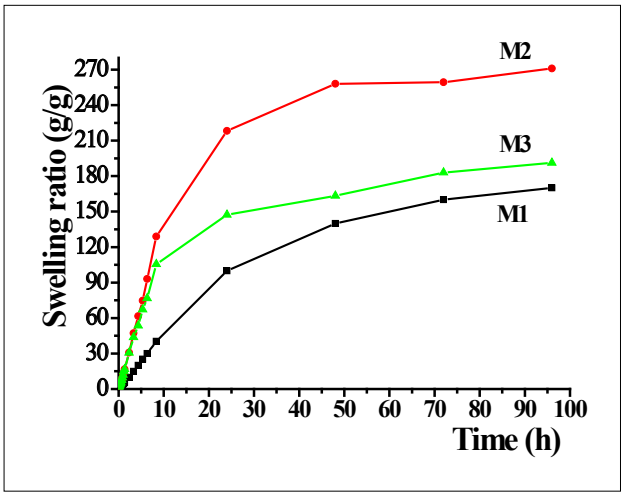

Figure 1 – Time-dependent swelling of poly (DMA-co-AAc) hydrogels

N,N-methylene-bis-acylamide was used as a crosslinking agent in the synthesis of Poly(DMA-co-AAc) hydrogel. Hydrogels with DMA monomer content of 50% (M2) at three different concentrations of the crosslinking agent (0.05 (a); 0.1 (b) and 0.3 (c) mol.%) were synthesized, and their swelling ability in aqueous medium was studied by gravimetric method. As shown in Figure 2, the higher crosslinking content in the hydrogel (Figure 5a), the lower the degree of swelling in water compared to other conditions (a = 128 g/g), and the lower the gel fraction yield (G = 17.42). This is because the frequent stitching of Poly(DMA-co-AAc) hydrogel prevents water from entering the gel and expanding the grid. Although Poly(DMA-co-AAc) hydrogel contains a small amount of crosslinking agent (Figure 5b), despite the high gel-sol fraction yield (G = 46.68) and swelling degree in water (a = 387 g/g), the gel absorbs a large amount of water. It retains its stable form tends to collapse easily without saving, which causes inconvenience to use. The most favorable condition for synthesizing poly (DMA-co-AAc) copolymer is 0.1 mol. % of the crosslinking agent in the gel. The swelling degree of the gel was 270 g/g, and the gel yield of the fraction was around G = 34. Furthermore, hardness and softness of this hydrogel are very favorable compared to others, and the gel can retain its stable shape.

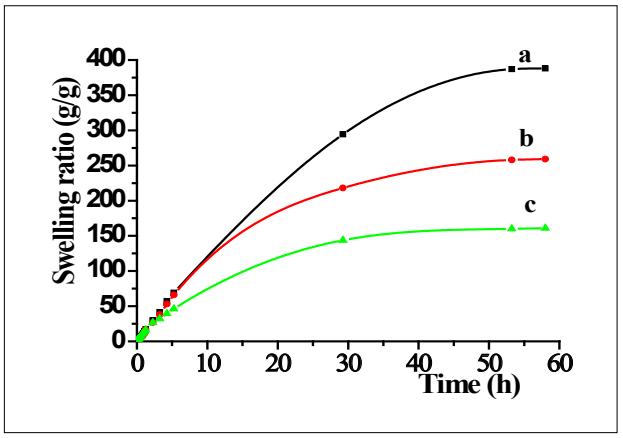

Figure 2 – Effect of the crosslinking agent content on the swelling ratio of poly(DMA-co-AAc) (M2).
a – 0.05; b – 0.1; c – 0.3 mol. % (crosslinking agent)

The swelling degree of hydrogel, along with crosslinking agents, affects the time of synthesis. During polymer synthesis, the longer the temperature is kept below the optimum temperature (in thermostat), the harder the gels are obtained, and the shorter the time, the opposite is true. Therefore, both the synthesis time and the amount of crosslinking are especially important in describing polymerization. Synthesize hydrogels at different times (10, 20 and 40 minutes) of Poly(DMA-co-AAc) hydrogels of swelling kinetics were studied. The initial monomeric composition of the study was 50-50 mol. % (M2) of hydrogel was obtained. The swelling degree of gel for more than two days, kept for 10 minutes at 60 □ in hydrogel preparation, was 387 g/g. The gel reaches its maximum swelling level, it tends to explode faster without retaining its shape. Such Poly(DMA-co-AAc) hydrogels are useless in terms of use. It was proved that the hydrogel, which has a longer fusion time in the thermostat (Figure 3c), can absorb only a small amount of water. This proved ineffective. We consider the optimal time to be 20 minutes (Figure 3b).

For Poly(DMA-co-AAc), the hydrogel properties for metal ions absorption at various concentrations of metal ion, i.e. copper salts ($CuSO_4$), were investigated by the gravimetric method related to time. The degree of metal ions absorption of poly (DMA-co-AAc) hydrogel samples (M1 and M2) is lower than another sample hydrogel.

The hydrogel containing the greatest amount of DMA (sample M3) possessed the highest degree of swelling as compared with the other prepared copolymers (Figure 4, M3).

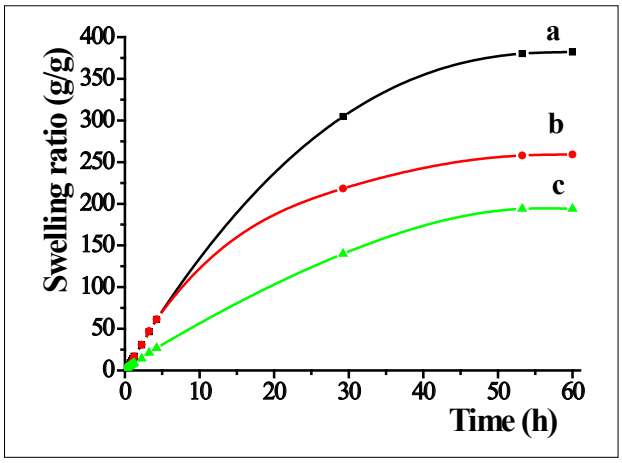

Figure 3 – Swelling kinetics of the prepared Poly(DMA-co-AAc) hydrogels (M2) as a function of the time of synthesis. a – 10 minutes; b – 20 minutes; c – 40 minutes

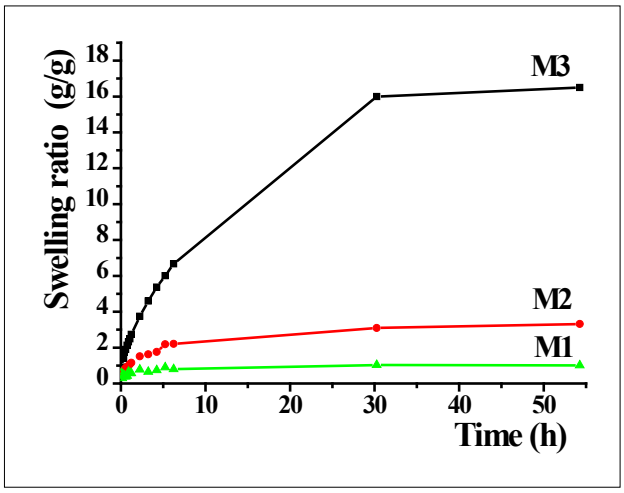

Figure 4 – Kinetics of sorption of Cu (II) ions (0.1M ($CuSO_4$)) of Poly(DMA-co-AAc) hydrogel

The kinetics of sorption various of Cu (II) ion in presence of copolymer hydrogel (M3) is presented on Figure 5.

The swelling degree of the hydrogel containing 0.001M of Cu (II) ions is higher than solutions containing 0.01 and 0.1M. However, the swelling ratios increase with increasing time from 10 to 90 hours. Oil and water are substances that do not mix and become a heterogeneous mixture where oil is at the top and water at the bottom. This is attributed to their density.

Washing of the obtained hydrogels with distilled water was several days for cleaning the hydrogels from monomers unreacted. It was noted that hydrogels performed a high swelling ratio, and initial volume increased several times while immersed in distilled water. It reaches saturation levels by absorbing water. The necessary part of this swollen hydrogel is placed in a cylinder with a diameter of 30 mm and fixed on a tripod, as presented on Figure 6.

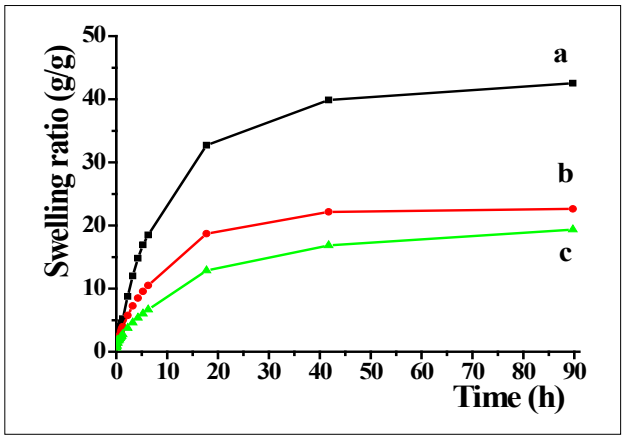

Figure 5 – Kinetics of absorption of Cu (II) ions by poly (DMA-co-AAc) (M3) hydrogel. 0.001M (a); 0.01M (b) and 0.1M (c) solution of $CuSO_4$

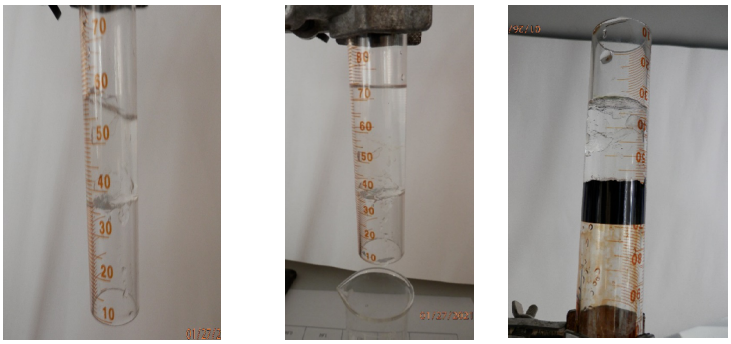

A B C

Figure 6 – The potential capability of hydrogel applied to the treatment of oil-contaminated water. Note: A – hydrogel, B – hydrogel with water, C – hydrogel with the oil emulsion

While pouring distilled water from the top, the water was filtered. As shown in Figure 6c, the hydrogel can hold the oil emulsion without letting it go down. The oil emulsion's viscosity was very close to the water and was obtained from the Kyzylkiya field (Kazakhstan). Due to the hydrophobic nature of the oil, Poly(DMA-co-AAc) hydrogel did not absorb the oil's emulsion. As shown by our results the water accumulating in the oil underside can be cleaned by passing through hydrogels.

Conclusion

Poly(DMA-co-AAc) hydrogels were prepared using free radical polymerization in water media. All the hydrogel copolymers are characterized by swelling properties. Highly swelling ratios distinguish the hydrogel copolymers in the crosslinking agent where is the highest content of crosslinking gave the highest swelling ratios. The optimum time for synthesis of hydrogel was studied. Synthesis time (20 minutes) was the optimum time for hydrogel, but 10 minutes gave soft hydrogel and 40 minutes gave rigid hydrogel. The potential capability of hydrogel in the treatment of oil-contaminated water was investigated. Hydrogel gave the highest swelling ratio for solution containing lowest concentration of Cu (II) ion than for solution containing highest concentration of Cu (II) ion. Based on the results of the study, Poly(DMA-co-AAc) hydrogel can be applied to remove oil from oil-contaminated water.

References

1 Ashok Kumar, Akshay Srivastava, Igor Yu Galaev, Bo Mattiasson. (2007) Smart polymers: Physical forms and bioengineering applications. Progress in Polymer Science. Vol 32, № 10, PP 1205-1237 https://doi.org/10.1016/j.progpolymsci.2007.05.003

2 Louise Van Gheluwe, Igor Chourpa,Coline Gaigne and Emilie Munnier (2021) Polymer-Based Smart Drug Delivery Systems for Skin Application and Demonstration of Stimuli-Responsiveness. Polymers 13(8), 1285; https://doi.org/10.3390/polym13081285

3 Qu Jin, Zhao Xin, Ma Peter X., Guo Baolin. (2018) Injectable antibacterial conductive hydrogels with dual response to an electric field and pH for localized "smart" drug release. Acta Biomaterialia. Vol.72, PP. 55–69. http://dx.doi.org/10.1016/j.actbio.2018.03.018.

4 Srivastava A, Yadav, T, Sharma, S, Nayak, A, Akanksha Kumari, A. and Mishra, N. (2016) Polymers in Drug Delivery. Journal of Biosciences and Medicines, №4, PP. 69-84. doi: 10.4236/jbm.2016.41009.

5 Brighenti R, Li Y and Vernerey F.J (2020) Smart Polymers for Advanced Applications: A Mechanical Perspective Review. Front. Mater. №7, P.196. doi: 10.3389/fmats.2020.00196

6 María V. Martinez, Maria Molina, (2018) Poly(N-isopropylacrylamide) cross-linked gels as intrinsic amphiphilic materials: swelling properties used to build novel interphases. J. Phys. Chem. B vol.122, № 38, P.9038–9048. https://doi.org/10.1021/acs.jpcb.8b07625

7 Nakan, U.; Mun, G.A.; Shaikhutdinov, E.M.; Bieerkehazhi, S.; El-Sayed, (2020) Hydrogels based on N-isopropylacrylamide and 2-hydroxyethylacrylate: Synthesis, characterization, and investigation of their antibacterial activity. Polym. Int. Vl. 69, PP. 1220–1226. https://doi.org/10.1002/pi.6065.

8 Nakan, U; Mun, G.A. (2021) Thermosensitive N-isopropylacrylamide -co-2-hydroxyethyl acrylate hydrogels interactions with Poly(acrylic acid) and surfactants. Polym. Adv. Technol. Vol. 32, PP.2676–2681. https://doi.org/10.1002/pat.5070.

9 Mao, J.; Yu, Q.J.; Wang, S. (2021) Preparation of multifunctional hydrogels with pore channels using agarose sacrificial templates and its applications. Polym. Adv. Technol. Vol.32, PP. 1752–1762. https://doi.org/10.1002/pat.5211.

10 Nakan U, K Rahmetullaeva, A Mun, M Shaihutdinov, Zh Yeligbaeva, El-Sayed Moussa. (2016) Linear Copolymer of N-Isopropylacrylamide and 2-Hydroxyethylacrylate: Synthesis, Characterization and Monomer Reactivity Ratios. Oriental Journal of Chemistry. Vol.5, № 32, PP. 2347–2354. http://dx.doi.org/10.13005/ojc/320505

11 Sadia Afroz, Fariha Afrose, A. K. M. M. Alam, Ruhul A. Khan & Md. Ashraful Alam. (2019) Synthesis and characterization of polyethylene oxide (PEO)-N,N-dimethylacrylamide (DMA) hydrogel by gamma radiation. Advanced Composites and Hybrid Materials vol. 2, pp.133–141 DOI: 10.1007/s42114-018-0058-x

11 Ulantay Nakan, Balgyn Tolkyn, Dinara Adikanova, El-Sayed Moussa Negim, (2021) Characterization and swelling properties of copolymer Poly(N, N-dimethyl acrylamide -co-acrylic acid) and homopolymer Poly (acrylic acid) // Egyptian Journal of Chemistry DOI: 10.21608/ejchem.2021.95005.4465

12 Ayatzhan Akhmetzhan, Nurgeldi Abeu, Sotirios Nik. Longinos. (2021) Synthesis and Heavy Metal Sorption Studies of N,N Dimethylacrylamide Based Hydrogels Polymers №13, PP 3084. https://doi.org/10.3390/polym13183084

13 Shahid Bashir, Fatin Saiha Omar, Maryam Hina, Arshid Numan, Javed Iqbal, S. Ramesh, K. Ramesh, (2020) Synthesis and characterization of hybrid poly (N,N-dimethylacrylamide) composite hydrogel electrolytes and their performance in supercapacitor. Electrochimica Acta, vol. 332, P. 135438. https://doi.org/10.1016/j.electacta.2019.135438

14 Ulantay Nakan.; Bieerkehazhi, S.; Tolkyn, B.; Mun, G.A.; Assanov, M; Nursultanov, M.E.; (2021) Synthesis, characterization and antibacterial application of copolymers based on N,N-dimethyl acrylamide and acrylic acid. Materials, №14, P.6191. https://doi.org/10.3390/ma14206191

15 A.R. Hernandez-Martíneza, J.A. Lujan-Montelongob, C. Silva-Cuevasb, Josué D. Mota-Moralesa (2018) Swelling and methylene blue adsorption of poly(N,N-dimethylacrylamideco-2-hydroxyethyl methacrylate) hydrogel. Reactive and Functional Polymers Vol. 122, Pages 75-84 https://doi.org/10.1016/j.reactfunctpolym.2017.11.008

16 Fariba Ganji, Samira Vasheghani-Farahani, and Ebrahim Vasheghani-Farahani (2010). Theoretical Description of Hydrogel Swelling: Iranian Polymer Journal vol.5, №19, PP. 375-398

17 Nermin Orakdogen, Talin Boyaci Charge density dependence of elasticity of anionically modified N,N-dimethylacrylamide-based gels with (meth)acrylic acid segments: an insight by quantitative analysis of electrostatic contributions, European Polymer Journal 2017; 94; 484-500 https://doi.org/10.1016/j.eurpolymj.2017.07.032

IRSTI 87.35.91 https://doi.org/10.26577/ijbch.2021.v14.i2.012

S. Satayeva[1], F.Zh. Akhmetova[1*], R. Jusupkaliyeva[1], D. Nazarova[1], I. Kazarinov[2], M. Mambetova[1], B. Salim[1], Y. Hahaleva[1]

[1]Zhangirkhan West-Kazakhstan agrarian technical university, Uralsk, Kazakhstan
[2]Saratov State University N G Chernyshevsky, Saratov, Russia
*e-mail: firuza.92@mail.ru

Study of the new composite sorbents for water treatment

Abstract. Water pollution has become one of the key global environmental problems. Heavy metal ions are the main pollutants of water. Current study focuses on the manufacture of a highly efficient filter that absorbs heavy metals for water purification using inexpensive materials. The article discusses and shows the possibilities of using new sorption materials for water softening purposes. Experimental data on the study of sorption properties of the developed material are presented. Possible ways to improve the water treatment existing scheme of the enterprise are proposed. The study object was natural mineral sorbents, promising for use in water purification and conditioning processes. The work aim was to experimentally evaluate the use effectiveness of natural mineral sorbents for water purification. Research by using modern physical and chemical methods, it has been shown that natural mineral sorbents effectively purify water from pollution. The most promising natural mineral sorbents turned out to be the flask of the Taskala deposit of the West Kazakhstan region to purify water from heavy metal ions. Natural mineral sorbents purify water from excess iron ions and have pronounced sorption properties.
Key words: opoka, water softening, natural mineral sorbents, siliceous microporous sedimentary rocks.

Introduction

Heavy metal pollution threatens the environment and human health, therefore the effective removal of these toxic pollutants from various complex substrates is of great importance. Until now, adsorption is still one of the most effective approaches [1].

Achieving the required quality of various compositions groundwater purification involves a variety of technological solutions. The technological scheme choice should be made on the basis of a comprehensive analysis of groundwater quality indicators, considering the efficiency of water treatment schemes established in practice. Effective measures are improvement of technological processes, reduction of specific water consumption, reduction of reagent consumption.

To date, various methods of iron removal are used to obtain drinking-quality water [2–4]. Methods based on filtration through modified loading and purification technology are often used, including aeration and filtration through sand loading. Their disadvantages include abrasion, short operating time of the catalytic layer, low cleaning efficiency by the end of the filtration cycle, a large amount of water required for filter regeneration [5]. Sorption is a simple and effective way to remove iron and manganese cations from water. Particular attention is paid to sorption systems, where natural materials are used as sorbents: minerals of various origins and structures. The presence of local effective natural sorbents makes it possible to expand the possibilities of implementing adsorption technological processes for local groundwater treatment systems [6,7].

The opoka have proven themselves as sorbents in the purification of natural and washing waters [8]. This is due to their porous structure with a predominance of micro- and mesopores. They are formed by silica particles, the mass content of which ranges from 75 to 92% depending on the deposit. The density ranges from 1100 to 1600 kg/m^3, the porosity is about 55%. The opoka mainly consist of clay minerals, but at the same time they differ in lightness, rough surface of a cancellous and squamous fracture [9,10].

Materials and methods

The study objects are the natural sorbent – the opoka of the Taskala deposit and the water of the Shagan river of the West-Kazakhstan region.

Siliceous rock – the opoka of the Taskala deposit is a light, hard, microporous rock. According to geological data, opoka occurs in Paleogene and Cretaceous sediments, are formed in marine basins due to compaction and cementation of diatomites and trepels. Their density is 1.3-1.5 g/cm^3.

The main components of the opoka are silicon and aluminum oxides, the contents of which range from 44.351% to 48.126% for SiO_2 and from 38.928% to 39.028% for $A1_2O_3$. The content of SiO_2 and Al_2O_3 corresponds to the values of the maximum permissible concentrations in clays used in the production of sorbent for water purification. However, magnesium and sulfur (VI) oxides play an important role, which are contained in small amounts, in the sedimentary rock of the Taskala deposit, their content reaches 1.149%. These impurities are undesirable, as they negatively affect the quality of the sorbent for water purification from heavy metals. Proceeding from this, it can be concluded that while the Taskala deposit is most suitable as a natural sorbent for removing heavy metal cations from water.

– X-ray phase analysis was used, which allows to determine the qualitative and quantitative composition of the clinker with high accuracy to control the quality of the obtained sorbent. X-ray phase analysis of the flask was performed on a diffractometer D2 Phaser (Bruker, USA). The sorbent under study was averaged, and a sample of 20-25 g was taken from it, which was crushed into fine grits in a metal mortar. After averaging the grits, 5-7 g of material was taken from it, which was crushed in the agate composition of the raw mixture and clinker was carried out in a powder mortar by periodic screening on a 006-sieve using a soft brush. The remaining residue on the sieve was ground again and sieved until the initial sample of the material was completely passed. The test substance sample was stuffed into a cuvette made of organic glass and having a diameter of 20-25 mm with a recess on one of the planes up to 3 mm. The stuffing was carried out gradually, in layers, until the recess in the cuvette was completely filled, after which the surface of the material under study was carefully aligned so that the material planes and the collar of the cuvette ring coincided. A cuvette filled with material was installed in a goniometer sample holder, where the material was irradiated with X-rays with a certain wavelength at a variable angle of incidence.

The sorption efficiency of natural mineral sorbent was studied under flow conditions. To do this, the mineral, crushed to the required particle size, was placed in a plastic column with a diameter of 6 cm and a height of 23 cm between two polypropylene gaskets on top and bottom to eliminate the leaching of small particles of material from the filter. The introduced material volume was 0.5 liters. The water supply rate to the filters was set in the range of 2-3 ml/min.

Concentrations of divalent copper ions of 0.5 mg/l, 5 mg/l and 10 mg/l were created in model solutions by introducing the necessary amounts of 1M copper sulfate solution. The copper content in water was determined by colorimetric method with sodium diethyldithiocarbamate

Results and discussion

The phase composition of the siliceous microporous sedimentary rock of the Taskala deposit is shown in Figure 1.

In the technology of sorbent production for water purification, a range of various additives is widely used. One of these additives is carbon, which has a particle size of no more than 5 microns. Based on the chemical composition of the raw material (siliceous microporous sedimentary rock of the Taskala deposit), an X-ray phase analysis of the obtained flask was carried out. The carbon use as an additive makes it possible to increase technological efficiency and environmental safety. Thus, based on the conducted studies, it is advisable to use the flask of the Taskala deposit as a sorbent for removing heavy metal ions from water.

The suitability of water for drinking is primarily determined by its organoleptic properties. Therefore, at the first stage of the work, studies of the effect of the sorbent on these indicators were carried out. Table 1 demonstrates the organoleptic parameters and pH of the water before and after passing it through filters with a sorbent. The original tap water had increased color and turbidity.

Water treatment with a sorbent in filtration mode leads to a significant improvement in the organoleptic properties of water. The sorbents effectiveness for water purification was evaluated by comparing the organoleptic, physical and chemical, microbiological and toxicological parameters of the source, and treated water. Organoleptic and physical and chemical parameters were evaluated in accordance with the methods.

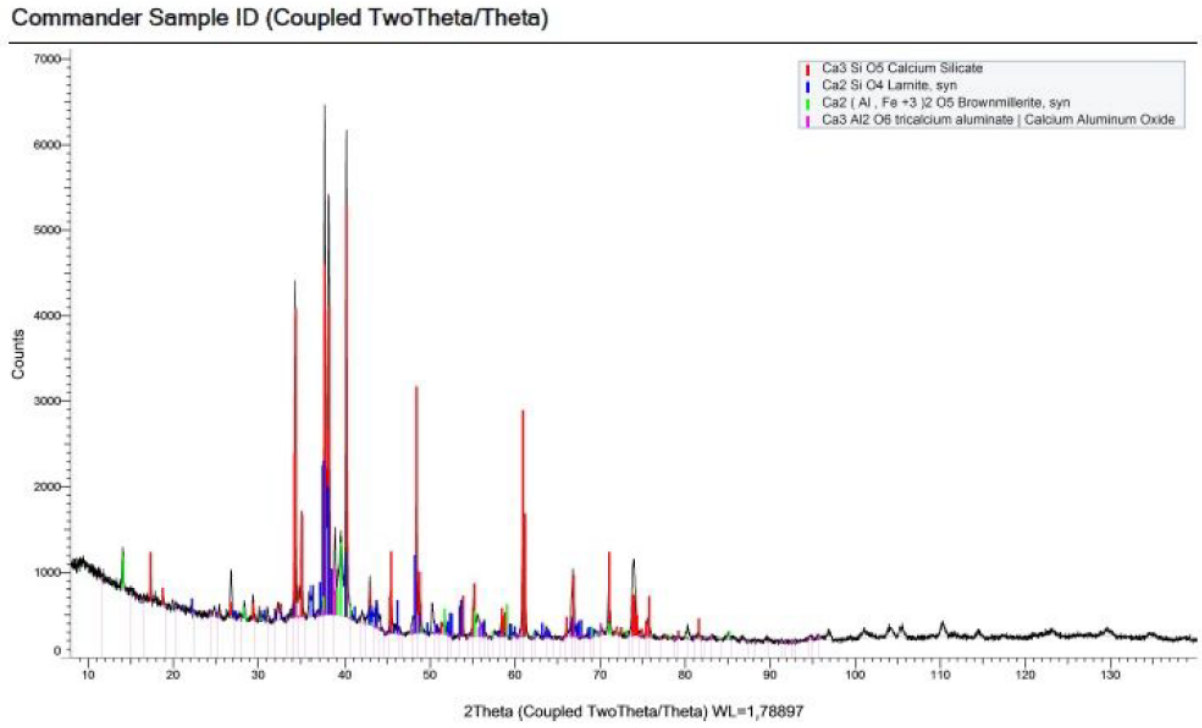

Figure 1 – Phase composition of the siliceous rock of the Taskala deposit

Table 1 – Organoleptic parameters of the Shagan River water

Indicators	Source water	Sorbent	Thermal modification of the sorbent at the		Standard 22.1.4.1074-01
			400 ºC	800 ºC	
pH	7.4	7.8	8.5	8.5	6-9
Aftertaste	3	0	0	0	2
Chroma	29	0	0	0	20
Turbidity	4	0	0	0	2.6
Smell	3	0	0	0	6.0-9.0

Iron and divalent copper ions were chosen as a model of heavy metals. The maximum permissible concentration of copper in drinking water is 1 mg/l, which is several orders of magnitude higher than the MPC of mercury, lead, and cadmium. This gives reason to believe that the effective sorption of copper will correspond to the effective sorption of other heavy metals.

The most typical result of secondary contamination of drinking water in distribution networks is a significant excess of iron ions, the usual is an excess of iron concentration by 1.5-3 times.

Table 2 presents the results of studying the use effectiveness of filters with sorbent for water purification from iron and divalent copper ions. The use effectiveness of filters with a support for water purification from heavy metal ions were studied, which are one of the priority pollutants of the hydrosphere. Divalent copper ions were used as a model toxicant.

It can be concluded that the use of filters with siliceous rock makes it possible to purify water from the excess content of iron ions and divalent copper.

Table 2 – Physical and chemical parameters of the water of the Shagan river

Indicators	Unit of measurement	Source water	Sorbent	Thermal modification of sorbent		Standard 22.1.4.1074-01
				400 ºC	800 ºC	
pH	-	7.4	7.8	8.5	8.5	6-9
General hardness	mg-eq./l	6.4	4.5	3.65	3.5	< 7
Iron	mg/l	0.32	0.22	0.18	0.013	< 0.3
Copper		0.90	0.38	0.29	0.28	< 1.0

The concentration of iron in water during water purification decreased from 0.32 mg/l to 0.18 mg/l – thermal modification of the sorbent at the 400 ºC: to 0.013 mg /l – thermal modification of the sorbent at the 800 ºC, and the concentration of copper, respectively, from 0.90 mg/l to 0.28 mg/l. This means that the sorbent cleans heavy metals well from water, thermal modification improves its sorption properties. The tables show that the heat-treated sorbent removes iron and copper ions from the water well. At the same time, a degree of purification of up to 95% is achieved. This means that the rock of the Taskala deposit is a suitable sorbent for water degreasing.

Conclusion

The conducted studies allowed to formulate the following conclusions: for water purification from heavy metal ions, the most promising sorbents are the siliceous microporous sedimentary rock of the Taskala deposit. Their efficiency remains at a high level with different initial parameters of the treated water (low and high hardness, color). The siliceous microporous sedimentary rock of the Taskala deposit exhibits specific activity in removing particles of radical and ion-radical nature from the water, significantly surpassing both flint and glauconite limestone in this respect. The studied sorbent purifies water from excess iron ions in the studied concentration range from 0.32 to 0.013 mg/l. Thus, the conducted studies have revealed that the natural rock of the Taskala deposit can be used as a sorbent for the removal of iron and copper ions. Water treated with a natural sorbent improves its biological properties due to deep purification from chemical contaminants, reduced toxicity, as well as enrichment with essential macro- and microelements. The investigated natural mineral sorbent – siliceous microporous sedimentary rock of the Taskala deposit is promising for use in systems and means of improving water quality.

References

1 K.P.W. Lankathilaka, R.M. de Silva, M.M.M.G.P.G. Mantilaka, K.M.N. de Silva, Magnetite nanoparticles incorporated porous kaolin as a superior heavy metal sorbent for water purification, Groundw. Sustain. Dev. 14 (2021) 100606. https://doi.org/10.1016/J.GSD.2021.100606.

2 D.T. Nguyen, K. –S Kim, Controlled synthesis of monodisperse magnetite nanoparticles for hyperthermia-based treatments, Powder Technol. 301 (2016) 1112–1118. https://doi.org/10.1016/J.POWTEC.2016.07.052.

3 A.A. Zaki, M.I. Ahmad, K.M.A. El-Rahman, Sorption characteristics of a landfill clay soil as a retardation barrier of some heavy metals, Appl. Clay Sci. 135 (2017) 150–167. https://doi.org/10.1016/J.CLAY.2016.09.016.

4 R. Amen, H. Bashir, I. Bibi, S.M. Shaheen, N.K. Niazi, M. Shahid, M.M. Hussain, V. Antoniadis, M.B. Shakoor, S.G. Al-Solaimani, H. Wang, J. Bundschuh, J. Rinklebe, A critical review on arsenic removal from water using biochar-based sorbents: The significance of modification and redox reactions, Chem. Eng. J. 396 (2020) 125195. https://doi.org/10.1016/J.CEJ.2020.125195.

5 F. Wang, X. Lu, X.Y. Li, Selective removals of heavy metals (Pb2+, Cu2+, and Cd2+) from wastewater by gelation with alginate for effective metal recovery, J. Hazard. Mater. 308 (2016) 75–83. https://doi.org/10.1016/J.JHAZMAT.2016.01.021.

6 T.K. Sen, S.P. Mahajan, K.C. Khilar, Adsorption of Cu2+ and Ni2+ on iron oxide and kaolin and its importance on Ni2+ transport in porous media, Colloids Surfaces A Physicochem. Eng. Asp.

211 (2002) 91–102. https://doi.org/10.1016/S0927-7757(02)00235-2.

7 S. Andrejkovičová, A. Sudagar, J. Rocha, C. Patinha, W. Hajjaji, E.F. Da Silva, A. Velosa, F. Rocha, The effect of natural zeolite on microstructure, mechanical and heavy metals adsorption properties of metakaolin based geopolymers, Appl. Clay Sci. 126 (2016) 141–152. https://doi.org/10.1016/J.CLAY.2016.03.009.

8 H. Nadaroglu, E. Kalkan, N. Demir, Removal of copper from aqueous solution using red mud, Desalination. 251 (2010) 90–95. https://doi.org/10.1016/J.DESAL.2009.09.138.

9 N. Timmer, D. Gore, D. Sanders, T. Gouin, S.T.J. Droge, Application of seven different clay types in sorbent-modified biodegradability studies with cationic biocides, Chemosphere. 245 (2020) 125643. https://doi.org/10.1016/J.CHEMOSPHERE.2019.125643.

10 M. Mohammadian, R. Sahraei, M. Ghaemy, Synthesis and fabrication of antibacterial hydrogel beads based on modified-gum tragacanth/poly(vinyl alcohol)/Ag0 highly efficient sorbent for hard water softening, Chemosphere. 225 (2019) 259–269. https://doi.org/10.1016/J.CHEMOSPHERE.2019.03.040.

IRSTI 53.37.35; 61.33.31 https://doi.org/10.26577/ijbch.2021.v14.i2.013

R.R. Tokpayev, T.N. Khavaza, Z.T. Ibraimov*, A.A. Atchabarova, K.K. Kishibayev, M.K. Nauryzbayev

Center of physical-chemical methods of research and analysis,
Al-Farabi Kazakh National University, Almaty, Kazakhstan
*e-mail: ibraimov.zair@mail.ru

Study of cerium and neodymium leaching from Kazakhstan phosphogypsum

Abstract. The processes of extraction of cerium and neodymium from Kazakhstan phosphogypsum, a large-tonnage waste of mineral fertilizer production of "Kazphosphate" LLP, have been studied. The influence of the nature of the leaching agent, temperature and duration of the process on the efficiency of cerium, neodymium leaching using the methods of X-ray fluorescence, X-ray phase and energy dispersive elemental analysis was studied. It has been found that the use of hydrogen peroxide as an oxidizer in the leaching of rare earth metals intensifies the process of recovery from phosphogypsum by 20% for cerium and by 28% for neodymium. Optimal parameters of cerium and neodymium leaching under atmospheric and autoclave conditions have been found. In atmospheric conditions, recovery of cerium and neodymium were 70.3% and 92.0%, in autoclave conditions 72.9% and 87.5%, respectively. The obtained results allow us to hope for the processing possibility of these wastes with the aim of rare-earth metals and other valuable products recovery.

Key words: phosphogypsum, leaching, microwave sample preparation, hydrogen peroxide, rare-earth metals, cerium, neodymium.

Introduction

It is well known that the concept of "integrated use of mineral raw materials" is not implemented at existing enterprises for a number of reasons, the main of which is the need to redo multiple technological processes, which ultimately leads to additional costs. The rate of extraction and processing of natural raw materials grows annually, and the volume of man-made waste increases accordingly. The accumulation of such waste in nature leads to environmental pollution. For example, the waste dumps of the Caspian Mining and Chemical Combine and phosphogypsum (PG) dumps of "Kazphosphate" LLP contain toxic compounds. The content of valuable components in these wastes is sufficient for their industrial development. One of the perspective sources for separation of rare-earth metals (REMs) is phosphogypsum, mentioned above. Processing of 1 ton of Karatau phosphorites produces 4.27-6.43 tons of PG, which is stored in the dumps of "Kazphosphate" LLP. It is known that more than 30 mln. tons of PG have been accumulated on the territory of the enterprise [1].

One of the problems of processing PG is the complexity of the composition, which includes the residues of mineral acids, insoluble salts and moisture. It is worth noting that the composition includes yttrium, light (lanthanum), medium (samarium) and heavy (terbium) groups of REMs, the total content of which is 0.4-0.6% wt. [2].

In recent years, there has been a growing consumption for rare earth products, driven by increased demand in a number of industries. [3-5]. Production of REM is one of the priority tasks of the rare-earth industry in Kazakhstan today [6, 7]. In this connection, the development of new, highly effective technologies for obtaining REMs from both natural and anthropogenic raw materials is important. Complex processing of PG in order to isolate REM and other components will initiate the development of rare-earth industry in the country, and will help to improve the environmental situation of the region as a whole. Waste recycling is one of the principles of low-waste and non-waste technology, which is a significant factor in the level of development of the country.

As a result of preliminary studies, it has been established that in the initial PG of "Kazphosphate" the following REM elements prevail: cerium, neodymium, yttrium and lanthanum [8]. Cerium and

neodymium are widely used in production of catalysts for magnets, in metallurgy, etc., respectively, are the most attractive elements of lanthanum series contained in PG.

The aim of this work is to determine optimal conditions of cerium and neodymium leaching from Kazakhstan PG.

In [9] processes of REM leaching from PG were studied. REMs leaching was carried out from 10%-sulphuric acid solutions, at a temperature of 60°C and 120 minutes. The leaching was carried out in two stages. As a result of leaching the total REMs recovery was 86%. The following results were obtained: cerium content was 103.13 and 105.78 ppm for neodymium in the first leaching stage; 50.85 and 50.71 ppm, respectively, in the second stage.

In [10, 11] the effect of temperature, duration of leaching processes on REM extraction from PG was also studied. The authors achieved the maximum REMs extraction at time – 120 minutes and temperature – 50 °C. The leaching was carried out in the presence of 5% sulphuric acid. The total REM extraction rate was 43%, REMs content in the leaching solution was 124 ppm.

The authors of works [12-14] conducted studies aimed at studying the influence of the nature of acid on the leaching efficiency. The influence of such parameters as S:L ratio, temperature, process time and acid concentration were studied. It was found that hydrochloric (R(Ce)=65%, R(Nd)=75%) and nitric acids (R(Ce)=62%, R(Nd)=75%) extract REM better than sulphuric acid (R(Ce)=22%, R(Nd)=32%) under normal conditions. At S:L ratio = 1:8, temperature 80°C, 20 min for 1.5 M sulphuric acid the recovery of cerium and neodymium is not more than 10 ppm. For 3.0 M hydrochloric acid not more than 15 ppm at the same parameters. The authors of [15] leached REM from PG by organic acids (malonic and citric acid). The maximum REM extraction (42% in total) was with citric acid with concentration of 1.0 M, at temperature 90 °C, S: L = 2:1, time – 15 minutes.

In [16] the authors studied the leaching with 0.5 M sulphuric acid and 3 M nitric acid from aged PG. The leaching was carried out between 2 and 8 hours at a ratio of S: L = 1:20. The most effective extraction was observed with nitric acid (t=8 h), cerium 67% (24 ppm), neodymium 90% (43.2ppm).

In [17, 18] it was found that catalytic decomposition of hydrogen peroxide contributes to barbotage of the system, which can improve the efficiency of REM extraction. It is also worth noting that in an acidic environment hydrogen peroxide oxidizes cerium to the state Ce^{4+}, which has a positive effect on its further selective extraction from the leaching solution [19].

As it is seen from literature review, the proposed methods do not allow to extract completely rare-earth metals from PG. That is why it is necessary to develop effective methods for their maximum extraction.

Materials and methods

The object of the study is waste PG from the "Mineral Fertilizer Plant" enterprise Kazphosphate LLP. PG was crushed on a planetary mono-mill "Pulverisette 6", "Fritsch" (Germany) and classified to a fraction of 0.056 mm.

Study of elemental and phase composition of PG was carried out on X-ray fluorescent wave dispersive combined spectrometer Axios ("PANalyical", the Netherlands) and energy dispersive analyzer. Study of PG surface morphology before and after leaching was carried out by EDAX on a scanning electron microscope Quanta 200i 3D (FEI Company, USA) at the National Nanotechnology Open Lab, Al-Farabi Kazakh National University.

The first stage of cerium, neodymium extraction from PG is acidic leaching. It was carried out in closed (autoclave) and open (atmospheric) modes by different mixtures of acids (HCl, HNO_3, H_2SO_4). All reagents used were classified as chemically pure (CP). The ratio S:L was kept constant at 1:40. Cerium and neodymium concentrations were analysed by ICP-MS method (Agilent 7500Series spectrometer). Leaching under atmospheric conditions was carried out at T=110 °C, τ=60 min. Autoclave dissociation of REM from PG was carried out in teflon vessels in microwave sample preparation system (Speed wave four "Berghof", Germany). Leaching process conditions: T=180 °C, τ=7.5 min, P=60 bar, ν=2500 Hz.

Results and discussion

The content of the target components in the initial PG sample was determined by quantitative chemical and XRF analyses and given in tables 1,2.

According to the XRF analysis (Figure 1, Table 3) the investigated PG is a phosphohydrate; the content of the main phase – bassanite is 73.3% wt. It is known from literature [20], that recovery of REM from semi-aqueous gypsum technologically requires less energy and water resources than processing of dihydrous gypsum.

Fluorite is found in PG composition – a consequence of incomplete decomposition of initial phosphorite. Quartz occurs together with phosphorite, after decomposition of which it remains in PG. Sodium hexafluorosilicate is a product of PG decomposition.

Table 1 – Results of XRF analysis

Element	O	F	Na	Mg	Al	Si	P	S	K	Ca
C, % wt.	42.00	7.90	3.26	0.41	0.61	7.23	1.10	12.02	0.56	20.42
Element	Ti	Cr	Mn	Fe	Ni	Zn	Sr	Y	Pb	
C, % wt.	0.07	0.03	0.06	0.63	0.01	0.02	0.07	0.01	0.02	

Table 2 – Results of quantitative chemical analysis of main REM in phosphogypsum

Element	Y	La	Ce	Nd
C, % wt.	0.0216	0.0201	0.0204	0.0123

Table 3 – Results of X-ray phase analysis

Name of phase	Formula	Content, % wt.
Bassanite	$CaSO_4 \times 0{,}5H_2O$	73.3
Quartz	SiO_2	16.3
Calcium pyrophosphate	$Ca_2P_2O_7$	2.7
Sodium hexafluorosilicate	Na_2SiF_6	2.6
Fluorapatite	$Ca_5(PO_4)_3F$	2.2
Potassium magnesium phosphate	$KMgPO_4$	1.6
Calcium Kutonarite	$Ca(Mn,Ca)(CO_3)_2$	1.3

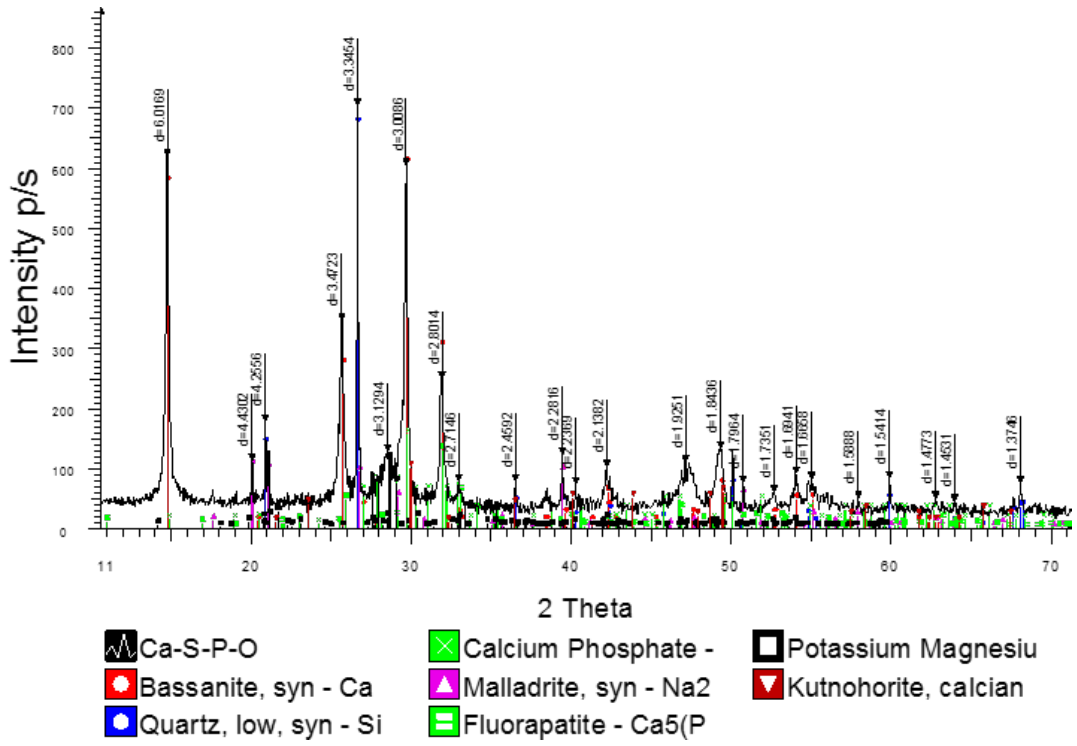

Figure 1 – Diffractogram of composition of initial PG

The migration of major elements during leaching was estimated by energy dispersive elemental analysis of PG before and after leaching (Figure 2, 3).

The absence of REMs on PG surface before leaching indicates the isomorphic replacement of calcium by cerium and other REMs in the PG structure [21-23]. The peak corresponding to cerium indicates the formation of insoluble cerium compounds during its leaching (Figure 3). The decrease of calcium content in the sample after leaching indicates the migration of calcium ions from PG into the solution. A scheme of isomorphic replacement of calcium by REMs is shown below:

$$REM^{3+} + Na^{+} + 2CaSO_4 = REMNa(SO_4)_2 + 2Ca^{2+}$$

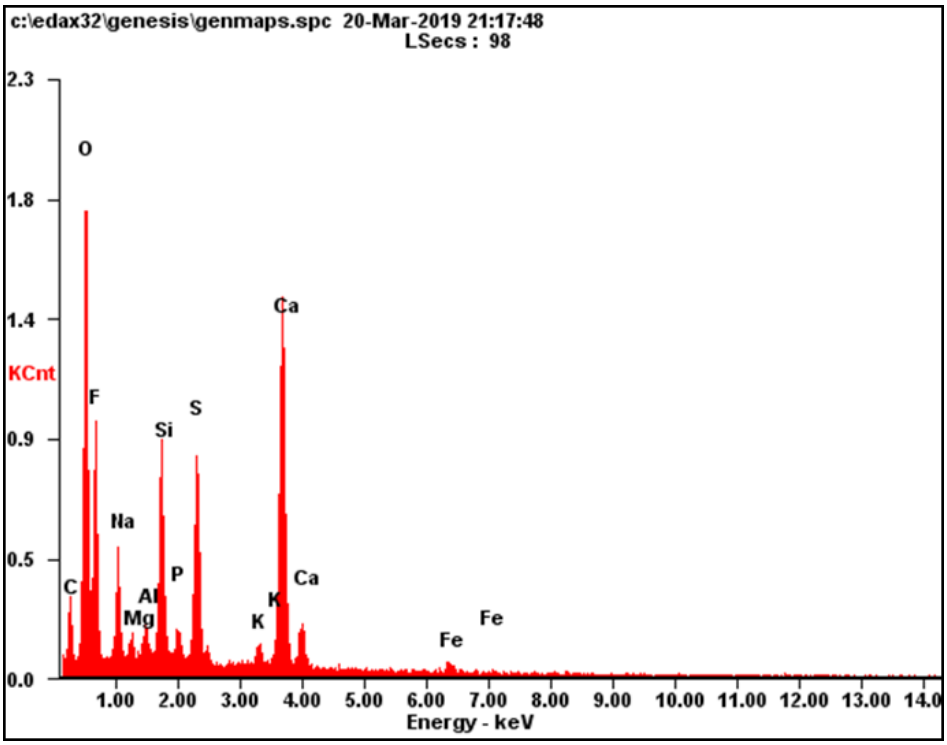

Figure 2 – EDAX analysis of PG sample before leaching

Nitric acid leaching of PG. A 56% nitric acid solution and a 30% hydrogen peroxide solution were used to extract cerium and neodymium from PG. The highest recovery of

REM in solution after leaching was observed at a ratio of HNO_3:H_2O_2 = 3:1 (Figure 4).

Nitric acid is not thermally stable and therefore cerium and neodymium leaching in autoclave mode is worse than in open mode [24], this is one of the reasons why technologies involving nitric acid stripping of REM are much less common than sulphuric acid technologies. The results of cerium and neodymium leaching are presented in Tables 4,5.

Decomposition of PG by a mixture of nitric and hydrochloric acids. Cerium and neodymium leaching with a mixture of nitric and hydrochloric acids is worse than with free nitric acid (Tables 6,7). This is explained by the fact that the solubility of $CaSO_4$ in hydrochloric acid is lower than in nitric acid [25].

Decomposition of PG by sulphuric acid. When PG is decomposed by sulphuric acid solution, the solubility of calcium sulphate is increased, causing cerium leaching from PG. The leaching process may proceed until equilibrium is reached; then further dissolution of gypsum is stopped due to saturation of solution with sulphate ions. Effective REMs extraction was observed using 10% sulphuric acid (Table 8).

The addition of a 30% hydrogen peroxide solution (Table 9) to sulphuric acid solution increases the leaching efficiency of cerium by 20%, of neodymium by 28% under autoclave conditions; by 19% for cerium, 11% for neodymium under open conditions, respectively.

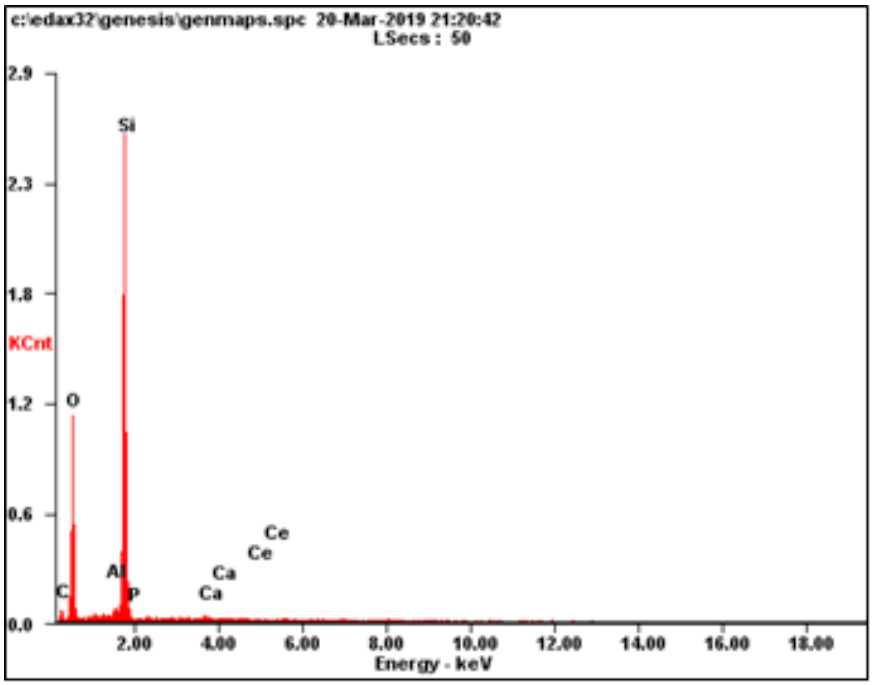

Figure 3 – EDAX analysis of PG sample after leaching

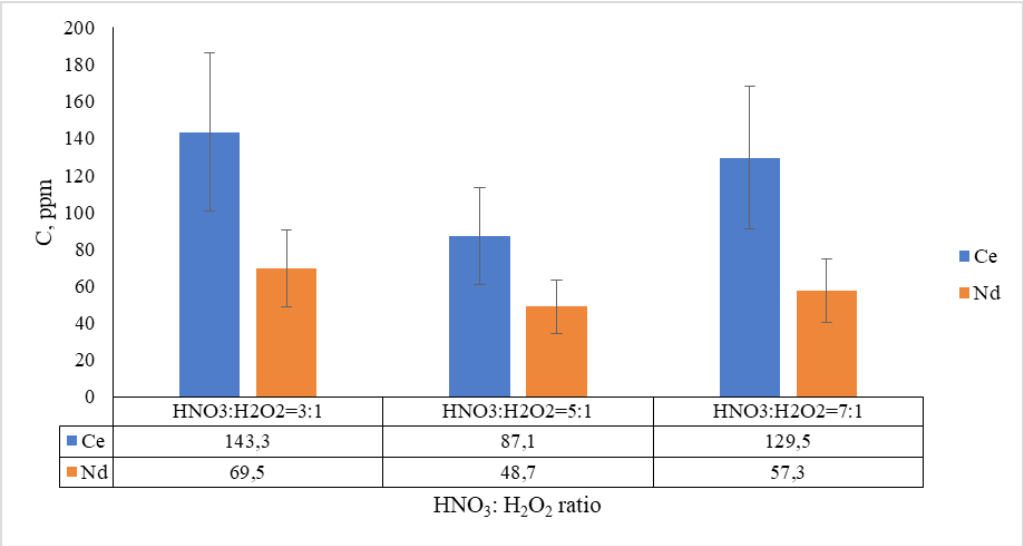

Figure 4 – Histogram of REMs concentration dependence on volume ratio of nitric acid and hydrogen peroxide

Table 4 – Results of cerium and neodymium leaching with nitric acid

C_{Me}, ppm	Autoclave leaching		Atmospheric leaching	
	$C(HNO_3)$, %			
	15	56	15	56
Ce	75.2±8.1	67.9±8.7	76.0±3.6	119.7±18.8
Nd	57.3±4.4	62.5±6.5	47.1±2.3	43.1±3.9

Table 5 – Results of cerium and neodymium leaching with nitric acid and hydrogen peroxide

C_{Me}, ppm	Autoclave leaching		Atmospheric leaching	
	$C(HNO_3)$, %			
	15	56	15	56
Ce	83.1±9.1	74.5±6.3	115.0±21.9	143.3±26.3
Nd	77.5±6.9	55.7±12.0	68.2±5.7	113.2±19.2

Table 6 – Results of cerium and neodymium leaching with a mixture of nitric and hydrochloric acids ("aqua regia")

C_{Me}, ppm	Autoclave leaching	Atmospheric leaching
Ce	55.9±1.2	53.0±4.1
Nd	51.6±0.9	33.5±1.2

Table 7 – Results of cerium and neodymium leaching with a mixture of nitric and hydrochloric acids (aqua regia) and hydrogen peroxide

C_{Me}, ppm	Autoclave leaching	Atmospheric leaching
Ce	65.1±5.2	75.3±6.9
Nd	57.4±3.3	56.9±8.3

Table 8 – Results of cerium and neodymium leaching with sulphuric acid

C_{Me}, ppm	Autoclave leaching			Atmospheric leaching		
	$C(H_2SO_4)$, %					
	5	10	20	5	10	20
Ce	79.0±3.3	147.8±27.7	115.5±16.3	35.4±5.0	58.1±9.6	16.8±3.3
Nd	81.3±5.2	99.4±11.3	77.2±1.5	25.7±0.6	38.6±1.3	1.5±0.2

Table 9 – Results of cerium and neodymium leaching with sulphuric acid with addition of hydrogen peroxide

C_{Me}, ppm	Autoclave leaching			Atmospheric leaching		
	$C(H_2SO_4)$, %					
	5	10	20	5	10	20
Ce	32.5±6.9	148.8±19.6	144.2±12.5	33.0±4.3	71.3±6.2	41.0±2.6
Nd	29.1±4.2	107.6±15.9	107.6±9.8	17.6±2.9	43.5±9.3	18.9±2.6

The results of investigation of temperature and process duration influence on efficiency of cerium and neodymium sulphuric acid leaching from PG are given in tables 10, 11. The leaching was carried out at conditions S: L = 1:40, T = 100°C, with mixture of H_2SO_4 (10%) + H_2O_2 (30%) (table 10). Autoclave leaching of Ce, Nd was carried out at S:L = 1:40, τ=15 min, with mixture of H_2SO_4 (10%) + H_2O_2 (30%).

Table 10 – Study of autoclave leaching time influence on recovery of cerium and neodymium from PG

C_{Me}, ppm	Leaching time, min		
	7.5	15	30
Ce	84.6±4.3	148.8±10.6	133.0±10.5
Nd	29.7±4.7	107.6±8.3	97.7±5.7

Table 11 – Study of temperature influence on recovery of cerium and neodymium from PG under autoclave conditions

C_{Me}, ppm	Temperature, °C		
	160	180	200
Ce	135.7±10.0	148.8±15.0	130.1±10.2
Nd	96.4±9.3	107.6±9.8	94.5±8.9

Conclusion

According to the XRF of PG sample from Kazphosphate LLP, the main compound is the mineral bassanite, which content is 73.3% wt. Cerium and neodymium, together with other REM are in isomorphic form in the crystal structure of bassanite. The total content of cerium and neodymium in the initial raw material was 3.27×10^{-2} % wt.

The optimum conditions of Ce, Nd stripping in atmospheric and autoclave conditions have been determined. The maximum recovery of neodymium (C(Nd)= 113.2±19.2 ppm, recovery rate – 92.03%) in simple conditions is achieved when using 15%-HNO_3 + H_2O_2, S:L = 1:40, t = 60 min, T = 80-100 °C. For cerium: 56%-HNO_3 + H_2O_2, S: L = 1:40, t = 60 min, T = 80-100 °C, (C(Ce) – 143.3±26.3 ppm, recoveries – 70.25%). At autoclave stripping of PG the maximum values for neodymium and cerium (C(Nd) = 107.6±9.8 ppm, recovery – 87.48 %; C(Ce) = 148.8±15.0 ppm, recovery – 72.94 %), were achieved at the following conditions: 10%-H_2SO_4 + H_2O_2, S:L = 1:40, t = 15 min, T = 180 °C, P = 60 atm, ν = 2 500 Hz.

Funding

This work was supported financially by the Committee of Science of the Ministry of Education and Science of the Republic of Kazakhstan, Project No. AP08957404.

References

1 Aimbekov D.S., Dyusembayev E.S., Aituraev I.Zh., Aituraev N.I. and Brener A.M. (2010) Short analytical analysis of the technological waste of phosphorogypsum of Kazphosphate LLP (MU). Bulletin of the ENU named after L.N. Gumileva., vol 4, pp. 274–278.

2 Mullakhodzhayev T.I., Olifson A.L. (2014) Method for extracting rare earth elements from PG [Sposob izvlecheniya redkozemel'nykh elementov iz FG]. Patent RF, no. 2509726.

3 Kudrin V.S. and Chistov L.B. (1996) State of the mineral raw material base of rare earth metals, prospects for its development and development. Mineral resources of Russia., vol. 15, pp. 6–12.

4 Pan F., Zhang J., Chen H., Su Y., Kuo C., Su Y-H., Chen S., Lin K., Hsieh P., Hwang W. Effects of rare earth metals on steel microstructures. Materials (Basel). 2016. Vol.9. No. 6. P. 1–19. https://doi.org/10.3390/ma9060417

5 Charalampides G., Vatalis K. I., Apostoplos B. and Ploutarch-Nikolas B. Rare Earth Elements: Industrial Applications and Economic Dependency of Europe. Procedia Economics and Finance. 2015. Vol. 24. No. 15. P. 126–135. https://doi.org/10.1016/S2212-5671(15)00630-9

6 Mukanov D. (2005) Metallurgy of Kazakhstan: state, innovation potential, development trend [Metallurgiya Kazakhstana: sostoyanie, innovaczionny`j potenczial, trend razvitiya] Almaty: Republican State Enterprise National Center for Complex Processing of Mineral Raw Materials of the Republic of Kazakhstan, 209 p.

7 Alshanov R.A. (2004) Metallurgiya Kazakhstana: sostoyanie, innovaczionny`j potenczial, trend razvitiya [Metallurgy of Kazakhstan: state, innovation potential, development trend] Almaty: Republican State Enterprise National Center for Complex Processing of Mineral Raw Materials of the Republic of Kazakhstan, 220 p.

8 Khavaza T.N., Tokpayev R.R., Atchabarova A.A., Beknazarov K.I., Zlobina E.V., Nauryzbayev M.K. (2019) Supercritical fluid extraction of rare earth elements from nitric acid solutions. Materials 17th European Meeting on Supercritical Fluids – 7th European Meeting on High Pressure Technology. Cuidad Real, Spain. P. 84-85.

9 Hammas-Nasri I., Horchani-Naifer K., Férid M., Barca D. (2016) Rare earths concentration from phosphogypsum waste by two-step leaching method. International Journal of Mineral Processing. Vol. 149. P. 78–83. https://doi.org/10.1016/j.minpro.2016.02.011

10 Liang H., Zhang P., Jin Z., and DePaoli D. (2017) Rare earths recovery and gypsum upgrade from Florida phosphogypsum. Minerals and Metallurgical Processing. Vol. 34. No. 4. P. 201–206. https://doi.org/10.19150/mmp.7860

11 Masmoudi-Soussi A., Hammas-Nasri I., Horchani-Naifer K. and Férid M. (from October 23, 2018, corrected November 17,2019, accepted January 5, 2020) Rare earths recovery by fractional precipitation from a sulfuric leach liquor obtained after phosphogypsum processing. https://doi.org/10.1016/j.hydromet.2020.105253.

12 Walawalkar M., Nichol C. K., Azimi G. (2016) Process investigation of the acid leaching of rare earth elements from phosphogypsum using HCl, HNO3, and H2SO4. Hydrometallurgy. Vol. 166. P. 195–204. https://doi.org/10.1016/j.hydromet.2016.06.008

13 Lambert A., Anawati J., Walawalkar M., Tam J. and Azimi G. (2018) Innovative Application of Microwave Treatment for Recovering of Rare Earth Elements from Phosphogypsum. ACS Sustainable Chemical Engineering Journal. Vol. 6. No. 12. P. 16471–16481. https://doi.org/10.4236/nr.2019.109021

14 Cánovas C. R., Chapron S., Arrachart G. and Pellet-Rostaing S. (2019) Leaching of rare earth elements (REEs) and impurities from phosphogypsum: A preliminary insight for further recovery of critical raw materials. Journal of Cleaner Production. Vol. 219. P. 225–235. https://doi.org/10.1016/j.jclepro.2019.02.104

15 Gasser M.S., Ismail Z.H., Abu E. Elgoud M., Abdel Hai F., Ali O.I., Aly H.F. (2019) Process for lanthanides-Y leaching from phosphogypsum fertilizers using weak acids. Journal of Hazardous Materials. Vol. 378. https://doi.org/10.1016/j.jhazmat.2019.120762

16 Rychkov V. N. et al. (2018) Recovery of rare earth elements from phosphogypsum. Journal of Cleaner Production. Vol. 196. P. 674–681. https://doi.org/10.1016/j.jclepro.2018.06.114

17 Buseva V.A. and Trofimov N.V. (1984) Metody` razlozheniya v analiticheskoj khimii [Methods of decomposition in analytical chemistry] Moscow: Chemistry, 430 p.

18 de Vasconcellos M. E., da Rocha S. M. R., Pedreira W. R., Carlos C. A., Abrão A. (2006) Enrichment of yttrium from rare earth concentrate by ammonium carbonate leaching and peroxide precipitation. Journal of Alloys and Compounds. Vol. 418. No. 1–2. P. 200–203. https://doi.org/10.1016/j.jallcom.2005.10.076

19 McNeice J., Kim R., Ghahreman A. (received November 14, 2019, received in revised form February 5, 2020, accepted April 4, 2020) Oxidative precipitation of cerium in acidic chloride solutions: Part II – oxidation in a mixed REE system.

20 https://doi.org/10.1016/j.hydromet.2020.105331

21 Lokshin E.P. (2014) Production of concentrate from sulfocationites saturated with rare-earth metals of sulphate solutions for leaching phosphogypsum. Chemical technology. Vol. 15. No. 12. P. 738–745.

22 Lokshin E.P., Tareeva O.A., Elizarova I. P. (2010) A study of the sulfuric acid leaching of rare-earth elements, phosphorus, and alkali metals from phosphodihydrate. Russian Journal of Applied Chemistry. Vol. 83. No. 6. P. 958–964. https://doi.org/10.1134/S1070427210060054

23 D.S. Zinin. Fazovye prevrasheniya pri poputnom izvlechenii RZE iz ekstrakcionnoi fosfornoi kisloty. Dokt, Diss. Moscow, 2018, 145 p.

24 Al-Thyabat S., Zhang P. (2015) REE extraction from phosphoric acid, phosphoric acid sludge, and phosphogypsum. Mineral Processing and Extractive Metallurgy: Transactions of the Institutions of Mining and Metallurgy: Section C. Vol. 124. No. 3. P. 143–150. https://doi.org/10.1179/1743285515Y.0000000002

25 Kravchenko I.V., Dyshlova V.I., Zabirko E.V. (2011) Mechanism of thermal decay of nitric acid. Energy technologies and resource conservation. Vol. 2. P. 41–45.

26 Wu S. et al. (2018) Recovery of rare earth elements from phosphate rock by hydrometallurgical processes – A critical review. Chemical Engineering Journal. Vol. 335. P. 774–800. https://doi.org/10.1016/j.cej.2017.10.143

IRSTI 65.35.03 https://doi.org/10.26577/ijbch.2021.v14.i2.014

N.V. Alexeyeva[1*], M.I. Satayev[1,2], A.M. Azimov[1], Z.M. Shakiryanova[1], Samonin V.V.[3]

[1] M. Auezov South Kazakhstan University Shymkent, Kazakhstan,
[2] InnovTechProduct LLP, Shymkent, Kazakhstan
[3] Saint-Petersburg State Technological Institute, Saint Petersburg, Russia
[*]e-mail: nina_vadimovna@mail.ru

Features of the chemical composition and technological properties of large-fruited purple cherry plum to justify its use for the production of dried fruits

Abstract. This article presents the results of studies of large-fruited purple cherry plum, large-fruited yellow and large-fruited red cherry plum. The fruits of the large-fruited purple plum contain a higher percentage of pectin compounds and fiber. The authors drew attention to this fruit due to its widespread growth in the south of Kazakhstan. Due to the presence of useful constituents, the authors justified the possibility of using this fruit and the dried fruit obtained from it for the prevention of cardiovascular diseases and anemia. The problem of these diseases is relevant for Kazakhstan, in particular, for the south of Kazakhstan. Dried fruit is the product that allows to get a balanced diet in the autumn-winter-spring period. Modern methods of drying allow you to preserve the appearance and useful composition of dried fruits. Cherry plum is a perishable and perennial plant. It is drought-resistant, not fastidious to growing conditions. Based on the results of a comparative analysis of the mineral composition of the ash residues of cherry plums of different sizes and colors growing in the Turkestan region, conclusions are drawn about the high content of useful components in cherry plums. It is proved that the formation of biocomponents in cherry plum fruits is also influenced by soil and climatic conditions and environmental factors of vertical zonation.

Key words: dried fruits, canning, processing of vegetable raw materials, nutrition, vitamins.

Introduction

The modern concept of a healthy diet assumes that one of the main parameters that a daily diet should satisfy is diversity and balance. But such a diet is impossible to achieve all year round. In the period of exacerbation of chronic diseases (in spring and autumn), as well as in winter to compensate for the lack of vitamins, micro- and macronutrients, the food industry offers a wide range of chemically synthesized multi-component vitamin and mineral complexes. Such complexes differ significantly from the native forms and are characterized by insufficient assimilation by the body. In this regard, it is advisable to turn to the traditional and effective way to compensate for the deficiency of vitamins, macro-and microelements in the body-dried fruits. They are fruits and berries dried in a natural industrial way. It should be noted that modern technologies of industrial drying allow you to preserve most of the biologically active compounds in dry fruits, while their amount will be higher than in fresh raw materials due to the removal of moisture from the fruit.

We propose to use large purple cherry plum for production. This species is common in the south of Kazakhstan. Cherry plum is a fruit woody plant; a species of the genus plum of the subfamily plum family Rosaceae. Cherry plum is drought-resistant, not very demanding to the level of agricultural technology. It is affected by diseases only in a weak degree. Another advantage of cherry plum is its unique rapidity. The potential yield of cherry plum is very high. This is due to the huge number of flower buds that the plant annually lays on both perennial and annual wood. And the tree enters fruiting after a year or two after planting. The fruits of the cherry plum are large (their average weight ranges from 25 to 35 g) and beautiful. The color is bright, rich, from light yellow to almost black [1].

In the paper presented, we will consider the following varieties of cherry plum:

- a variety of large-fruited yellow cherry plum. The tree is medium-sized. The fruits are sweet, large, yellow, weighing up to 35g. Very early maturation period. The yield is high [1].

- a variety of large red cherry plum. The tree is weakly grown. The fruits are ovoid, maroon, weighing about 30 g. Early maturation period. Yield of 30 kg per tree [1].

- a variety of large purple cherry plum. The tree is medium-sized. The fruits are sweet, large, dark purple, weighing up to 37g. This variety of cherry plum is resistant to diseases and pests and is famous for the excellent sweet and sour taste of the fruit. The flesh is very sweet. [2]

Materials and methods

The object of the study was the varieties of cherry plum that grow widely in the south of Kazakhstan. Experimental studies were carried out in the research laboratory of the Department of "Food Engineering", in the test regional laboratory of the engineering profile "Structural and biochemical materials" of M.Auezov South Kazakhstan University and InovTechProduct LLP (Shymkent, Kazakhstan).

To implement the research tasks, we used generally accepted, standard methods of raw materials research:

1. Methods for determining moisture according to all-Union State Standard 28561-90 [3].

2. Methods for determining titratable acidity according to all-Union State Standard 25555.0-82 [4].

3. Method for determining the pH according to all-Union State Standard 26188-2016 [5].

4. Methods for determining sugar according to all-Union State Standard 5903-89 [6].

5. Determination of the chemical composition of cherry plum and the content of toxic elements according to all-Union State Standard 32896-2014 [7,9,10].

Results and discussion

Below are the results of studies of the chemical composition of three types of cherry plum grown in the territory of the Turkestan region, since the ability of fruits to accumulate vitamins and minerals is largely determined by the climatic conditions of growth and the mineral composition of soils [1,7,9,10].

From Table 1, it can be seen that in the above varieties of cherry plum, the dry matter content is from 10.34% to 11%, with highest content in large purple cherry plum. The content of pectin compounds varies from 0.47% to 0.92%. The content of fiber from 0.50% to 0.58%. Among analyzed varieties, large-fruited purple cherry plum contains pectin compounds and fiber above. Pectin compounds have a positive effect on the human body for the number of reasons. They reduce the level of cholesterol what justifies the use of cherry plum and its products for the prevention of cardiovascular diseases. The presence of fiber helps to slow down the digestive process, therefore the prolonged effect of the feeling of satiety is preserved what makes possible to use cherry plum for a low-calorie diet [8].

The formation of components in cherry plum fruits is also influenced by soil and climatic conditions and environmental factors of vertical zonation table 2 [9,10].

Table 1 – Chemical composition of cherry plums of various colors

Indicators	Purple large-fruited cherry plum, %	Yellow large-fruited cherry plum, %	Red large-fruited cherry plum, %
Humidity, %	89	88.69	89.14
Free acids, %	2.19	2.94	2.80
Total sugar, %	5.35	4.71	4.37
Invert sugar, %	2.38	1.84	1.76
Pectin compounds, %	0.92	0.80	0.47
Tannins, %	0.23	0.12	0.11
Cellulose, %	0.58	0.52	0.50
Nitrogenous compounds, %	0.20	0.16	0.23
Ash, %	0.44	0.48	0.47

Table 2 – Influence of soil and climatic conditions and environmental factors of vertical zonation on the formation of biocomponents in cherry plum fruits

Fruit zone	Mass concentration				
	Sugar, g/100 sm^3	Titratable acids, g/dm^3	Pectin compounds, %	Vitamin C, mg/dm^3	Vitamin P, mg/dm^3
Plain, 50 m above sea level	7.6	12.8	2.52	69	1017
Submountain, 475 m above sea level	7.2	13.5	2.64	72	1063
Mountain-valley, 750 m above sea level	6.9	13.7	2.71	75	1105

The analysis of the chemical composition and the presence of biocomponents of cherry plum is carried out in order to obtain a non-finished product in the form of dried fruit. Shymkent and the south of Kazakhstan have both flat, and foothill and mountain-valley zones. This indicates that the mass concentration of ascorbic acid, pectin compounds, etc. will change in the purple large-fruited cherry plum. indicators.

Based on the indicators in Table 1, which describes the chemical and biochemical composition of cherry plums of various colors and sizes, it can be assumed that a more promising fruit raw material for the production of dried fruits is purple cherry plums. It is distinguished from other types by a greater amount of raw fiber, tannins and pectin compounds [1].

Next, we will focus on the mineral composition of cherry plums of various colors. The mineral composition is nothing more than the content of macro-and microelements in plant raw materials. They enter the human body with food and ensure the constancy of the osmotic pressure of cellular and extracellular fluids, acid-base balance, the processes of absorption, secretion, hematopoiesis, bone formation, blood clotting, determine the state of water-salt metabolism; without them, the functions of muscle contraction, nerve conduction, and intracellular respiration would be impossible. Minerals are of great importance for the formation and formation of protein [1]. The results of the comparative analysis are presented in Table 3.

Table 3 – Results of a comparative analysis of the mineral composition of ash residues of different size and color, growing in the Turkestan region [7,9,10]

№	Name of indicators, units of measurement	Actual results (in ash residues)		
		Purple large-fruited cherry plum	Yellow large-fruited cherry plum	Red large-fruited cherry plum
1	Mass fraction of ash, in %	0.6	0.6	0.6
2	Li, mg/kg	190.3597	113.5896	128.5248
3	Na, mg/kg	13506,55	12386,35	11756,58
4	Mg, mg/kg	5996,664	2758,364	4895,325
5	Al, mg/kg	553,0761	412,0586	338,8798
6	P, mg/kg	10633,99	9633,56	10183,69
7	S, mg/kg	3929,015	2989,569	3129,786
8	K, mg/kg	228908,7	218689,3	222898,2
9	Ca, mg/kg	7849,244	6876,875	7448,247
10	Sc, mg/kg	0,820179	0,688667	0,785868
11	Ti, mg/kg	48,25451	47,25451	48,18765
12	V, mg/kg	0,714911	0,658633	0,707897

Table continuation

№	Name of indicators, units of measurement	Actual results (in ash residues)		
		Purple large-fruited cherry plum	Yellow large-fruited cherry plum	Red large-fruited cherry plum
13	Cr, mg/kg	8,567634	8,045896	8,367931
14	Mn, mg/kg	54,33446	52,86786	54,03245
15	Fe, mg/kg	308,2083	300,5685	304,9762
16	Co, mg/kg	0,266295	0,187697	0,206258
17	Ni, mg/kg	7,468304	6,768965	7,058967
18	Cu, mg/kg	42,99411	40,89647	42,02356
9	Zn, mg/kg	153,0272	150,5788	151,8955
20	Ga, mg/kg	8,635938	6,669689	8,025668
21	Ge, mg/kg	0,051071	0,037863	0,044333
22	As, mg/kg	25,89674	23,56987	25,25984
23	Se, mg/kg	1,878348	1,023658	1,558456
24	Rb, mg/kg	112,3865	102,2569	111,2569
25	Sr, mg/kg	87,82339	85,25686	86,55874
26	Zr, mg/kg	9,831518	8,256984	9,023659
27	Nb, mg/kg	0,043438	0,002355	0,025589
28	Mo, mg/kg	4,843839	3,256987	4,255545
29	Ag, mg/kg	1,168884	0,955866	1,023659
30	Cd, mg/kg	0,305848	0,202556	0,302365
31	Sb, mg/kg	0,138929	0,098863	0,110256
32	Te, mg/kg	0,034286	0,012563	0,023658
33	Cs, mg/kg	0,212009	0,125638	0,202369
34	Ba, mg/kg	722,3696	716,3458	720,5986
35	La, mg/kg	0,11817	0,56866	0,86689
36	Ce, mg/kg	0,24817	0,63565	0,63396
37	Pr, mg/kg	0,009286	0,577557	0,635689
38	Nd, mg/kg	0,066384	0,065366	0,065897
39	Sm, mg/kg	0,004196	0,002569	0,003588
40	Gd, mg/kg	0,006696	0,006589	0,006659
41	Tb, mg/kg	0,003438	0,003025	0,003236
42	Dy, mg/kg	0,00183	0,00156	0,00176
43	Yb, mg/kg	0,002991	0,002578	0,002948
44	Hf, mg/kg	0,189554	0,125369	0,143639
45	Ta, mg/kg	0,009732	0,009023	0,009658
46	W, mg/kg	0,179821	0,102365	0,158964
47	Pb, mg/kg	8,154063	8,112566	8,558899
48	U, mg/kg	0,038259	0,030255	0,032588

As it is shown in Table 3, purple cherry plum contains a higher content of useful components compared to the other two: Fe, Ca, K, P, Mg, Zn, Cr, Ag.

Actually, one of the vital trace elements is iron. It is part of hemoglobin, which is responsible for transporting oxygen to all cells and tissues, and is involved

in the synthesis of proteins, enzymes, and hormones. The body is not able to produce iron on its own, and a person can only get it with food [11].

According to the World Health Organization, iron deficiency anemia affects about 600 million people worldwide. Latent iron deficiency is observed in 30% of the European population [11,12]. The problem of anemia is relevant for Kazakhstan due to its high prevalence on the territory of the republic. According to the Statistics Agency of the Republic of Kazakhstan, anemia in pregnant women has doubled over the past fifteen years. Economic damage due to anemia and folic acid deficiency in Kazakhstan is up to 5% [13]. In Kazakhstan, 41.9% of the population, or more than seven million people, suffer from anemia [11].

It is known from the works that iron is optimally absorbed in the presence of vitamin C, significant presence of vitamin C in cherry plum is supported by the data in the Table 2 [11]. The proposed type of cherry plum and the food products obtained from it, in particular, dried fruits, can be recommended as a preventive tool in the fight against anemia.

Conclusion

The biochemical composition of the fruits of 3 varieties of cherry plum was studied and their varietal differences were established. The perspective directions of processing of cherry plum fruits for dried fruits were revealed. The fruit of the cherry plum in view of the usefulness of the composition is recommended for the production of dried fruits. The high content of pectin, fiber, and ascorbic acid in the cherry plum indicates the need for further research in order to use it for therapeutic and preventive purposes. For the prevention of iron levels, we suggest using dried fruits based on large-fruited red purple cherry plum.

Funding

These studies were carried out with the support of the Ministry of Education and Science of the Republic of Kazakhstan, grant AP08855596 (2020-2022)

References

1 Ezhov V. N., Polonskaya A. K. (2003) Biochemical justification of the directions of plant processing for obtaining therapeutic and prophylactic products. Newsletter GBS. Issue 186. – pp. 214-226.

2 Ezhov, V. N., Polonskaya, A. K., Gorin V. M., Cucelapa E. M. (2002) Biochemical rationale for the different areas of processing of fruits plum // New technology of production and application of biologically active compounds: Report. International. Scientific and practical conference-Alushta, Crimea, Ukraine, pp. 238-239.

3 GOST (all-Union State Standard) 28561-90 (2016) Fruit and vegetable processing products. Methods for determining dry matter. – M.: Standards publishing house. P. 2.

4 ISO 750-2013 Products of fruit and vegetable processing. Determination of titratable acidity (Reissue) – Moscow: Standards publishing house, P. 4.

5 GOST (all-Union State Standard) 26188-2016 (2017) Fruit and vegetable processing products, canned meat and meat-growing products. Method for determining pH (with Correction) – Moscow: standards publishing house, P. 2

6 GOST (all-Union State Standard) 5903-89 (2017) Confectionery products. Methods for determining sugar. – Moscow: Standards publishing house. P 13.

7 GOST (all-Union State Standard) 32896-2014 (2017) Dried fruit. General technical conditions. – M.: Standards publishing house. P. 15.

8 Davidyuk L. P., Vshivkova G. F. (1985) Complex-forming ability of pectins of fruit crops Proceedings of the State Nikitinsky Botanical Garden. Vol. 95. – pp. 94-103.

9 Kriventsov V. I. (1982) Methodological recommendations for the analysis of fruits for biochemical composition. Proceedings of the State Nikitinsky Botanical Garden, P.22

10 Kriventsov V. I. (1989) Non-carbazol method of quantitative spectrophotometric pectin compounds. Proceedings of the State Nikitinsky Botanical Garden, Vol. 109, pp. 128-137.

11 URL:https://www.pravda.ru/navigator/defitsit-zheleza-v-organizme.html/(accessed: 03.02.2021).

12 URL:http://ikaz.kz/anemiya-v-kazakhstane/ (accessed: 03.02.2021).

13 Abdikarimova R. K. (2011) Analysis of the prevalence of iron deficiency anemia in Kazakhstan// Journal of the Almaty State Institute of Advanced Medical Training. P. 67

IRSTI 31.19.15 https://doi.org/10.26577/ijbch.2021.v14.i2.015

I.Yu. Silachyov

Institute of Nuclear Physics, Almaty, Kazakhstan
e-mail: silachyov@inp.kz

Determination of indium in its mineral resources by comparative neutron activation analysis

Abstract. The application of comparator instrumental neutron activation analysis (INAA) was considered to determine indium by the short-lived radionuclide ^{116m}In it its mineral resources such as different types of polymetallic ore, copper, lead-zinc, tin, tin-tungsten ores, and similar. Cu and Zn contents of the samples were determined by X-ray fluorescence method (XRF) using a laboratory energy dispersive XRF spectrometer RLP-21T, Kazakhstan. If Cu mass fraction exceeded 0.4–0.5% or that of Zn exceeded 3% (that is often characteristic of polymetallic, copper, and lead-zinc ores), then their contents were used in comparator INAA as the internal standards measured by an independent method. If none of the conditions were met, then the standard addition method was applied using a 10 mg addition of reagent ZnO to each sample. A range of the samples of polymetallic ore reference material certified for indium content (CRMs) were used to verify accuracy of the method. The proposed variant of comparator INAA was shown to insure accuracy of a routine analysis of indium-bearing ores of nonferrous metals fir indium content by the III category of precision according to the industrial standard OST 41-08-221-04 (Russian Federation). The method was tried out for several dozens of ore samples presenting various indium mineral resources including the ones from the gold-polymetallic deposit Maikain in North-Eastern Kazakhstan.
Key words: indium, neutron activation analysis, mineral resources.

Introduction

Indium is a typical dispersed rare element with the average crustal abundance ~56 ppb [1]. About two tens of indium minerals are currently identified [2], and a range of other minerals can occur as its carriers due to the closeness of In ion radius to that of some more abundant elements [3]. An overwhelming majority of the minerals are extremely rare and hence are far beyond any industrial importance. The other more common ones (chalcopyrite, cassiterite, sphalerite) can concentrate indium in sufficient quantities to be extracted as a by-product of primary Cu, Sn and Zn production [4]. So, main indium suppliers in the world at present are polymetallic [5, 6], tin [2, 3, 7], and complex tin-polymetallic deposits [8]. Kazakhstan possesses great opportunities of indium mining and production from polymetallic deposits in its eastern, southern and south-eastern regions.

Bulk indium contents of geological samples are usually determined together with the other elements for whole rock geochemistry using high-sensitive analytical methods such as mass-spectrometry with inductively coupled plasma (ICP-MS) and instrumental neutron activation analysis (INAA) [6, 9]. Synchrotron radiation X-ray fluorescence and atomic absorption spectrometry can be occasionally employed as well [7]. Despite ICP-MS is applied most frequently [10, 11], necessity of total rock digestion presents a serious disadvantage of the method, often turning into rather a laborious, time-consuming, and expensive procedure [12]. Laser ablation ICP-MS [7, 8] is deprived of this drawback, but it's rather a variant of local analysis of the specially prepared doubly polished thin sections due to a very small beam spot 15–25 μm across diameter and superficial sampling depth below 100 μm [13]. The method is hardly applicable for indium analysis in highly heterogeneous solids such as blende (ZnS) [3]. Moreover, both indium isotopes ^{113}In and ^{115}In overlap in mass with ^{113}Cd and ^{115}Sn; substantial contents of the latter usually accompany indium mineral resources.

In spite of the increasing challenges from the newer methods, INAA can still offer a range of advantages of rocks and minerals analysis for indium content. The most significant of them include supreme sensitivity [14], absence of sample decomposition and spectral interferences, moderate cost, and promptness owing to short half-live of ^{116m}In (54 min). In contrast to X-ray fluorescence and ICP-MS, Sn-rich samples with tin content >1%

can be successfully investigated [15]. High resonance integral value of ^{115}In implies epithermal activation to obtain better detection limit. This may be useful in geochemical exploration but is apparently out of need if indium mineral resources are analyzed.

In case of geological samples investigation, k_0-method had long proved its convenience and effectiveness for concentration standardization [16]. Based on the external standard (an Au-containing sample), this variant of single-comparator INAA still inherits some drawbacks of the relative method [17]; therefore, a range of corrective procedures should be considered. Main drawbacks of k_0-INAA are overcome using internal standardization with comparator content of the samples determined by k_0- or relative methods [18, 19]. However, all the advantages of comparator INAA may be realized only by joint application of the internal standard method (ISM) and an independent method to analyze comparator content [20].

Element Fe is chosen as an internal standard most frequently owing to its favorable mineralogical and activation properties [21]. It's also important that iron content of rock samples may be reliably and promptly determined by X-ray fluorescence method (XRF), rather successfully complementing INAA [22, 23]. Some other elements resulting in long-lived radionuclides after neutron activation are occasionally used as internal comparators too [17]. Though no references to short-lived radionuclides were found, Mn can basically supersede Fe in the respect of rock analysis, but scarcely in case of indium mineral resources investigation. Mn content of tin and polymetallic ores is often lower the value guaranteeing its reliable determination by XRF (≈0.03%). Moreover, Mn$K\alpha$ X-ray line is not resolved with Ba$L\gamma_{2,3}$ lines which can superimpose severely with the former in barite-polymetallic and similar ores with high Ba content more than 1%.

In this work comparator INAA was tried to analyze indium in polymetallic, nonferrous, tin, and tungsten ores, and some others. Taking into account element composition of the objects, activation and X-ray properties of their main components, short-lived radionuclides ^{66}Cu and ^{69m1}Zn were used as the internal standards when one of the next conditions was met: Cu was reliably determined by XRF; statistical uncertainty of ^{69m1}Zn analytical line count rate was sufficiently low. Otherwise standard addition method (SAM) was applied with comparator INAA using an appropriate zinc reagent.

Materials and methods

The certified reference materials (CRMs) of indium-containing ores together with the real samples from a Kazakhstan's ore deposit were used in the investigation. X-ray fluorescence analysis of the samples for Cu and Zn mass fractions was carried out using an energy dispersive spectrometer RLP-21T ("AspapGeo" LLP, Almaty, Kazakhstan) designed to study element composition of rocks, minerals, ores, and concentrates. Sample preparation for elemental analysis was performed following a standard procedure including raw material grounding to a particle size of <0.071 mm controlled by a FRITSCH Gmbh (Germany) sieve. Several grams of the assays were pressed manually in stainless steel dishes to provide "the saturated layer geometry" and smoothed down with a laboratory glass. The assays were counted in the automatic operating mode for 15 minutes each.

Accuracy of RLP-21T software was repeatedly confirmed with the help of different corresponding CRMs. The ascribed uncertainty of Cu and Zn mass fractions determination is below 10% (P = 0.95) for the contents exceeding 0.5%. RLP-21T is enrolled in the State Register of Measuring Devices, and the corresponding analytical technique is registered by the National Body for Certification of Kazakhstan.

To implement short-time activation analysis, an automated pneumatic transport system (PTS) was used [24]. The irradiation terminal of the PTS is installed in a "dry" horizontal channel of INP research reactor WWR-K close to the outer side of its tank. The samples are thus activated by more thermalized neutron flux comparing with the vertical peripheral irradiation channels within the reactor's active zone, as it is shown below.

About 100 mg of the assays were sealed in plane polyethylene bags (≈1 mm of the thickness) and fixed inside HDPE transport capsules across the neutron flux to minimize its gradient effect. If SAM was realized where necessary, then 10 mg of the analytical reagent ZnO (≥99% of zinc oxide, produced according to GOST 10262-73, Russian Federation) were placed into the same bags. In these cases assay and addition masses were fixed up to the forth decimal with a Mettler Toledo analytical balance. Only one bag was put into in each capsule. The capsules were irradiated one by

one usually for 30–90 s by the thermal neutron flux density n × 10^{12} cm^{-2} s^{-1}. Activation time was selected empirically mainly based on Mn contents of the samples by XRF and was sometimes corrected to avoid over-irradiation.

Gamma-spectrometric measurements of the assays were conducted for 5 min. 20–30 min of the decay time was chosen to allow the count rate of the radionuclides with the shorter half-lives (^{28}Al first of all) substantially reduced. To optimise counting geometry, the bags were taken out of the capsules and placed at the distances of 50 mm to the detector cap. A coaxial HPGe detector GC2018 (Canberra) coupled to an analyzer DSA-1000 was used, both incorporated into PTS. Relative efficiency of the detector amounted to 20% and its energy resolution was not worse than 1.80 keV. GC2018 was calibrated for relative detection efficiency ε(E) where E is a gamma-ray energy, with the help of a multi-gamma ray standard MGS-1 (^{152}Eu, ^{154}Eu, ^{155}Eu) and an isotopic source ^{133}Ba (Canberra). ε(E) values were evaluated in the interval from the 81.0 keV (^{133}Ba) to 1408.0 keV (^{152}Eu). The calibration curve was fitted by a fourth power polynomial.

GENIE 2000 software was used for the spectra collection. Spectra treatment was carried out by "AnalGamma" software developed in INP to provide gamma-ray spectrometric analysis. This software approximates a part of gamma-ray spectrum in the treatment window by Gaussian curves and a flat background and calculates peak count rates J in cps. Partly overlapping peaks can be reliably resolved. Quality of the approximation is checked by the X^2 test.

Table 1 – Main nuclear data to determine indium by comparator INAA using Cu and Zn as internal comparators

Activated isotope	θ, %	σ_0, barn	I_0, barn	Target radionuclide	$T_{1/2}$, min	E_γ, keV	P_γ, %
^{115}In	95.7	161	2705	^{116m}In	54.4	416.90	27.2
						818.68	12.1
						1097.3	58.5
						1293.6	84.8
						1507.6	9.92
						2112.3	15.1
^{65}Cu	30.8	1.99	2.01	^{66}Cu	5.12	1039.2	9.23
^{68}Zn	18.8	0.0701	0.224	^{69m1}Zn	13.76 h	438.6	94.9

Main nuclear data to determine indium content by comparator INAA are presented in Table 1: isotopic abundance θ, thermal neutron cross-section σ_0, and resonance integral I_0 of an activated isotope, half-life $T_{1/2}$, energies of gamma-lines E_γ, and their quantum yields P_γ of the target radionuclide [25]. Only the main gamma-lines of ^{116m}In with higher P_γ values are listed. The most suitable one (1293.6 keV) practically coincides in E_γ with the single intensive gamma-line of ^{41}Ar (P_γ = 99.1%, $T_{1/2}$ = 110 min) ever present in spectra after short-time activations. Among the other gamma-lines of ^{116m}In the 416.9 keV one reveals the highest count rate considering GC2018 detection efficiency and absence of significant spectral interferences. That is why it was selected as the analytical gamma-line. Both ^{66}Cu and ^{69m1}Zn gamma-lines are not encumbered with any noticeable spectral overlapping with other radionuclide lines.

Results and discussion

In case of ISM application indium content C_a (%) of the analyzed samples was calculated according to the next equation of simple comparator method of standardization in INAA [26] (lower case indices a and c mean an analyzed element and the comparator, respectively):

$$C_a = C_c \frac{k_{0,c} J_a \varepsilon(E_c)(f + Q_0^c)(SDC)_c G_c F_c}{k_{0,a} J_c \varepsilon(E_a)(f + Q_0^a)(SDC)_a G_a F_a} K_{a,c}, \quad (1)$$

where C_c is the element comparator content of the sample (%), k_0 is k_0-factor relatively to 411.8 keV gamma-line of radionuclide ^{198}Au for the gamma-lines of the comparator and an analyzed element [25], J is the full-energy peak count rate of the corresponding radionuclide analytical gamma-ray (cps), Q_0 is the resonance integral to the thermal neutron cross-section ratio, f is the thermal to epithermal neutron flux ratio, $S = 1 - \exp(-\lambda t_{irr})$ is saturation factor, $D = \exp(-\lambda t_d)$ is decay factor, $C = (1 - \exp(-\lambda t_m))/\lambda t_m$ is the counting factor (t_{irr}, t_d, and t_m are irradiation, decay and measuring time), G is the correction factor for neutron self-shielding by the sample, F is the correction factor for analytical gamma-ray self-absorption by the sample.

The empirical correction factor $K_{a,c}$ is applied to compensate for an analytical bias caused by the errors of detector calibration for detection efficiency, absence of Q_0 correction for the deviation of thermal neutron flux from $1/E$ law, and by other reasons. In particular, using the same counting geometries, there is no need to correct J for true coincidences. $K_{a,c}$ values were assessed by the repeated irradiation and counting of the CRMs certified for indium, copper, and zinc contents. $K_{\mathrm{In,Cu}}$ and $K_{\mathrm{In,Zn}}$ coefficients didn't differ substantially from unity amounting to 0.993 and 0.957, correspondingly.

If SAM was applied, another variant of equation (1) must be used as follows:

$$C_a = (C_c + \frac{m_c^{add}}{M_s} \cdot 100) \frac{k_{0,c} J_a \varepsilon(E_c)(f + Q_0^c)(SDC)_c G_c F_c}{k_{0,a} J_c \varepsilon(E_a)(f + Q_0^a)(SDC)_a G_a F_a} K_{a,c}, \quad (2)$$

where m_c^{add} is the standard addition (Zn) mass (mg) and M_s is the sample mass (mg).

Since greatly prevailing isotope ^{115}In is distinguished by large values of σ_0 and I_0 (Table 1), thermal and resonance neutron self-shielding by the samples might be expected. The problem was studied by M.Ebihara, et al. [27]; no apparent effect due to self-shielding was revealed up to the indium mass equal to 1 mg, i.e. to $C_{\mathrm{In}} = 1\%$ in a 100 mg assay. Such high indium content is never found in its mineral resources with the exception of blende [3], therefore G factor can be ignored.

On the other side, some sources of indium by-product production like barite-polymetallic ores are characterised by high contents of heavy metals, Pb and Ba first of all, with these elements mass-fractions reaching 5% and 40–45% correspondingly. Gamma-ray self-absorption of ^{116m}In and ^{66}Cu analytical gamma-lines (differing in E_γ most of all) by similar samples was evaluated in the approximation of a thin irradiating layer [28]. Photon mass attenuation coefficients were picked up from an NIST database [29]. Due to high E_γ values, photoelectric absorption and scattering of the gamma-lines are distinct from each other by no more than 1% even in such heavy matrixes.

The model ratio of $1/f$ was evaluated using the "bare bi-isotopic method" [30] with the help of a monitor of the neutron flux spectral composition – a ZrO_2 sample [17]:

$$\frac{1}{f} = \frac{\sigma_{0,2} - B\sigma_{0,1}}{BI_{0,1} - I_{0,2}}, \; B = \frac{N_{p,2}\varepsilon(E_1)\theta_1 P_{\gamma,1}(SDC)_1}{N_{p,1}\varepsilon(E_2)\theta_2 P_{\gamma,2}(SDC)_2}, \quad (3)$$

where lower indices 1 and 2 correspond to two zirconium isotopes: ^{94}Zr ($Q_0 = 5.31$) and ^{96}Zr ($Q_0 = 251.6$). Small polyethylene bags containing ≈100 mg of ZrO_2 were prepared and installed into the transport capsules as described above. A range of the samples were independently irradiated for 5 min in different days, even months, using the same PTS and counted for 20 min after one day of decay. The calculated individual $1/f$ values revealed great stability from one irradiation to another resulting in the average one 0.0121 ± 0.007 ($P = 0.95$). This is approximately thrice as low as that of the WWR-K's peripheral vertical channel № 10-6 used in INAA for long-time irradiations.

While accuracy of different element determination by comparator INAA using Fe content of geological samples by RLP-21T as the internal standard was repeatedly confirmed [17, 22, 28], Cu and Zn were tried by the author with that end in view for the first time. Careful XRF analysis of several tens of various ore CRMs showed that Cu mass fractions of the samples can be reliably

measured by RLP-21T to use them as the internal comparator beginning from 0.4–0.5%. Relative discrepancy between the analysed and certified values, in this case, didn't exceed 4%. On the other hand, due to favorable nuclear data (Table 1), these contents are high enough to determine ^{66}Cu count rate of a 100 mg sample irradiated for 1 min and counted as noticed above with relative uncertainty below 1.5%. Sensitivity of Zn analysis by the short-lived radionuclide is considerably worse than that of Cu, therefore Zn can be reliably (with count rate uncertainty <2.5%) used as the internal standard if its mass fraction exceeds 3%. Usually, there are no problems in such sample analysis by XRF with sufficient precision. The estimated Cu and Zn contents to implement internal standard based INAA can be generally found in polymetallic ores as one of the main sources of indium production. To analyse other indium mineral resources by comparator INAA SAM should be evidently applied. Zinc is more appropriate than copper then, since a bigger standard addition mass is necessary. If a 10 mg addition is used, uncertainty of its measuring by an analytical balance is 1% and can be ignored comparing with the other sources of uncertainty.

Table 2 – Indium content of polymetallic ore CRMs by comparator INAA using Cu and Zn as the internal standards (P = 0.95)

CRM name	CRM type	Element, % (XRF)		In, mg/kg		E_n-number
				Certified value	Measured value	
OSO 207	Pyrite-barite-polymetallic ore	Cu	1.331 ± 0.081	0.7 ± 0.1	0.67 ± 0.07	-0.25
		Zn	6.75 ± 0.30		0.73 ± 0.07	0.25
OSO 208	Pyrite-barite-polymetallic ore	Cu	1.574 ± 0.081	1.2 ± 0.1	1.17 ± 0.12	-0.19
		Zn	4.87 ± 0.17		1.16 ± 0.12	-0.26
OSO 209	Pyrite-copper-zinc ore	Cu	3.58 ± 0.17	6.5 ± 0.3	6.35 ± 0.64	-0.21
		Zn	7.53 ± 0.30		6.30 ± 0.63	-0.29
OSO 210	Sulfide-barite-pyrite-polymetallic ore	Cu	2.14 ± 0.17	4.6 ± 0.2	4.77 ± 0.48	0.33
		Zn	17.00 ± 0.45		4.84 ± 0.48	0.46
OSO 211	Sulfide-pyrite-copper-zinc ore	Cu	2.46 ± 0.17	3.6 ± 0.2	3.51 ± 0.35	-0.22
		Zn	3.23 ± 0.17		3.53 ± 0.36	-0.17
OSO 213	Sulfide-pyrite-copper-zinc ore	Cu	4.81 ± 0.17	28.0 ± 1.0	29.0 ± 2.9	0.33
		Zn	6.25 ± 0.30		29.5 ± 3.0	0.47

Accuracy of indium determination by comparator INAA was assessed with the help of several CRMs presenting different types of polymetallic ores (Table 2) produced by the Central laboratory (CL) of the Industrial Geological Association “EastKazGeology”, Kazakhstan. The CRM samples were prepared, irradiated and analyzed as described above. A single measurement of each CRM was carried out. Both Cu and Zn contents of the samples were high enough to implement ISM, so the values determined by XRF were used as the internal standards.

Relative expanded uncertainty of the INAA results $U(C_a)$ was estimated as follows (P = 0.95):

$$U(C_a) \approx 2C_a\sqrt{\frac{u(J_a)^2}{J_a^{\,2}} + \frac{u(J_c)^2}{J_c^{\,2}} + \frac{u(C_c)^2}{C_c^{\,2}} + \delta_a^{\,2}}\,, \qquad (4)$$

where $u(J_a)$, $u(J_c)$, and $u(C_c)$ are standard uncertainties of the corresponding values as in Eq. 1, δ_a is the standard deviation of element analysis (methodical uncertainty) by comparator INAA (all the ratios and δ_a are in %). δ_a value assessed earlier with the help of the CRMs equals ≈3% for both comparators. Standard uncertainty of Cu and Zn contents of a sample by XRF is equated to the ascribed values according to the certified analytical technique.

The measured indium mass fractions of the CRMs are well comparable with the certified ones

with <6% of discrepancy irrespective of the internal comparator. Maximum relative difference (≈9%) between each two results of indium determination corresponds to their lowest values (OSO 207) and is <2% for the other samples. Expanded uncertainty of all six CRMs analysis by comparator INAA doesn't exceed the allowable standard deviation of the results of their determination directed by the III category of precision (common analysis) – namely 24–30% for these content intervals, according to OST 41-08-221-04 [31].

E_n-number of indium determination was additionally evaluated as a criterion recommended by IUPAC to verify the laboratory performance [32]:

$$E_n = \frac{C_a - C_r}{\sqrt{U(C_a)^2 + U(C_r)^2}}, \qquad (5)$$

where $U(C_r)$ is expanded uncertainty of the analyzed element certified value C_r ($P = 0.95$). E_n-number values within $-1<E_n<1$ interval are considered admissible if the relative deviation $C_a - C_r$ doesn't exceed a predetermined quantity. In the present investigation maximum deviation ±10% was accepted. Since E_n-number absolute values appeared less than unity (Table 2) and the relative bias – less than 10%, the results of In analysis can be considered acceptable by E_n-number criterion too.

Low indium content of CRM OSO 207 permitted to assess its limit of detection (*LOD*) in polymetallic ores. Two gamma-lines of ^{116m}In – 416.90 keV and 1097.3 keV – were used with that end in view. A part of gamma-ray spectrum of CRM OSO 207 including these lines is presented in Fig. 1 in a log-linear scale after 28 min of decay. The sample was irradiated and counted for 1.5 min and 5 min, correspondingly; the analyzer dead time reached 22%. Both internal comparator gamma-lines together with that of some major elements are lettered in Fig. 1. The zoomed fragments of the spectrum demonstrating net peak areas of ^{116m}In gamma-lines above the background are shown in the treatment window of the "AnalGamma" software (Fig. 2(a) and 2(b)).

LOD values were estimated according to the next expression commonly applied in spectroscopic methods: $LOD = 3.3\sigma_b/b$ [33], where σ_b is standard deviation of the blank signal (counting statistics of the background count rate at the peak area) and b is concentration sensitivity of the method. If a linear calibration function is used like in INAA, b is a constant: $b = \Delta J / \Delta C$. *LOD* of indium in the polymetallic ore sample equaled to ≈0.06 mg/kg by its 416.90 keV gamma-line and ≈0.04 mg/kg by 1097.3 keV one, correspondingly. The last value appeared better formally due to a lower spectral background under the more high-energy gamma-line. Nevertheless, both assessments can be considered practically the same comparing with indium lower content of typical polymetallic ores (tenth of mg/kg) supplying 70–75% of indium in the world [3].

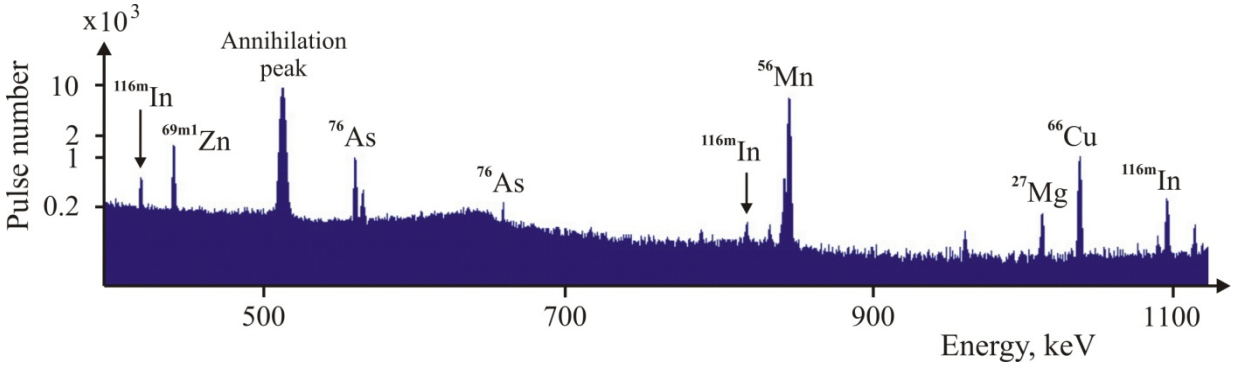

Figure 1 – A part of gamma-ray spectrum of CRM OSO 207 counted by GC2018 after 28 min of decay (in a log-linear scale)

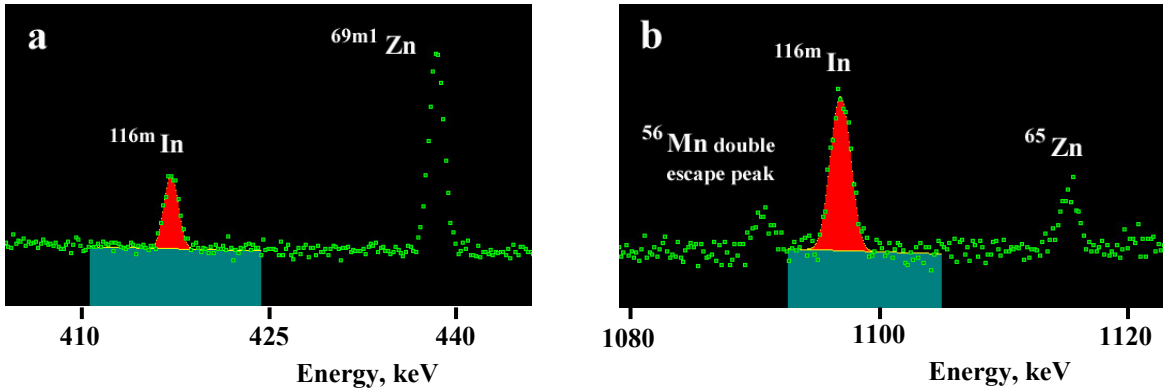

Figure 2 – net peak area of ^{116m}In gamma-lines in "AnalGamma" treatment window: 416.90 keV (a) and 1097.3 keV (b) (vertical scaling is different)

So, an opportunity was demonstrated to analyze indium in different types of polymetallic ores by comparator INAA. Both Cu and Zn contents of the samples exceeded the values making possible to use ISM with the internal standard mass fractions found by XRF. To verify this approach, it should be tried for the ore samples characterized by different contents of the accompanying indium elements and presenting various types of indium mineral resources.

The corresponding CRM samples which were not certified for indium mass fraction were selected at first. Table 3 presents the ones with higher contents of copper and zinc as some of the main indium companion elements. These CRMs include several types of copper and polymetallic ores, a lead-zinc ore and even a gold-bearing ore. The last type is not typical as an indium mineral resource and was involved into investigations due to enhanced copper and zinc contents (often accompanying gold deposits). The CRMs were produced by CLs "EastKazGeology" and "CentreKazGeology" (Kazakhstan) and by LLP "Tula Scientific Research Geological Enterprise" (Russian Federation). Six of ten samples were analyzed using Cu or Zn by XRF as the internal comparator. Both elements were applied with that end in view measuring indium content of SOP 2-89 and SOP 3-89 analogous to OSO 210 from Table 2. Since none of Cu and Zn mass fractions of the other four CRMs were sufficient to use them as the internal comparators the method of Zn standard addition was realized in this case. Then zinc content of these samples was evaluated according to equation (2). The added masses of zinc are much higher than its initial quantity (mg) in the samples found by XRF (thirteen times greater for GSO 6585 as the most rich of them). Therefore the relative standard uncertainty of zinc content of such a sample $u(C_c)/C_c$ slightly differs from the value of zinc standard addition uncertainty and can be ignored in (4) for the majority of the samples.

Table 4 includes tin ore and tungsten ore CRMs, the latter ones since they are characterized by the enhanced Sn contents. Tungsten itself doesn't relate to indium companion elements, so its mass fractions are not presented. Tin contents are certified in some CRMs and were defined by XRF in the others. Cu and Zn mass fractions of the samples were measured too to select XRF-based ISM, or SAM, making possible implementation of comparator INAA. The CRMs were produced by the Kyrgyz branch of the All-Union Scientific Research Center of Reference Materials (Kyrgyz Republic), by "CentreKazGeology", and by LLP "GEOTEHVIMS" (Russian Federation). Only one sample – GSO 323 – allowed using an independent method to determine internal comparator (Cu) content. GSO 2040 could be analyzed in the same way, but ^{66}Cu count rate appeared severely insufficient due to a very low irradiation time – 6 s caused by too high Mn mass fraction (0.951%). So SAM was applied in all the other cases. High Mn contents being inherent to all five tungsten ore CRMs resulted in the diminished irradiation time followed by the increased uncertainty.

Table 3 – Indium content of Cu-Zn-bearing CRMs by comparator INAA using ISM and SAM methods (P = 0.95)

CRM name	CRM type	Cu, %	Zn, %	In, mg/kg
OSO 47-85	Skarn copper ore	0.415 ± 0.048	0.0204 ± 0.0048	3.14 ± 0.32 [a]
MSO 1071	Porphyry copper ore	1.450 ± 0.081	0.0180 ± 0.0023	0.56 ± 0.07
OSO 118	Lead-zinc ore	0.101 ± 0.020	4.70 ± 0.17	0.68 ± 0.08
GSO 1433	Barite-polymetallic ore	0.332 ± 0.048	0.558 ± 0.080	1.00 ± 0.10 [a]
GSO 1434	Barite-polymetallic ore	0.423 ± 0.048	0.060 ± 0.010	0.80 ± 0.08 [a]
GSO 1435	Barite-polymetallic ore	0.132 ± 0.020	3.48 ± 0.17	1.68 ± 0.17
GSO 3584	Polymetallic ore	0.626 ± 0.048	10.23 ± 0.45	0.63 ± 0.07
SOP 2-89	Sulfide-barite-pyrite-polymetallic ore	2.14 ± 0.17	4.56 ± 0.17	0.22 ± 0.03 0.23 ± 0.03
SOP 3-89	Sulfide-barite-pyrite-polymetallic ore	1.870 ± 0.081	13.71 ± 0.45	0.22 ± 0.03 0.21 ± 0.03
GSO 6585	Gold-bearing ore	0.074 ± 0.010	0.618 ± 0.080	1.34 ± 0.13 [a]

[a] Zn standard addition

Table 4 – Indium content of Sn- and W-Sn-bearing CRMs by comparator INAA using ISM and SAM methods (P = 0.95)

CRM name	CRM type	Sn, %	Cu, %	Zn, %	In, mg/kg
GSO 168	Tinstone ore	1.55 ± 0.04 [b]	0.112 ± 0.020	0.0187 ± 0.0023	1.68 ± 0.17 [a]
GSO 169	Tinstone ore	1.085 ± 0.04 [b]	0.318 ± 0.048	0.0199 ± 0.0023	8.75 ± 0.88 [a]
GSO 322	Tinstone ore	0.34 ± 0.01 [b]	0.051 ± 0.010	0.0115 ± 0.0023	2.62 ± 0.26 [a]
GSO 323	Tin-tungsten-beryllium ore	2.81 ± 0.03 [b]	1.401 ± 0.081	0.090 ± 0.010	17.0 ± 1.7
GSO 324	Tin-tungsten-beryllium ore	0.40 ± 0.01 [b]	0.150 ± 0.020	0.0280 ± 0.0048	1.02 ± 0.10 [a]
GSO 576	Tinstone ore	0.93 ± 0.03 [b]	0.0377 ± 0.0048	0.0296 ± 0.0048	0.85 ± 0.09 [a]
NFS-4	Tin ore	0.466 ± 0048 [b]	0.196 ± 0.020	0.078 ± 0.010	6.68 ± 0.67 [a]
NFS-13	Tungsten-tin ore	0.121 ± 0.005 [b]	0.0350 ± 0.0048	0.147 ± 0.020	4.85 ± 0.49 [a]
GSO 1714	Tungsten ore	0.131 ± 0.020	0.0251 ± 0.0048	0.0374 ± 0.0048	0.97 ± 0.12 [a]
GSO 2039	Tungsten ore	0.0067 ± 0.0013	0.304 ± 0.048	0.097 ± 0.010	3.70 ± 0.48 [a]
GSO 2040	Tungsten ore	0.0104 ± 0.0023	0.421 ± 0.048	0.104 ± 0.020	6.27 ± 0.82 [a]
GSO 2041	Tungsten ore	0.00311 ± 0.00083	0.0466 ± 0.0048	0.0300 ± 0.0048	1.22 ± 0.15 [a]
GSO 2042	Tungsten ore	0.0105 ± 0.0023	0.107 ± 0.020	0.061 ± 0.010	4.59 ± 0.60 [a]

[a] Zn standard addition
[b] certified values

The results of indium content determination by comparator INAA in real samples of copper-pyrite ore and several types of polymetallic ore are presented in Table 5. The samples were collected from the ore veins of the gold-polymetallic deposit Maikain in North-Eastern Kazakhstan to implement geochemical investigations. Due to low Mn mass fraction of the samples (≤200 mg/kg) all of them were irradiated for the same time – 1 min. Cu content by XRF was used to determine indium in the majority of the samples. One of them allowed to use Zn content as well; relative discrepancy amounted to <4%, that is lower than the relative uncertainty of the results. The other samples were analyzed using Zn standard addition method. Maximum indium content of the samples (65.9 mg/kg) approximately reaches that of some pyrite-polymetallic deposits of Rudny Altai (Eastern Kazakhstan) [3] which is the main region of indium production in Kazakhstan at present.

Table 5 – Indium content of polymetallic ore and copper-pyrite ore samples by comparator INAA using ISM and SAM methods ($P = 0.95$)

Sample number	Description	Cu, %	Zn, %	In, mg/kg
1859	Pyrite-barite-polymetallic ore	0.499 ± 0.048	4.14 ± 0.17	4.27 ± 0.44
1992	Copper-pyrite ore	6.57 ± 0.30	0.0162 ± 0.0023	65.9 ± 6.5
1998	Copper-pyrite ore	0.330 ± 0.048	0.0478 ± 0.0048	2.28 ± 0.23 [a]
2026	Copper-pyrite ore	2.46 ± 0.17	0.330 ± 0.048	2.69 ± 0.27
2036	Copper-pyrite ore	3.25 ± 0.17	0.464 ± 0.048	7.18 ± 0.72
2050	Polymetallic ore	2.92 ± 0.17	0.685 ± 0.080	4.29 ± 0.43
2052	Copper-pyrite ore	0.731 ± 0.080	0.0380 ± 0.0048	2.33 ± 0.27
2082	Copper-pyrite ore	0.577 ± 0.080	0.0200 ± 0.0023	1.73 ± 0.24
2108	Copper-pyrite ore	0.251 ± 0.048	0.0368 ± 0.0048	1.39 ± 0.14 [a]
2115	Barite-polymetallic ore	0.674 ± 0.080	1.218 ± 0.081	9.3 ± 1.1
2124	Pyrite-barite-polymetallic ore	0.230 ± 0.048	0.359 ± 0.048	2.85 ± 0.29 [a]
2146	Copper-pyrite ore	1.254 ± 0.081	0.088 ± 0.010	1.63 ± 0.16
2157	Copper-pyrite ore	0.275 ± 0.048	0.0336 ± 0.0048	0.40 ± 0.04 [a]

[a] Zn standard addition

Conclusion

A simple, prompt, and reliable variant of comparator INAA was used to analyze indium content of its ore mineral resources by the short-living radionuclide ^{116m}In. Instead of commonly applied relative method or k_0-INAA, both based on the external standards, two ways of internal standardization was tried using Cu and/or Zn contents of the samples as some of the main indium companion elements. Mass fractions of the elements were found by an independent method – XRF often used at present to complement INAA in ores, rocks, and minerals investigation. These element contents ≈0.5% for Cu (by XRF spectrometer RLP-21T) and >3% for Zn are usually sufficient to realize the internal standard method by their short-living radionuclide studying different types of pollymetalic and similar ores. Otherwise, the standard addition method with ZnO reagent was used to analyze indium content of other main types of its resources such as tin- and tin-tungsten-bearing ores.

The assessed expanded uncertainty of indium determination usually didn't exceed 10% depending mainly on the uncertainties of the internal standards analysis by XRF and increased to ≈14% due to a higher component of the analytical

line statistical uncertainty in case of indium lower contents (<1 mg/kg).

By the example of INAA of different ore samples including the CRMs (certified and non-certified for indium mass fractions) and the samples from the gold-polymetallic deposit Maikain, the possibility of indium routine determination in the similar objects by the III category of precision (common analysis) according to OST 41-08-221-04 was demonstrated.

Mere advantages of the approach, its sensitivity and flexibility promote its applicability in different geological object analysis including geochemical investigations.

Funding

The work was supported by a grant from Ministry of Energy of the Republic of Kazakhstan (BR09158958).

References

1 Rudnick R.L., Gao S. (2014) 4.1 – Composition of the continental crust. *Treatise Geochem*, 2d edition, vol. 4, pp. 1-51. https://doi.org/10.1016/B978-0-08-095975-7.00301-6.

2 Lerouge C., Gloaguen E., Wille G., Bailly L. (2017) Distribution of In and other rare metals in cassiterite and associated minerals in Sn ± W ore deposits of the western Variscan Belt. *Eur J Mineral*, vol. 29, pp. 739-753. https://doi.org/10.1127/ejm/2017/0029-2673.

3 Gaskov I.V., Gushchina L.V. (2020) Physicochemical conditions of the formation of elevated indium contents in the ores of tin-sulfide and base-metal deposits in Siberia and Far East: evidence from thermodynamic modeling. *Geochem Int*, vol. 58, pp. 291-307. https://doi.org/10.1134/S0016702920030052.

4 Werner T.T., Mudd G.M., Jowitt S.M. (2017) The world's by-product and critical metal resources part III: A global assessment of indium. *Ore Geol Rev*, vol. 86, pp. 939-956. https://doi.org/10.1016/j.oregeorev.2017.01.015.

5 Valkama M., Sunblad K., Nygård R., Cook N. (2016) Mineralogy and geochemistry of indium-bearing polymetallic veins in the Sarvlaxviken area, Lovisa, Finland. *Ore Geol Rev*, vol. 75, pp. 206-219. https://doi.org/10.1016/j.oregeorev.2015.12.001.

6 Jovic S.M., Guido D.M., Ruiz R., et al. (2011) Indium distribution and correlations in polymetallic veins from Pingüino deposit, Deseado Massif, Patagonia, Argentina. *Geochem*: *Explor*, *Environ*, *Anal*, vol. 11, pp. 107-115. https://doi.org/10.1144/1467-7873/09-IAGS-013.

7 Pavlova G.G., Palessky S.V., Borisenko A.S., et. al. (2015) Indium in cassiterite and ores of tin deposits. *Ore Geol Rev*, vol. 66, pp. 99-113. https://doi.org/10.1016/j.oregeorev.2014.10.009.

8 Murakami H., Ishihara Sh. (2013) Trace elements of indium-bearing sphalerite from tin-polymetallic deposits in Bolivia, China and Japan: A femto-second LA-ICPMS study. *Ore Geol Rev*, vol. 53, pp. 223-243. http://dx.doi.org/10.1016/j.oregeorev.2013.01.010.

9 Valkama M., Sunblad K., Cook N., Ivashchenko V.I. (2016) Geochemistry and petrology of the indium-bearing polymetallic skarn ores at Pitkäranta, Ladoga Karelia, Russia. *Miner Deposita*, vol. 51, pp. 823-839. http://dx.doi.org/10.1007/s00126-016-0641-4.

10 Liu J., Gu X., Shao Y., et al. (2016) Indium mineralization in copper-tin stratiform skarn ores at the Saishitang-Rilonggou ore field, Qinghai, Northwest China. *Resour Geol*, vol. 66(4), pp. 351-367. http://dx.doi.org/ 10.1111/rge.12108.

11 Ishihara Sh., Murakami H., Marquez-Zavalia M.F. (2011) Inferred indium resources of the Bolivian tin-polymetallic deposits. *Resour Geol*, vol. 61(2), pp. 174-191. http://dx.doi.org/ 10.1111/j.1751-3928.2011.00157.x.

12 Zhang Q., Zhu X., He Yu., et al. (2006) Indium enrichment in the Meng'entaolegai Ag-Pb-Zn deposit, Inner Mongolia, China. *Resour Geol*, vol. 56(3), pp. 337-346. http://dx.doi.org/10.1111/j.1751-3928.2006.tb00287.x.

13 Cook N., Ciobanu C.L., George L., et al. (2016) Trace element analysis of minerals in magmatic-hydrothermal ores by laser ablation inductively-coupled plasma mass spectrometry: approaches and opportunities. *Minerals*, vol. 6(4), pp. 111-145. https://doi.org/10.3390/min6040111.

14 Dybczyński R. (2001) Neutron activation analysis and its contribution to inorganic trace analysis. *Chem Anal* (*Warsaw*, *Pol*), vol. 46(2), pp. 133-160.

15 Frenzel M., Bachmann K., Carvalho J., et al. (2019) The geometallurgical assessment of by-products – geochemical proxies for the complex mineralogical deportment of indium at Neves-

Corvo, Portugal. *Miner Deposita*, vol. 54, pp. 959-982. https://doi.org/10.1007/s00126-018-0849-6.

16 Jaćimović R., Lazaru A., Mihajlović D., et al. (2002) Determination of major and trace elements in some minerals by k_0-instrumental neutron activation analysis. *J Radioanal Nucl Chem*, vol. 253(3), pp. 427-434. https://doi.org/10.1023/A:1020421503836.

17 Silachyov I. (2016) Rare earths analysis of rock samples by instrumental neutron activation analysis, internal standard method. *J Radioanal Nucl Chem*, vol. 310(2), pp. 573-582. https://doi.org/10.1007/s10967-016-4903-5.

18 Acharya R., Nair A.G.C., Sudarshan K., et al. (2007) Development and applications of the k_0-based internal mono standard INAA method. *Appl Radiat Isot*, vol. 65, pp. 164-169. https://doi:10.1016/j.apradiso.2006.08.005.

19 Silachyov I. (2020) Elemental analysis of vegetation samples by INAA internal standard method. *J Radioanal Nucl Chem*, vol. 324(1), pp. 97-108. https://doi.org/10.1007/s10967-020-07051-6.

20 Silachyov I.Yu. (2020) Neutron activation analysis of rare earth raw material using a planar detector and thorium as an internal standard. *IJBC*, vol. 13(2), pp. 117-129. https://doi.org/10.26577/ijbch.2020.v13.i2.14.

21 Tiwari S., Nair A.G.C., Acharya R., et al. (2007) Analysis of uranium bearing samples for rare earth and other elements by k_0-based internal monostandard INAA method. *J Nucl Radiochem Sci*, vol. 8(1), pp. 25-30. https://doi.org/10.14494/JNRS2000.8.25.

22 Silachyov I.Yu. (2020) Combination of neutron activation analysis with X-ray fluorescence spectrometry for the determination of rare-earth elements in geological samples. *J Analyt Chem*, vol. 75(7), pp. 878-889. https://doi.org/10.1134/S106193482007014X.

23 Silachyov I.Yu. (2018) Determination of rare earths in uranium raw material by neutron activation analysis and X-ray fluorescence. *News of the Academy of Sciences of RK*, *ser. chem. & technol.*, vol. 429(3), pp. 28-38.

24 Ismail S.S. (2010) A new automated sample transfer system for instrumental neutron activation analysis. *J Autom Methods Manage Chem*, vol. 2010(1), 8 pp. https://doi.org/10.1155/2010/389374.

25 Nuclear data sub-committee. K0-neutron activation analysis link page (accessed Nov 12, 2021). http://www.kayzero.com/k0naa/k0naaorg/Links.html.

26 Pushkin S.G., Mikhailov V.A. (1989) Komparatornyi neitronno-aktivatsionnyi analiz. Izuchenie atmosfernyh aerozolei (Comparator neutron activation analysis. Study of atmospheric aerosols). Novosibirsk, Nauka, 125 p. (in Russian).

27 Ebihara M., Nemoto A., Akaiwa H. (1988) Epithermal neutron activation analysis of geological materials for trace indium. *Anal Sci*, vol. 4(2), pp. 169-173. https://doi.org//10.2116/analsci.4.169.

28 Silachyov I.Yu. (2020) Instrumental neutron activation analysis of rhenium in uranium raw material. *IJBC*, vol. 13(1), pp. 161-169. https://doi.org/10.26577/ijbch.2020.v13.i1.17.

29 Hubbell J.H., Seltzer S.M. X-ray mass attenuation coefficients. NIST standard reference database 126 (accessed Nov 12, 2021). https://www.nist.gov/pml/x-ray-mass-attenuation-coefficients.

30 Simonits A., De Corte F., Hoste J. (1976) Zirconium as a multi-isotopic flux ratio monitor and a single comparator in reactor-neutron activation. *J Radioanal Nucl Chem*, vol. 31, pp. 467-586.

31 OST 41-08-212-04 (2004) Standart otrasli. Upravlenie kachestvom analiticheskih rabot. Normy pogreshnosti pri opredelenii himicheskogo sostava mineralnogo syr'ya i klassifikatsiya metodik laboratornogo analiza po tochnosti rezultatov (Idustrial standard. Quality management of analytical work. Error guidelines for chemical analysis of mineral resources and precision classification of laboratory analytical techniques). Moscow, VIMS, 23 p. (in Russian).

32 ISO 13528:2015 (2015) Statistical methods for use in proficiency testing by interlaboratory comparisons. Genève, Switzerland, 89 p.

33 Desimoni E., Brunetti B. (2015) About estimating the limit of detection by the signal to noise approach. *Pharm Anal Acta*, vol. 6, 4 pp. http://dx.doi.org/10.4172/2153-2435.1000355.

IRSTI 31.23.17 https://doi.org/10.26577/ijbch.2021.v14.i2.016

Zh.A. Koshetova[1,2], K.D. Praliyev[1], V.K. Yu[1],
T.E. Li[3], N.A. Zhumanova[2], E. Turaç[4]

[1] A.B. Bekturov Institute of Chemical Sciences, Almaty, Kazakhstan
[2] Kazakh National Women's Pedagogical University, Almaty, Kazakhstan
[3] Institute of Plant Biology and Biotechnology, Almaty, Kazakhstan
[4]Nigde Omer Halisdemir University, Turkey, Nigde
*e-mail: zhanar.kozhetova@gmail.com

Novel 3,5- bis(fluorobenzylidene)piperidin-4-ones as regulators of wheat growth

Abstract. In plant growing, the practical value of growth regulators is determined by the ability to significantly accelerate the development and increase the productivity of most agricultural crops. One of the most important tasks of the technology of wheat production is a target search for novel effective growth regulators. To determine the effect of the presence of fluoride in a molecule with the binding fragment of N-(2-ethoxyethyl)piperidine, as well as the substitution of ethoxyethyl substituent at nitrogen of piperidine cycle on benzyl it had been synthesized fluorine-containing piperidines. It turned out that the pre-treatment of seeds of spring wheat varieties Kazakhstanskaya-10, Severyanka and Miras with 0.01% solutions of 3,5-bis (fluorobenzylidene)piperidin-4-ones as complexes with *β*–cyclodextrin regulates the effect on germination and development. Dienone with ethoxyethyl substitute at nitrogen of piperidine cycle stimulates growth, and its N-benzyl analogue is a retardant. Target 3,5-bis(fluorarylidene)-4-piperidones were synthesized via the conditions of the Kleisen-Schmidt reaction by the interaction of piperidine-4-ones with fluorobenzaldehyde in ethanol in the presence of sodium hydroxide with a yield of 40.8-50.9%: Synthesized dienones are crystalline substances, limited soluble in water.
Key words: Fluorine-containing piperidin-4-ones, stimulants of wheat growth, retardant.

Introduction

Modern agriculture in many countries, including Kazakhstan, is characterized by the transition to organic farming and the biologization of processes in obtaining agricultural products in crop production [1-2]. And during the reproduction of green spaces, modified bioorganic fertilizers with additives of growth stimulants are used to increase the survival rate of tree crops. Biomineral and bioorganic fertilizers are widely used for cleaning (bioremediation) of oil-contaminated lands. It is known that a biotechnological solution to increase the productivity of the most important agricultural crops on irrigated soils while minimizing energy and resource consumption, as well as environmental protection, is associated with the creation of highly efficient plant and microbial systems that allow more fully realize the potential of plants [3-4]. Optimization of organo-mineral nutrition of plants and their adaptation to unfavorable conditions can be achieved by selecting complementary associative plants, in particular nitrogen-fixing and ammonifying microorganisms and effective preparations [5-8]. Since the mechanism of action of these ones is the optimization of the vital activity of nitrogen-fixing microorganisms in terms of water supply and nutrition, therefore, the vegetation cover has a significant effect on the quantitative and qualitative composition of bacteria in the soil. In turn, bacteria actively produce enzymes that decompose difficult-to-disintegrate plant residues. Finally, thanks to the activity of microorganisms, the soil is enriched with valuable nutrients and freed from many harmful organisms and products. Stimulating plant growth as a whole helps to restore soil fertility. The research interest to modifiers (additives) of biomineral and bioorganic fertilizers, which not only stimulate plant growth, but enhance their protective functions to natural and man-made stress situations (adaptogens for plants), is great all over the world. The chemical aspect is the search for new substances with the aforementioned properties, both natural and synthetic origin.

The use of growth regulators in agricultural production pursues many goals: improving fruit setting, preventing lodging of grain and industrial crops, rooting cuttings, accelerating ripening, improving the quality of grown products. These substances can affect frost and drought resistance of plants, increase their immunity, and reduce the content of nitrates and radionuclides in cultivated products [9].

Growth regulators – retardants, are used to slow down the growth of plant stems in height in order to increase yields. In particular, cereals treated with retardants stop growing upward, but at the same time their root system becomes more developed, ears gain significantly in weight, and plant resistance to phytopathogenic damage increases [10]. Under the action of retardants, the stem becomes lower and increases in volume, while the division of cells of the young growing stem in length is inhibited and their division in the transverse direction increases, and the branching of the root system also occurs. The shortening of the vegetative part of the shoot is accompanied by increased spike growth and better filling of wheat grain. These preparations are widely used on cereals, as well as on rapeseed, grapes, cucumbers and many other crops [11-13]. With the correct use of retardants, the yield can increase up to 15%, while the harvest will be easier to harvest, and its quality will be higher.

One of the main methods of increasing the yield of grain crops is the preparation of seed material in order to disinfect it, protect seedlings from external pathogenic factors and increase their resistance to them, as well as stimulate the growth and development of plants, both during the germination of seeds and during the growing season. This is achieved by dressing seeds, processing them with growth regulators.

A targeted search for new effective regulators of grain growth is an urgent problem of wheat cultivation technology. This Research presents the synthesis of novel fluorine-containing piperidines, the use of which regulates seed germination and development of spring wheat seedlings of varieties Kazakhstanskaya-10, Severyanka and Miras.

Materials and methods

The reaction path and the identity of the compounds were controlled by thin layer chromatography (TLC) on aluminum oxide of the II degree of activity, with the following staining of spots with iodine vapor. The IR spectra were recorded on a Nicolet 5700 FT-IR spectrometer in KBr tablets and in a thin film, in the range from 4000 to 500 cm^{-1}. The ^{1}H and ^{13}C NMR spectra were taken on a JNM-ECA Jeol 400 spectrometer (frequency 399.78 and 100.53 MHz, respectively) using a $CDCl_3$ solvent. Chemical shifts were measured relative to the signals of residual protons or carbon atoms of chloroform.

1-(2-Ethoxyethyl)-3,5-bis(2-fluorobenzylidene) piperidin-4-one (3). In a flask equipped with a reflux condenser, a thermometer, a stirrer and a dropping funnel, 5.8 g of NaOH are placed in 55 ml of water and 55 ml of ethanol. Half a freshly prepared mixture of 5.0 g (0.029 mol) of 1-(2-ethoxyethyl) piperidone-4 (1) and 7.19 g (0.058 mol) of *o*-fluorobenzaldehyde is poured. After 15 min, add the second half of the mixture. The reaction is carried out at 20-25°C. The reaction mixture was stirred for 4 h. The precipitate that formed was filtered off, washed with water until neutral, dried, and recrystallized from iso-Propanol. 1-(2-ethoxyethyl)-3,5-bis (2-fluorobenzylidene) piperidin-4-one (3) was obtained in a yield of 4.57 g (40.8%), Rf 0.8 (Al_2O_3, eluent – benzene: dioxane = 7: 1), m.p. 150-151°C.

Calculated for $C_{23}H_{23}F_2O_2N$: C, 71.98; H, 5.99; N, 3.65. Found: C, 72.01; H, 6.02; N, 3.64.

IR spectrum cm^{-1}: 1093.9 (ν_{C-N}); 1218.8 (ν_{C-F}); 1601,2 ($\nu_{C=C}$); 1670.3 ($\nu_{C=O}$).

^{1}H HMR δ, ppm: 3.93 (s, 4H, $H_{2,6}$); 7.29-7.32 м.д. (m, 8H, $2C_6\underline{H}_4F$); 7.75 (s, 2H, $C_{3(5)}$=C$\underline{H}$); 2.75 (t, $C\underline{H}_2CH_2OCH_2CH_3$); 3.48 (t, $CH_2C\underline{H}_2OCH_2CH_3$); 3.37 (t, $CH_2CH_2OC\underline{H}_2CH_3$); 1.07 (q, $CH_2CH_2OCH_2C\underline{H}_3$) .

^{13}C NMR δ, ppm: 57.51 ($C_{2,6}$); 133.75 ($C_{3,5}$); 136.21 $C_{3(5)}$=$\underline{C}$H); 186.99 (C_4); 161.73, 164.23 (C-F); 132.03 ($\underline{C}_q$,C_4H_4CF), 115.97-117.04 ($\underline{C}_q$,C_4H_4CF); 54.39 ($\underline{C}H_2CH_2OCH_2CH_3$); 68.71 ($CH_2\underline{C}H_2OCH_2CH_3$); 66.97 ($CH_2CH_2O\underline{C}H_2CH_3$); 14.85 ($CH_2CH_2OCH_2\underline{C}H_3$).

Complex of 1-(2-ethoxyethyl)-3,5-bis(2-fluorobenzylidene)piperidin-4-one with β-cyclodextrin (5). To obtain an inclusion complex, mix solutions of 1.26 g (0,003mol) of 1-(2-ethoxyethyl)-3,5-bis(2-fluorobenzylidene) piperidin-4-one (3) in 35 ml of ethanol and 3.73 g (0,003mol) of β-cyclodextrin in 35-40 ml of distilled water. The mixture is placed in an oven, ethanol and water are evaporated at 50-55^{0}C. The inclusion complex of 1-(2-ethoxyethyl)-3,5- bis(2-fluorobenzylidene)piperidin-4-one with β-cyclodextrin (5) was obtained in a yield of 4.36 g (87.5%) as a light yellow powder.

Calculated for $C_{65}H_{93}O_{37}NF_2$: C, 51.40; H, 6.12; N, 0.92. Found: C, 51.43; H, 6.15; N, 0.90.

N - Benzyl - 3, 5 - bis (p - fluorobenzylidene) piperidin-4-one (4). NaOH (2.6 g) in 25 ml of water and 25 ml of ethanol are placed in a flask equipped with a reflux condenser, a thermometer, a stirrer and a dropping funnel. Half a freshly prepared mixture of 2.5 g (0.013 mol) of 1-benzylpiperidone-4 (2) and 3.38 g (0.026 mol) of *p*-fluorobenzaldehyde is poured. After 15 min, add the second half of the mixture. The reaction is carried out at 20-25°C. The reaction mixture was stirred for 4 h. The formed precipitate is filtered off, washed with water until neutral, dried and recrystallized from iso-Propanol. 1-Benzyl-3,5-bis(*p*-fluorobenzylidene)piperidin-4-one (4) was obtained in a yield of 5.3 g (50.9%), Rf 0.7 (Al_2O_3, eluent – benzene:dioxane=7:1), m.p. 153-155^{0}C.

Calculated for $C_{26}H_{21}F_2ON$: C, 77.80; H 5.23; N, 3.49. Found: C, 77.83; H, 5.26; N, 3.48.

IR spectrum cm^{-1}: 1006.6 (C-N); 1190.1 (C-F); 1601.3 (C=C); 1670.0 (C=O).

^{1}H HMR δ, ppm: 3.69 (s, 2H, $H_{2a,6a}$); 3.81 (s, 4H, $H_{2e,6e}$, $C\underline{H}_2Ph$); 7.03-7.07, 7.29-7.32 м.д. (m, 8H, $2C_6\underline{H}_4F$); 7.23 (s, $C_6\underline{H}_5$); 7.75 (s, 2H, $C_{3(5)}$=C<u>H</u>).

^{13}C NMR δ, ppm: 54.34 ($C_{2,6}$); 131.39 ($C_{3,5}$); 187.60 (C_4); 135.59 ($C_{3(5)}$=<u>C</u>); 161.71, 164.21 (C-F); 132.96 ($\underline{C}_qC_4H_4CF$); 115.45-128.49 ($C_q\underline{C}_4H_4CF$); 61.52 (CH_2); 137.23 ($\underline{C}_qC_5H_5$); 127,57-129.06 ($C_q\underline{C}_5H_5$).

Complex of N-benzyl-3,5-bis(p-fluorobenzylidene)piperidin-4-one with β-cyclodextrin (6). To obtain an inclusion complex, mix solutions of 0.78 g (0,002 mol) of N-benzyl-3,5-bis(*p*-fluorobenzylidene)piperidin-4-one (4) in 30 ml of ethanol and 2.21 g (0,002 mol) of β-cyclodextrin in 35-40 ml distilled water. The mixture is placed in an oven, ethanol and water are evaporated at 50-55^{0}C. The inclusion complex of N-benzyl-3,5-bis(*p*-fluorobenzylidene)piperidin-4-one with β-cyclodextrin (6) was obtained in a yield of 2.93 g (98.3%) as a light yellow powder.

Calculated for $C_{68}H_{91}O_{36}NF_2$: C, 53.15; H, 5.92; N, 0.91. Found: C, 53.10; H, 6.02; N, 0.90.

Biological experimental. The studies were carried out on model samples of spring wheat *Triticum aestivum* varieties Kazakhstanskaya-10, Severyanka and Miras. Severyanka and Miras were drought tolerant varieties, and Kazakhstanskaya-10 was studied as a standard. Presowing treatment of wheat with aqueous solutions of samples 3, 4 at a concentration of 0.01% was carried out in Petri dishes during germination of seeds for 2 days. Then, the seedlings were transferred to floating rafts for germination in hydroponics up to 10 day-old seedlings. Then biometric indicators were taken in comparison with control.

Water was used as the basis for the germination of grain crops. Experimental samples were laid in 15 replicates for each culture and the tested growth regulator. As a control option, we used tap water, settled for three days. The experiment lasted 10 days.

For each sample, the degree (%) of stimulation or inhibition was calculated in comparison with the control of its series of experiments.

Results and discussion

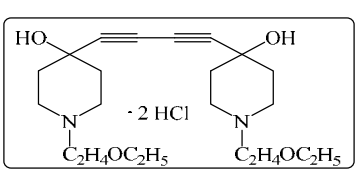

Kaz-4

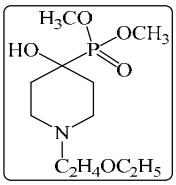

Kaz-6

In crop production, the practical importance of growth regulators is determined by the ability to significantly accelerate growth and increase the yield of most agricultural crops. Earlier, we found the stimulation of seed germination when they were treated with solutions Kaz-4 [14] and Kaz-6 [15], which have a fragment of N-(2-ethoxyethyl)piperidine. It was hypothesized that the introduction of fluorine into the molecule with the obligatory N-(2-ethoxyethyl) piperidine would have more effect on the development of wheat. In addition, it was interesting to investigate the effect of replacing the ethoxyethyl substituent at the nitrogen of the piperidine ring with a benzyl substituent.

The target 3,5-bis(fluoroarylidene)-4-piperidones (3,4) had been synthesized under the conditions of the Kleisen-Schmidt reaction by the interaction of piperidin-4-ones (1,2) with fluorobenzaldehyde in ethanol in the presence of sodium hydroxide with a yield of 40.8% and 50.9%:

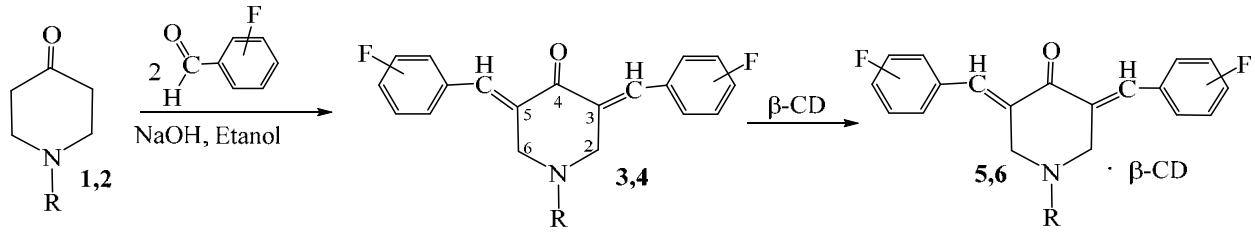

The synthesized dienones (3,4) are crystalline substances, limitedly soluble in water. Structure 3,4 was established on the basis of IR spectra, ^{1}H and ^{13}C NMR. IR spectra were characterized by the presence of absorption bands at 1670.0-1670.3 cm^{-1} (C=O), 1601.2-1601.3 cm^{-1} (C=C). The band of the double C=C bond was more intense than that of the carbonyl group. This indicates the formation of a dienone of symmetric conformation and flattening of the piperidine ring [16]. Due to the high symmetry of these molecules, the ^{1}H and ^{13}C NMR spectra are simplified. The spectra of protons 3,4 have a singlet for four methylene protons at $C_{2,6}$ at δ 3.69-3.93 ppm, a singlet for protons $C_{3,5}$=CH at 7.75 ppm. The ^{13}C NMR spectra were of double intensity for equivalent carbon atoms, with the exception of the carbonyl group (C_4, 186.99 3 and 187.60 4 ppm). Alkenyl carbon signals were observed in a weak field ($C_{3,5}$ – s, 133.75 3 and 131.39 4; $C_{3.5}$ =CH – d, 136.21 3 and 135.59 4 ppm). NMR spectra have signals of protons and carbons of substituents (ethoxyethyl and benzyl) at the carbon atom of the piperidine ring.

When wheat germinated in Petri dishes with pre-sowing treatment with 1-(2-ethoxyethyl)-3,5-bis(2-fluorobenzylidene)piperidin-4-one (3), no significant differences were observed against the background of control (water). The stimulation of the growth and development of wheat seedlings was noted. Compound 3 increased the height of Kazakhstanskaya-10 plants by 4.5%, Severyanka – by 8.5%, and Miras – 3%. Table 1 shows the mean and standard deviation for 1-(2-ethoxyethyl)-3,5-bis(2-fluorobenzylidene) piperidin-4-one (3) compared to controls.

Table 1 – Biometric data of wheat of three varieties in the control and in the presence of **3**, n = 15

	Kazakhstanskaya-10		Severyanka		Miras	
	Stem length	Root length	Stem length	Root length	Stem length	Root length
Control	19,58±1,14	14,46±2,19	18,4±1,17	9,7±1,46	17,6±1,68	10,93±2,61
3	20,47±0,88 *4,5%*	9,87±1,68	19,97±0,9 *8,5%*	7,9±0,88	18,14±1,19 *3%*	8,89±2,63

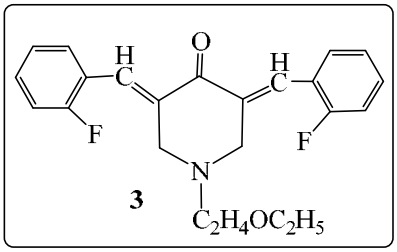

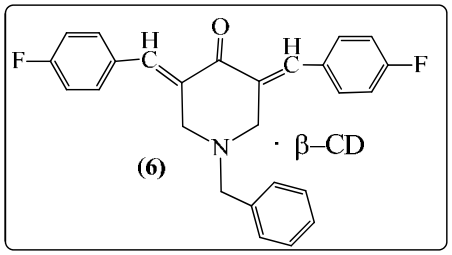

The trials results of 1-benzyl-3,5-bis(4-fluorobenzylidene) piperidin-4-one as complex with β-cyclodextrine (**6**) on the growth and development of the wheat root system are presented in Table 2. It is shown that the treatment of seeds and of plants by compound 6 led to inhibition, to varying degrees, of plant height and root length – by an average of 12% and root length by an average of 36% (Table 2 , Figure 1).

Table 2 – Biometric data of three varieties of wheat in the control and in the presence of 6; n = 15

Object	Kazakhstanskaya-10		Severyanka		Miras	
	Stem length	Root length	Stem length	Root length	Stem length	Root length
Control	19,71±1,13	9,29±1,35	19,5±1,29	10,27±1,97	17,96±1,05	11±2,06
6	18,91±1,14	6,56±1,03 29,4%	17,38±1,11 11,9%	7,08±0,96 31,1%	17,53±0,74	7±0,77 36,4%

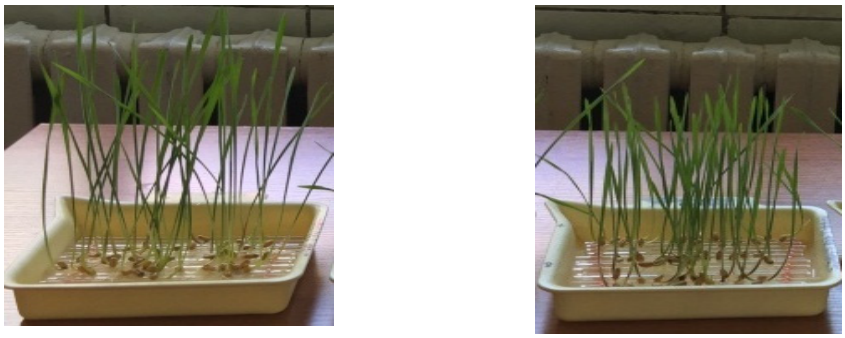

Control (water) 6

Figure 1 – 10-day-old wheat seedlings of varieties Kazakhstanskaya-10, Miras and Severyanka with treatment of seeds and plants 6 in comparison with control (water)

It was found that 1-benzyl-3,5-bis(4-fluorobenzylidene)piperidin-4-one as complex with β-cyclodextrine (**6**) has an inhibitory effect of phytohormones, shortening the vegetative part of the shoot and increasing the growth of the root system. In this case, the root system is shortened and thickened relative to the control.

Conclusion

Target 3,5-bis(fluoroarylidene)-4-piperidones were synthesized via the conditions of the Kleisen-Schmidt reaction by the interaction of piperidine-4-ones with fluorobenzaldehyde in ethanol in the presence of sodium hydroxide with a yield of 40.8% and 50.9%: Synthesized dienones are crystalline substances, limited soluble in water. Structure of 3,5-bis(2-fluorobenzylidene)piperidin-4-one were identified by IR and NMR spectra.

The stimulation of the growth and development of wheat seedlings was noted. When wheat germinated in Petri dishes with pre-sowing treatment with 1-(2-ethoxyethyl)-3,5-bis(2-fluorobenzylidene)piperidin-4-one as complex with β–cyclodextrin increased the height of plants Kazakhstanskaya-10 by 4.5%, Severyanka – by 8.5%, Miras – 3%. It is shown to stimulate the development of grain seedlings in the presence of a complex of 1- (2-ethoxyethyl) -3.5-bis (2-fluorobenzylidene) piperidine-4-one with β-cyclodextrin compared with the control.

The novel synthesized complexes 3,5-bis(fluorobenzylidene)piperidones-4 with β-cyclodextrin after the treatment of seeds of three wheat varieties affect the germination and development of seedlings. It had found, that 3,5-bis(2-fluorobenzylidene)piperidin-4-one·β-cyclodextrin with an ethoxyethyl substituent at the nitrogen of the piperidine cycle stimulates growth, and its N-benzyl analogue is retardant.

Funding

Research was funded by the Committee of Science of the Ministry of Education and Science of the Republic of Kazakhstan, BR10965255.

References

1 Orlov D.S., Sadovnikova L.K., Sukhanova N.I. Soil chemistry // M .: Higher school. – 2005. – 558 p. (rus.)

2 Kruglov Yu.V. Microbiological aspects of soil fertility and the problem of sustainable agriculture // Fertility. – 2006. – No. 5. – P. 9-12. (rus.)

3 Kravchenko L.V., Makarova N.M., Azarova T.S. Isolation and phenotypic characteristics of growth-stimulating rhizobacteria (PGPR), combining high activity of root colonization and inhibition of phytopathogenic fungi // Microbiology. – 2002. – T. 71. – No. 4. – S. 521-525. (rus.)

4 Kravchenko L.V., Azarova T.S., Makarova N.M., Tikhonovich I.A. The role of tryptophan in root exometabolites for the phytostimulating activity of rhizobacteria // Microbiology. – 2004. – T. 73. – No. 2. – S. 195-198. (rus.)

5 Posypanov G.S., Dozorov A.V., Dozorova T.A. Biological nitrogen and its ecological and economic significance in crop production // Grain cultures. – 2000. – No. 2.- P. 24-26. (rus.)

6 Zahir, Z. A. Plant growth promoting rhizobacteria: application and perspectives in agriculture // Adv. Agron. – 2004. – V. 81. – P. 97-169.

7 Zehr J. P., B. D. Jenkins, S. M. Short, G. F. Steward. Nitrogenase gene diversity and microbial community structure: cross-sestem comparison // Environ. Microbiol. – 2003. – V. 5. – # 7 – P. 539-554.

8 Akkoprii A., Deneir S. Biological control of fusarium wilt in tomato caused by Fusarium oxysporum f. sp. Lucopersici by AMF Glomus intraradices and some rhizobacteria // J. Phytopathol. – 2005. – V. 153. – #9. – P. 544-550. (rus.)

9 Shapoval O.A., Mozharova I.P., Korshunov A.A. Plant growth regulators in agricultural technologies // Plant protection and quarantine. – 2014. – No. 6. – P. 16 – 20. (rus.)

10 Bogomazov S.V., Kochmin A.G., Tikhonov N.N., Kudin S.M .. The effectiveness of the use of retardant growth regulators in the technology of growing seed crops of winter wheat // Niva Volga region. – 2017. -No. 1 (42). – S. 15-20. (rus.)

11 Privalov F.I. Retardants in spring barley crops // Plant protection and quarantine. – 2012. – No. 12. – P. 24-26. (rus.)

12 Utility model patent No. 3810 RK. Salt of naphthoxybutynylpiperazine hydrochloride with retardant properties / Sycheva E.S., Mukanova M.S., Yu V.K., Li T. / by application No. 2019 / 0022.2 dated 10.01.2019; publ. 04/05/2019, Bul. No. 14. – 3c. (rus.)

13 Patent 258235C1 RU. Retardant for the growth of vegetative organs of cucumbers and a method for its production / Protsenko A.N., Shakirova O.G. by application No. RU2015108229 / 13A dated 10.03.2015; publ. 04/27/2016. (rus.)

14 Prev. Pat. 218 RK. The application of 1,4-[1-(2-ethoxyethyl)-4-hydroxypiperidyl-4]-1,3-butadiyne dihydrochloride as a plant growth stimulator // Praliev KD, Yu V.K., Bazunova G.G. Publ. 12/30/93. Bull. No. 6. (rus.)

15 Prev. Pat. 5011 RK. 1-(2-Ethoxyethyl)-4-(dimethoxyphosphoryl)-4-hydroxypiperidine, which possesses plant growth stimulating activity / Yu V.K., Praliyev K.D.; claimed. 28.12.95; publ. August 15, 1997. Bul. №3 (rus.).

16 Bellamy L. J. The infrared spectra of complex molecules//Halsted Press, a division of John Wiley & Sons, Inc.: New York. – 1975. – Vol. 1 (3rd ed.). – 433 pp. https://doi.org/10.1002/pol.1976.130140217

IRSTI 31.27.21 https://doi.org/10.26577/ijbch.2021.v14.i2.017

A.A. Taldybai[1*], D K. Aidarbayeva[1], A. Aksoy[2], J. Jenis[3*], B. Oxikbayev[4]

[1]Abai Kazakh National Pedagogical University, Almaty, Kazakhstan
[2]Akdeniz University, Antalya, Turkey
[3]Research Center for Medicinal Plants, Al-Farabi Kazakh National University, Almaty, Kazakhstan
[4]I. Zhansugurov Zhetysu University, Taldykorgan, Kazakhstan
*e-mail: aknur666@mail.ru

Prospects of studying and using *Saussurea elegans* Ledeb. in the foothills of the Zhetysu Alatau

Abstract. The conservation and rational use of plant resources combined with global warming and other environmental stresses and human activities can lead to the rapid destruction of existing ecosystems, especially in arid regions, which include most of the territory of Kazakhstan (Kazakhstan's Second National Communication, 2009). The article represents the results of studies of a promising medicinal plant *Saussurea (S.) elegans* Ledeb including of phytochemical research, the compositional analysis of the main groups of biologically active compounds. The quantitative content of *S.elegans* was determined such as polysaccharides, flavonoids, alkaloids, saponins, extractives, free organic acids, vitamin B2 (riboflavin), vitamin C, and groups of 15-component fatty acid. Additionally, ethnobotanical studies have shown the purpose of this plant usage (forage, ornamental, etc.) by geobotanical, floristic, ethnobotanical, resource, physico-chemical methods. The resource data of *S. elegans* are presented in three gorges (the Krutoe tract, the right bank of the Terekti River valley (Topolevka), the Karasyryk Gorge) of the Zhetysu Alatau. *S. elegans* is practical interest for introduction into medical practice as a source of biologically active substances. At the moment, the anthropogenic load on the *S. elegans* site leads to their gradual reduction (haymaking, fires, plowing the land for agricultural purposes), or causes a succession of phytocenosis. A detailed literature overview shows the distribution and resources together with chemical composition of the *S. elegans* have not been properly studied in the Zhetysu Alatau.

Key words. *Saussurea elegans* Ledeb, Asteraceae Dumort., flavonoids, alkaloids, saponins, polysaccharides, vitamins, resources.

Introduction

Currently, despite a number of studies conducted in this area, one of the most pressing challenges is the study of plants in some remote areas of Kazakhstan, including the possibility of searching for useful plant species, their distribution, estimation of their volume, and their effective use. Many plant species have lost substantial distribution areas due to environmental changes in Kazakhstan. Thus, due to insufficient coverage of the majority of useful plants' studies require additional research in order to preserve, restore, and augment biological diversity at the population, species, and genus levels of the gene pool of Kazakhstan's flora.

S.elegans is an important object for study and a promising plant on the territory of Zhetysuyskiy Alatau. The purpose of this study is the phytochemical and resource study of *Saussurea (S.) elegans* Ledeb. According to S. Smirnova in the Altai Mountains there are up to 47 species of the genus [1].

S. elegans is included into the list of alkaloid plants and terms of biological activity as a herbicide by the Institute of Botany. According to previous reports the phytochemical constituents of this plant include rubber and sesquiterpenoids (elegin, chlorohissopifolin B, salegin, saelin, aguerin A, aguerin B), triterpenoids (B-amerine acetate), steroids (B-sitosterol, stigmasterol, campesterol), alkaloids (elegantin), coumarines 0.44%, flavonoids (hispidulin, pectolinarigenin) are considered as main constituents of *S.elegans* [3-5].

S. elegans has been studied and its reserves have been estimated in Kazakhstan for the first time. *S. elegans* is a potential plant to study its chemical composition and biological activity. As a result of research in the northwestern part of the Zhetysu Alatau, *S. elegans* was observed in 3 gorges.

Phytochemical analysis was made from the collected materials of the species *S. elegans*, and some biologically active substances were identified.

Materials and methods

The geobotanical survey was carried out in 3 stages: preparatory, field, and laboratory. In the preparatory stage the literature analysis was made, and routes were defined. In the field stage the route method was used to conduct field research in the northwestern part of the Zhetysu Alatau in August 2020. The coordinates of the studied areas were obtained with the help of the Garmin GPSMAP 62sGPS navigator. In the course of the work, geobotanical characterization and floristic analysis of the community were carried out using generally accepted methods.

The identification of the *S. elegans* species was carried out according to the "Flora of Kazakhstan" [6]; Illustrated determinant of Kazakhstan plants [7]. The list of plants was checked according to S.K. Cherepanov's publications [8].

The quantitative and qualitative analysis. The quantitative and qualitative analysis of the biologically active components of *S. elegans* was carried out by the method described in the State Pharmacopoeia [9].

For quantitative analysis of flavonoids, 2 g (actual size) of ground raw material together with a thin section was put in a 150 ml flask, then 30 ml of 90% ethyl alcohol a solution of 1% concentrated hydrochloric acid or 10% sulfuric acid (for hydrolysis of glycosides) added, and reflux in the water bath for 1 hour, let it cool at room temperature and filtered through filter paper to a 100 ml flask. This procedure of the extraction process was repeated 2 times using the above method, washed with 90% ethyl alcohol using the filter, and filled up alcohol to the mark on the flask (solution A). Poured out 2 ml of solution A in 25 ml flask and added into it 1 ml of 1% aluminum chloride solution in 95% alcohol and filled up 95% alcohol to the mark on the flask. After 20 minutes, the optical density of the solution (in a cuvette of 10 mm thickness) was measured by the spectrophotometer at 430 nm wavelength. For reference, several times was made the measurements using initially prepared solution A [9].

For quantitative determination of vitamin B_2 (riboflavin), 5 g of ground raw material put into 100 ml cone flask, then 2 ml of glacial acetic acid and 98 ml of water was added and heated in a water bath for 10 minutes. When the solution cooled down it filtered through a paper filter. 10 ml of filtrate poured to 100 ml measuring flask, then 3.5 ml of 0.1M sodium acetate solution added and filled up with water to the mark of the flask. The optical density of the resulting solution was determined on a spectrophotometer with a wavelength at 430 nm in a 10 ml thick measuring cuvette.

For determination of vitamin C, 100 ml of water added to 5 g of raw material and left for 1 hour, then 1ml of 2% salt solution, 1 ml of testing solution, 6.5 ml of water poured into a 50-100 ml flat-bottomed flask and titrated with 0.001 M until the purple color with 1 ml 0.001 mol, 2,6-dichlorophenol-indophenol sodium solution equivalent to 0.000088 g of ascorbic acid.

The sample was pre-ground to the size passing through a sieve with a hole diameter of 1 mm. The regrounded product in the amount of 0.1 g was selected by the quartering method and subjected to acidic methanolysis of 0.1N HCl/MeOH for 40 minutes. The resulting components were extracted with hexane for 5 minutes. The hexane layer was dried in a drying cabinet, and the dry residue was diluted in hexane. The fatty acid composition of *S. elegans* was determined by gas chromatography. The determination of the fatty acid composition was preceded by the conversion of fatty acids to methyl esters according to GOST 31665-2012 [10]. The derived fatty acid methyl esters were analyzed on a gas chromatograph Chromos GC-1000 (Chromos, Russia) with a flame ionization detector using a capillary column CP-Sil 88 with the parameters of 100 m × 0.25 mm × 0.20 microns (Agilent Technologies, USA). The analysis was carried out in the following temperature range: 100 °C – exposure time of 4 minutes – heating at a rate of 5 °C/min to 170°C – exposure time of 20 minutes. Then the temperature was raised at a rate of 5°C/min to 240°C with exposure at the final temperature of 18 min. The total duration of the chromatographic analysis was 70 minutes. The obtained chromatograms of fatty acid methyl esters were identified and the quantitative content of fatty acids was calculated by the peak areas as a percentage, using a standardized technique. The qualitative analysis is based on a comparison of the retention times of the corresponding mixtures of standard substances (Supelco® 37 Component FAME Mix, Sigma-Aldrich fatty Acid Methyl Ester Mix).

Results and discussion

The vegetation cover of the northwestern part was investigated, and expeditionary work was carried out in the Zhetysuyskiy Alatau in August 2020. As a

result of field studies in the Zhetysu Alatau, *S. elegans* were observed in 3 gorges: The Krutoe tract, the right bank of the Terekti River valley (Topolevka), the Karasyryk Gorge. The herbal raw material was collected to identify the phytochemical composition of *S. elegans*, and the plant's herbarium [6].

Saussurea is a genus of about 400 species in the Asteraceae family that can be found in Asia and Europe. Sesquiterpenes, triterpenes, flavonoids, and lignans, among other compounds, have been isolated from the *Saussurea* genus. The characteristic components of *Saussurea* plants, sesquiterpenes, are discussed first. Antitumor, antibacterial, antimararial, anti-inflammatory, and anti-ulcer effects have been discovered in compounds isolated from the *Saussurea* family. The most common behavior identified in the last decade is cytotoxicity [17]. Its last revision in the world volume was carried out by S.Yu. Lipschitz (1979). The genus *Saussurea* has a complex specific and intraspecific composition. The history of its study in Siberia is connected with the works of A.R. De Candolle, K. F. Lcdebour, N.S. Turchaninov, P.N. Krylov, L.P. Sergievskaya, M.G. Popov, S.Yu. Lipschitz et al. [11]. There are 115 species in the CIS, and among them 41 species are distributed in Kazakhstan [6]. The genus is well distinguished by morphological features, the anthuriums are usually smaller (up to 3-4 cm wide), numerous, rarely solitary, but then the primordial leaves are not expanded in the squamella. Perennial, rarely biennial grasses, sometimes semi-shrubs; leaves alternate, smooth-edged, sinuate-dentate, sinuate-lobate or pinnated incised [6,12,13].

The genus was separated into an independent taxon by the outstanding French botanist O.P. De Candolle in 1810 and named in honor of two naturalists, father and son *Saussure* [1]. For the first time, plants of the genus *Saussurea* DC. were described by I.G. Gmelin (1749) in the second volume of Flora Sibirica and assigned by the author to the genus *Cirsium* Hill. The *Saussure* species was assigned to the genus *Serratula* by Carl Linnaeus, the inventor of binomial nomenclature [14].

The new genus *Saussurea* DC. was introduced by De Candol in his first monograph on the revision of composite plants ("Observations sur les plantes Composées ou Syngeneses") presented to the French Institute on January 18, 1808. It was published only in 1810 in the proceedings of the Paris Museum of Natural History. In the monograph of the genus *Saussurea*, De Candol compares the established by himself new genus with the genera *Serratula* L. and *Cirsium* Hill. According to the author the genus *Saussurea* DC. differs from *Serratula* L. in the presence of pinnate seta of pappus, and from *Cirsium* Hill. in the absence of a prickly involucre.

Following De Candolus, a significant contribution to the study of the species composition of the *Saussurea* was made by K.F. Ledebourg. Based on the results of floristic studies of the Altai and Eastern Kazakhstan, he conducted an inventory of the species composition of the *Saussurea* in Russia in 1829-1831. Ledebourg's first work, Icônes plantarum novarum vel imperfecte cognitarum, floram rossicam, imprimis altaicam illustrantes (1829, 1833), covered 25 species of *Saussurea*.

K.F. Ledebur identified 6 groups of species based on the following main features:

a. two groups of species are distinguished by the relationship of the length of the leaves of the involucre:

- outer leaves of the involucre, almost equal in length to the inner ones;
- the leaves of the involucre are much shorter than the inner ones, i.e., the involucre is clearly imbricate;

b. the two groups of species differ in the main features of the basal appendages of the anthers. The first of them is distinguished by the presence of bicetal appendages, the second-by tufted-woolly or tufted-ciliated appendages;

c. two groups of species are distinguished by the presence or absence of appendages on the top of the leaves of the involucre. Representatives of the first group are characterized by the presence of glumal appendages, representatives of the second group do not have them [15].

Botanical aspects. S. elegans has oblong or oblong-ovate basal and lower stem leaves, along the edge of the pinnate-lobate or almost lyre-shaped-pinnate-separate, glabrous or pubescent, but not scabrous; anthuriums 0.5-0.8 cm wide, collected in a corymbose panicle. Perennial herbaceous plants 60 cm in height. The stems are erect, numerous, thin, with numerous shortened vegetative branches, glabrous and shiny below, web-like pubescent, glandular, evenly leafy above. The leaves are scabrous above and along the edge due to short bristles, greyish below, web-like, to white felt, glandular-pubescent. It grows on the meadow, meadow-steppe, steppe, rocky, loess and gravelly mountain slopes, among shrubs and stones, along the banks of rivers. Blooms in July-August. Meadow, shrubby and fescue steppes, rocky slopes [6,13].

Figure 1 – *S. elegans* from the north-western part of the Zhetysu Alatau. From the authors' personal archive

The Krutoe tract is located in the northern part of the Zhetysu Alatau ridge, on the right side of the Lepsi River valley. A combination of apple and aspen forests with meadow vegetation.

N 45°33 '19, 8" E 80°42'57, 3" Height 1377m. *S.elegans* is in satisfactory condition. Accompanying species: *Vicia crassa, Erigeron caucasicus, Origanum vulgare, Fallopia convolvulus, Oberna Behen, Serratula coronata, Crepis sibirica, Inula brittanical.*

The right bank of the Terekti River valley (near the village of Topolevka). Mountain dry mixed herb – grass steppe with Meadowsweet, at the pass of the northern macroslope of the Zhetysu Alatau.

The Terekti massif is located in the south-eastern part of the Aksai Mountains. The gorge is very deep, the Terekti river flows along the bottom. The slopes are steep with many flakes.

N 45°27'10, 7" E 80°22'56, 3" Height 1183m, *S.elegans* in satisfactory condition. The species grows among mixed grasses together with *Polonia* Pall., *Nepeta pannonica* L., *Ajania fastigiata* Poljak., *Potentilla impolita*., *Paeonia hybrida*, *Pao angustifolia, Stipa capillata*, *Eremurus altaicus*, *Origanum vulgare*, *Leymus angustus*.

Karasyryk gorge. Rocky-scree slope. Deep, with numerous flakes. In many places, the slopes are steep, difficult to access, rocky-scree slope. *S.elegans* is in satisfactory condition. N 45°12 '33, 7" E 80°01'52, 5" Height 1476 m. Accompanying species: *Artemisia sublessingiana, Juniperus sabina, Gentiana tianchanica, Artemisia frigida, Berberis sphaerocorpa, Ephedra equisetina, Sedum hybridum, Pao angustifolia.*

Biologically active compounds of S. elegans. Biologically active compounds (BAC) – chemicals that participate or can participate in the implementation of the functions of the body, affecting the course of biological processes. They have a high specificity of action. BAC include enzymes, vitamins, and hormones. These are vital and necessary compounds, each of which performs an irreplaceable and very important role in the vital activity of the body.

To determine the qualitative content of the *S. elegans* according to the methodology of the State Pharmacopoeia of the Republic of Kazakhstan moisture content of raw materials, extractive substances, quantitative BAC content was studied. BAC content is presented in Table 1. Place of growth: Right side of the Terekti River valley (near the village of Topolevka). Study part: Aerial.

These materials prove the dependence of the content of biologically active substances of plants on environmental conditions, especially on the place of growth. In terms of biological productivity and content the plant can be considered suitable for complex use. Thus, the analysis of the literature data and the results of the in-house study suggest that plants of the genus Saussurea containing a valuable set of biologically active components, widely distributed in the territory of Kazakhstan, are deserving plants. Currently, it is established that flavonoids are synthesized mainly in aboveground organs. Cases of detection of these substances in the roots are quite rare [16].

The fatty acid composition of *S. elegans* is shown in Table 2 and the chromatogram is given in Figure 2.

Table 1 – Quantitative composition of biologically active compounds of *S. elegans* (dry weight, %)

Quantitative composition quality of raw materials, (%)			Quantitative composition of BAC (%)						
Plant moisture content	Extractive substance (90% alcohol)	Extractive substance (70% alcohol)	Flavo-noids	Free organic acids	Alkaloids	Saponins	Polysac charides	Vitamin B_2 (riboflavin)	Vitamin C
7.2	44.18	37.71	0.005	1.27	8.69	1.53	4.7	0.008	0.05

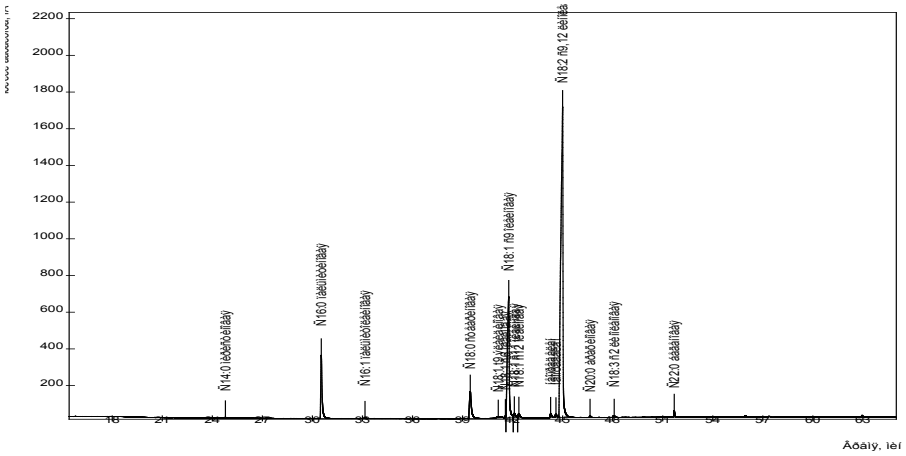

Figure 2 – GC-MS chromatogram of *S. elegans* extract

Table 2 – Composition of fatty acids in *S. elegans* extract

Name of the acid	Mass fraction, %
Total saturated fatty acids	18.002
C14:0 – Myristic acid	0.154
C16:0 – Palmitic acid	11.463
C18:0 – Stearic acid	4.900
C20:0 – Arachidic acid	0.324
C22:0 Begenic acid	1.161
The sum of monounsaturated fatty acids	25.417
C16:1 Palmitoleic acid	0.128
C18:1 t9 Elaidic acid	0.273
C18:1 c6 Oleic acid	0.317
C18:1 c9 Oleic acid	21.918
C18:1 c11 Oleic acid	0.830
C18:1 c12 Oleic acid	0.762
undefined	0.628
undefined	0.561
The sum of polyunsaturated fatty acids	56.581
C18:2 c9, 12 Linoleic acid	56.269
C18:3 c2 Linolenic acid	0.312

According to the results of GC analysis (Table 2), it was found that linoleic C18:2 (56.269 %), oleic C18:1 (25.289 %), and palmitic C16:0 (11.463 %) acids predominate in *S. elegans*. The following fatty acids were also found in this *S. elegans* extract: myristic C14: 0 (0.154 %), palmitoleic C16:1 (0.128%), stearic C18:0 (4.9%), elaidic C18:1trans (0.273%), linolenic C18:3 (0.312%), arachidic C20:0 (0.324%), and begenic C20:0 (1.161%). According to the obtained results, *S. elegans* is a source of essential fatty acids (linoleic and linolenic), which indicates the prospects of using this raw material as a source of biologically active substances.

During the field survey in the area of the north-western part of the Zhetysu Alatau, a current estimate of the distribution and stocks of *S. elegans* was performed. The *Saussurea elegans* was found on the northern macroslope of the ridge. The operational reserve of dry raw materials of the *S. elegans* amounted to 15.5 tons of aboveground phytomass on a total area of 68.0 hectares. The volume of possible annual harvesting of raw materials considering the period of renewal of *S. elegans* after harvesting should not exceed 4.5-5.0 tons of aboveground phytomass in dry form.

Plants of the genus *Saussurea* are widely used in folk medicine. People of the Far East, Siberia, Tibet, and Mongolia, used it in the treatment of a wide variety of diseases. Residents of Zhetysu Alatau use *S. elegans* as pet food and as an ornamental plant. *Saussurea* performs a decorative function, but at the same time, it can have a therapeutic effect on the human body.

Conclusion

S. elegans grows at altitudes of 1183-1476 m of the Zhetysu Alatau. As a result of field studies, *S.elegans* was observed in three gorges: the Krutoe tract, the right side of the Terekti River valley (Topolevka), and the Karasyryk Gorge. Materials were collected for chemical analysis and herbarium.

Biological active constituents, such as flavonoids 0.005%, alkaloids 8.69%, saponins 1.53%, extractives 44.18% (90% alcohol) 37, 71% (70% alcohol) free organic acids 1.37%, polysaccharides 4.7%, vitamin B_2 (riboflavin) 0.008%, vitamin C 0.05% together with plant moisture 7.2% of *S. elegans* growing in the northwestern part of the Zhetysu Alatau were determined. The main contents of fatty acids were linoleic acid (56.269 %) and oleic acid (25.289 %), and palmitic acids (11.463 %). In addition, unsaturated linolenic acids are found in small amounts (0.312%).

In our study is given the current estimation of the distribution and stocks of *S. elegans* in the area of the north-western part of the Zhetysu Alatau. Ethnobotanical studies have shown that the locals use *S.elegans* only as pet food and as ornamental plants.

Based on the above, the Saussurea elegans plant can be used to make natural cosmetics that will not harm the human body in the future, as well as natural medicines for use in the treatment, alleviation, healing or prevention of disease.

References

1 Smirnov S.V. Synopsis of the genus Saussurea DC. (Asteraceae) of the Altai Mountains // Journal Turczaninowia. – 2007. – Vol. 10, No 3-4. – P. 5-35.

2 Gemedzhiyeva N.G. Alkaloid-bearing plants of Kazakhstan and prospects for their use (by the example of the Dzungarian-North Tian Shan province). – Almaty. – 2012. – P. 117.

3 Sham'yanov D., Mallabaev A., Sidyakin G.P. Saelin – a new sesquiterpene lactone from Saussurea elegans // Journal Khimiya Prirodnykh Soedinenii. – 1980. – No 2. – P. 258.

4 Sham'yanov D., Mallabaev A., Sidyakin G.P. Aguerins A and B from Saussurea elegans // Journal Khimiya Prirodnykh Soedinenii. – 1983. – No 6. – P. 788-789.

5 Sokolov P.D. Plant resources of the USSR, flowering plants, their chemical composition, use, Asteraceae Family. – Saint-Petersburg: "Nauka", 1993. – 166 p.

6 Flora of Kazakhstan. Vol. 9. – Alma-Ata. – 1966. – 248 p.

7 Illustrated determinant of Kazakhstan plants. Vol. 1. – Alma-Ata. – 1972. – 644 p.

8 Cherepanov S.K. Vascular plants of Russia and neighboring countries. – St. Petersburg: Mir i semya, 1995. – 182 p.

9 Mashkovsky M.D., Babayan E.A., Oboymakova A.N. Gosudarstvennaya pharmacopoeia SSSR [State Pharmacopoeia of the USSR]. – M.: Medicine, 1968. – 1080 p.

10 GOST 31665-2012 Vegetable oils and animal fats. Preparation of methyl esters of fatty acids.

11 Lipschitz S.Yu. Saussurea, Lactarius Rufus. – Bashbigea BS. / S.Yu. Lipschitz, B.K. Shishkin, E.G. Bobrov / ed. acad. V.L. Komarov / Flora of the USSR. – M.L.: Publishing House of the USSR Academy of Sciences, 1962. – 361 p.

12 Flora of the USSR. – M.L.: Publishing House of the USSR Academy of Sciences, 1962. V 27. – p. 423

13 Baitenov M.S. Flora of Kazakhstan. Vol. 1. Illustrated determinant of families and genera. – Almaty: Gylym, 1999. – 125 p.

14 Species plantarum [Electronic resource] / Carolus Linnaeus / 1753. – Available at: http://manybooks.net/titles/linnaeusc2077120771-8.html

15 Janssen K.P., Mensink R.P., Cox F.J., Harryvan J.L., Hovenier R., Hollman P.C., Katan M.B. Effects of the flavonoids quercetin and apigenin on hemostasis in healthy volunteers: results from an in vitro and a dietary supplement study // The American journal of clinical nutrition. – 1998. – Vol. 67, No 2. – P. 255-262.

16 Kukenov M.K. Flavonoid-containing plants of the South-East of Kazakhstan. – Almaty: Science KazSSR, 1984. – P. 10

17 Ting Zhao, Shao-Jing Li, Zhao-Xin Zhang, Man-Li Zhang, Qing-Wen Shi, Yu-Cheng Gu, Mei Dong and Hiromasa Kiyota. Chemical constituents from the genus Saussurea and their biological activities // Heterocyclic Communications. – 2017. – Vol. 23, Iss. 5. – P. 55-63.

Content